FUSED-RING HETEROCYCLIC AROMATIC COMPOUNDS

A Dissertation

by

YIRUI CAO

Submitted to the Graduate and Professional School of
Texas A&M University
in partial fulfillment of the requirements for the degree of

DOCTOR OF PHILOSOPHY

Chair of Committee,	Lei Fang
Committee Members,	Daniel Singleton
	Quentin Michaudel
	Choongho Yu
Head of Department,	Simon North

May 2022

Major Subject: Chemistry

ABSTRACT

Fused-ring heterocyclic aromatic compounds represent an intriguing family of organic π-systems for fundamental chemistry and practical properties. The term "hetero-" indicates the presence of heteroatoms in the aromatic backbone. In the past two decades, the requirement for precisely functionalized nanographenes sparked interest in nanographenes with heteroatoms. Various heteroatoms, including nitrogen, boron, oxygen, sulfur, *etc*., were incorporated into polycyclic aromatic compounds to manipulate the chemical and electronic properties of nanographene-like compounds. This dissertation describes my work on the synthesis and investigation of fused-ring heterocyclic aromatic compounds containing nitrogen and/or boron atoms.

This dissertation starts with a brief introduction to the field of aromatic compounds with heteroatoms. First, the background of this topic and underlying motivations are summarized. Then selected literature examples of π-systems containing B—N bonds and azahelicenes are presented. The unexplored areas and challenges related to this field are identified. Finally, the choice of topics as the main focuses of this dissertation is discussed.

Chapter II describes the design and synthesis of a B←N coordination-containing molecule with an extended conjugation composed of 23 fused rings. The synthesis towards this novel molecule and the impact of incorporating B←N bonds are the focuses of this chapter. Chapter III presents my work on the manipulation of molecular bandgaps based on the installation of various aryl groups on the B←N bond-containing compounds, and the impact on structure and optical properties.

In Chapter IV, motivations and efforts towards the synthesis of centripetal azahelicenes are discussed. A combination of synthetic strategies and theoretical simulations is illustrated along with iterative modification on the reaction conditions to complete the synthetic route. The preliminary observations of metal binding are discussed as well.

Chapter V describes the development of undergraduate teaching labs for the broader impact of the research described above. Well-known “Nobel prize-winning reactions”, including Suzuki coupling and ring closing metathesis, are optimized, and implemented in undergraduate organic laboratory course.

Finally, Chapter VI concludes the entire dissertation by giving an overview of the results presented in the previous chapters, followed by perspectives of research that would strengthen the insight into this field.

DEDICATION

Parents, Shengbo Cao and Dongmei Li

Teachers who led me into chemistry, Zhen Jia and Feifei Mao

My Beloved Homeland

ACKNOWLEDGEMENTS

First and foremost, I would like to express my gratitude to my advisor Dr Lei Fang for providing me an opportunity to pursue Ph.D. degree, guiding and supporting me during my academic journey. He gave me valuable feedbacks on research progress through my entire graduate study. I still remember his advice that I should work hard mentally instead of only physically during my first year. Beyond academic affairs, he supported my decision to pursue industrial career outside chemistry, which had been critically important to me. Dr Fang no doubt contributed most significantly in my completion of this dissertation.

I would also like to thank Dr Daniel Singleton, Dr Quentin Michaudel and Dr Choongho Yu for their service on my committee. They provided me with not only valuable feedbacks on my research progress, but also methodologies about how to conduct scientific research. Besides, I am grateful to all the staff in the Department of Chemistry and Material Characterization Facility at Texas A&M University for their professional service to aid my research. In particular, I would like to thank Dr Yohannes Rezenom who manages mass spectroscopy facilities. His kindness and professionalism helped me tremendously.

I feel so lucky to have been working in a nice and supportive group for the past five years. Everyone I work with in our group is so kind and helpful to me. The list includes Dr Jongbok Lee, Dr Tianyu Yuan, Dr Congzhi Zhu, Dr Alex Kalin, Dr Xiaozhou Ji, Dr Chenxu Wang, Dr Sai Che, Dr Bailey Phillips, Anthony Mu, Bo-Ji Peng, Chenxuan Li, Octavio Miranda, Mingwan Leng, Abani, Steven Hodge, Shao-Jiun Yang and Guanghua Yu. I would like to specially mention my three mentors, Dr Jongbok Lee, Dr Congzhi Zhu

and Dr Xiaozhou Ji. They taught me a lot when I first joined the lab, including experimental skills and helpful scientific habits. Special thanks to Steven Hodge who joined the group as an undergraduate mentee about two years ago and decided to stay in the group as a graduate student. I learnt a lot during communication with him.

I am also grateful for financial assistance and awards from Texas A&M University for OGAPS travel award to support my trip to Japan to attend ISNA conference.

Besides these people and organizations who directly helped me in my academic career, there are so many others who have been standing behind me with their unconditional support. First, my parents provided me with love and support all the time. Owing to the pandemic, it is barely possible to go back to hometown to see them. I know how much they miss me. We can only rely on video streaming for communication. I still clearly remember the crying tones of my mother when she called me after I passed the Customs and safety inspection. She did not have the courage to wave me goodbye before that. I was too young and naïve to understand this, but as I am increasingly aged, such a feeling deeply craved my heart.

I have had so many good friends who made me feel I am not alone on this lonely journey. Yi Han, who is currently a postdoc in National University of Singapore, encouraged me a lot, and I was often impressed with his knowledge and professionalism in Chemistry. The work from his group inspired me a lot. Herein I would like to wish him all the best in the future. The friendship with my best friend Zhaozhong Li, whom I have known since high school, has never faded away and during the hard Ph.D. journey, it is

even becoming more important. There are so many other good friends of mine, including Jian Ding, Fengjiao Yan, Ruiqi Sun *etc.* who made me feel the warmth of friendship.

Reading the acknowledgement of my undergraduate thesis, it feels like a dream that the past five years finally lead to the contemporary moment when I am writing this Ph.D. dissertation. I was a person so ambitious about pursuing an academic career, and I feel honored to have such a trip to win the Ph.D. title. It has been 12 years since I participated in the Chemistry Olympiad, and this Ph.D. title serves a nice period to conclude all of it. Although I might not continue the academic path, but the experiences these years gave me courage to embrace challenges that are about to come.

CONTRIBUTORS AND FUNDING SOURCES

Contributors

This works was supervised by a dissertation committee consisting of Professor Lei Fang, Professor Daniel Singleton, Professor Quentin Michaudel of the Department of Chemistry, and Professor Choongho Yu of the Department of Mechanical Engineering.

The single crystal structure of **BN-2** in Chapter II was obtained and analyzed by Dr Nattamai Bhuvanesh. The mass spectra of all the compounds mentioned in this dissertation were collected by Dr Yohannes Rezenom. In Chapter V, the proposal of feasible teaching lab experiments was made by undergraduate student Nicholas Nguyen and the optimization of those conditions were conducted by Steven Hodge in our group and the author.

The GIWAXS data of **Ph-IDCZ-Cl-BTh**, **Ph-IDCZ-BTh**, **Th-IDCZ-Cl-BTh** and **Th-IDCZ-BTh** in Chapter III and **BN-1** in Chapter II were measured by Anthony Mu in Argonne National Laboratory, and the mobilities of OFET devices fabricated with **Ph-IDCZ-Cl-BTh**, **Ph-IDCZ-BTh**, **Th-IDCZ-Cl-BTh** and **Th-IDCZ-BTh** were measured by him in Lawrence Berkeley National Laboratory.

All other research mentioned in this dissertation was conducted by the author student Yirui Cao independently.

Funding Sources

The research described in this dissertation was supported by National Science Foundation under Award Numbers DMR-1654029 and CHE-2003733, and Welch Foundation research grant A-1898. The chance to present the relevant research work in

ISNA-18 conference in Sapporo Japan was sponsored by the Travel Award by OGAPS of TAMU.

NOMENCLATURE

HOMO	Highest Occupied Molecular Orbital
LUMO	Lowest Unoccupied Molecular Orbital
P3HT	Poly(3-hexyl)thiophene
OSC	Organic Solar Cell
OLED	Organic Light Emitting Diode
OFET	Organic Field Effect Transistor
CV	Cyclic Voltammetry
GIWAXS	Grazing Incidence Wide Angle X-ray Scattering
DFT	Density Functional Theory
THF	Tetrahydrofuran
RCM	Ring Closing Metathesis
DMF	N,N-Dimethylformamide
DCM	Dichloromethane
DMAP	4-Dimethylaminopyridine
ESI	Electron Spray Ionization
Fc	Ferrocene
NMR	Nuclear Magnetic Resonance
BHT	Butylated Hydroxytoluene

TABLE OF CONTENTS

Page

LIST OF FIGURES

Page

LIST OF TABLES

Page

CHAPTER I

INTRODUCTION

1.1 Overview of Polycyclic Heteroaromatic Molecules

The chemistry of heteroaromatic compounds has attracted ongoing attention since around two centuries ago, encompassing many topics including synthetic and physical organic chemistry, natural product research, pharmaceuticals, and material science, *etc*. In the very initial stage of this field, much attention was paid to the investigation of natural and synthetic dyes.[1] Some pioneering examples included flavanthrone, xylindein, coerulein, tricycloquinazoline, *etc*. These molecules, among others, received attention due to their special fused-ring backbones and, more importantly, their industrial values. However, the early stages of the development were hindered due to the lack of versatile synthetic methodologies and precise characterization methods.

Beginning in the 1970s, the rapid development of various synthetic strategies, especially transition metal-catalyzed cross coupling reactions, enabled the synthesis of a wide variety of polycyclic aromatic compounds without the harsh conditions that were previously required. Cross coupling reactions have been extensively employed to synthesize fully-fused aromatic compounds, from the oligomerization of precursors to the final annulation steps. In addition, the discoveries of novel catalysts and ligands that could satisfy substrates with distinct electronic and structural features have strengthened the toolbox towards the evolution of these fascinating aromatic compounds.

Entering the 21st century, the significant advancement of knowledge on graphene and graphene nanoribbons sparked interest in large polycyclic aromatic compounds. As an extensive π-conjugated system of carbon atoms, graphene has attracted tremendous attention due to the extraordinary properties including remarkable charge-carrier mobility, mechanical strength, and quantum hall effect.[2] However, its conductive nature prevents its application as semiconducting materials. In contrast, graphene segments with locally confined structures show non-zero bandgaps, which are tunable by their size and functionalization.[3] Conventionally, there are two major ways to achieve graphene nanoribbons, namely, top-down strategy and bottom-up strategy.[4] Top-down strategy represents trimming or deforming a larger piece of carbon-enriched material, like graphene or carbon nanotube to form the desired structure. Although it enjoys the benefit of the ability to address the location of the desired entity, it suffers from the drawback of the low resolution limit and poor control over the edge structure and the molecular size. Bottom-up strategy on the other hand, endows these materials with desirable precision, scalability and can be undoubtedly characterized by various characterization methods.[5,6]

Incorporation of heteroatoms into graphene strongly impacts its electronic properties, implying various new possibilities of applications in biosensing,[7] batteries,[8] supercapacitors,[9] catalysis[10,11], *etc*. However, it is still a formidable challenge to control the precise local structure and distribution of heteroatoms during the heteroatom incorporation process. In this context, bottom-up synthesized, fused polycyclic aromatic systems decorated with heteroatoms can be regarded as functionalized nanographenes, which enjoy both the structural uniformity of graphene and tunable electronic structures.

Dr Perepichka's group theoretically proved that enhanced dimension of conjugation witnessed a quicker contraction of HOMO-LUMO bandgap with increased molecular size.[12] By modifying the geometry, size, and heteroatom content of these fused nanographenes, electronic structures could be flexibly tuned to further control bandgaps, optical properties, redox behavior, *etc*. This structure-property correlation serves as the guidance for the development of various promising heteroatom-containing carbon materials, including NIR dyes,[13,14] two-photon absorbers,[15] sensors[16,17] *etc*. Thus far, there has been significant improvement in fundamental investigations, where heteroatom-containing aromatic compounds have found application in bench stable cations,[18] spin-active organic molecules[19] and ligands to chelate transitional metals.[20-23]

By careful design of ring fusion patterns, the location of heteroatoms, and conformational control, a wide variety of polycyclic aromatic compounds can be rationally designed to serve both fundamental and application purposes. Inspired by such a diversity of active stimuli, there have been numerous compounds with different elements, the most common ones being sulfur, nitrogen, oxygen, silicon, phosphorous, boron, *etc*., synthesized and investigated in detail.

1.2 Polycyclic Aromatic Systems Containing Boron Atoms

Boron (atomic number = 5) and nitrogen (atomic number = 7) can form a B—N bond isoelectronic to a C—C bond. Depending on the bond order of B—N bond, they can be classified into B—N covalent bond or B←N coordination bond. Swapping a C—C bond with a B—N bond creates a polar bond due to their different electronegativities.

An early report of the appearance of B—N covalent bond dated back to 1926, when the synthesis and properties of $B_3N_3H_6$ were discussed[24]. When incorporated into a polycyclic π-system, boron plays an important role in tuning the energy levels of molecular orbitals and bandgaps. Thereby, the resulting compounds have found promising optoelectronic applications, including field transistors,[25] light-emitting diodes,[26] solar cells,[27,28] stimuli-responsive luminescent devices,[29,30] *etc*. In the last two decades, there have been significant advances in this field, contributing to the fundamental insights and practical applications. In this section, recent advances are summarized according to the type of B—N bond. For boron embedded systems, the main focus is on molecules featuring B—N bonds, while those with only B—C bonds are excluded.

1.2.1 B—N Covalent Bond Embedded Systems

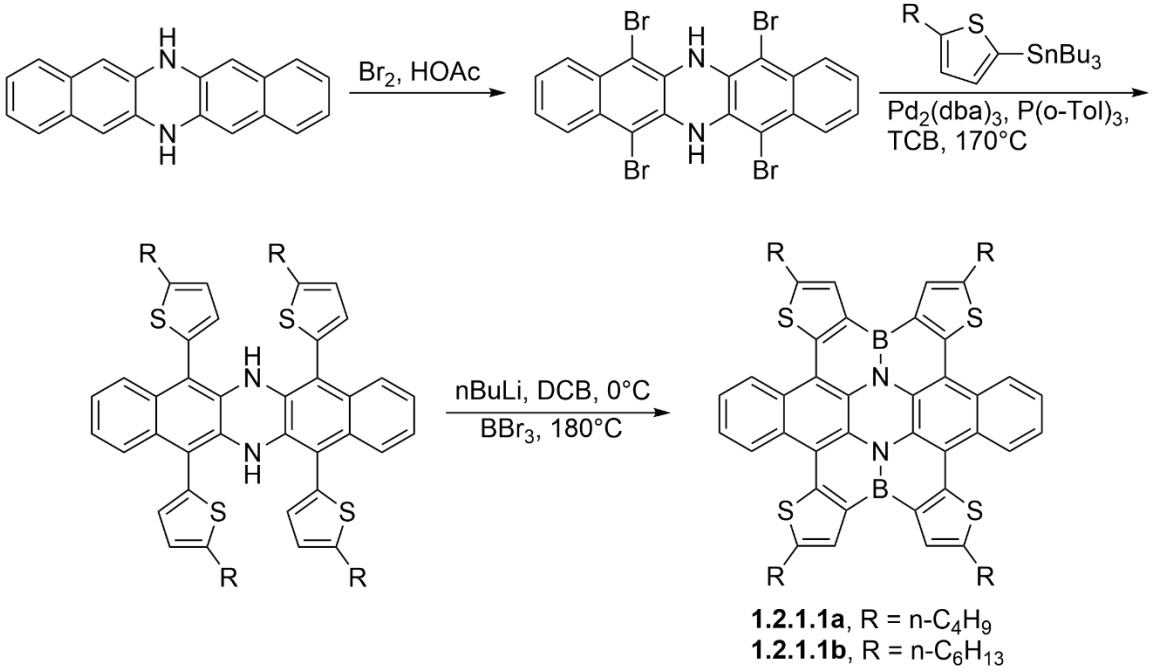

Figure 1. Synthetic scheme of a coronenoid with thiophenes and B—N covalent bond. Adapted from *J. Am. Chem. Soc*. 2014, 3764-3767.

To construct this π-system with B—N covalent bonds, electrophilic cyclization method between boron and the aromatic motif is usually required. The aromatic unit should be electron rich to facilitate this type of reaction, and the boron source is typically BX_3, where X is a halogen. Pei et al. reported the synthesis of a system containing four thiophene rings and two B—N bonds (**Figure 1**).[31] The synthesis started from the Stille coupling between a tetrabromo derivative and a stannylated thiophene. Next, electrophilic borylation was conducted on the lithiated intermediate to form the final product **1.2.1.1a** and **1.2.1.1b**

featuring a coronene center. The optical properties and self-assembly behavior of these molecules were investigated in detail to find that the molecule **1.2.1.1b** adopted photoconductivity behavior.

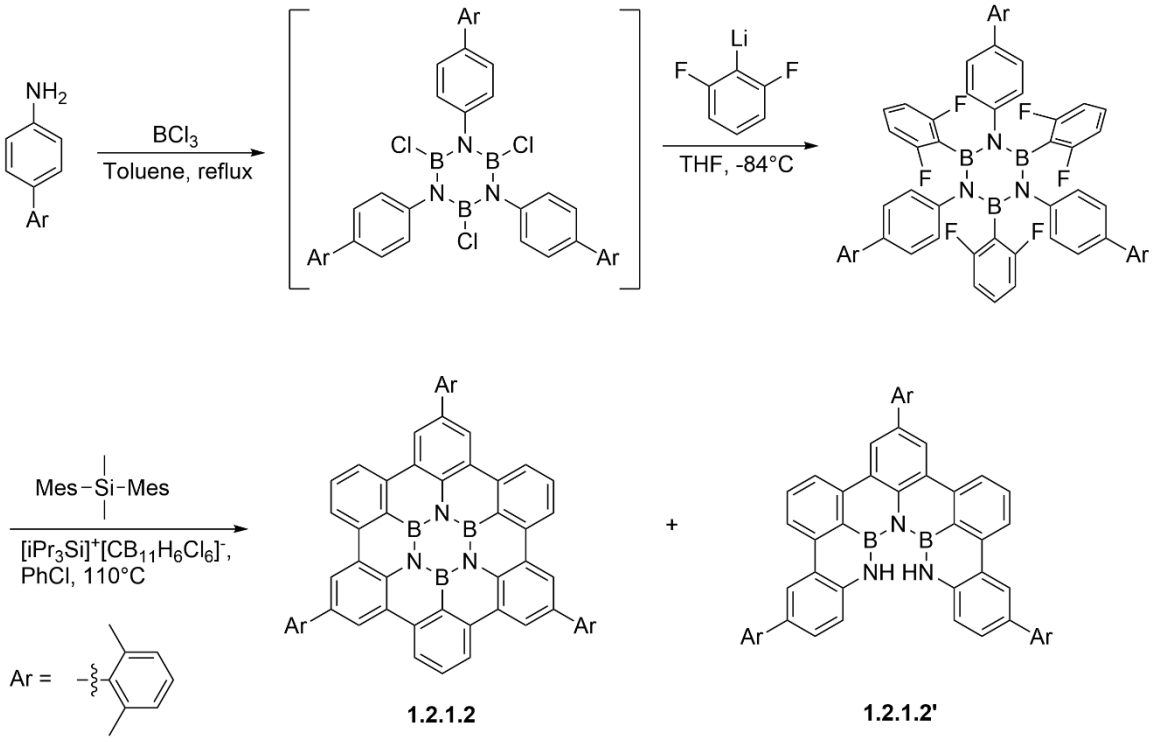

Figure 2. Synthetic scheme of a coronene derivative with the core fully replaced by B—N bond. Adapted from *Angew. Chem., Int. Ed*. 2017, 4483−4487.

The range of B—N bond could be further expanded. Bonifazi et al. successfully achieved a structure where the central ring was fully replaced with B—N bond (**Figure 2**).[32,33] Despite the success, the yield for the last step planarization was particularly low,

demonstrating the difficulty of the removal of fluoride in Friedel-Crafts type coupling of fluoroarenes.[34] In fact, the partial annulated product **1.2.1.2'** was separated as the major product. The desired final product **1.2.1.2** displayed strong blue-violet emission and green phosphorescence.

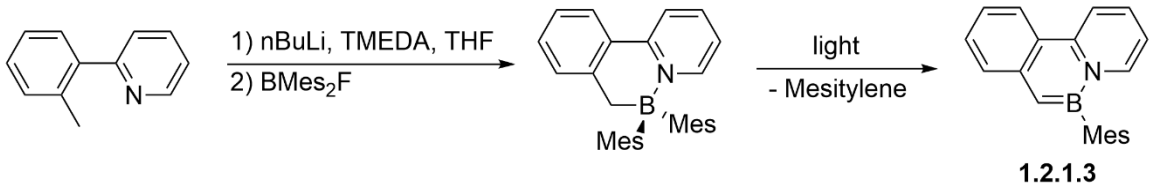

Figure 3. Synthetic scheme towards a ladder type small molecule with photoelimination. Adapted from *Angew. Chem., Int. Ed*. 2013, 4544-4548.

In recent years, a novel photoelimination reaction was discovered which could afford boron embedded ladder type small molecules with a fully fused backbone (**Figure 3**).[29] In this reaction, the methyl group was first borylated following lithiation. Afterwards, the mesityl group will be eliminated when subjected to irradiation. In the photo elimination step, arene was eliminated and a new C—B double bond was formed to rigidify the backbone. The detailed mechanism has not been fully known yet, and subsequent investigations have been underway, including the impact of chelation,[35] substituent,[36] the linker and location of BN units[37] *etc*.

1.2.2 B←N Coordination Bond Embedded Systems

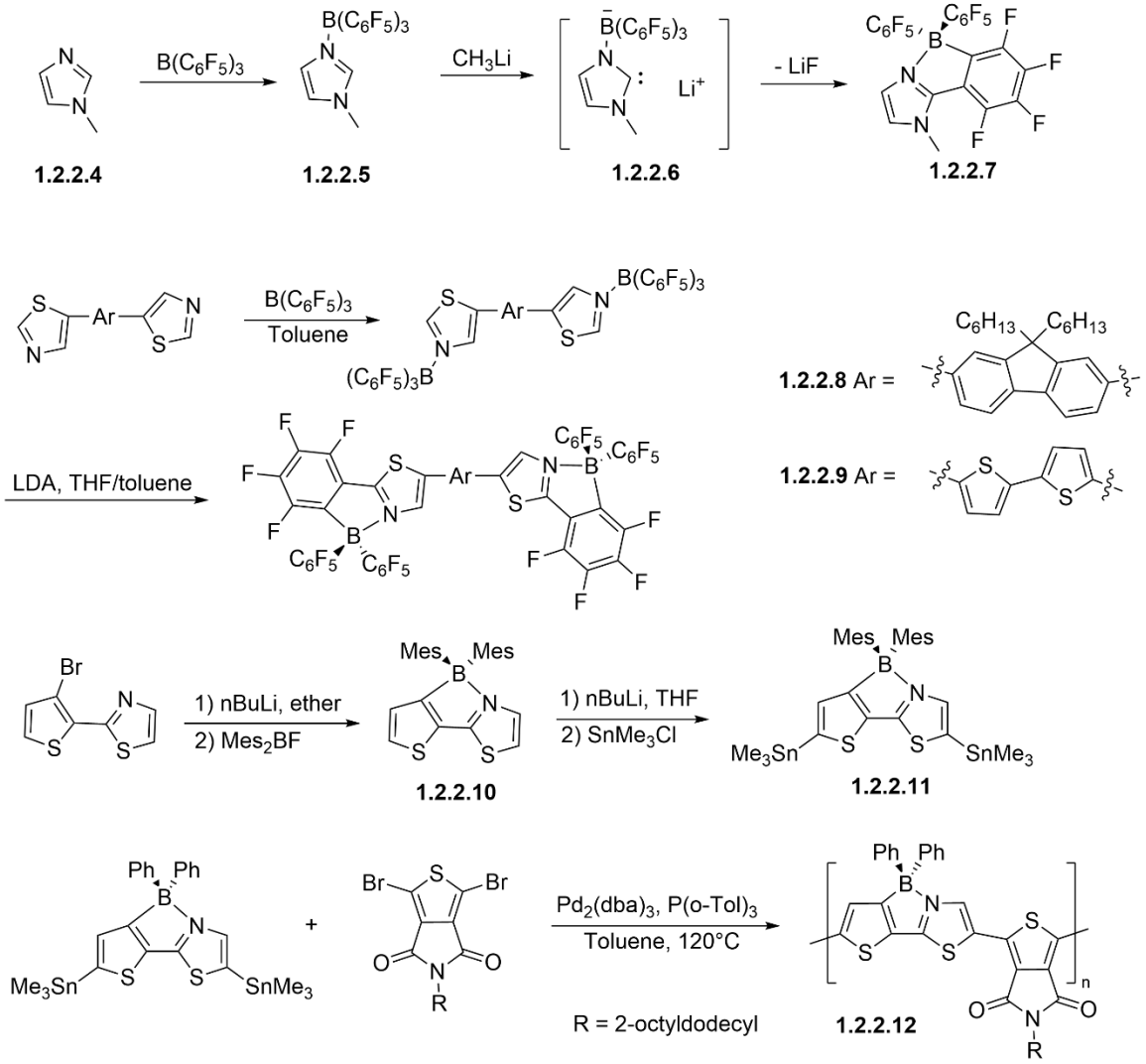

Figure 4. a) An example reaction demonstrating the synthesis of an aromatic molecule featuring B←N coordination bonds by BBr_3 and hindered base and b) a few other compounds synthesized by this method. Synthetic scheme adapted from *J. Org. Chem*. 2010, 8709–8712.

The vacant p orbital of boron atoms enables it to accommodate another lone pair of electrons to form a tetravalent center. This extra coordination bond can lock the conformation of the molecule, potentially favoring properties like faster transport of charges, phonons, excitons *etc*.[38]

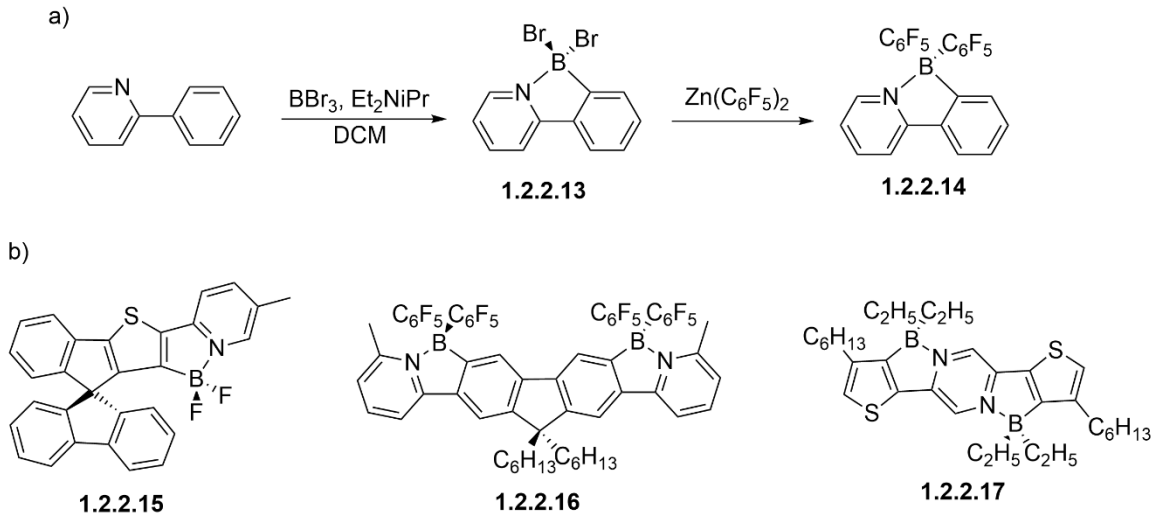

Figure 5. Synthetic schemes towards a series of compounds with coordinative B←N bonds by a mixture of BR_3 /$BR_2X$and base. Adapted from *Eur. J. Inorg. Chem*. 2002, 2015–2021, *Org. Lett*. 2010, 5470–5473, *Angew.Chem.Int.Ed*. 2006, 3170–3173, *Angew. Chem. Int. Ed*. 2015, 3648 –3652.

An early example dated back to 2002 when Erker et al. reported the synthesis of a triple ring structure with B←N coordination bond (**Figure 4**).[39] In their synthesis, imidazole moiety **1.2.2.4** reacted with $B(C_6F_5)_3$ to form the adduct **1.2.2.5**. Deprotonation on the imidazole would afford the carbene-like intermediate **1.2.2.6**, followed by a rapid

intramolecular nucleophilic substitution on one of the -C_6F_5 groups to form the final product **1.2.2.7**. Following the same protocol, Yamaguchi et al. reported the synthesis of two compounds with extended conjugation, which were found to have enhanced electron affinity due to the extra cyclization.[40] The same group modified the protocol to use $BMes_2F$ as the boron source to synthesize the building blocks **1.2.2.10** and **1.2.2.11**.[41] Based on this building block, Wang et al. synthesized a polymer containing B←N coordination bond **1.2.2.12**, and by comparing its counterpart with C—C bonds, it was elucidated that the introduction of B←N coordination bonds lowered the HOMO and LUMO, and also showed acceptor behavior when mixed with a polythiophene donor.[27]

Besides the systems mentioned above, C—B←N bonds have also been formed through direct borylation by the addition of BX_3 in the presence of hindered base. In 2010 Murakami et al. reported the synthesis of a series of compounds bearing B←N coordination[42] by using this strategy (**Figure 5**). Many other compounds with B←N coordination bonds were synthesized to show desirable coplanarity, red-shifted absorption and depressed energy levels.[43-45]

The formation of N—B←N bonds represents another important strategy to incorporate boron into π-systems. This approach gives molecular moieties resembling BODIPY, a well-known dye. This strategy typically requires an amino group that could be deprotonated and an aromatic nitrogen that provides a suitable position for chelation. $BF_3{\cdot}OEt_2$ with Et_3N is the most prevalent combination to realize the deprotonation and chelation. A number of compounds synthesized from this strategy have found wide

applications in OSCs, OLEDs, sensing *etc*.[46-48] Our group has gained much expertise in this field, and more specific introduction is provided in Chapter III.

1.3 Polycyclic Aromatic System Containing Nitrogen Atoms

Nitrogen might be one of the most prevalent heteroatoms seen in polycyclic aromatic systems, on account of the availability of synthetic methods, versatility and stability of N-containing motifs. The most common local aromatic N-containing moieties include pyrrole, pyridine, pyrimidine *etc*., which display distinct electronic properties and can be used to tune the overall property of the entire molecule.

For nitrogen embedded molecules, according to the location of the nitrogen atom, they can be classified into coronenoids,[49,50] perylenoids,[51] pyrenoids,[52,53] phenalenoids,[54] circulenoids,[55,56] or acenaphthylene[57] *etc*. To narrow down the scope of compounds presented herein, only helicenoids will be summarized considering the relevance.

Thanks to the exquisite molecular design and successful employment of diverse synthetic methods, nitrogen-incorporated mono-helicenic and multi-helicenic scaffolds have been synthesized. The varieties of nitrogen environments diversified the properties of resultant helicene compounds, such as electron-density, aromaticity, redox behavior etc. For example, the lone pair on pyridine rings does not participate in the conjugation so that it renders the system electron-deficient and enables coordination capacity. In contrast, the lone pair on pyrrole participates in the ring aromaticity. Herein, some representative nitrogen-embedded helicenoids are presented to demonstrate the impact of nitrogen on the overall properties of these molecules. In the discussion below, the nomenclature by IUPAC

is employed to refer this family of compounds as “azahelicenes”. Considering the relevance and prevalence of examples, some examples of azahelicenes with pyridine rings are presented herein.

Due to the special properties of pyridine especially as a common ligand, incorporation of pyridine rings into helicenes attracted a lot of attention and a large variety of structures have been synthesized. Among these synthetic strategies, the most common one is light induced oxidative photocyclization. The key idea of this strategy is following the formation of the stilbene connecting two oligomers via a double bond, conrotatory electrocyclization generates a primary dihydroaromatic intermediate which is oxidized to recover aromaticity.

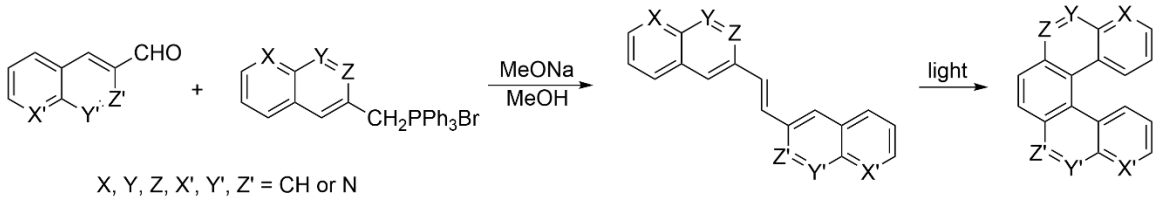

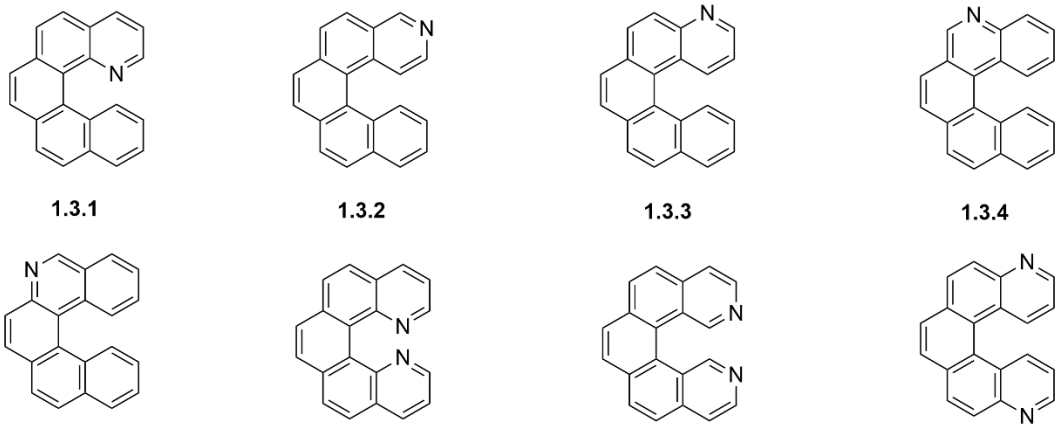

1.3.1 **1.3.2** **1.3.3** **1.3.4**

Figure 6. Synthetic scheme of aza[5]helicenes by oxidative photocyclization and some representative molecules. Adapted from *Eur. J. Org. Chem*. 2005, 1247-1257.

Caronna et al. demonstrated the successful application of this strategy in 2005 by synthesizing a series of aza[5]helicenes and diaza[5]helicenes.[58] In their synthesis, Wittig olefination was utilized to construct the double connecting two aromatic building blocks, followed by the oxidative photocyclization to annulated the ring. Some of these molecules are depicted in **Figure 6** (**1.3.1 ~ 1.3.8)**. Following the synthesis of this family of compounds, the racemization barrier parameters were examined using the Eyring plot.[59,60] It was found that the free energy barrier for racemization was around 21 kcal/mol across these molecules, equivalent to around a 40-min half-life, which implied a rapid racemization process and the requirement for storage at low temperatures.

Regarding the enantioselective separation between P/M enantiomers, HPLC with chiral stationary phase was employed as a common method. When the racemization time scale was longer than the separation, the separation between enantiomers was rendered possible after careful screening of chromatography conditions. Apart from chiral HPLC, if these molecules were able to react with another chiral guest to form a diastereomer, they could possibly be purified with column chromatography. Dehaen et al. synthesized chlorinated diaza[5]helicenes which were further subjected to Buchwald-Hartwig coupling to form the diastereomer which could be separated by column chromatography (**Figure 7**).[61] This result verified the feasibility of using non-chiral column chromatography to separate respective diastereomers.

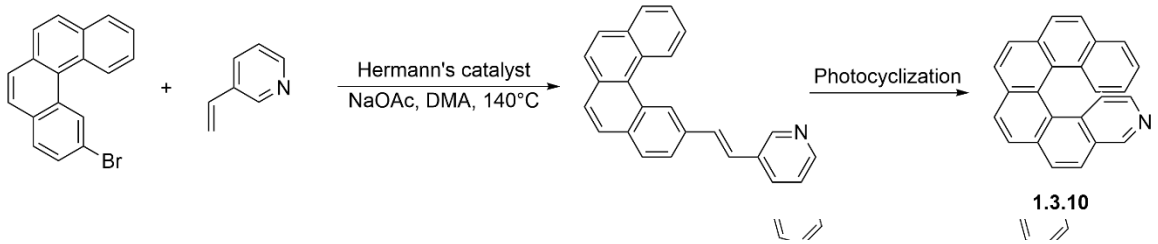

Figure 8. Synthetic scheme to aza[6]helicene by Heck reaction followed by oxidative photocyclization. Adapted from *Tetrahedron Lett.* 2008, 1455−1457.
Figure 7. Synthetic scheme of diaza[5]helicenes derivatives and their diastereomers for column chromatography separation. Adapted from *J. Org. Chem*. 2012, 10176–10183.

Having witnessed the successful synthesis of aza[5]helicenes, the efforts naturally turned towards aza[6]helicenes.[62,63] There was a slight difference in the preparation of aza[6]helicenes that in the first step stilbene derivatives were synthesized by Heck reaction instead of Wittig reaction, but the key ring formation reactions were commonly oxidative photocyclization (**Figure 8**). Following the successful synthesis of these molecules, other properties of this series of aza[6]helicenes were investigated in detail, including racemization process,[64] proton affinities,[65] chiroptical properties,[66] intersystem crossing[67], *etc*.

A noteworthy example to mention here is the successful employment of this strategy to synthesize a terpyridine ligand, in which the Lewis basicity of pyridine nitrogen atoms was exploited. Srebro-Hooper and Crassous et al. reported a bis-helicenic ligand in 2016.[68] The key synthesis(**Figure 9**) started from a Wittig reaction between a di-aldehyde

compound **1.3.11** and a phosphonium salt **1.3.12** to get intermediate **1.3.13**. Afterwards, the backbone was annulated via oxidative photocyclization to afford the final product **1.3.14**. Due to the existence of two chiral helicene motifs, the final product was obtained in the form of four enantiomers, two of them being *meso*. They can be separated by chiral

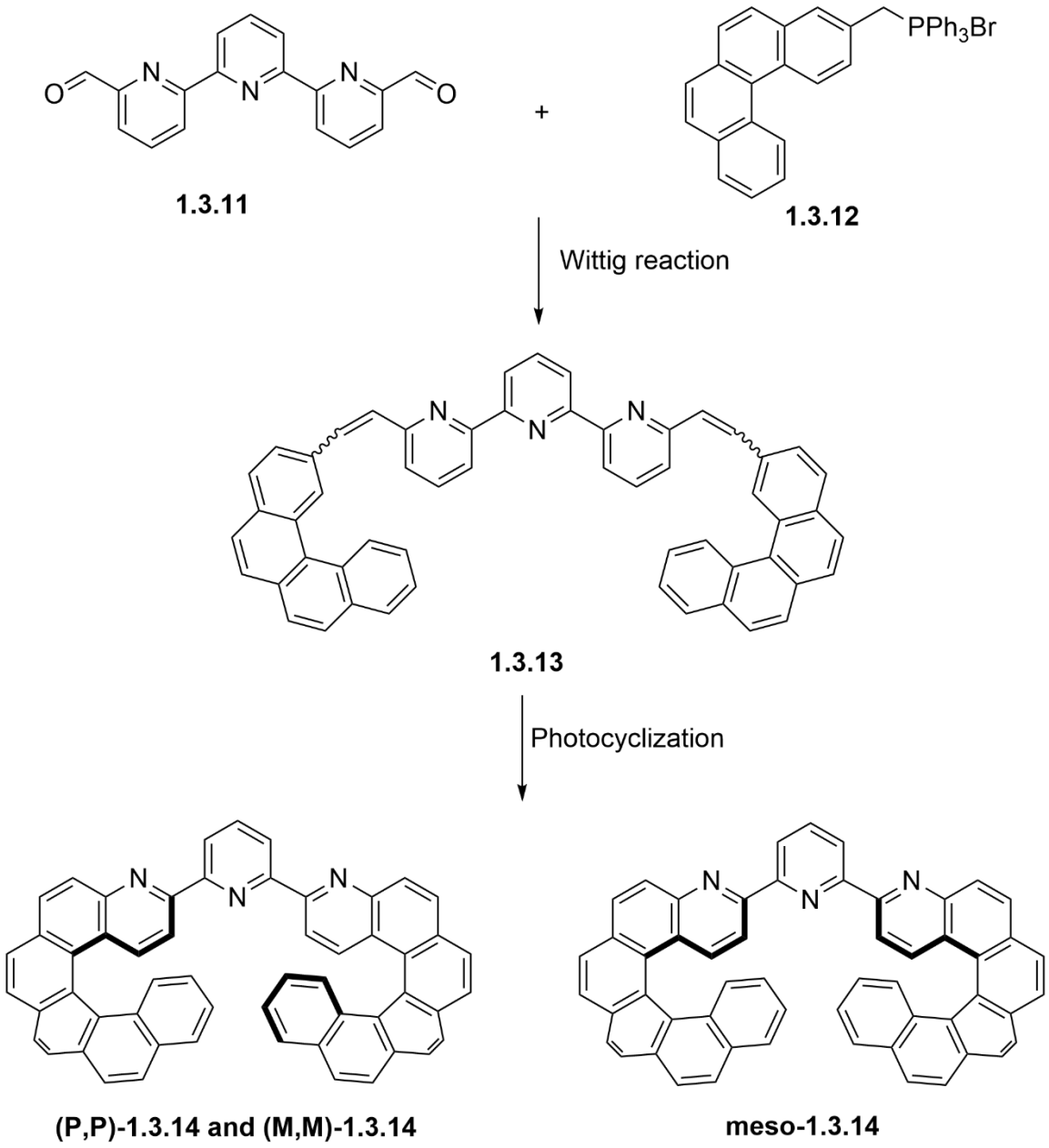

Figure 9. Synthetic scheme towards a terpyridine ligand featuring the bi-helicenic structure synthesized by photocyclization method. Adapted from *Chem. Commun*. 2016, 52, 5932−5935.

HPLC. The pure enantiomer exhibited high molar optical rotation values, agreeing with

the bi-helicenic feature of this compound. It is a special instance since the cases where the helicenes incorporated polypyridyl and served as effective ligands remained rare even up till now. In this work, it was observed that upon binding to Zn (II), the two helicenic wings had to rotate to form the *cis* terpyridine conformation, which took extra preorganization energy. This work sets ground for our future work regarding the construction of fully fused polypyridyl ligands.

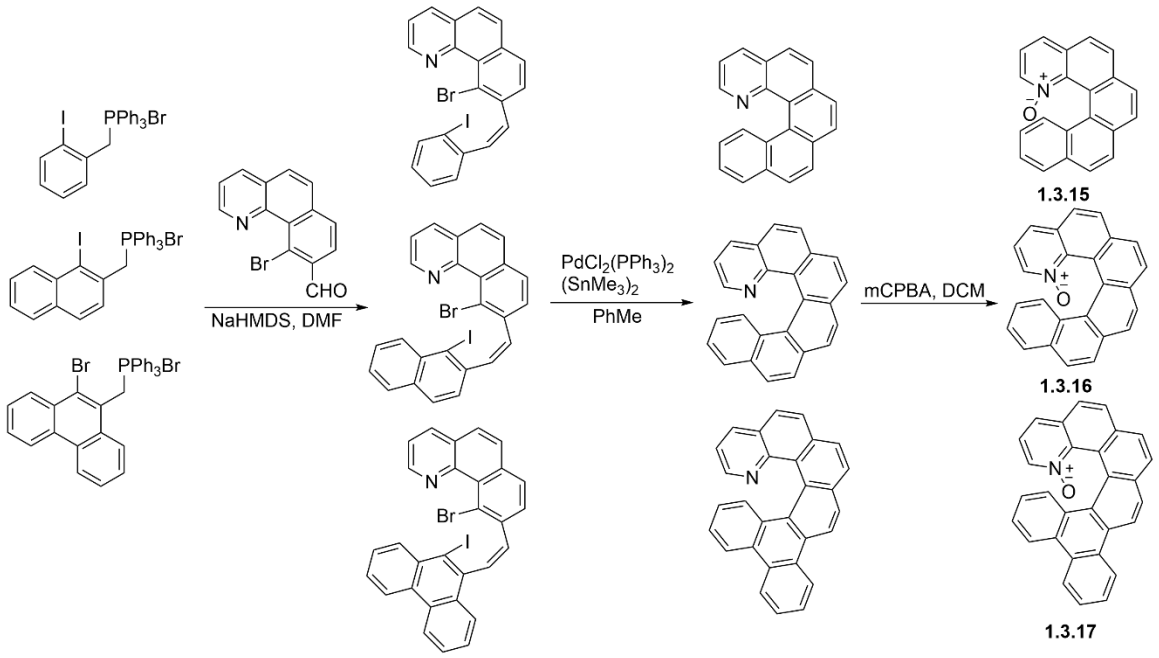

Figure 10. Synthetic scheme of three N-oxide based helical asymmetric catalysts with Stille coupling. Adapted from *Chem. - Eur. J*. 2009, 7268−7276.

Apart from the powerful photocyclization method, versatile cross coupling reactions represent another class of important methods to construct helical N-containing π-systems. Among them, tandem Stille coupling was often used to form a new C—C bond between where there was halogen before. The advantage of Stille coupling over photocyclization was that it enabled better stereoselectivity. In 2008, Takenaka reported the synthesis of three helical pyridine N-oxides **1.3.15**, **1.3.16**, **1.3.17** as novel asymmetric catalysts (**Figure 10**).[69] The first step was the *Z*-selective Wittig reaction between an aldehyde and phosphonium salt to afford the olefin intermediate, which was subsequently subjected to tandem Stille coupling to annulate the ring. Afterwards, the pyridine ring was oxidized to form the corresponding N-oxide. They also studied the asymmetric catalytic behavior of these chiral catalysts on desymmetrization of *meso* epoxides with chlorosilanes. This work suggested the desirable configurational stability of azahelicenes to promote asymmetric catalysis.

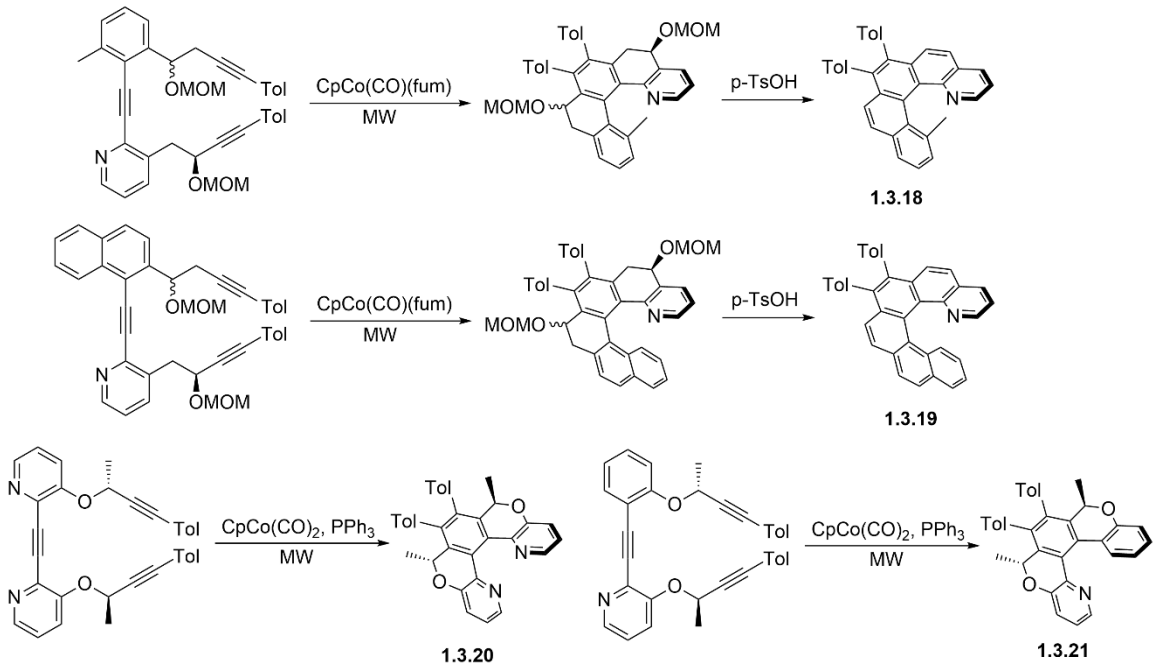

Figure 11. Synthetic scheme of metal catalyzed cyclotrimerization towards pyridinic helicenes. Adapted from *Angew. Chem., Int.* Ed. 2012, 5857−5861 and *J. Am. Chem. Soc*. 2015, 8469−8474.

Another metal-involved process to synthesize pyridinic helicenes is alkyne cyclotrimerization, typically catalyzed by cobalt. This type of reaction features triple bonds forming aromatic rings when arranged in a reasonable manner. Besides the successful application of this strategy towards some of the compounds aza[5]helicenes and aza[6]helicenes mentioned above, more delicate structures were achieved through this strategy by Stary's and Stara's group.[70-72] A significant advance made there was the stereoselective synthesis of these helicenes by introducing chiral induction groups (**Figure 11**), so that the subsequent separation of enantiomers/diastereomers was avoided.

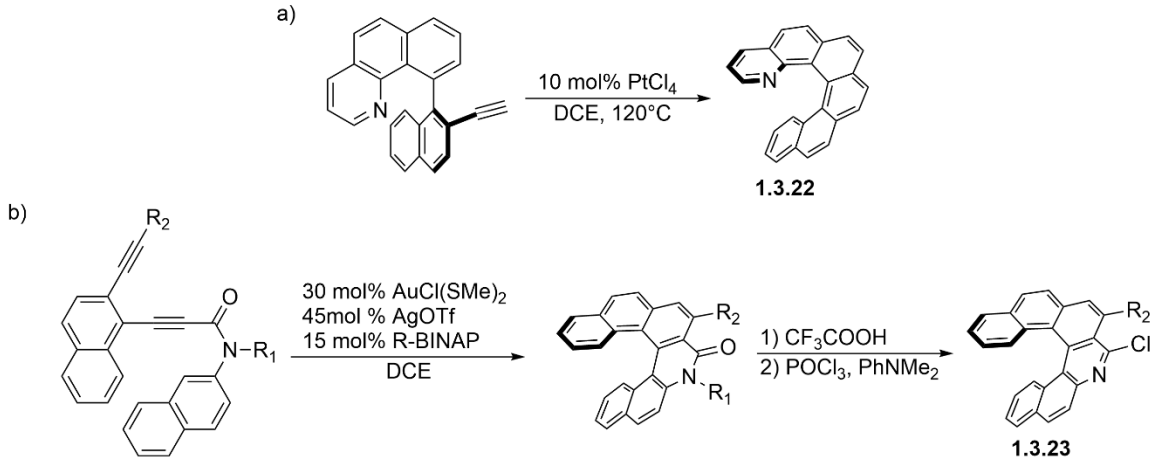

Figure 12. Synthetic schemes towards pyridinic helicenes with a) alkyne-arene cycloisomerization and b) intramolecular hydroarylation. Adapted from *Org. Lett.* 2013, 1706−1709 and *J. Am. Chem. Soc*. 2014, 5555−5558.

Apart from these strategies, some other examples included alkyne-arene cycloisomerization,[73] intramolecular hydroarylation,[74,75] *etc*. (**Figure 12**). Although they were not so common as the ones mentioned above, they also enriched the toolbox to synthesize pyridinic helicenoids.

1.4 Challenges and Motivations

As mentioned earlier in this chapter, the incorporation of heteroatoms into polycyclic aromatic systems is a thriving research topic. The vast varieties of heteroatoms and their respective functionalization open endless possibilities of possible structures to

synthesize. The requirement for establishment of structure-property correlation, practical applications including light harvesting, charge transport, energy conversion, *etc*., and even aesthetic appeal is calling for the rational design, synthesis and investigation of sophisticated model molecules.

There are thousands of such molecules, conservatively speaking, that have been investigated and published, featuring different backbone, heteroatom identities and incorporation pattern. It can be seen that two of the major advantages of heteroatom incorporation are the extra bandgap tunability and the functionalization they bring about to the molecules. Based on this argument, I focus my attention on two kinds of π-systems: B←N coordinative bond incorporated systems and pyridinic helicene systems. First, for the molecules with B←N coordinative bonds, despite some success in the design of novel compounds and some respective preliminary device data, it still has a long way to go before it can be put into practical production to compete with the contemporary silicon-based semiconductors. There are many challenges to overcome, including synthetic scalability, suboptimal fabrication conditions, instability of organic semiconductors,[76] *etc*. To better modulate the energy level of such molecules, I performed research on two aspects. First, the range of delocalization was expanded by connecting different π-fused molecules together and locking their conformation to maximize the conjugation. Second, to better understand the structure-property relationship, aryl groups were coupled with different electron densities to the indolocarbazole core that our group had already investigated[77] and explore their properties. By doing this, a deeper insight of molecular design principles towards optimal device performances was expected.

Regarding the pyridinic helicenes, there are many important hypotheses and intriguing possibilities unexplored yet. First, despite the plenty of synthetic strategies mentioned above, they usually result in helicenes with limited number of nitrogen atoms compared to the number of rings. Second, the distribution of nitrogen is usually scattered, and there are only very few cases where the nitrogen atoms are arranged to form polypyridine ligands. The contemporary research is either focused on helicenes with one or two nitrogen atoms, or the backbone is not fully fused so that it takes extra preorganization energy to orient nitrogen atoms. To address this concern, I devised a series of molecules where there were multiple nitrogen atoms where each pair of adjacent nitrogen atoms was arranged in a phenanthroline manner with a fused backbone. It was expected that this design would lead to a powerful ligand to host metal ions, since the entropy penalty to bind metal ions should be reduced.

CHAPTER II

ELECTRON-DEFICIENT POLYCYCLIC Π-SYSTEM FUSED WITH MULTIPLE B←N COORDINATE BONDS*

2.1 Introduction

Polycyclic π-systems are ubiquitous in organic molecules that are essential for a wide range of applications including organic electronics, bioimaging, and pharmaceutics.[78-81] In these molecules, the fused-ring constitution of the backbone promotes extensive π-conjugation, enhances the backbone rigidity, and reduces conformation disorder.[38] As a result, polycyclic aromatic molecules typically exhibit narrow optical bandgaps, strong intermolecular π-π interactions, and excellent chemical stability.[81]

The synthesis of polycyclic aromatic molecules can be accomplished through either (i) stepwise cross-coupling of smaller molecular building blocks, followed by ring annulation, or (ii) one-step annulative π-extension.[78,79] The first method, in which an efficient ring-fusing annulation takes place after the assembly of all structural components, is highly versatile and allows for the construction of polycyclic systems with a wide scope of structural diversity. Most known polycyclic aromatic molecules, such as oligoacenes,[82,83] thienoacenes,[84] quinacridones,[85] nanographenes,[86-89] and carbon

* Reprinted with permission from "Electron- Deficient Polycyclic π-System Fused with Multiple B←N Coordinate Bonds" Yirui Cao, Congzhi Zhu*, Maciej Barłóg, Kayla P. Barker, Xiaozhou Ji, Alexander J. Kalin, Mohammed Al-Hashimi*, and Lei Fang*. *J. Org. Chem.*, **2021**, *86*, 3, 2100–2106. Copyright 2021 American Chemical Society.

nanobelts,[90,91] are electron-rich or exhibit p-type semiconducting properties. However, it remains challenging to render electron-deficient characteristics to polycyclic aromatic molecules, while electron-deficient polycyclic molecules hold great promise as *n*-type semiconductors in organic electronics and non-fullerene electron acceptors in organic photovoltaics.[76,92-96] The synthetic challenges include (1) the low reactivity of electron-deficient aromatic units in commonly employed ring-annulation reactions, such as electrophilic aromatic substitution or oxidative C−C coupling, and (2) the limited synthetic methods to precisely functionalize polycyclic aromatic molecules with electron-withdrawing substituents.[97,98] To date, examples of electron-deficient polycyclic arenes are mostly limited to those containing azacene units,[99] or those with pendant electron-withdrawing groups such as imide or cyanide groups.[80,93,95-97,100] Efficient synthetic methodologies and molecular design principles beyond these classes of compounds are desired in order to broaden the structural scope of *n*-type fused-ring π-systems.

Replacing C−C bonds in polycyclic aromatic hydrocarbons with isoelectronic B←N coordinate bonds represents a powerful strategy to modulate their electronic structures, optical properties, and reactivities.[31,77,101-109] It typically decreases the energy level of the lowest unoccupied molecular orbital (LUMO), while imposing a smaller impact on the highest occupied molecular orbital (HOMO).[103,110,111] This in turn facilitates intermolecular electron transfer[112] and narrows the optical band gaps of aromatic molecules.[102,103,110] The strength of a B←N coordinate bond can be as high as 30 kcal/mol.[113] Therefore, it can serve as a strong conformational lock to maintain the structural rigidity and desirable molecular conformation, such as a coplanar conformation

that is favorable for π-delocalization.[41,110,113] A number of representative B←N bond-containing conjugated compounds demonstrated high electron mobilities and, therefore, emerged as a novel class of *n*-type organic electronic materials.[107,114] Despite recent advances in this field,[77,101,104,108,110,111] it is still challenging to construct extensive polycyclic π-systems fully fused with B← N coordinate bonds, and to achieve deep LUMO levels (below −3.8 eV) in these systems without introducing pendant electron-withdrawing groups.[28,115,116] Herein, we report a 23-ringfused polycyclic π-system constructed by simultaneously incorporating four B←N bonds. This extensive π-system features high molecular rigidity, π-delocalization, and electron-deficient characteristic.

2.2 Results and Discussion

In order to construct an extended polycyclic π-system containing multiple B←N coordinate bonds, it is challenging, but crucial, to develop a ring-annulation reaction that can take place at each desirable reaction site with high efficiency. In this context, the target molecule **BN-1** (**Figure 13**) was designed to feature boron dipyrromethene (BODIPY)-like units, in which a boron center is covalently bound to one nitrogen atom (originating from an acidic N−H group) and datively coordinated to another Lewis basic nitrogen atom. To construct these BODIPY-like units in an efficient manner, indolo[3,2-b]carbazole was selected as a ditopic N−H donor,[117] instead of aniline analogues that are usually employed in previously reported systems.[27,116] In this case, the stronger acidity of the N−H functionalities in indolo[3,2-b]carbazole[118] will better facilitate the formation of covalent B−N bonds in the ring-annulation reaction performed under basic conditions. Moreover,

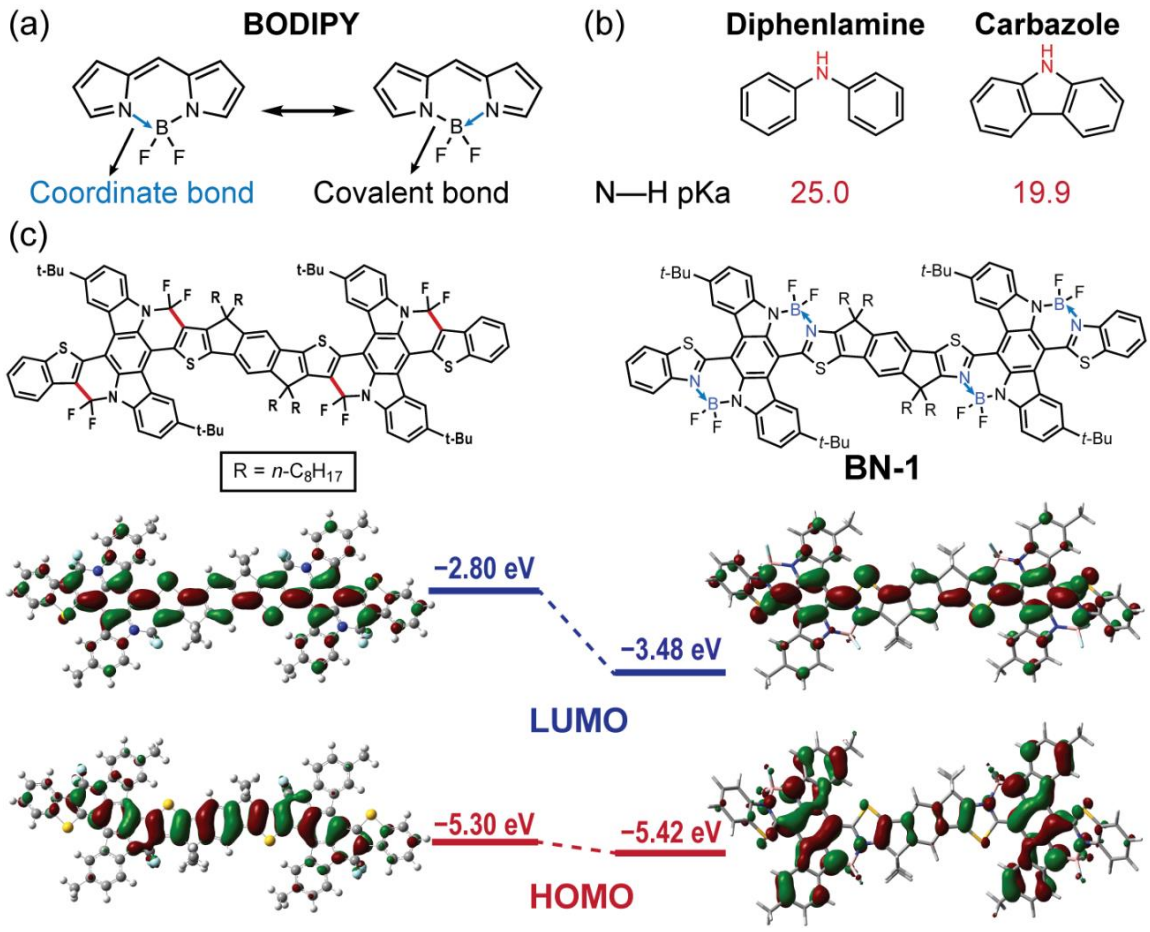

Figure 13. Structural formulas, DFT calculated diagrams, and energy levels of frontier orbitals of BN-1 featuring multiple B←N coordinate bonds and its structural analogue fused by C−C bonds [B3LYP/6- 311G(d,p), isovalue = 0.02].

these N−H functionalities are fused with the backbone and thus preorganized to provide the anchoring point for multiple boron centers. Centrosymmetric indaceno[2,1-d:6,5-d′]dithiazole was selected as the ditopic building block to form the B←N coordinate bonds. The two Lewis basic nitrogen atoms are far away from one another, so that the mutual deactivation on their Lewis basicity is avoided to ensure full installation of all B←N

coordinate bonds. The indaceno[2,1-d:6,5-d′]dithiazole unit also carries four octyl chains to promote the solubility of the final product (**Figure 13**).[119] Initial density functional theory (DFT) computation revealed that, in comparison with its structural analogue in which the B←N coordinate bonds are replaced by C−C bonds (**Figure 13**), the LUMO energy level of **BN-1** was 0.68 eV lower, confirming its electron-deficient characteristics. The orbital diagram showed an extended quinoidal LUMO (**Figure 13**) and an extended HOMO on the backbone of **BN-1**, facilitated by the nearly coplanar conformation.

The synthesis toward **BN-1** started with a Stille coupling reaction between the dibromo-indolo[3,2-b]carbazole derivative **1** and 2-(tri-n-butylstannyl)benzo[d]thiazole (**Figure 14a**) to afford a mono-coupled intermediate **2**. The remaining bromide group on **2** was transformed into a pinacol boronic ester group through Miyaura borylation to give intermediate **3**. Compound **3** was subsequently subjected to Suzuki coupling with the dibrominated indaceno[2,1-d:6,5-d′]bisthiazole derivative to afford the alternating donor-acceptor-type precursor **4**, which features four acidic N−H functional groups and four Lewis basic thiazole units ready for the borylative annulation to form four BODIPY-like units. Borylation of 4 with $BF_3{\cdot}OEt_2$ and N,N-diisopropylethylamine was performed at 130 °C to give **BN-1** with a remarkable isolated yield of 94%. Compared to previously reported syntheses of polycyclic molecules with multiple B←N coordinate bonds,[107,108,120] the borylation reaction developed here exhibits a much higher conversion owing to the dedicated molecular design principles. The diagnostic disappearance of the N−H resonance signals in the range from 9.5 to 10 ppm suggested a nearly quantitative conversion in this step (**Figure 14b**). In this reaction, one-pot formation of four B−N covalent bonds and four

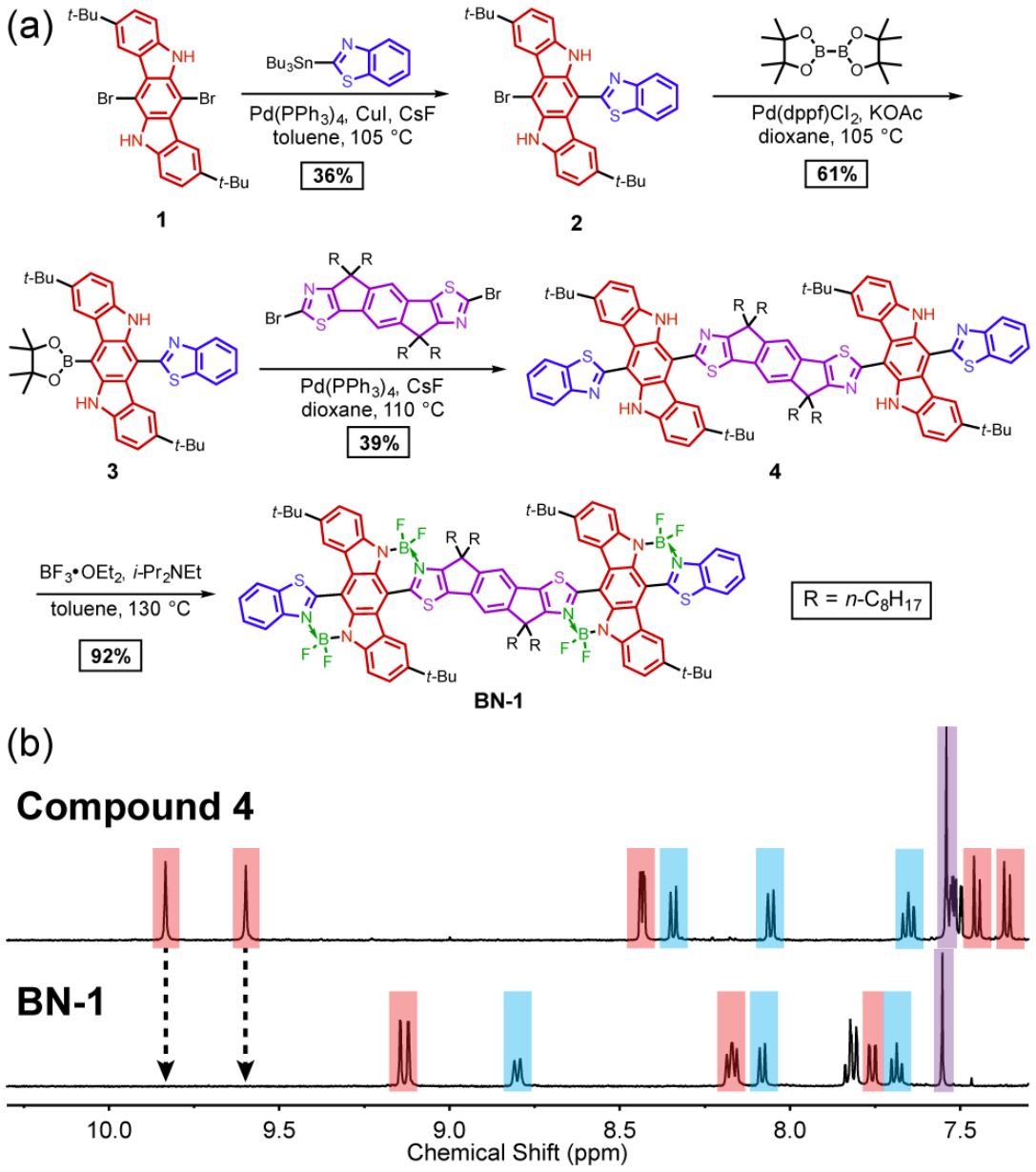

Figure 14. (a) Synthesis of BN-1, (b) Comparison of the characteristic ^{1}H NMR (500 MHz) resonance signals of 4 and BN-1 in $CDCl_3$ at room temperature. The resonance signals from indolo[3,2-*b*]carbazole units are colored in red, those from benzo[d]thiazole units in blue, and the singlet from the central indaceno[2,1-*d*:6,5-*d'*]dithiazole unit in purple.

B←N coordinate bonds took place in each molecule. Despite its rigid structure and

extended fused-ring architecture, **BN-1** exhibited an excellent solubility in organic solvents such as chloroform and chlorobenzene.

To better understand the molecular conformation and the nature of the B←N coordinate bonds in **BN-1**, a smaller, yet similar, π-system **BN-2** was synthesized as a model for structural elucidation. The synthesis of **BN-2** was accomplished through an approach similar to that of **BN-1** (**Figure 15a**). It is noteworthy that the annulation reaction took place at room temperature and afforded **BN-2** in a yield of 94%. Single crystals of **BN-2** suitable for X-ray diffraction structural determination were grown by vapor diffusing pentane into a diluted dichloromethane solution of **BN-2**. In the solid state, **BN-2** showed a rigid and nearly coplanar backbone with a dihedral angle of 9.9° between the indolo[3,2-b]carbazole unit and the thiazole units (**Figure 15b**). The conformation twist, although small, was attributed to the steric repulsion between thiazole and indolo[3,2-b]carbazole, as evidenced by the short distance (2.460 Å) between the sulfur and the closest hydrogen on the indolo[3,2-b]carbazole unit. The bond length of the B←N coordinate bond is 1.564(12) Å, only slightly longer than the B−N covalent bond [1.510(12) Å] (**Figure 15b**). The formation of such a short B←N coordinate bond was attributed to the resonance effect observed in BODIPY units,[121] which ensures strong B←N coordination and good chemical stability of such compounds. Given the structural similarity between **BN-2** and **BN-1**, it is believed that **BN-1** also adopts a nearly coplanar conformation with a small dihedral angle around 10° between the building blocks.

To evaluate the bond strength of the intramolecular B←N coordinate bonds, the torsional energy landscape of **BN-2** was examined by DFT calculation. The molecular

potential energy in the gas phase was computed while the dihedral angle between the central indolo[3,2-b]carbazole unit and one of the thiazole units was varied (**Figure 15c**) from 0° to ±180°. As the dihedral angle deviated from 10°, the potential energy increased, leading to a deep energy well of 30.3 kcal/mol. This value is comparable to the reported complexation enthalpy values between organic bases and BF_3,[122] suggesting a strong coordination between the boron and nitrogen centers, which is sufficient to maintain the extended π-system in a stable rigid conformation.

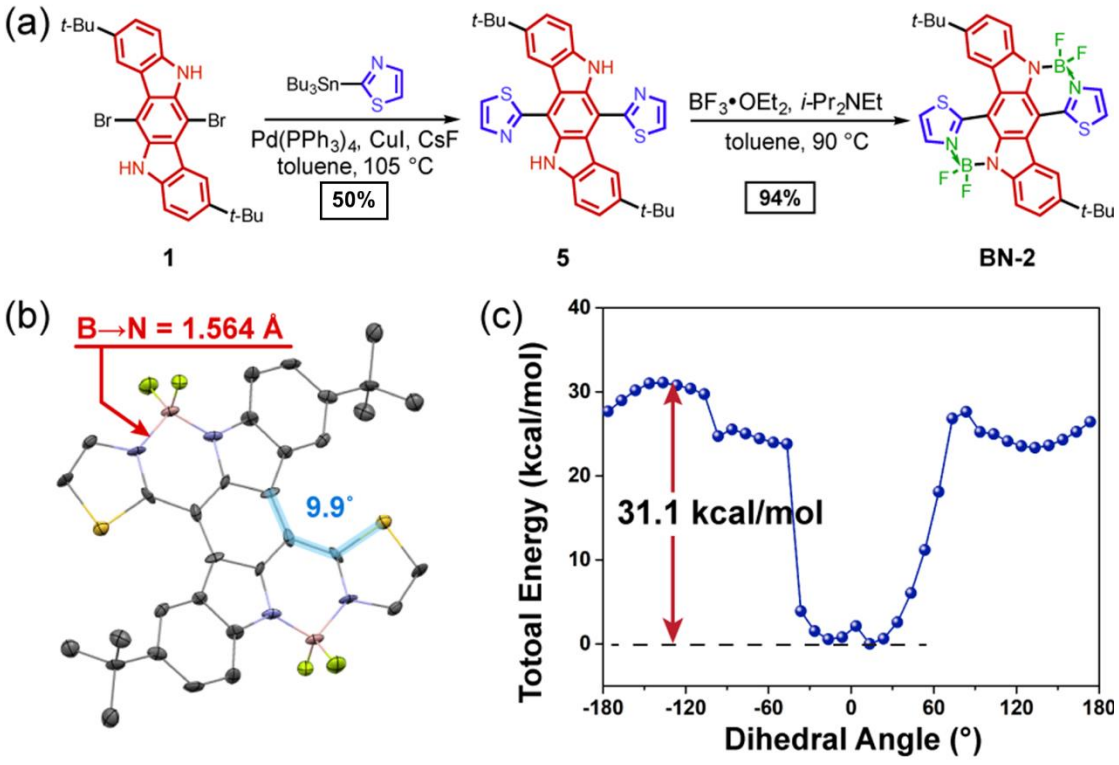

Figure 15. (a) Synthesis of BN-2. (b) The single-crystal structure of BN-2. (c) The potential energy surface scan of BN-2 by changing the dihedral angle between indolo[3,2-b]carbazole and one of the flanking thiazoles (highlighted in cyan color in (b)).

It was anticipated that the introduction of multiple B←N coordinate bonds can significantly impact the optical properties of conjugated molecules. The photo-absorption onset of precursor **4** is around 590 nm with a λ_{max} of 494 nm. Its fluorescence spectrum exhibits an emission band at 583 nm. In comparison, upon introducing the B←N coordinate bonds, **BN-1** exhibited a red-shifted, intensive absorption band spanning from 600 to 800 nm (λ_{max} = 700 nm) in $CHCl_3$ solution, corresponding to the narrowed band gap of the HOMO to LUMO transition (**Figures 16a** and **27**). The fluorescence emission band of **BN-1** in $CHCl_3$ was found to be centered at 723 nm, which was also red-shifted compared to that of **4**. It is also worthy to note that the Stokes shift of **BN-1** was much smaller than that of **4**, indicating the less significant vibrational energy loss in its excited state due to the rigid structure of **BN-1** (**Figure 16a**). Compared to **BN-1**, the absorption spectrum and fluorescence emission spectrum of **BN-2** were blue-shifted, on account of its smaller size of π-conjugation. The quantum yields of **BN-1** and **BN-2** in chloroform were estimated to be 6.6% and 12.9%, respectively, using zinc phthalocyanine as a standard. The absorption spectrum of **BN-1** was also measured in the thin film state, thanks to its good solubility and film-forming ability. The solid-state spectrum was similar to that in solution, suggesting that no significant intermolecular aggregation or conformational changes took place from the solution phase to the solid state for **BN-1**, further corroborating its rigid backbone. Grazing incidence wide angle X-ray diffraction of the thin film showed ring-like diffraction patterns, revealing the semi-crystalline character of **BN-1** (**Figure 28**), suggesting the weak π-π interactions between these molecules in the thin film.

The solvatochromism of **BN-1** and **BN-2** was examined in a series of organic solvents. Unlike many reported BODIPY dyes whose absorption maxima were insensitive to solvent polarity changes or show slight shifts of only 2−10 nm,[123,124] significant solvatochromsim was observed for **BN-1** and **BN-2** (**Figures 33** and **34**). For both compounds, it was observed that, as the solvent polarity increased, the absorption and emission spectra underwent blue shifts. For instance, the λ_{max} of the absorption of **BN-2** was shifted from 645 to 611 nm when the solvent was changed from toluene to dimethylformamide. Such a significant solvatochromism revealed the strong solvation effect on the ground state of **BN-1** and **BN-2** in polar solvents, as a result of the intramolecular charge transfer character in these rigid conjugated molecules.

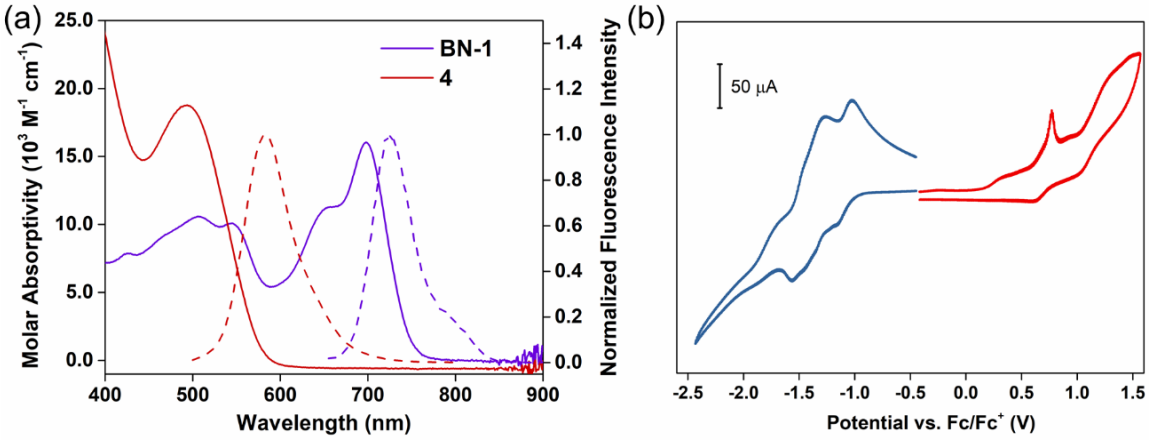

Figure 16. (a) UV−vis−NIR absorption spectra (solid lines) fluorescence emission spectra (dashed lines) of BN-1 and 4 in a diluted CHCl3 solution. (b) Cyclic voltammogram of a BN-1 thin film.

The introduction of intramolecular B←N coordinate bonds was expected to increase the electron affinity of conjugated molecules. Cyclic voltammetry was performed on a thin film of **BN-1**, which was drop-casted on the surface of a glassy carbon electrode. **BN-1** underwent two semi-reversible reduction processes in the range from −1.6 to −1.0 V vs the ferrocene/ferrocenium redox couple (**Figure 16b**). Multiple redox processes were also observed on differential pulse voltammetry (**Figure 31**). The reduction peak of **BN-1** shifted cathodically for 0.46 V compared to that of compound 4 (**Figure 29**). The LUMO energy level of **BN-1** was determined to be −3.82 eV, much lower than that of **4** (−3.36 eV in **Table 2**), and close to those of high-performance *n*-type organic semiconductors[27,76,94] and non-fullerene acceptors in organic photovoltaics.[92,93]

2.3 Conclusion

In conclusion, we established the molecular design and synthesis of an extensive electron-deficient polycyclic π-system featuring multiple B←N coordinate bonds. A 23-ring-fused molecule was constructed via a highly efficient borylation reaction, in which four B−N covalent bonds and four B←N coordinate bonds were formed in one pot. The high efficiency in simultaneously fusing multiple rings promises its utility in future synthesis of B←N bridged ladder polymers. These B←N coordinate bonds not only rigidified the backbone and promoted a near-coplanar conformation but also decreased the LUMO energy level to −3.82 eV and led to the intensive absorption in the near-infrared region. This work unveiled that the introduction of multiple B←N coordinate bonds serves dual purposes of (i) fusing the π-system into a rigid polycyclic constitution and (ii)

imparting *n*-type characters for the development of new organic molecules and macromolecules for electronic and photovoltaic applications.

2.4 Experimental Section

2.4.1 General Methods and Materials

Starting materials and reagents were purchased from commercial sources and were used as received without further purification. THF was dried and distilled under nitrogen from sodium using benzophenone as the indicator. Toluene was dried using an inert pure solvent system and used without further treatment. An oil bath was used for those reactions that required heating. 6,12-Dibromo-2,8-di-tert-butyl-5,11-dihydroindolo[3,2-b]-carbazole (**1**) and 2,7-bis(triisopropylsilyl)-s-indaceno[2,1-d:6,5-d′]- bis(thiazole)-4,9-dione were prepared according to reported procedures.[77,125] ^{1}H and ^{13}C NMR spectra were recorded on a 500 MHz or 400 MHz spectrometer. The ^{1}H and ^{13}C{^{1}H} NMR chemical shifts were reported in ppm relative to the signals corresponding to the residual non-deuterated solvents ($CDCl_3$: ^{1}H 7.26 ppm, ^{13}C 77.23 ppm) or the internal standard (tetramethylsilane: ^{1}H 0.00 ppm). The ^{19}F NMR chemical shifts were reported in ppm relative to the signal corresponding to $BF_3{\cdot}OEt_2$ (−153.0 ppm) as the external standard. Abbreviations for reported signal multiplicities are as follows: s, singlet; d, doublet; t, triplet; q, quartet; m, multiplet; br, broad. The broad singlet at ∼1.55 ppm on ^{1}H NMR spectra represents the resonance signal of H_2O in $CDCl_3$. High-resolution mass spectra were obtained via electrospray ionization (ESI), atmospheric pressure chemical ionization (APCI) with a hybrid quadrupole-orbitrap analyzer, or matrix-assisted laser desorption

ionization (MALDI) mode with a time-of-flight analyzer. Column chromatography was carried out on a normal phase SiO_2. Preparative size exclusive chromatography (SEC) purifications were performed at room temperature using chloroform as the eluent at a flow rate of 14 mL/min. UV−vis absorption spectra were recorded in a 1.0 cm pathlength cuvette, and the neat solvent was used as baseline. Fluorescence emission spectra were recorded in a 1.0 cm path-length cuvette. Cyclic voltammetry was carried out in nitrogen-purged acetonitrile at room temperature. Tetra-n-butylammonium hexafluorophosphate (0.1 M) was used as the supporting electrolyte. The conventional three-electrode configuration consists of an ITO working electrode, a platinum wire auxiliary electrode, and a Ag/AgCl electrode with ferrocenium/ferrocene as the standard. Cyclic voltammograms were obtained at a scan rate of 200 mV/s. The absorption spectra of **4** and **BN-1** were recorded at room temperature at concentrations of 2.2×10^{-5} M and 2.1×10^{-5} M, respectively. The emission spectra of **4** and **BN-1** were recorded at room temperature at concentrations of 2.2×10^{-6} M and 2.1×10^{-5} M, respectively. The excitation wavelengths for **4** and **BN-1** were set at 620 and 650 nm, respectively.

2.4.2 Synthesis

2-(12-Bromo-2,8-di-tert-butyl-5,11-dihydroindolo[3,2-b]-carbazol-6-yl)benzo[d]thiazole (2). 1 (690 mg, 1.31 mmol) and tri-n-butylstannylbenzothiazole (680 mg, 2.28 mmol) were suspended in toluene (13 mL). The suspension was degassed by three cycles of freeze-pump-thaw before $Pd(PPh_3)_4$ (151 mg, 0.13 mmol), CuI (12.5 mg, 0.066 mmol), and CsF (996 mg, 6.55 mmol) were added under N_2. The reaction mixture was

stirred at 105 °C for 36 h. After cooling to room temperature, the mixture was extracted with CH_2Cl_2 and washed with 1 M HCl once, brine twice, water once, and dried with $MgSO_4$. Volatile solvents were removed under reduced pressure. The crude product was purified through column chromatography (SiO_2, hexane/CH_2Cl_2 1:1 to 1:9) to give **2** as an orange solid (96.2 mg, 36%). ^{1}H NMR (400 MHz, $CDCl_3$) δ = 9.69 (s, 1H), 8.84 (d, *J* = 1.6 Hz, 1H), 8.38 (d, *J* = 1.6 Hz, 1H), 8.36 (s, 1H), 8.29 (d, *J* = 7.6 Hz, 1H), 8.03 (d, *J* = 7.6 Hz, 1H), 7.63 (m, 1H), 7.53 (m, 3H), 7.45 (d, *J* = 8.0 Hz, 1H), 7.36 (d, *J* = 8.0 Hz, 1H), 1.51 (s, 9H), 1.32 (s, 9H). ^{13}C{^{1}H} NMR (100 MHz, $CDCl_3$) δ = 164.5, 153.6, 142.5, 142.2, 139.2, 139.0, 136.1, 135.6, 134.9, 126.7, 125.8, 125.2, 125.1, 123.5, 122.6, 122.6, 121.8, 121.8, 120.6, 120.3, 118.7, 110.6, 110.4, 108.6, 100.7, 35.0, 32.2, 32.1. APCI-MS: m/z [M + H]$^+$ Calcd for $C_{33}H_{31}N_3SBr$ 580.1417; Found 580.1400.

2-(2,8-Di-tert-butyl-12-(4,4,5,5-tetramethyl-1,3,2-dioxaborolan-2-yl)-5,11-dihydroindolo[3,2-b]carbazol-6-yl)benzo[d]- thiazole (3). **2** (106 mg, 0.18 mmol), bis(pinacolato)diboron (91 mg, 0.36 mmol), and KOAc (35 mg, 0.36 mmol) were suspended in dioxane (3 mL). The suspension was degassed by three cycles of freeze-pump-thaw before Pd(dppf)Cl_2 (13 mg, 0.018 mmol) was added under N_2. The reaction mixture was stirred at 105 °C for 36 h. After cooling to room temperature, the mixture was extracted with CH_2Cl_2 and washed with 1 M HCl once, brine twice, water once, and dried with $MgSO_4$. Volatile solvents were removed under reduced pressure. The product was purified through preparative size exclusion chromatography to give compound **3** as an orange solid (69 mg, 61%). ^{1}H NMR (400 MHz, $CDCl_3$) δ = 9.95 (s, 1H), 9.50 (s, 1H), 9.04 (d, *J* = 2.0 Hz, 1H), 8.33 (d, *J* = 8.4 Hz, 1H), 8.28 (d, *J* = 2.0 Hz, 1H), 8.04 (d, *J* = 7.6

Hz, 1H), 7.64 (m, 1H), 7.53−7.50 (m, 3H), 7.48 (d, *J* = 8.4 Hz, 1H), 7.37 (d, *J* = 8.4 Hz, 1H), 1.61 (s, 12H), 1.50 (s, 9H), 1.29 (s, 9H). $^{13}C\{^{1}H\}$ NMR (100 MHz, $CDCl_3$) δ = 165.2, 153.7, 143.9, 141.8, 141.0, 139.6, 135.9, 134.9, 128.6, 126.6, 125.8, 124.5, 123.9, 123.6, 121.8, 121.8, 121.0, 119.8, 119.3, 112.5, 110.1, 109.9, 84.4, 35.2, 34.9, 32.5, 32.1, 25.6. APCI-MS: m/z $[M + H]^+$ Calcd for $C_{39}H_{43}BN_3O_2S$ 628.3164; Found 628.3150.

Compound 4. 3 (75.0 mg, 0.12 mmol) and 2,7-dibromo-4,4,9,9- tetraoctyl-4,9-dihydro-s-indaceno[2,1-d:6,5-d′]bis(thiazole) (26.0 mg, 0.03 mmol) were suspended in anhydrous dioxane (2.0 mL) at room temperature. The suspension was degassed by three cycles of freeze-pump-thaw before $Pd(PPh_3)_4$ (3.5 mg, 0.003 mmol) and CsF (45.6 mg, 0.3 mmol) were added under N_2. The reaction mixture was stirred at 110 °C for 48 h. After cooling to room temperature, the mixture was extracted with CH_2Cl_2 and washed with 1 M HCl once, brine twice, water once, and dried with $MgSO_4$. Volatile solvents were removed under reduced pressure. After purification through column chromatography (SiO_2, hexane/CH_2Cl_2 1:1 to 1:9), all the red-colored solution that showed orange-colored fluorescence under a 365 nm UV lamp was collected. Volatile solvents were removed under reduced pressure to yield the crude product. The product was further purified through preparative size exclusion chromatography to give compound **4** as a red solid (20.0 mg, 39%). ^{1}H NMR (500 MHz, $CDCl_3$) δ = 9.86 (s, 2H), 9.62 (s, 2H), 8.46 (d, *J* = 2.0 Hz, 2H), 8.45 (d, *J* = 2.0 Hz, 2H), 8.37 (m, 2H), 8.08 (m, 2H), 7.67 (td, *J* = 8.0, 1.5 Hz, 2H), 7.57−7.52 (m, 6H), 7.56 (s, 2H), 7.47 (d, *J* = 8.5 Hz, 2H), 7.38 (d, *J* = 8.5 Hz, 2H), 2.45 (m, 4H), 2.18 (m, 4H), 1.36 (s, 18H), 1.33 (s, 18H), 1.25−1.15 (m, 48H), 0.80 (t, *J* = 7.0 Hz, 12H). $^{13}C\{^{1}H\}$ NMR (100 MHz, $CDCl_3$) δ = 170.7, 164.9, 153.6, 152.7, 141.8, 141.7,

139.5, 139.5, 136.3, 136.0, 135.9, 135.7, 134.7, 126.7, 125.8, 125.0, 124.9, 123.6, 121.9, 120.9, 120.6, 120.2, 119.7, 115.3, 113.0, 111.0, 110.8, 110.6, 53.6, 38.5, 35.0, 32.1, 32.0, 31.8, 30.4, 29.8, 29.6, 28.1, 27.3, 24.8, 22.8, 14.3. ESI-MS: m/z $[M + H]^+$ Calcd for $C_{112}H_{131}N_8S_4$ 1719.9413; Found 1719.9439.

BN-1. In a N_2-filled glovebox, **4** (20.0 mg, 0.012 mmol), anhydrous toluene (1.0 mL), diisopropylethylamine (0.1 mL), and $BF_3{\cdot}OEt_2$ (0.2 mL, 1.6 mmol) were added into a thick-walled reaction vessel, which was subsequently screw-sealed with a PTFE cap. The reaction mixture was stirred at 115 °C for 48 h and at 130 °C for 48 h. After completion of the reaction, the reaction was cooled to room temperature, and volatile solvents were removed under reduced pressure. The crude product was dissolved in CH_2Cl_2 (30 mL). To this solution, methanol (20 mL) was added. The mixture was stirred at room temperature for 30 min. CH_2Cl_2 was removed under reduced pressure using a rotary evaporator, affording a suspension of **BN-1** in methanol. The suspension was collected by filtration and washed with excessive methanol at room temperature to give **BN-1** as a deep purple solid (19.0 mg, 94%). ^{1}H NMR (500 MHz, $CDCl_3$) δ = 9.14 (d, *J* = 2.0 Hz, 2H), 9.12 (d, *J* = 2.0 Hz, 2H), 8.80 (d, *J* = 8.5 Hz, 2H), 8.17 (m, 4H), 8.08 (d, 2H), 7.84−7.80 (m, 4H), 7.77−7.75 (dd, *J* = 8.5, 2.0 Hz, 6H), 7.47 (td, *J* = 8.0, 1.0 Hz, 2H), 7.55 (s, 2H), 3.07 (m, 4H), 2.23 (m, 4H), 1.64 (s, 18H), 1.25 (s, 18H), 1.25−1.07 (m, 48H), 0.7 (t, *J* = 7.0 Hz, 12H). ^{13}C{^{1}H} NMR (125 MHz, $CDCl_3$) δ = 165.1, 164.5, 162.7, 154.3, 143.9, 143.0, 143.0, 142.7, 142.6, 138.7, 137.6, 136.0, 133.8, 129.9, 129.3, 127.7, 126.7, 122.1, 121.7, 121.6, 120.0, 119.5, 119.3, 118.8, 114.6, 114.0, 111.3, 108.1, 58.7, 38.1, 35.7, 35.5, 32.3, 32.3, 31.9, 29.8, 29.4, 29.3, 24.3, 22.7, 14.2. ^{19}F NMR (470.4 MHz, $CDCl_3$) δ = 133.23

(m), 135.39 (m). MALDI-MS: m/z $[M]^+$ Calcd for $C_{112}H_{126}N_8S_4B_4F_8$ 1907.9266; Found 1907.9115.

2,2′-(2,8-Di-tert-butyl-5,11-dihydroindolo[3,2-b]carbazole6,12-diyl)dithiazole (5). 6,12-Dibromo-2,8-di-tert-butyl-5,11- dihydroindolo[3,2-b]carbazole (**1**) (52.5 mg, 0.10 mmol) and 2- (tributylstannyl)thiazole (158.3 mg, 0.30 mmol) were added into toluene (1.0 mL). The suspension was degassed by three cycles of freeze-pump-thaw before $Pd(PPh_3)_4$ (11.6 mg, 0.010 mmol), CuI (3.8 mg, 0.020 mmol), and CsF (91.1 mg, 0.60 mmol) were added under N_2. The reaction mixture was stirred at 110 °C for 48 h. After cooling to room temperature, the mixture was extracted with CH_2Cl_2 and washed with 1 M HCl once, brine twice, water once, and dried with $MgSO_4$. The crude product was purified through column chromatography (SiO_2, hexane/ethyl acetate 9:1 to 7:3) to give **5** as a yellow solid (29.0 mg, 50%). ^{1}H NMR (500 MHz, $CDCl_3$) δ = 9.69 (s, 2H), 8.23 (d, *J* = 2.0 Hz, 2H), 8.22 (d, *J* = 3.5 Hz, 2H), 7.68 (d, *J* = 3.5 Hz, 2H), 7.50 (dd, *J* = 8.5 Hz, 2.0 Hz, 2H), 7.39 (d, *J* = 8.5 Hz, 2H), 1.35 (s, 18H). $^{13}C\{^1H\}$ NMR (125 MHz, $CDCl_3$) δ = 164.5, 143.4, 141.6, 139.5, 135.7, 124.8, 121.8, 120.8, 120.2, 119.5, 111.2, 110.6, 35.0, 32.1. ESI-MS: m/z $[M + H]^+$ Calcd for $C_{32}H_{31}N_4S_2$ 535.1985; Found 535.1983.

2,2′-(2,8-Di-tert-butyl-5,11-bis(difluoroboraneyl)-5,11- dihydroindolo[3,2-b]carbazole-6,12-diyl)dithiazole (BN-2). In a N_2-filled glovebox, **3** (53.5 mg, 0.10 mmol), anhydrous CH_2Cl_2(5 mL), triethylamine (0.2 mL), and $BF_3{\cdot}OEt_2$ (0.3 mL, 2.4 mmol) were added into a thick-walled reaction vessel, which was subsequently screw-sealed by a PTFE cap. The mixture was stirred at room temperature for 24 h. After completion of the reaction, the mixture was extracted with CH_2Cl_2 and washed with 1 M HCl once, brine twice, water

once, and dried with $MgSO_4$. The crude product was purified through column chromatography (SiO_2, hexane/ethyl acetate 9:1 to 1:2) to give **BN-2** as a blue solid (59.3 mg, 94%). ^{1}H NMR (500 MHz, CDCl3) δ = 8.93 (d, *J* = 2.0 Hz, 2H), 8.37 (d, *J* = 3.5 Hz, 2H), 8.03 (d, *J* = 8.5 Hz, 2H), 7.75 (d, *J* = 3.5 Hz, 2H), 7.71 (dd, *J* = 8.5 Hz, 2.0 Hz, 2H), 1.25 (s, 18H). ^{13}C{^{1}H} NMR was not obtained for **BN-2**, due to its limited solubility. ^{19}F NMR (470.4 MHz, $CDCl_3$) δ = 137.81 (m). APCI-MS: m/z $[M + H]^+$ Calcd for $C_{32}H_{29}N_4S_2B_2F_4$ 631.1945; Found 631.1950. Melting point: 304−310 °C.

4,9-Dioctylidene-2,7-bis(triisopropylsilyl)-4,9-dihydro-sindaceno[2,1-d:6,5-d′]bis(thiazole) (S1). Octyltriphenylphosphonium bromide (728 mg, 1.6 mmol) was dissolved in anhydrous THF (20 mL) at −78 °C. n-BuLi (1.0 mL, 1.6 M in hexane) was added dropwise. The mixture was stirred at −78 °C for 1 h. To the cooled mixture at −78 °C, a solution of 2,7-bis(triisopropylsilyl)-s-indaceno- [2,1-d:6,5-d′]bis(thiazole)-4,9-dione (366 mg, 0.60 mmol) in anhydrous THF (15 mL) was added dropwise over 30 min. After the addition, the mixture was stirred at −78 °C for 1 h and slowly warmed up to room temperature. The reaction mixture was further stirred at room temperature overnight. The reaction mixture was extracted with CH_2Cl_2 and washed with brine three times. The organic solution was dried over $MgSO_4$ and concentrated under reduced pressure. The residue was further purified through column chromatography (SiO_2, hexane/CH_2Cl_2 9:1) to give the product as a yellow solid. The product was identified as a mixture of three stereoisomers. One of the isomers was purified by column chromatography and characterized as follows. ^{1}H NMR (400 MHz, $CDCl_3$) δ = 7.67 (s, 2H), 6.77 (t, J = 8.0 Hz, 2H), 3.20 (q, J = 7.6 Hz, 4H), 1.63 (qunitet, J = 7.6 Hz, 4H), 1.48 (septet, J = 7.6 Hz, 6H),

1.40−1.25 (m, 20H), 1.20 (septet, J = 7.6 Hz, 36H), 0.87 (t, J = 6.8 Hz, 6H). $^{13}C\{^{1}H\}$ NMR (100 MHz, $CDCl_3$) δ = 171.3, 162.9, 140.5, 140.3, 132.5, 131.2, 130.8, 112.8, 32.1, 29.8, 29.4, 22.9, 18.8, 14.3, 12.0. ESI-MS: m/z $[M + H]^+$ Calcd for $C_{48}H_{77}N_2S_2Si_2$ 801.5061; Found 801.5058. All the isomers were combined (293 mg, 61%) and were used directly in the next step of the synthesis.

4,4,9,9-Tetraoctyl-2,7-bis(triisopropylsilyl)-4,9-dihydro-sindaceno[2,1-d:6,5-d′]bis(thiazole) (S2). To a suspension of $LiAlH_4$ in anhydrous THF (6 mL) at 0 °C, 1-bromooctane (868 mg, 4.5 mmol) was added. A solution of **S1** (366 mg, 0.45 mmol) in anhydrous THF (6.0 mL) was added dropwise. The mixture was stirred at 0 °C for 1 h and subsequently at 50 °C for 8 h. The solvent was then removed under reduced pressure. The residue was dissolved in CH_2Cl_2 and washed with water twice and dried with $MgSO_4$. After removing the solvent under reduced pressure, the crude product was purified through column chromatography (SiO_2, hexane/CH_2Cl_2 9:1 to 7:1) to afford **S2** as a pale yellow solid (297 mg, 64%). ^{1}H NMR (400 MHz, $CDCl_3$) δ = 7.36 (s, 2H), 2.22 (m, 4H), 1.89 (m, 4H), 1.49 (septet, *J* = 7.6 Hz, 6H), 1.3−1.0 (m, 76H), 0.9−0.7 (m, 20H). $^{13}C\{^{1}H\}$ NMR (125 MHz, $CDCl_3$) δ = 174.0, 171.3, 153.2, 137.3, 134.3, 115.4, 52.8, 38.4, 32.1, 30.1, 29.5, 29.3, 24.2, 22.8, 18.8, 18.8, 14.3, 12.0. ESI-MS: m/z $[M + H]^+$ Calcd for $C_{64}H_{113}N_2S_2Si_2$ 1029.7878; Found 1029.7887.

2,7-Dibromo-4,4,9,9-tetraoctyl-4,9-dihydro-s-indaceno[2,1-d:6,5-d′]bis(thiazole) (S3). S2 (206 mg, 0.20 mmol) was dissolved in a mixture of THF (4.0 mL) and MeOH (2.0 mL) at room temperature. A solution of TBAF (2.0 mL, 1.0 M in THF) was added dropwise. The mixture was stirred at 55 °C for 16 h. After cooling to room

temperature, the mixture was extracted with CH_2Cl_2 and washed with brine twice, water once, and dried with $MgSO_4$. After removing the solvent under reduced pressure, the deprotected product was used without further purification in the next step. It was dissolved in $CHCl_3$ (6 mL) at 0 °C. NBS (85 mg, 0.50 mmol) was added portion-wise. The reaction mixture was then stirred at room temperature for 24 h. After completion of the reaction, the mixture was extracted with CH_2Cl_2 and washed with 1 M HCl once, brine twice, water once, and dried with $MgSO_4$. The crude product was purified through column chromatography (SiO_2, hexane/CH_2Cl_2 9:1 to 4:1) to give S3 as a pale yellow solid (113 mg, 65%). ^{1}H NMR (400 MHz, $CDCl_3$) δ = 7.28 (s, 2H), 2.15 (m, 4H), 1.88 (m, 4H), 1.20−1.07 (m, 40 H), 0.82−0.73 (m, 20H). ^{13}C{^{1}H} NMR (100 MHz, $CDCl_3$) δ = 168.4, 151.5, 137.2, 135.4, 134.0, 115.0, 54.3, 38.2, 32.0, 30.0, 29.5, 29.4, 24.1, 22.8, 14.3. APCI-MS: m/z $[M + H]^+$ Calcd for $C_{46}H_{71}N_2S_2Br_2$ 875.3405; Found 875.3363. Melting point: 146−147 °C.

2.4.3 NMR Spectra

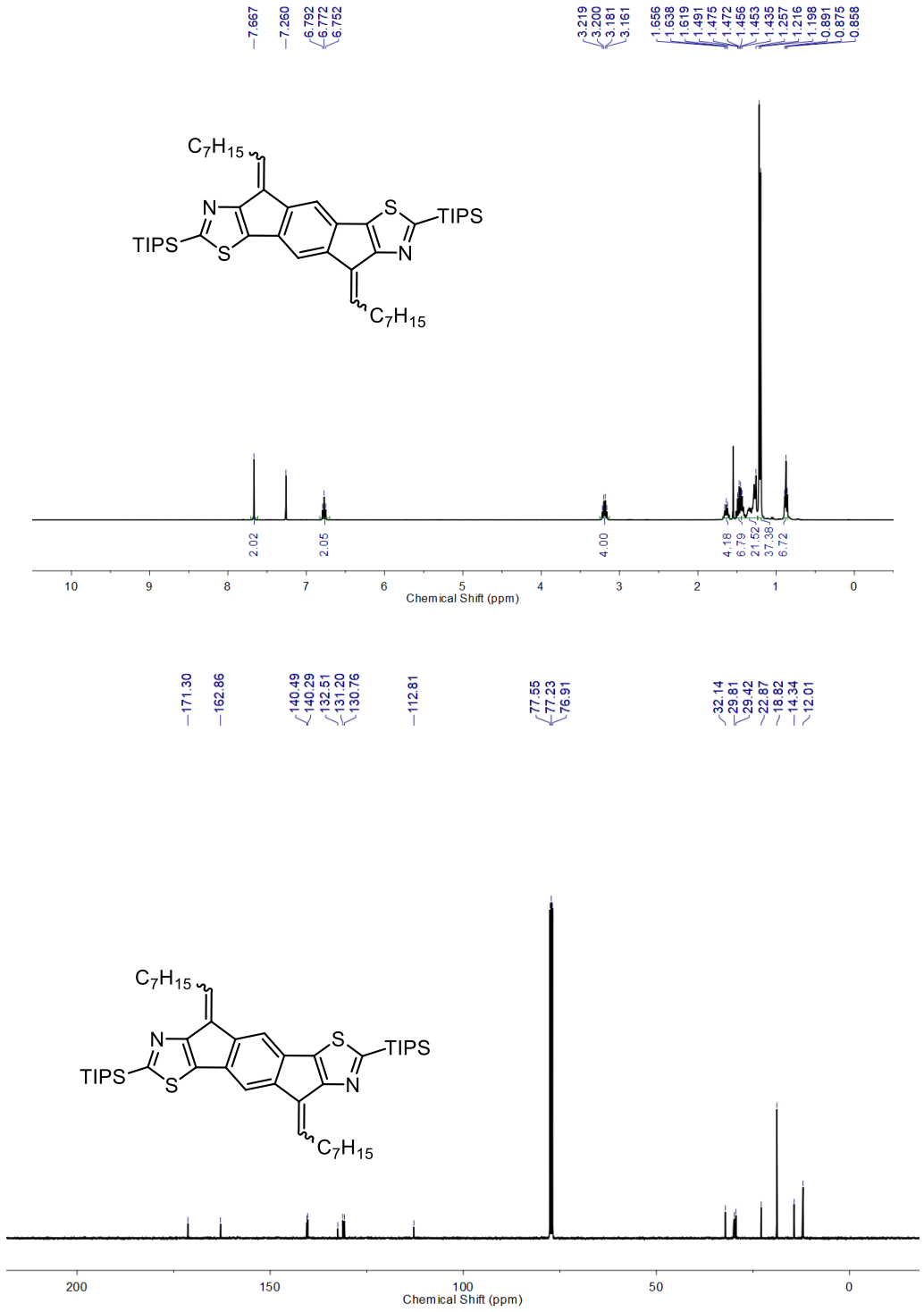

Figure 17. ^{1}H (400 MHz), ^{13}C{^{1}H} (100 MHz) NMR of S1 in $CDCl_3$ at room temperature.

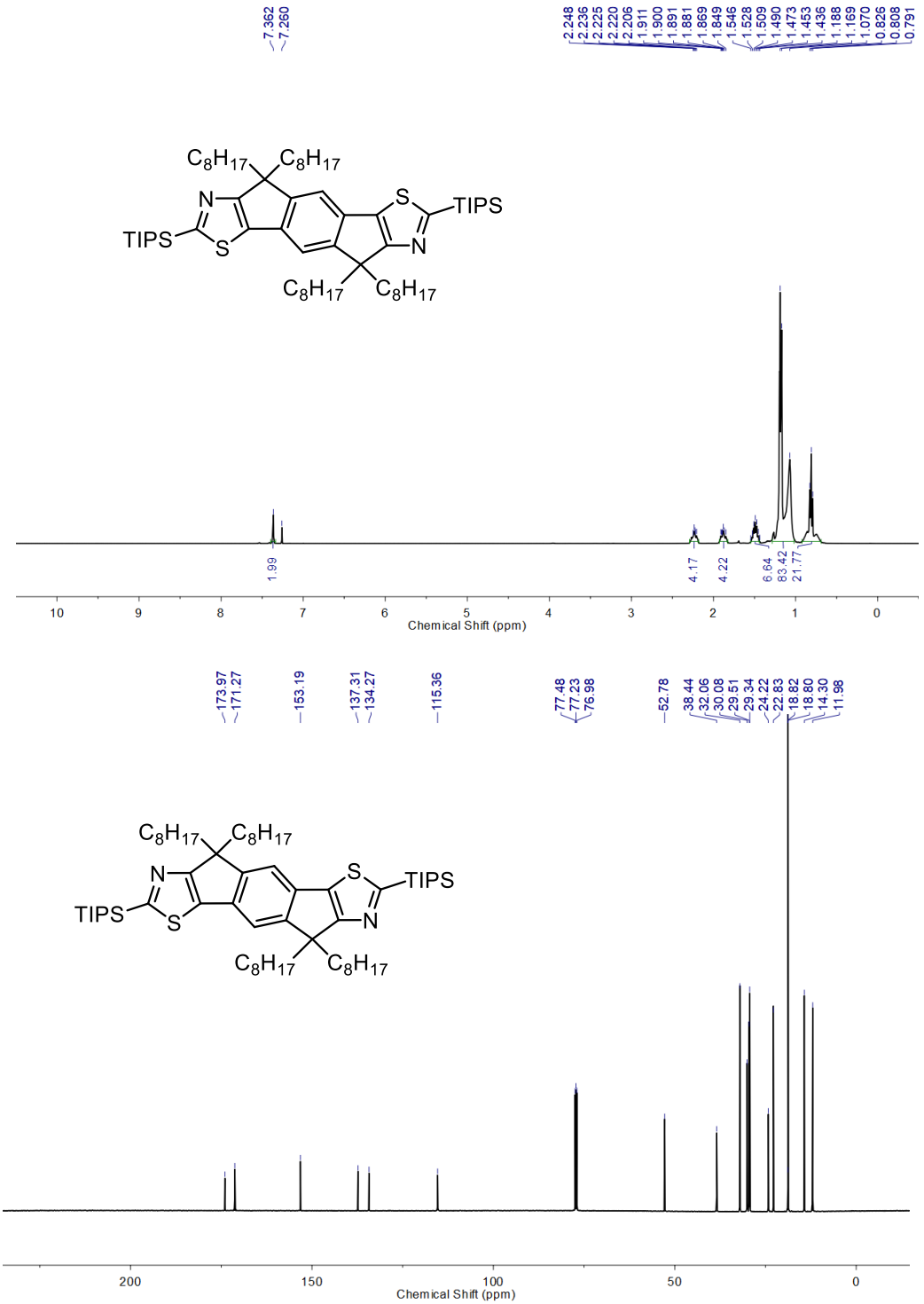

Figure 18. ^{1}H (400 MHz), $^{13}C\{^{1}H\}$ (125 MHz) NMR of S2 in $CDCl_3$ at room temperature.

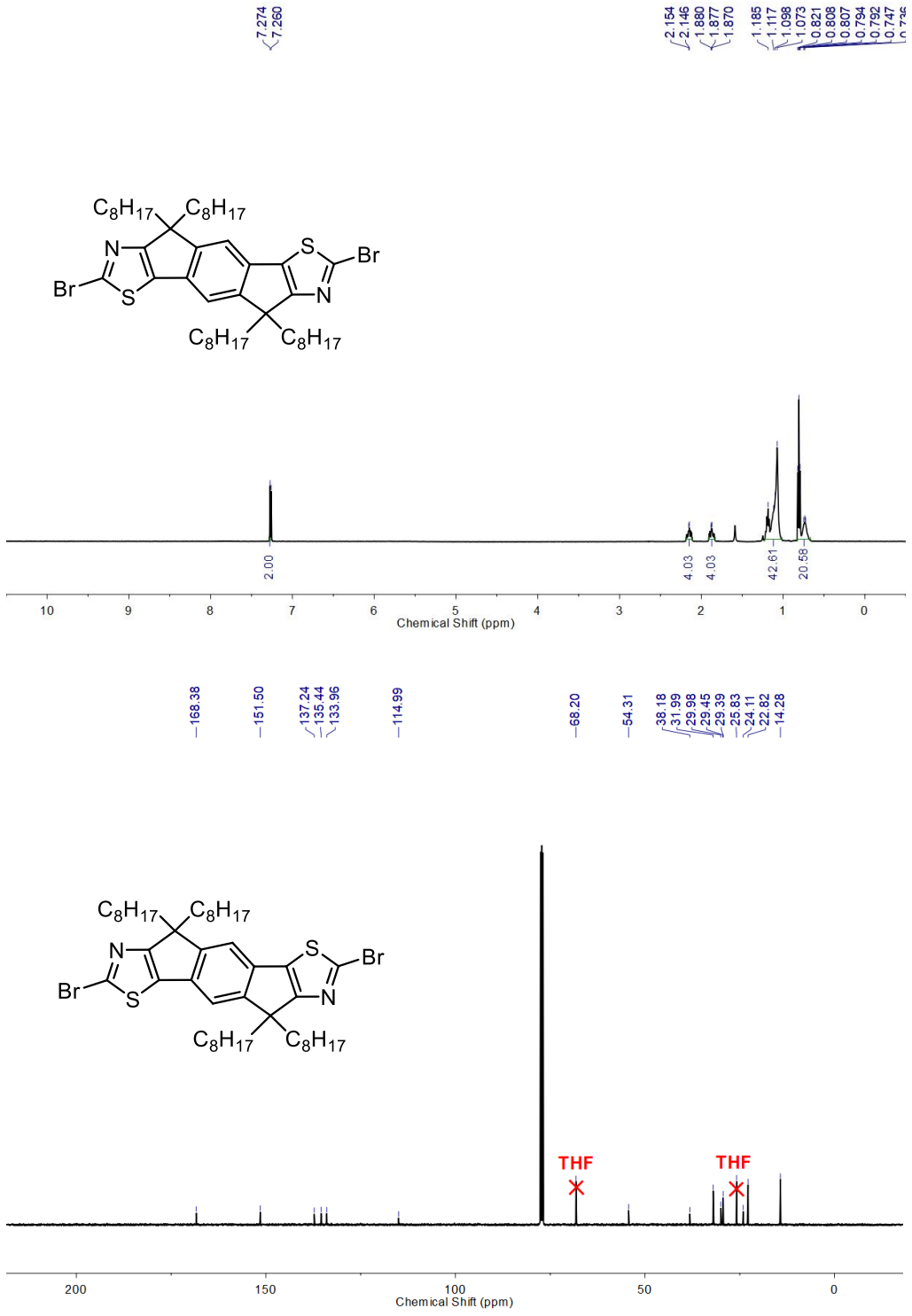

Figure 19. ^{1}H (400 MHz), $^{13}C\{^{1}H\}$ (100 MHz) NMR of S3 in $CDCl_3$ at room temperature.

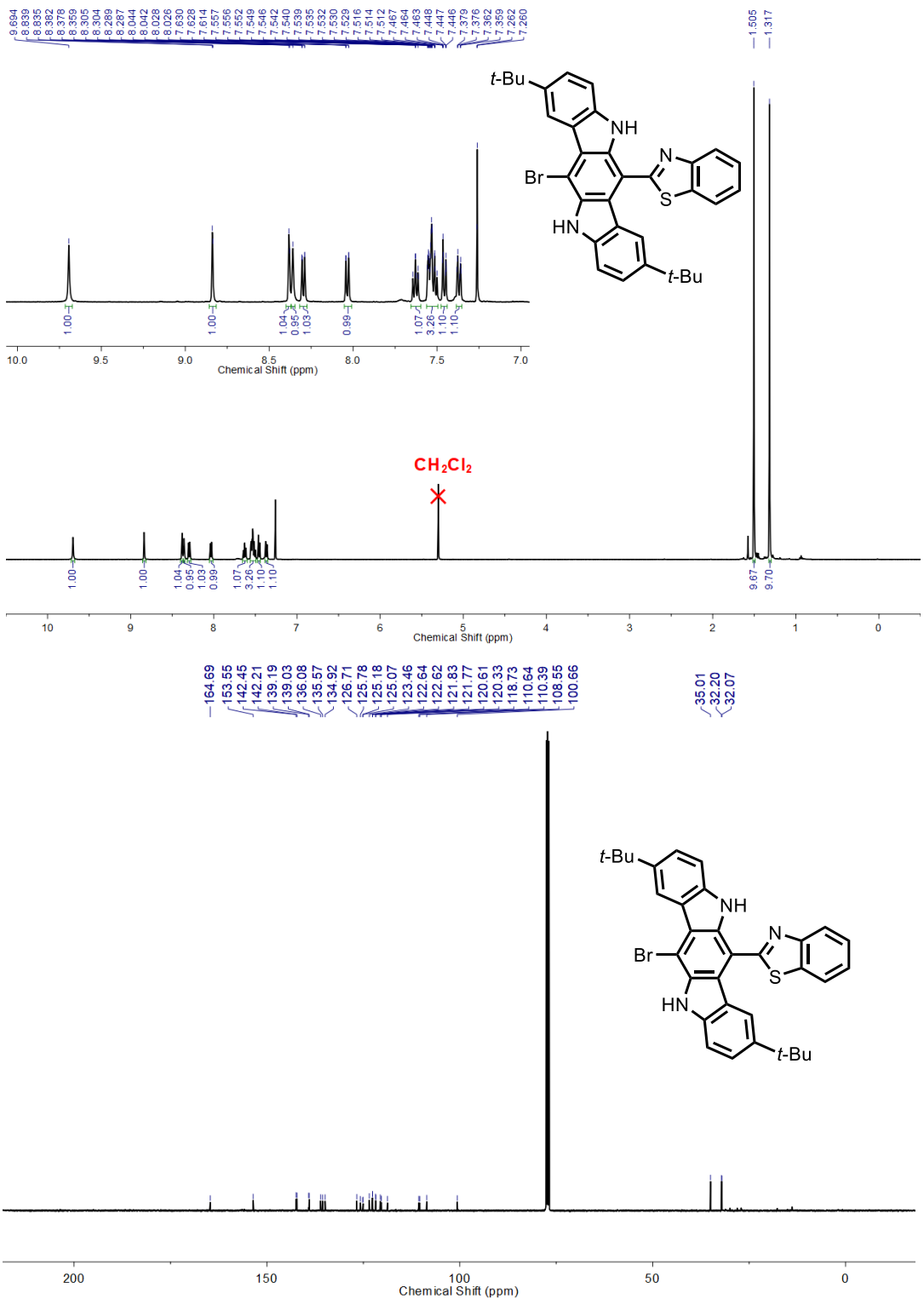

Figure 20. ^{1}H (400 MHz), $^{13}C\{1H\}$ (100 MHz) NMR of 2 in $CDCl_3$ at room temperature.

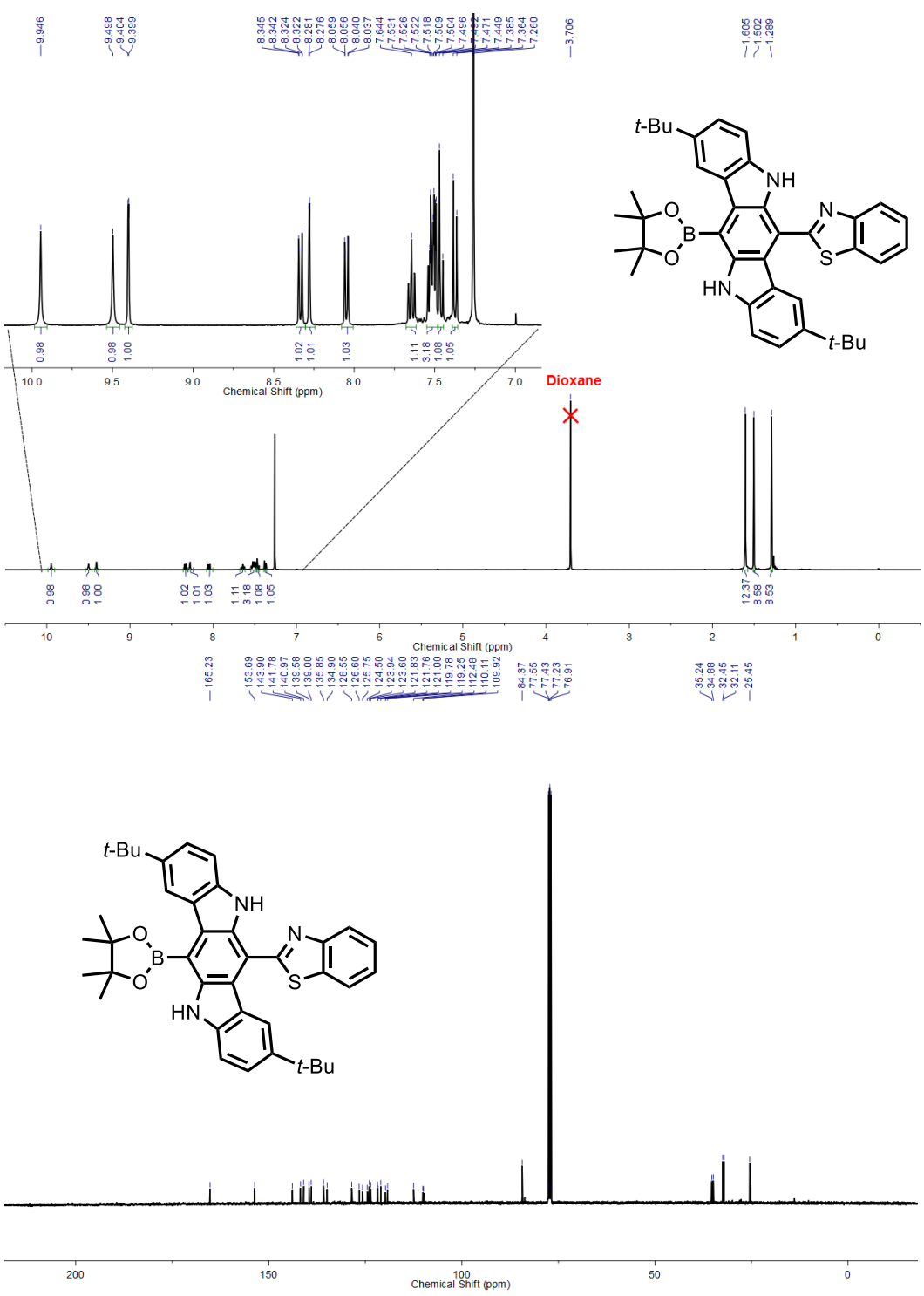

Figure 21. ^{1}H (400 MHz), $^{13}C\{^{1}H\}$ (100MHz) NMR of 3 in $CDCl_3$ at room temperature.

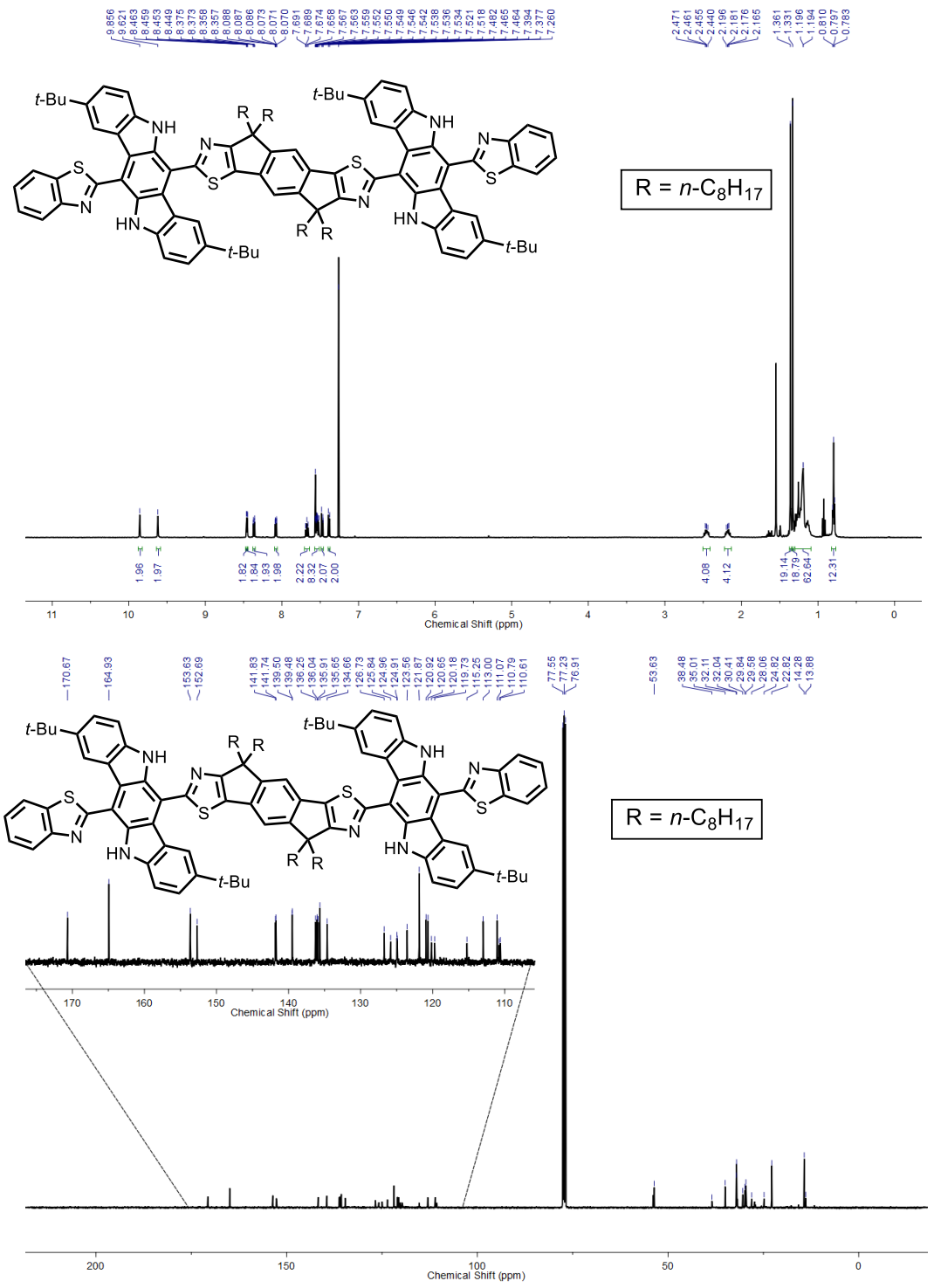

Figure 22. ^{1}H (500 MHz), ^{13}C{1H} (100 MHz) NMR of 4 in $CDCl_3$ at room temperature.

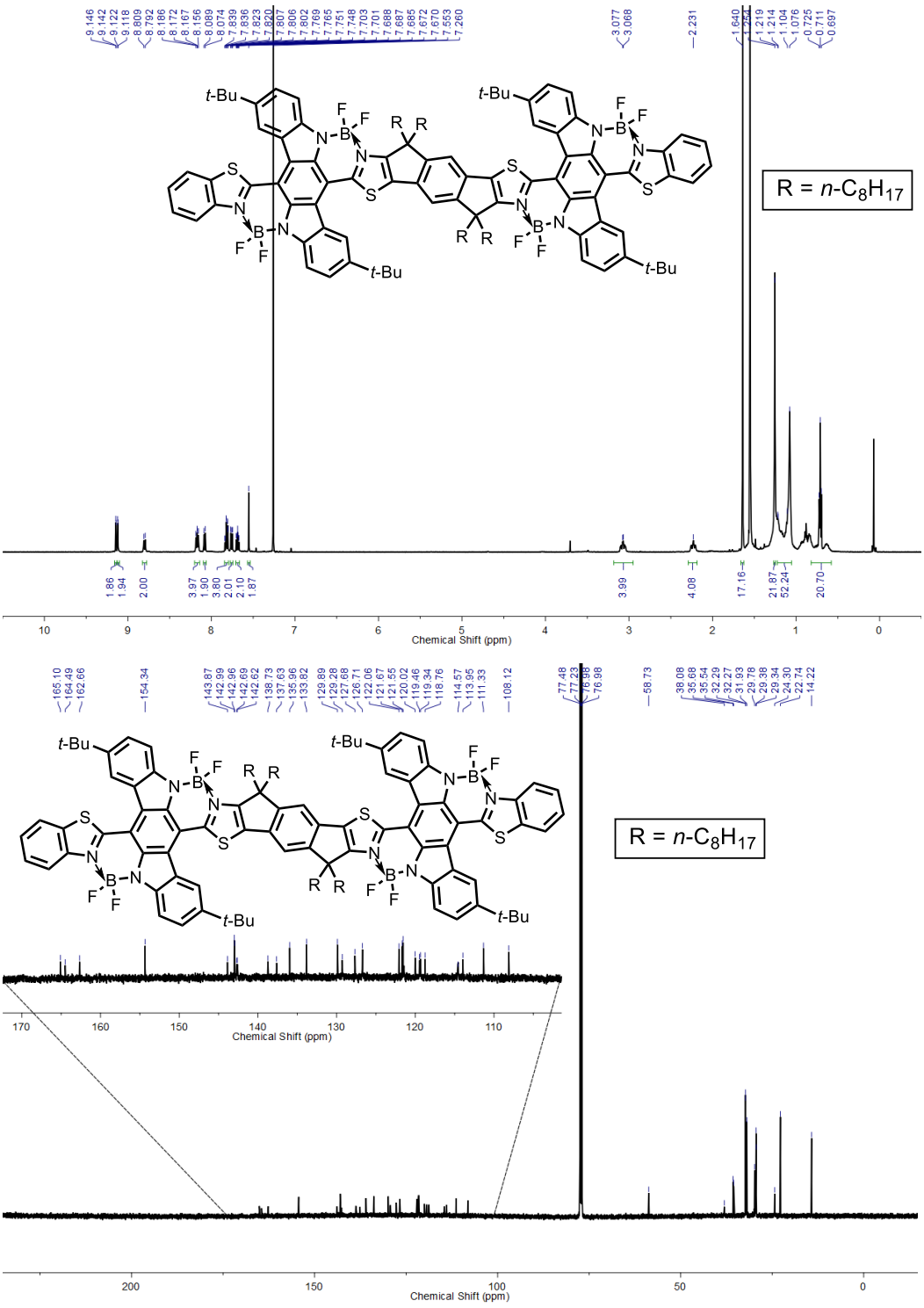

Figure 23. ^{1}H (400 MHz), ^{13}C{^{1}H} (125 MHz) NMR of BN-1 in $CDCl_3$ at room temperature.

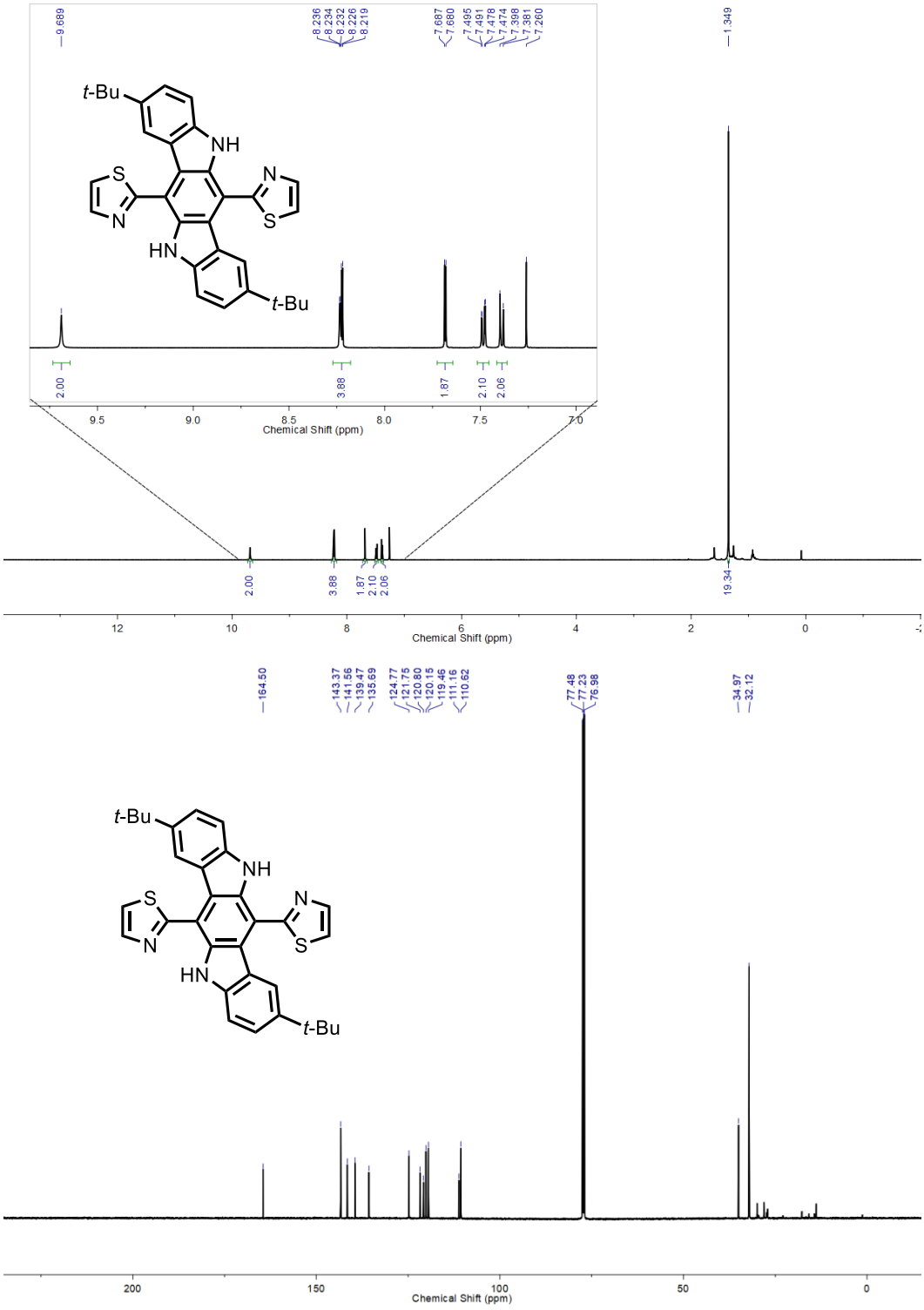

Figure 24. ^{1}H (500 MHz), ^{13}C{^{1}H} (125 MHz) NMR of 5 in $CDCl_3$ at room temperature.

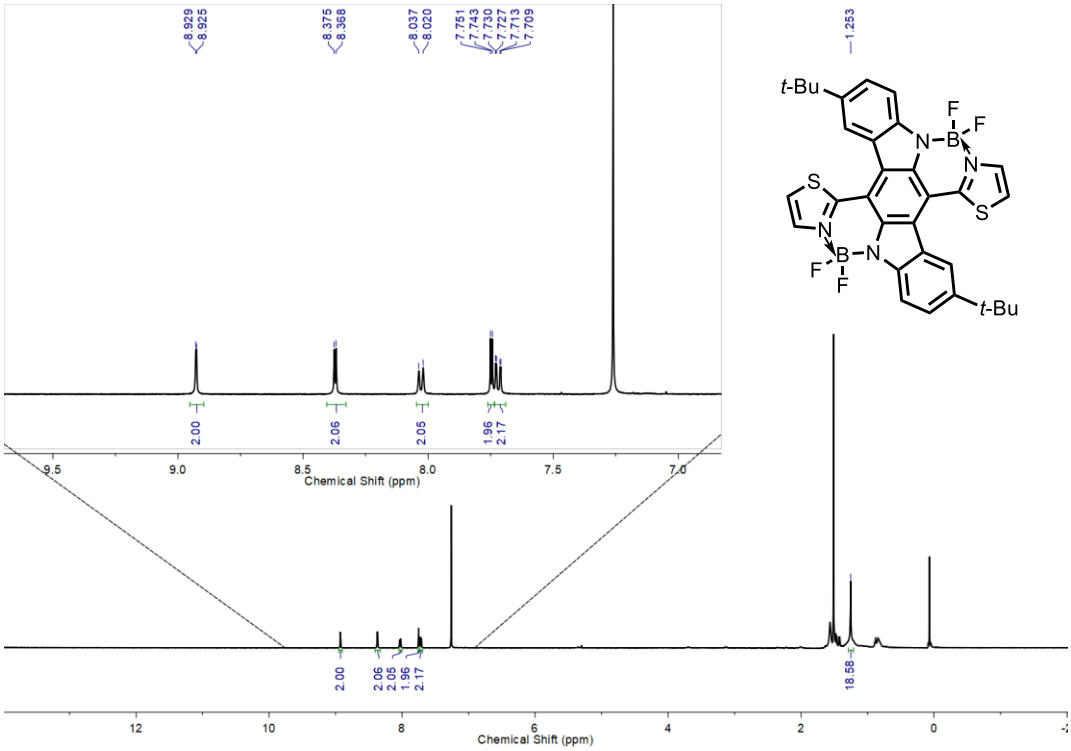

Figure 26. ^{1}H (500 MHz) NMR of BN-2 in $CDCl_3$ at room temperature.

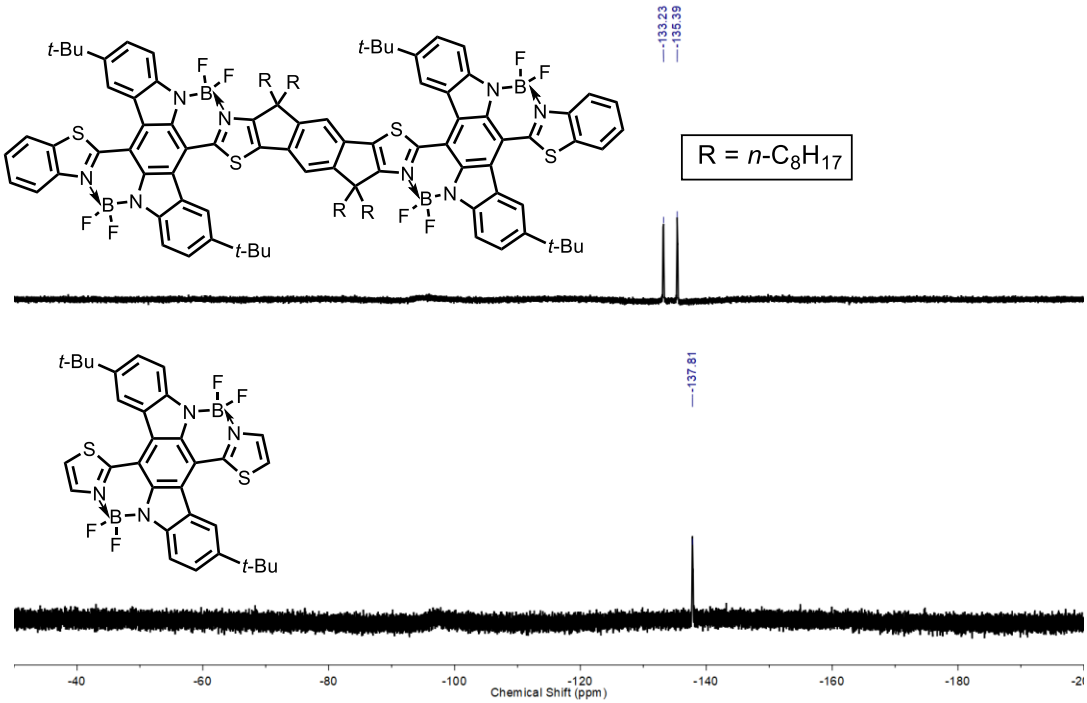

Figure 25. ^{19}F (470.4 MHz) NMR of BN-1 (top) and BN-2 (bottom) in $CDCl_3$ at room temperature.

2.4.4 DFT Calculation

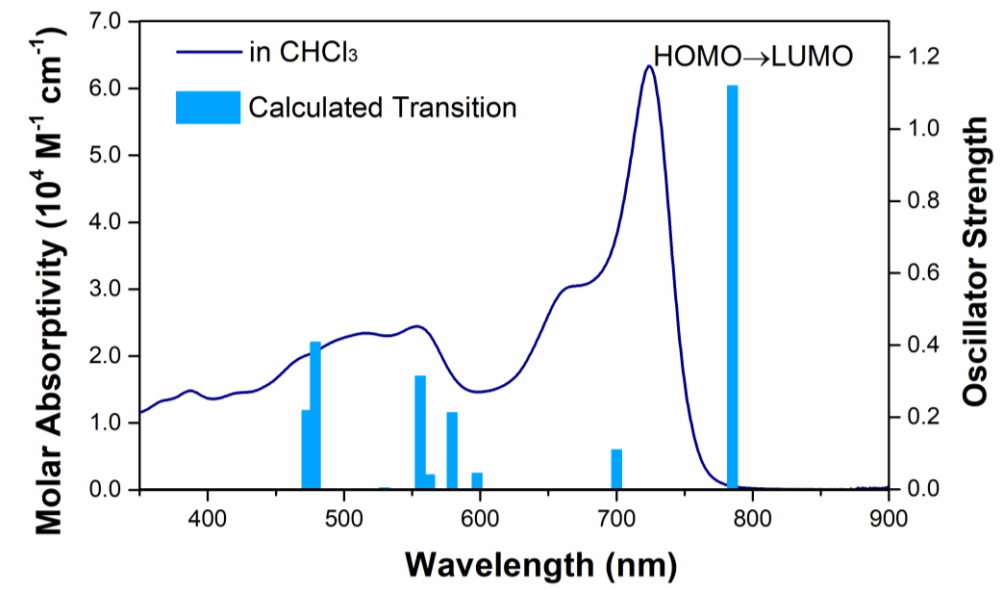

Figure 27. UV-vis-NIR absorption spectrum of BN-1 in a diluted $CHCl_3$ solution and TD-DFT computed transition energies of BN-1 with $CHCl_3$ solvation.

Table 1. Computed transition energies of BN-1 using time-dependent density functional theory.

Transition energies (nm)	Oscillator strength	Main contribution
785.12	1.1193	HOMO→LUMO
700.09	0.1091	HOMO−1→LUMO
597.71	0.0437	HOMO→LUMO+1
579.38	0.2119	HOMO−2→LUMO
562.76	0.0400	HOMO−1→LUMO+1
555.90	0.3136	HOMO−3→LUMO
530.59	0.0227	HOMO−4→LUMO
529.39	0.0035	HOMO−5→LUMO
478.90	0.4082	HOMO−6→LUMO+1
472.81	0.2186	HOMO−2→LUMO+2

2.4.5 Atomic Force Microscopy and Glazing-Incidence Wide Angle X-ray Scattering

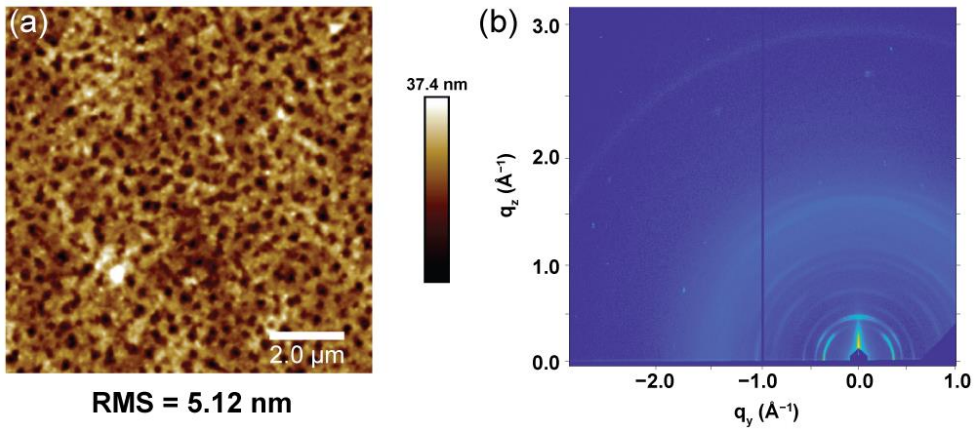

Figure 28. (a) Atomic force microscopy image and (b) glazing-incidence wide-angle X-ray scattering image of thin films of BN-1. The thin films of BN-1 were prepared by casting a solution of BN-1 in chlorobenzene (5 mg/mL) on ozone-cleaned silica wafer substrates followed up spinning coating at 1000 rpm/s for 60 s.

2.4.6 Cyclic Voltammetry

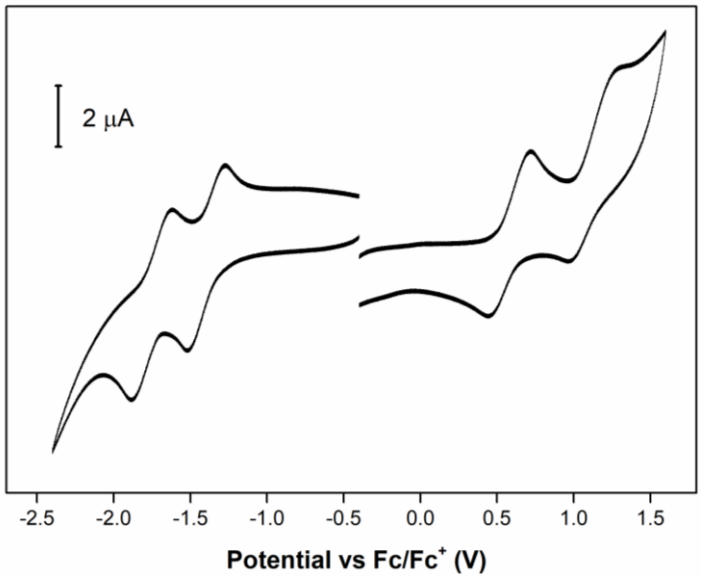

Figure 29. Cyclic voltammogram of Compound 4.

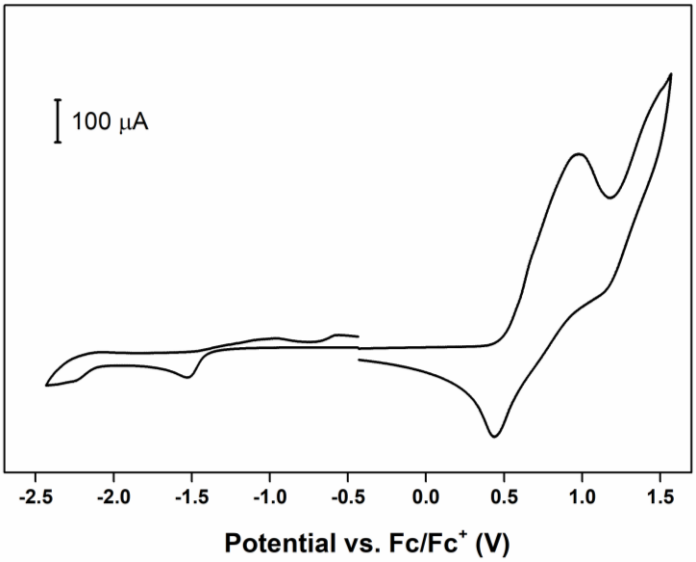

Figure 30. Cyclic voltammogram of BN-2 (1.0 mM BN-2 in CH_2Cl_2).

The energy levels were calculated using ferrocene/ferrocenium (Fc/Fc^+) as the standard reference. The potential of the Fc/Fc^+ redox couple was measured to be 0.45 V vs. Ag/AgCl. The energy levels of frontier molecular orbitals were calculated as follows and summarized in Table S5.

$E_{HOMO/LUMO} = -4.80 + (0.45 - E_{1/2})$ eV

E1/2 represented the onset of a redox process on cyclic voltammogram.

Table 2. Energy levels of frontier orbitals calculated from cyclic voltammetry.

	HOMO (eV)	**LUMO (eV)**
Compound **4**	−5.25	−3.36
BN-1	−5.34	−3.82
BN-2	−5.38	−3.41

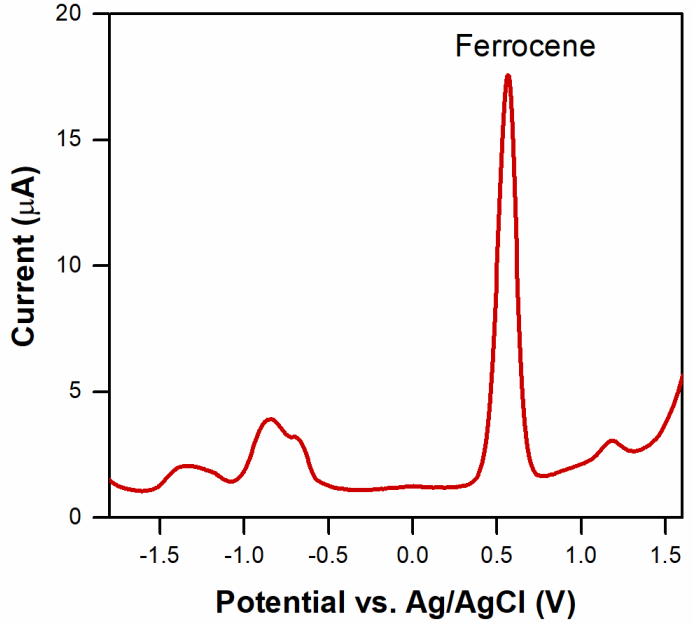

Figure 31. Differential pulse voltammetry of BN-1 in (0.1 mM in CH2Cl2). Ferrocene was used as an internal standard for this measurement.

2.4.7 X-ray Single Crystal Analysis

A Leica MZ 75 microscope was used to identify a suitable brown block with very well-defined faces with dimensions (max, intermediate, and min) 0.092 x 0.059 x 0.025 mm^3 from a representative sample of crystals of the same habit. The crystal mounted on a nylon loop was then placed in a cold nitrogen stream (Oxford) maintained at 100 K. A BRUKER Venture X-ray (kappa geometry) diffractometer was employed for crystal screening, unit cell determination, and data collection. The goniometer was controlled using the APEX3 software suite.[126] The sample was optically centered with the aid of a video camera such that no translations were observed as the crystal was rotated through all

positions. The X-ray radiation employed was generated from a Cu-Iμs X-ray tube (K_α = 1.5418Å with a potential of 50 kV and a current of 1.0mA). 45 data frames were taken at widths of 1°. These reflections were used to determine the unit cell. The unit cell was verified by examination of the *h k l* overlays on several frames of data. No super-cell or erroneous reflections were observed. After careful examination of the unit cell, an extended data collection procedure (11 sets) was initiated using omega and phi scans. Integrated intensity information for each reflection was obtained by reduction of the data frames with the program APEX3.[126] The integration method employed a three-dimensional profiling algorithm and all data were corrected for Lorentz and polarization factors, as well as for crystal decay effects. Finally, the data was merged and scaled to produce a suitable data set. The absorption correction program SADABS[127] was employed to correct the data for absorption effects. Systematic reflection conditions and statistical tests of the data suggested the space group P-1. A solution was obtained readily (Z = 1, Z' = 0.5) using XT/XS in APEX3.[126,128]1,3 Hydrogen atoms were placed in idealized positions and were set riding on the respective parent atoms. All non-hydrogen atoms were refined with anisotropic thermal parameters. SIMU and DELU restraints were used to keep the thermal ellipsoids of some of the atoms meaningful. Absence of additional symmetry or void were confirmed using PLATON (ADDSYM). The structure was refined (weighted least squares

refinement on F^2) to convergence.[128,129] Olex2 was employed for the final data presentation and structure plots.[129]

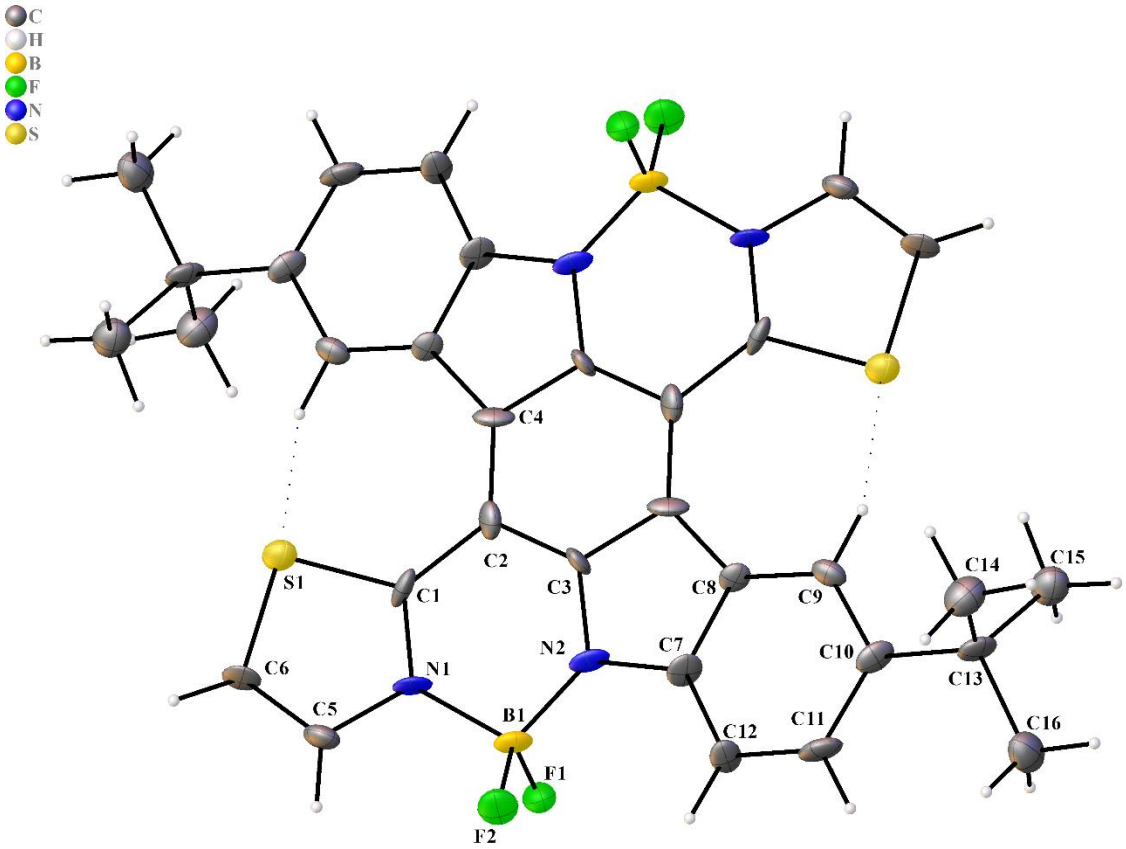

Figure 32. A thermal ellipsoid plot for the crystal structure of BN-2. The ellipsoid contour % probability level was set to be 50%.

2.4.8 UV-Vis Absorption and Fluorescence Emission

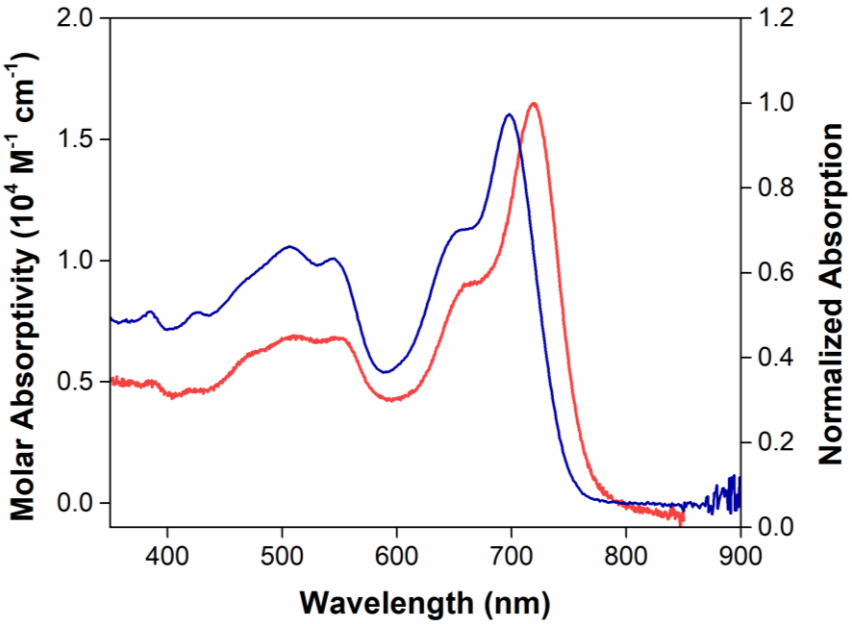

Figure 33. UV-vis absorption spectrum of BN-1 in chloroform (red) and in the solid state (blue). The absorption spectrum was taken at room temperature at a concentration of 2.1×10^{-5} M.

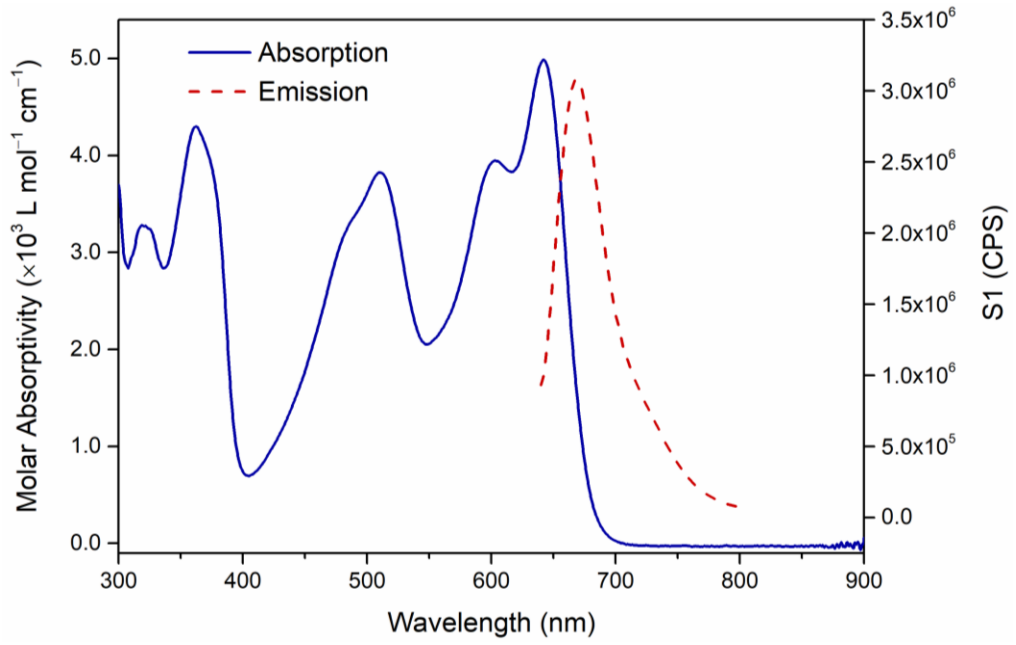

Figure 34. UV-vis absorption and emission spectrum of BN-2 in $CHCl_3$. The absorption spectrum was taken at room temperature at a concentration of 2.9×10^{-5} M. The emission spectrum was taken at room temperature at a concentration of 3.6×10^{-6} M with an excitation wavelength at 635 nm.

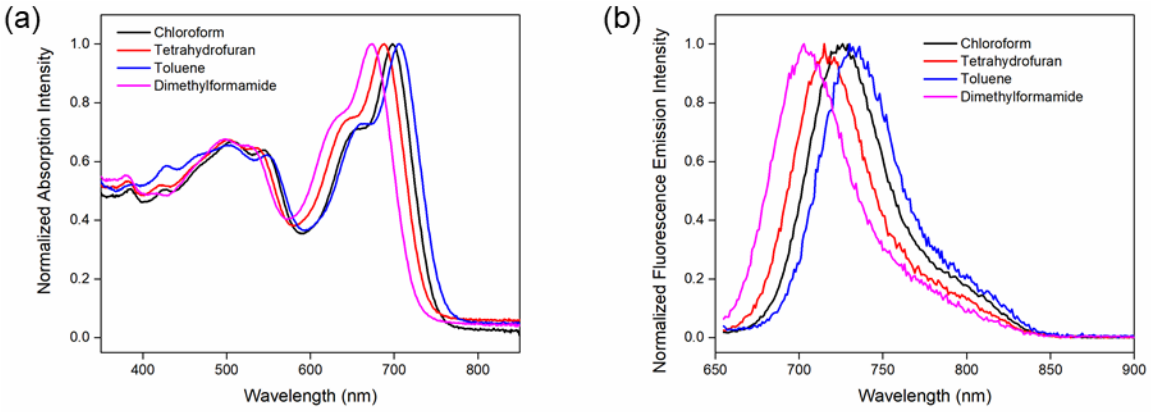

Figure 36. (a) UV-vis absorption and (b) emission spectrum of BN-1 in chloroform, toluene, tetrahydrofuran and dimethylformamide. The absorption spectrum was taken at room temperature at a concentration of 2.0×10^{-5} M. The emission spectrum was taken at room temperature at a concentration of 2.2×10^{-6} M with an excitation wavelength at 620 nm.

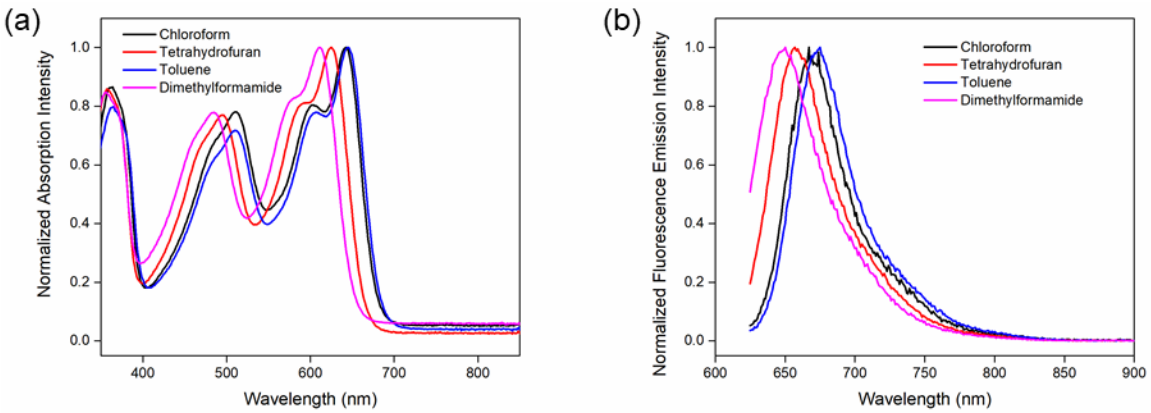

Figure 35. (a) UV-vis absorption and (b) emission spectrum of BN-2 in chloroform, toluene, tetrahydrofuran and dimethylformamide. The absorption spectrum was taken at room temperature at a concentration of 2.0×10^{-5} M. The emission spectrum was taken at room temperature at a concentration of 2.1×10^{-6} M with an excitation wavelength at 650 nm.

CHAPTER III

LADDER TYPE MOLECULES RIGIDIFIED WITH B←N COORDINATE BONDS WITH TUNABLE BANDGAP AS N-TYPE SEMICONDUCTING MATERIALS

3.1 Introduction

Over the last decades, there has been remarkable progress in the investigations in organic electronics, including organic thin film transistors (OFETs), organic solar cells (OSCs), organic light emitting diodes (OLEDs), *etc*.[130] These devices have revolutionized our lives by opening up opportunities for next-generation products, like wearable electronics, sensors, and bioelectronic interfaces, *etc*.[131,132] Compared to conventional inorganic semiconductors, organic electronic materials typically possess weaker intermolecular forces, often bringing about unfavorable properties, including slower transport of charges, phonons, excitons, and morphological instability.[38] Despite these potential drawbacks, there have been significant advances made in this field in terms of the development of novel molecules, modified processing strategies, and device architecture optimization.[119,133,134] Based on the guidance from these perspectives, both small molecules and polymers with high mobilities of up to 40 $cm^2\ V^{-1}\ s^{-1}$ have been achieved in OFETs.[135,136]

Most of these high mobilities were achieved on *p*-type semiconducting materials, which conduct holes in the OFET channel. Comparatively, the development of *n*-type organic semiconductors remains confined, in terms of the varieties of structures synthesized and the charge mobility achieved. One key factor that hinders the development

of *n*-type organic semiconductors is the difficulty to achieve low enough LUMO energy levels among a large selection of organic structures. When the energy level of LUMO is high, not only is it hard to inject electrons from the electrodes, but also renders it prone to reacting with ambient water and oxygen.[76,137]

Based on these principles, it is vital to tune the LUMO energy level so that it is reasonably low. Examples include those developed based on the backbone of naphthalene diimides (NDIs),[138-141] perylene diimides (PDIs),[142-145] N-heteroacenes,[146,147] quinoidal oligothiophenes,[148,149] and isoindigo derivatives,[150,151] *etc*. Moreover, it is ideal to adopt a planar, rigid molecular structure over the extended conjugation framework, which facilitates carrier transport. Previously, our group has demonstrated the incorporation of B←N coordinate bonds to rigidify and coplanarize the backbone of the molecules. A profound effect of this incorporation is that it stabilized the various redox states by forming quinoidal structures. Such transformation was verified by the bond length alternation (BLA) from not only the DFT simulation but also experimental data obtained from the single crystals of different redox states (**Figure 37**).[77] As a result of this, reversible oxidative and reductive peaks on CV were evidently witnessed.

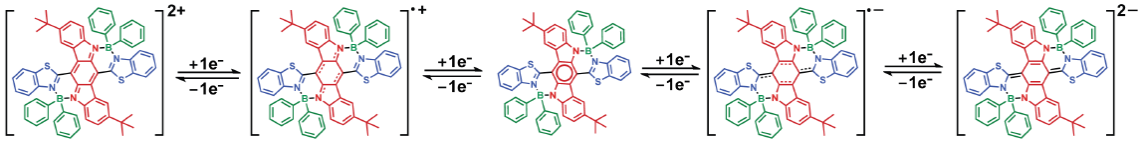

Figure 37. Constitutional structures of the five different redox states of previous work.

Based on the previous chapter, it is known that the incorporation of B←N coordinate bonds could effectively lower the LUMO energy level. Inspired by this result, I would like to further shed light on a feasible manner to tune the electronic properties of similar structures with the indolocarbazole backbone. Currently, the benzothiazole motif was installed on the central ring of the indolocarbazole backbone. In order to increase the dimension of modification to the molecular structures, instead of a tert-butyl group, different aryl groups were connected to the indolocarbazole motif via coupling reactions to afford tunability over the optical and electronic properties. In addition, an extra chlorine atom was installed on the benzothiazole motif to tune the electron density from the other direction. Based on such design (**Figure 38**), in this chapter the synthesis of these novel compounds accommodating B←N coordinate bonds and their device performances are discussed.

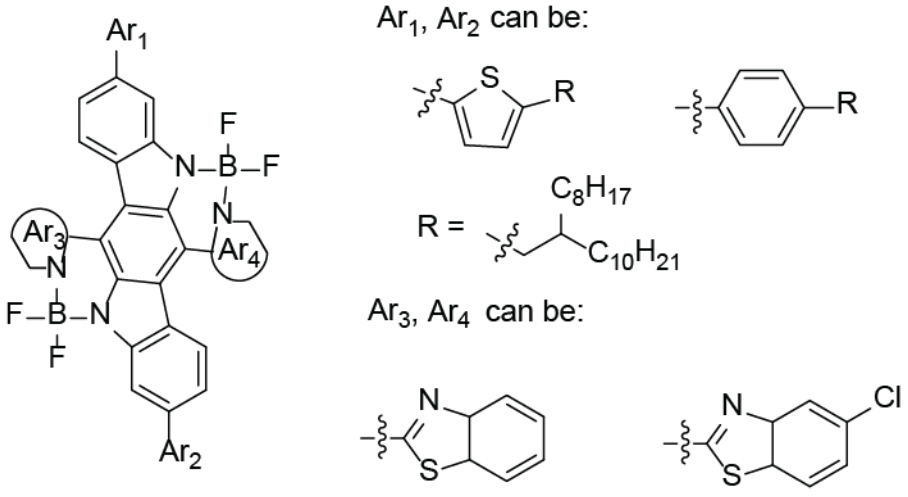

Figure 38. Molecular design of novel compounds with B←N coordinate bonds coupled with various aryl groups.

3.2 Results and Discussion

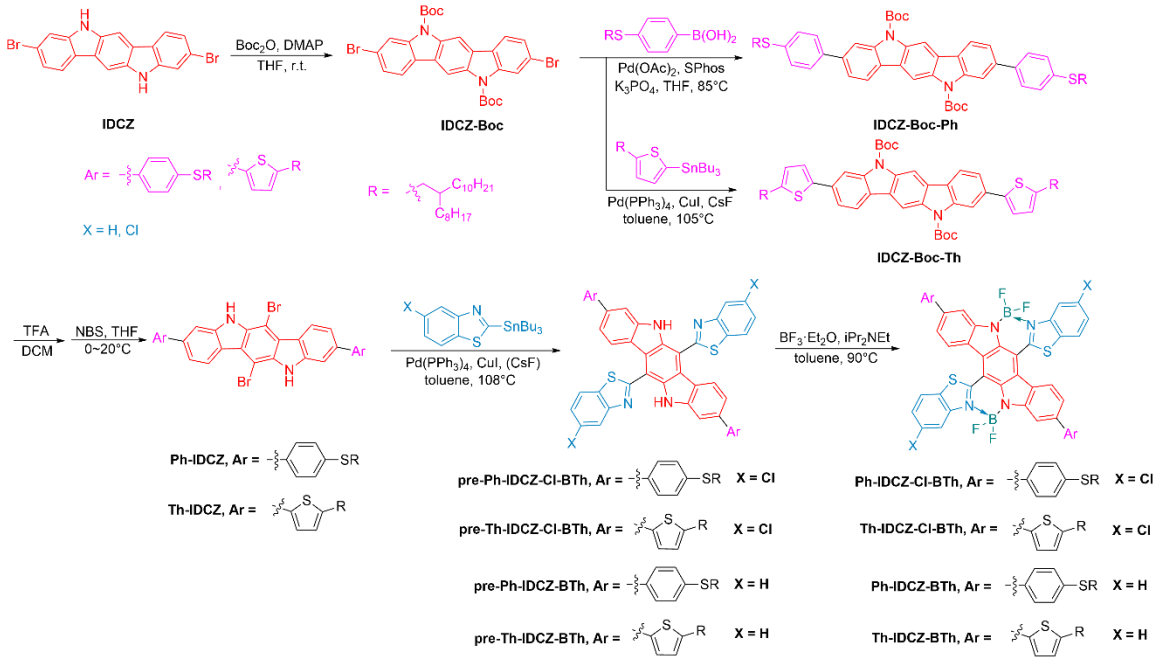

Figure 39. Synthetic scheme of the proposed four molecules with B←N coordinate bonds.

The synthetic route towards the proposed molecules is shown in **Figure 39**. The synthesis started from the indolocarbazole core that has been used in our group before.[152] Instead of directly conducting cross coupling on the starting material, the synthesis started from the protection of secondary amino groups on the starting material **IDCZ** by -Boc groups to afford intermediates **IDCZ-Boc**. This step served two purposes. First, the installation of -Boc groups enhanced the solubility to facilitate the further synthesis.

Second, the protection deactivated the amino groups so that side reactions and catalyst poisoning by nitrogen could be prevented.

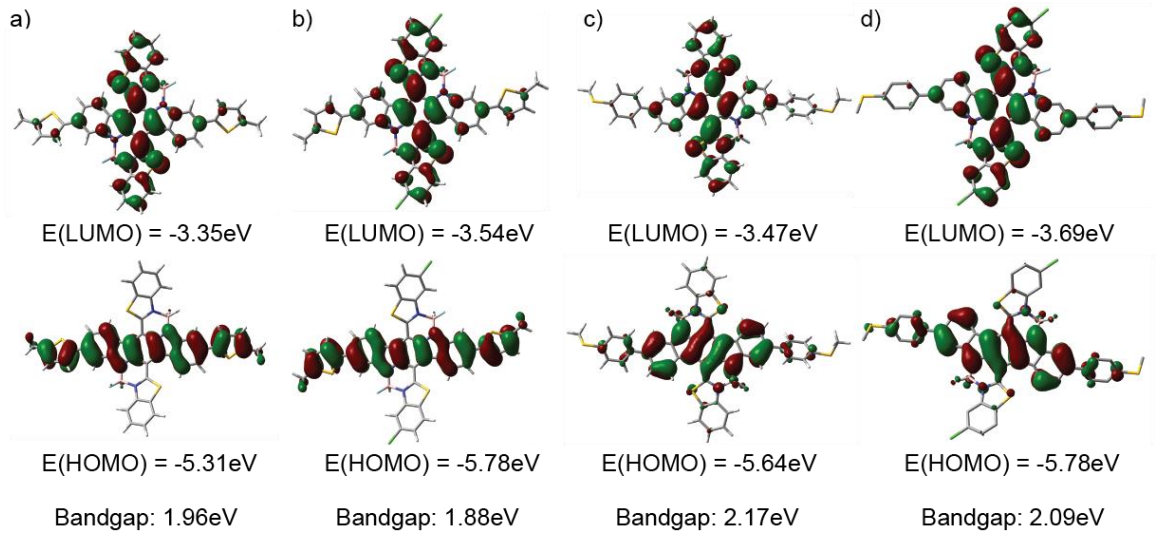

Figure 40. Molecular structures and frontier molecular orbitals of a) Th-IDCZ-BTh, b) Th-IDCZ-Cl-BTh, c) Ph-IDCZ-BTh, d) Ph-IDCZ-Cl-BTh, simulated by DFT calculation based on B3LYP/6-311g.

Afterwards, the proposed phenyl and thiophene derivatives were coupled with **IDCZ-Boc** to extend the conjugation backbone by Suzuki coupling and Stille coupling respectively. The conditions of these two reactions were carefully controlled to avoid deprotection of -Boc groups due to the known instability to heat.[153] After this step, two kinds of compounds, **IDCZ-Boc-Ph** and **IDCZ-Boc-Th** were generated. Next, these two intermediates were deprotected in acidic conditions, followed by selective two-fold

bromination on the central positions of indolocarbazole. These two sites were later subjected to Stille coupling with two types of benzothiazole derivatives to afford four kinds of precursors. Finally, borylations of these four precursors with $BF_3 \cdot OEt_2$ and N,N-diisopropylethylamine were performed at an elevated temperature of 90°C to guarantee high conversion towards the desired final products. In this step, two B←N coordinate bonds were constructed on each molecule to fuse the backbone via six-member rings.

Following the successful synthesis of these molecules, efforts were committed to better understand the structure-property correlation of these four molecules. Initially, I tried to grow single crystals of these molecules, but the growth of single crystals turned out difficult and no single crystals suitable for X-ray analysis were obtained due to the branched alkyl chain. As an alternative, density functional theory (DFT) simulations were carried out to reveal the structures and frontier molecular orbitals of these molecules, with isovalue of 0.1 and side alkyl groups omitted for clarity (**Figure 40**). It was shown that a rather rigid and coplanar backbone was adopted by all these four molecules. Additionally, they shared a common trend in terms of the distribution of frontier molecular orbitals. Regardless of the aryl groups in the molecule, the HOMO mostly resided on the direction where the indolocarbazole core was connected to phenyl/thiophene groups, but LUMO mostly resided on the benzothiazole motifs. This observation complied with the fact that benzothiazole motifs were more electron-deficient but either thiophene or phenyl groups were more electron-rich comparatively. In terms of the energy level, the impact of substituent groups was clearly demonstrated. When an extra chlorine atom was installed onto benzothiazole, both HOMO and LUMO were lowered. Because LUMO was lowered

by a stronger degree, the bandgap between HOMO and LUMO was also reduced. Similarly, when thiophene groups were changed to phenyl groups, *i.e.*, changed to less electron-rich aryl groups, a decrease in both HOMO and LUMO was observed, but since HOMO was more impacted, the observed bandgap was increased.

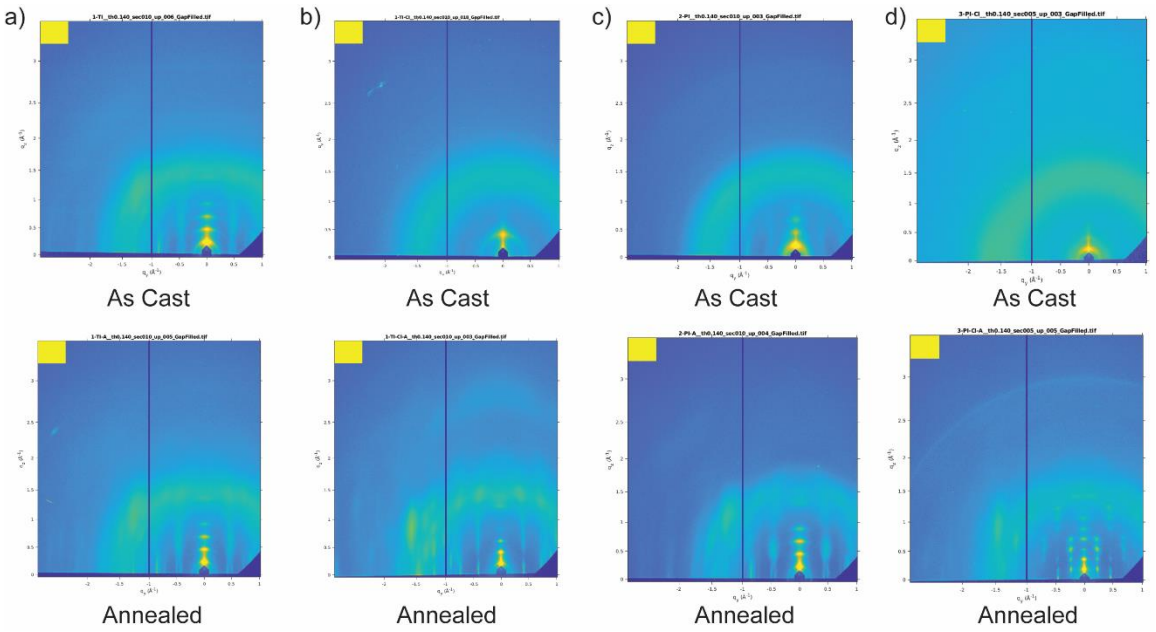

Figure 41. GIWAXS of thin films of a) Ph-IDCZ-BTh, b) Ph-IDCZ-Cl-BTh, c) Th-IDCZ-BTh, d) Th-IDCZ-Cl-BTh as cast and after thermal annealing.

Next, the absorption and emission spectrum of these four compounds were recorded in chloroform as the solvent. All these four compounds showed relatively small Stokes shifts of ~40 nm, indicating a rather rigid backbone. For both the absorption and emission spectra, all these four compounds showed similar patterns. The absorption peak ranged

from ~500 nm to ~800 nm, while the emission spectrum ranged from ~650 nm to 850 nm. There is a consistent red shift in the λ_{max} of both absorption and emission peaks when the aryl groups were changed from phenyl to thiophene, or when the chlorine atom was installed on the benzothiazole motif. Such red shifts reflected a reduction in the bandgap, which aligned with the DFT simulated results. In addition, the fluorescence weakened along with such changes.

Afterwards, grazing-incidence wide-angle X-ray scattering (GIWAXS) was employed to gain insight into the crystalline packing patterns of spin-cast thin film samples of these molecules (**Figure 41**). All the samples after annealing showed clear lamellar stacking peaks in the out-of-plane direction. Some of the samples after annealing displayed diagonal π - π stacking peaks. **Ph-IDCZ-Cl-BTh** showed the most intense diagonal π - π stacking peaks, which represented lessened grain-boundary effects between crystals. The combination of these two types of peaks suggested predominantly edge-on packing mode on the substrate. In addition, these molecules exhibited high crystallinity after annealing. These GIWAXS observations elucidated that these molecules were promising OFET semiconducting materials thanks to their crystalline edge-on packing mode on the substrate.

Table 3. Summary of device performance fabricated with these four molecules as the conducting layer.

Compound	Dielectric	Annealing	Avg μ_e (cm^2/Vs)	Highest μ_e (cm^2/Vs)	Avg μ_h (cm^2/Vs)	Highest μ_h (cm^2/Vs)
Ph-IDCZ-BTh	None	None	-	-	-	-
	None	110°C	-	-	-	-
	OTS	None	9.34×10^{-5}	1.01×10^{-4}	5.34×10^{-5}	1.32×10^{-4}
	OTS	110°C	-	-	2.08×10^{-5}	3.90×10^{-5}
Ph-IDCZ-Cl-BTh	None	None	-	-	-	-
	None	110°C	-	-	-	-
	OTS	None	5.65×10^{-4}	7.49×10^{-4}	-	-
	OTS	110°C	8.06×10^{-5}	2.28×10^{-4}	-	-
Th-IDCZ-BTh	None	None	-	-	-	-
	None	110°C	-	-	-	-
	OTS	None	1.56×10^{-5}	2.51×10^{-5}	6.51×10^{-5}	1.15×10^{-4}
	OTS	110°C	-	1.72×10^{-6}	1.33×10^{-5}	1.33×10^{-5}
Th-IDCZ-Cl-BTh	None	None	-	-	-	-
	None	110°C	-	-	-	-
	OTS	None	-	-	-	-
	OTS	110°C	-	7.61×10^{-9}	-	1.43×10^{-8}

These four compounds were tested as the active material in OFET devices to investigate their electron-transporting properties. The results for these devices are summarized in **Table 3**. During device fabrication optimization, samples on bare silicon or OTS treated silicon were prepared without annealing, and then another batch of these devices were made and annealed at 130°C for 1 h. Most of these devices showed *n*-type semiconducting behavior and gave electron mobility (μ_e) data in the magnitude of ~10^{-5}

cm^2/Vs. The highest average data (5.65×10^{-4} cm^2/Vs) came from the devices which had **Ph-IDCZ-Cl-BTh** as the conducting layer and OTS as the dielectric layer without thermal annealing. This result complied with the observation in GIWAXS that **Ph-IDCZ-Cl-BTh** displayed the most intense diagonal π - π stacking peaks. These values suggested preliminary achievements in the mobility, despite room for further improvements. First, these compounds were only purified by preparative size exclusion chromatography. Vacuum sublimation is a useful tool to increase the purities of samples, and it has been experimentally investigated that purification of organic semiconductors is a critical parameter to guarantee the device performances.[154] In addition, the architecture of devices could be altered to further increase the performances.

3.3 Conclusion

In conclusion, the molecular design and synthesis of four novel molecules featuring multiple B←N coordinate bonds with indolocarbazole core and various aryl groups were achieved. In the synthesis of these molecules, borylation reactions were performed in an efficient manner to rigidify the backbone. The incorporation of B←N coordinate bonds not only restricted the conformation of these molecules but also lowered the LUMO of these molecules to lower than -3.30 eV, which made them promising candidates as *n*-type organic semiconductors. The rigid backbone of these molecules made them easier to form crystalline areas, as suggested by GIWAXS characterizations.

However, the target of designing efficient *n*-type semiconductors has not been fully achieved yet, as the electron mobilities from these molecules were not remarkably high.

As predicted by DFT calculations, the LUMO energy levels of these molecules fell in the range of -3.30eV to -3.70 eV. Although the incorporation of B←N indeed decreased the LUMO energy level, but the strategy alone was not sufficient. It was suggested that a LUMO as low as -4.0 eV would be desirable for *n*-type semiconductor applications.[155] For example, Dr Liu's group employed the same strategy to design molecules which achieved electron mobility as high as 1.60 cm^2/Vs, and their LUMO is extraordinarily low as -4.58 eV.[107] Research regarding incorporation of other organic motifs like isoindigo into the B—N bonded π-system is underway in our lab.

3.4 Experimental Section

3.4.1 General Methods and Materials

Starting materials and reagents were purchased from commercial sources and were used as received without further purification. THF was dried and distilled under nitrogen from sodium using benzophenone as the indicator. Toluene was dried using an inert pure solvent system and used without further treatment. An oil bath was used for those reactions that required heating. 3,9-dibromo-5,11-dihydroindolo[3,2-b]carbazole (**IDCZ**) was synthesized according to previous literature.[152] ^1H and ^{13}C NMR spectra were recorded on a 500 MHz or 400 MHz spectrometer. The ^1H and $^{13}C\{^1H\}$ NMR chemical shifts were reported in ppm relative to the signals corresponding to the residual non-deuterated solvents ($CDCl_3$: ^1H 7.26 ppm, ^{13}C 77.23 ppm) or the internal standard (tetramethylsilane: ^1H 0.00 ppm). The ^{19}F NMR chemical shifts were reported in ppm relative to the signal corresponding to $BF_3{\cdot}OEt_2$ (−153.0 ppm) as the external standard. Abbreviations for

reported signal multiplicities are as follows: s, singlet; d, doublet; t, triplet; q, quartet; m, multiplet; br, broad. The broad singlet at ~1.55 ppm on ^{1}H NMR spectra represents the resonance signal of H_2O in $CDCl_3$. Column chromatography was carried out on a normal phase SiO_2. Preparative size exclusive chromatography (SEC) purifications were performed at room temperature using chloroform as the eluent at a flow rate of 14 mL/min. UV−vis absorption spectra were recorded in a 1.0 cm pathlength cuvette, and the neat solvent was used as baseline. Fluorescence emission spectra were recorded in a 1.0 cm path-length cuvette. The absorption spectra of **Th-IDCZ-BTh**, **Th-IDCZ-Cl-BTh**, **Ph-IDCZ-BTh**, **Ph-IDCZ-Cl-BTh** were recorded at room temperature at concentrations of 3.72×10^{-5} M, 3.55×10^{-5} M, 3.58×10^{-5} M, and 3.45×10^{-5} M respectively. The emission spectra of **Th-IDCZ-BTh**, **Th-IDCZ-Cl-BTh**, **Ph-IDCZ-BTh**, **Ph-IDCZ-Cl-BTh** were recorded at room temperature at concentrations of 3.72×10^{-6} M, 3.55×10^{-6} M, 3.58×10^{-6} M, and 3.45×10^{-6} M respectively. The excitation wavelengths for **Th-IDCZ-BTh**, **Th-IDCZ-Cl-BTh**, **Ph-IDCZ-BTh**, **Ph-IDCZ-Cl-BTh** were set at 640 nm, 625 nm, 681 nm and 699 nm, respectively.

Grazing-incidence wide-angle X-ray scattering (GIWAXS) measurements were carried out in Sector 8-ID-E at the Advanced Photon Source, Argonne National Laboratory.[156] Beamline 8-ID-E operates at an energy of 10.92 keV and the images were collected from a Pilatus 1MF camera (Dectris), with two exposures for different vertical positions of the detector. After flat field correction for detector nonuniformity, the images are combined to fill in the gaps for rows at the borders between modules, leaving dark only the columns of inactive pixels at the center. Using the GIXSGUI package[157] for MATLAB

(Mathworks), data are corrected for X-ray polarization, detector sensitivity and geometrical solid-angle. The beam size was 0.2 mm × 0.02 mm, and the incident angle was 0.14°, the resolution (ΔE/E) was 1×10^{-4}, and the sample detector distance was 217 mm.

Organic field effect transistors were fabricated by spin-coating on bare SiO_2/Si or OTS-modified SiO_2/Si with a bottom-gate/top-contact architecture. Spin-coating of 5 mg/mL solutions in chlorobenzene was done at 1000 RPM for 60 seconds. Then 50 nm Au as source and drain electrodes were deposited on the film by physical vapor deposition and templated by shadow masks with defined channel lengths of 125 μm and widths of 3.00 mm. The OFET characteristics were recorded using Lakeshore CPX-HF Probe Station under vacuum (~10^{-5} mbar). The mobility was calculated by the formula: $I_D = W/2L\mu C_i(V_G - V_T)^2$ where I_{DS} is the drain-source current, W and L are the channel width and length, C_i is the dielectric capacitance, V_G is the gate voltage, and V_T is the threshold voltage.

3.4.2 Synthesis

3,9-dibromo-5,11-dihydroindolo[3,2-b]carbazole (IDCZ). (3-bromophenyl)hydrazine hydrochloride (26 g, 111 mmol) was dispersed in 200 mL EtOH in 1 L flask, and sodium acetate trihydrate was dissolved in 100 mL water then poured into the flask. 1,4-cyclohexanedione (6.42 g, 55 mmol) was dissolved in 50 mL EtOH and added into the 1 L flask by addition funnel dropwise very slowly. Stir the dispersion for an extended period until it became cloudy yellow liquid. 50 mL AcOH was added into the

flask and the reaction mixture was stirred for 1 h at 50 °C and 1 h at 0 °C. Afterwards, the crude product was filtered under vacuum, washed with water and dried in vacuum overnight. The crude hydrazone was added into 75 mL hydrazone and 15 mL sulfuric acid in 250 mL flask at 10 °C. The mixture was allowed to warm up to room temperature and stirred for 10 min. The temperature was then raised to 65 °C and the mixture was stirred for 15 min and cooled down to room temperature to stir for 24 h. Afterwards, the precipitate was filtered and washed with water and methanol and put into boiling methanol for 6 h. The mixture was filtered when hot and dried in vacuum after rained with methanol. The crude product was recrystallized with DMF twice. The final product was collected by filtration under vacuum as pale-yellow powder (1.6 g, 6%). ^{1}H NMR (500 MHz, d_6-DMSO) δ = 11.23 (s, 1H), 8.17 (s mix with d, 2H), 7.62 (d, 1H), 7.26 (dd, 1H).

IDCZ-Boc. IDCZ (0.828 g, 2 mmol) and 4-dimethylaminopyridine (DMAP, 0.733 g, 6 mmol) was dispersed in anhydrous THF under N_2 protection and ice bath, and di-tert-butyl decarbonate (Boc_2O, 1.746 g, 8 mmol) was directly added into the flask slowly. The mixture was allowed back to room temperature naturally and stirred overnight. After the completion of the reaction, solvent THF was removed under vacuum and the solid was washed with methanol to remove impurities. No further purification was required and the product was collected as while powder (1.15 g, 93%). ^{1}H NMR (500 MHz, $CDCl_3$) δ = 11.23 (s, 2H), 8.50 (s, 2H), 7.91 (d, 2H), 7.51 (d, 2H), 1.81 (s, 18H).

IDCZ-Boc-Ph. IDCZ-Boc (94 mg, 0.153 mmol), (4-((2-octyldodecyl)thio)phenyl)boronic acid (200 mg, 0.460 mmol), 2-Dicyclohexylphosphino-2′,6′-dimethoxybiphenyl (SPhos, 6.3 mg, 0.0153 mmol) and $Pd(OAc)_2$ (4 mg, 0.0153

mmol), K_3PO_4 (0.196 g, 0.921 mmol) were mixed in anhydrous 4 mL THF in a Schlenk tube and the mixture was degassed by freeze-pump-thaw with liquid nitrogen three times. Afterwards, the reaction mixture was heated up to 80°C and stirred overnight. After the completion of the reaction, the crude mixture was washed with water and brine solution and extracted by DCM. After the removal of the solvent, the crude product was purified by column chromatography (SiO_2, hexane/CH_2Cl_2 1:1 to 1:9) to afford the product as yellow oil (107 mg, 57%). ^{1}H NMR (500 MHz, $CDCl_3$) δ = 8.93 (s, 2H), 8.56 (s, 2H), 8.10 (d, 2H), 7.62 (d, 4H), 7.60 (d, 2H), 7.43 (d, 2H), 2.97 (d, 4H), 1.86 (s, 18H), 0.86-1.32 (m, 78H). ^{13}C{^{1}H} NMR (100 MHz, $CDCl_3$) δ = 151.43, 140.04, 139.87, 139.06, 137.14, 135.89, 129.24, 127.81, 125.75, 125.65, 122.26, 120.05, 114.97, 107.04, 84.19, 38.66, 37.74, 33.37, 32.08, 32.07, 30.10, 29.85, 29.81, 29.76, 29.52, 29.50, 28.64, 26.71, 22.84, 14.27.

Ph-IDCZ. IDCZ-Boc-Ph (0.178 g, 0.144 mmol) was dissolved in 10 mL anhydrous DCM under ice bath, and 1 mL trifluoroacetic acid was added into the solution dropwise. The solution was stirred for 30 min, and then washed with 1 M NaOH solution and extracted with chloroform. The crude deprotected product was directly used for bromination without further purification. The crude product was dissolved into 4 mL anhydrous THF under ice bath, and freshly recrystallized NBS (49 mg, 0.271 mmol) was added to the solution slowly. The reaction mixture was gradually warmed up to room temperature and stirred overnight. Afterwards, the mixture was washed with water and brine solution and extracted with DCM. The volatile solvent was removed with reduced pressure, and the crude product was purified with column chromatography (SiO_2,

hexane/CH_2Cl_2 1:1 to 1:9) to afford the product as yellow solid (70 mg, 40%). ^{1}H NMR (500 MHz, $CDCl_3$) δ = 8.74 (d, 2H), 8.26 (s, 2H), 7.63 (d, 2H), 7.61 (d, 4H), 7.53 (d, 2H), 7.43 (d, 2H), 2.98 (d, 4H), 0.86-1.33 (m, 78H).

pre-Ph-IDCZ-Cl-BTh. Ph-IDCZ (70 mg, 0.0587 mmol), 5-chloro-2-(tributylstannyl)benzo[d]thiazole (0.162 g, 0.352 mmol), fresh tetrakis (7 mg, 0.00587 mmol) and CuI (1 mg, 0.00587 mmol) were mixed in 2 mL anhydrous toluene and the solution was degassed by freeze-pump-thaw with liquid nitrogen three times. The mixture was stirred at 110°C overnight. Afterwards, the reaction mixture was washed by water and brine and then extracted with DCM, dried over Na_2SO_4. The volatile solvent was removed under reduced pressure. The crude product was with column chromatography (SiO_2, hexane/CH_2Cl_2 1:1 to 1:9) to afford the product as gold-color solid (20 mg, 25%). ^{1}H NMR (500 MHz, $CDCl_3$) δ = 10.12 (s, 2H), 8.15 (d, 2H), 8.13 (d, 2H), 7.92 (d, 2H), 7.49-7.47 (m, 4H), 7.45 (d, 4H), 7.29 (d, 4H), 7.26 (dd, 2H), 2.90 (d, 4H), 1.30-0.86 (m, 78H).

Ph-IDCZ-Cl-BTh. pre-Ph-IDCZ-Cl-BTh (20 mg, 0.0147 mmol) was dissolved in 2 mL anhydrous toluene in a pressure tube in the glovebox, and diisopropylethylamine (0.2 mL) along with $BF_3{\cdot}OEt_2$ (0.4 mL) was added sequentially. The mixture in the pressure tube was heated up to 90°C and stirred overnight. Afterwards, the toluene was removed with reduced pressure, and the crude product was washed with methanol to remove residual salts. Afterwards, the collected solid was further purified by preparative size exclusion chromatography. Due to the low solubility and low amount of the product, the ^{1}H NMR did not yield well-defined peaks. ^{19}F NMR showed a single peak at -134.11ppm indicated the existence of fluoride and its unique chemical environment.

pre-Ph-IDCZ-BTh. **Ph-IDCZ** (110 mg, 0.0913 mmol), 2-(tributylstannyl)benzo[d]thiazole (0.233 g, 0.5479 mmol), fresh tetrakis (11 mg, 0.00913 mmol) , CuI (3 mg, 0.0183 mmol) and CsF (0.139 g, 0.913 mmol) were mixed in 2 mL anhydrous toluene and the solution was degassed by freeze-pump-thaw with liquid nitrogen three times. The mixture was stirred at 110°C overnight. Afterwards, the reaction mixture was washed by water and brine and then extracted with DCM, dried over Na_2SO_4. The volatile solvent was removed under reduced pressure. The crude product was with column chromatography (SiO_2, hexane/CH_2Cl_2 1:1 to 1:9) to afford the product as orange solid (37 mg, 31%). ^{1}H NMR (500 MHz, $CDCl_3$) δ = 10.02 (s, 2H), 8.38 (d, 2H), 8.33 (d, 2H), 8.07 (d, 2H), 7.67-7.65 (m, 4H), 7.59 (d, 4H), 7.55 (d, 2H), 7.39 (d, 4H), 7.34 (d, 2H), 2.94 (d, 4H), 1.30-0.85 (m, 78H).

Ph-IDCZ-BTh. pre-Ph-IDCZ-BTh (36 mg, 0.0284 mmol) was dissolved in 4 mL anhydrous toluene in a pressure tube in the glovebox, and diisopropylethylamine (0.36 mL) along with $BF_3{\cdot}OEt_2$ (0.72 mL) was added sequentially. The mixture in the pressure tube was heated up to 90°C and stirred overnight. Afterwards, the toluene was removed with reduced pressure, and the crude product was washed with methanol to remove residual salts. Afterwards, the collected solid was further purified by preparative size exclusion chromatography.

IDCZ-Boc-Th. **IDCZ-Boc** (0.123 g, 0.2 mmol), tributyl(5-(2-octyldodecyl)thiophen-2-yl)stannane (0.523 g, 0.8 mmol), fresh tetrakis (23 mg, 0.02 mmol) and CuI (4 mg, 0.02 mmol) were mixed in anhydrous 4 mL toluene in a Schlenk tube and the mixture was degassed by freeze-pump-thaw with liquid nitrogen three times.

Afterwards, the reaction mixture was heated up to 120°C and stirred overnight. After the completion of the reaction, the crude mixture was washed with water and brine solution and extracted by DCM. After the removal of the solvent, the crude product was purified by column chromatography (SiO_2, hexane/CH_2Cl_2 1:1 to 1:9) to afford the product as yellow oil (107 mg, 57%). ^{1}H NMR (500 MHz, $CDCl_3$) δ = 8.92 (s, 2H), 8.53 (s, 2H), 8.03 (d, 2H), 7.62 (d, 4H), 7.25 (d, 2H), 6.77 (d, 2H), 2.78i (d, 4H), 1.86 (s, 18H), 0.86-1.27 (m, 78H).

Th-IDCZ. IDCZ-Boc-Th (66 mg, 0.056 mmol) was dissolved in 3 mL anhydrous DCM under ice bath, and 3 mL trifluoroacetic acid was added into the solution dropwise. The solution was stirred for 30 min, and then washed with 1 M NaOH solution and extracted with chloroform. The crude deprotected product along with previous batch (together 0.156 g, 0.158 mmol) was directly used for bromination without further purification. The crude product was dissolved into 6 mL anhydrous THF under ice bath, and freshly recrystallized NBS (50 mg, 0.285 mmol) was added to the solution slowly. The reaction mixture was gradually warmed up to room temperature and stirred overnight. Afterwards, the mixture was washed with water and brine solution and extracted with DCM. The volatile solvent was removed with reduced pressure, and the crude product was purified with column chromatography (SiO_2, hexane/CH_2Cl_2 1:1 to 1:9) to afford the product as yellow solid (103 mg, 57%). ^{1}H NMR (500 MHz, $CDCl_3$) δ = 8.48 (d, 2H), 7.91 (s, 2H), 7.43 (d, 2H), 7.17 (d, 2H), 6.73 (d, 2H), 2.78 (d, 4H), 0.88-1.31 (m, 78H).

pre-Th-IDCZ-Cl-BTh. Th-IDCZ (103 mg, 0.0904 mmol), 5-chloro-2-(tributylstannyl)benzo[d]thiazole (0.249 g, 0.542 mmol), fresh tetrakis (11 mg, 0.00904

mmol) , CuI (1 mg, 0.0452 mmol) were mixed in 2 mL anhydrous toluene and the solution was degassed by freeze-pump-thaw with liquid nitrogen three times. The mixture was stirred at 110°C overnight. Afterwards, the reaction mixture was washed by water and brine and then extracted with DCM, dried over Na_2SO_4. The volatile solvent was removed under reduced pressure. The crude product was with column chromatography (SiO_2, hexane/CH_2Cl_2 1:1 to 1:9) to afford the product as orange solid (70 mg, 56%). ^{1}H NMR (500 MHz, $CDCl_3$) δ = 8.05 (d, 2H), 7.87 (d, 2H), 7.83 (d, 2H), 7.45 (dd, 2H), 7.27 (s, 2H), 7.17 (d, 2H), 6.96 (d, 2H), 6.63 (d, 2H), 2.71 (d, 4H), 1.30-0.85 (m, 78H).

Th-IDCZ-Cl-BTh. pre-Th-IDCZ-Cl-BTh (45 mg, 0.0329 mmol) was dissolved in 4 mL anhydrous toluene in a pressure tube in the glovebox, and diisopropylethylamine (0.45 mL) along with $BF_3{\cdot}OEt_2$ (0.9 mL) was added sequentially. The mixture in the pressure tube was heated up to 90°C and stirred overnight. Afterwards, the toluene was removed with reduced pressure, and the crude product was washed with methanol to remove residual salts. Afterwards, the collected solid was further purified by preparative size exclusion chromatography.

3.4.3 NMR Spectra

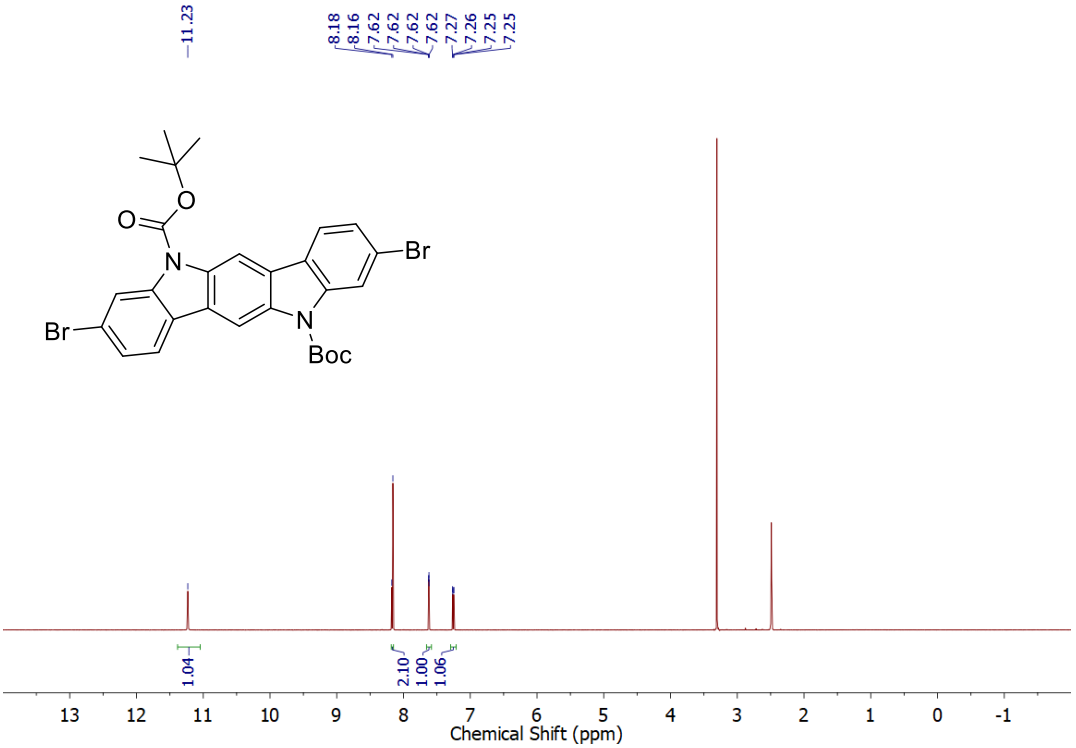

Figure 42. ^{1}H (500 MHz) NMR of IDCZ-Boc in d_6-DMSO at room temperature.

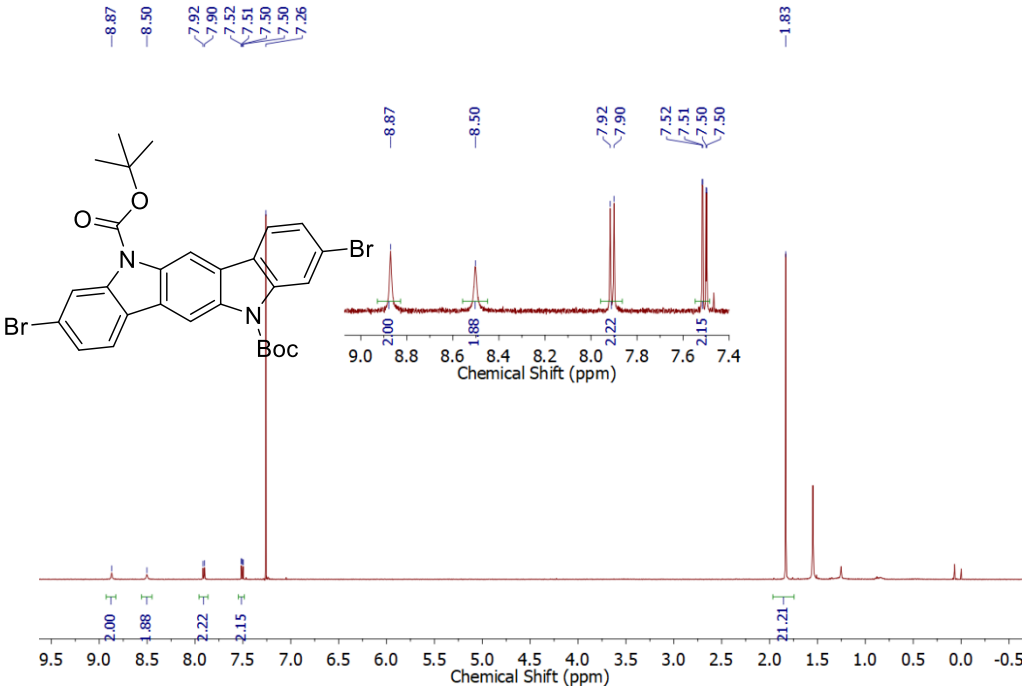

Figure 43. ^{1}H (500 MHz) NMR of IDCZ-Boc in $CDCl_3$ at room temperature.

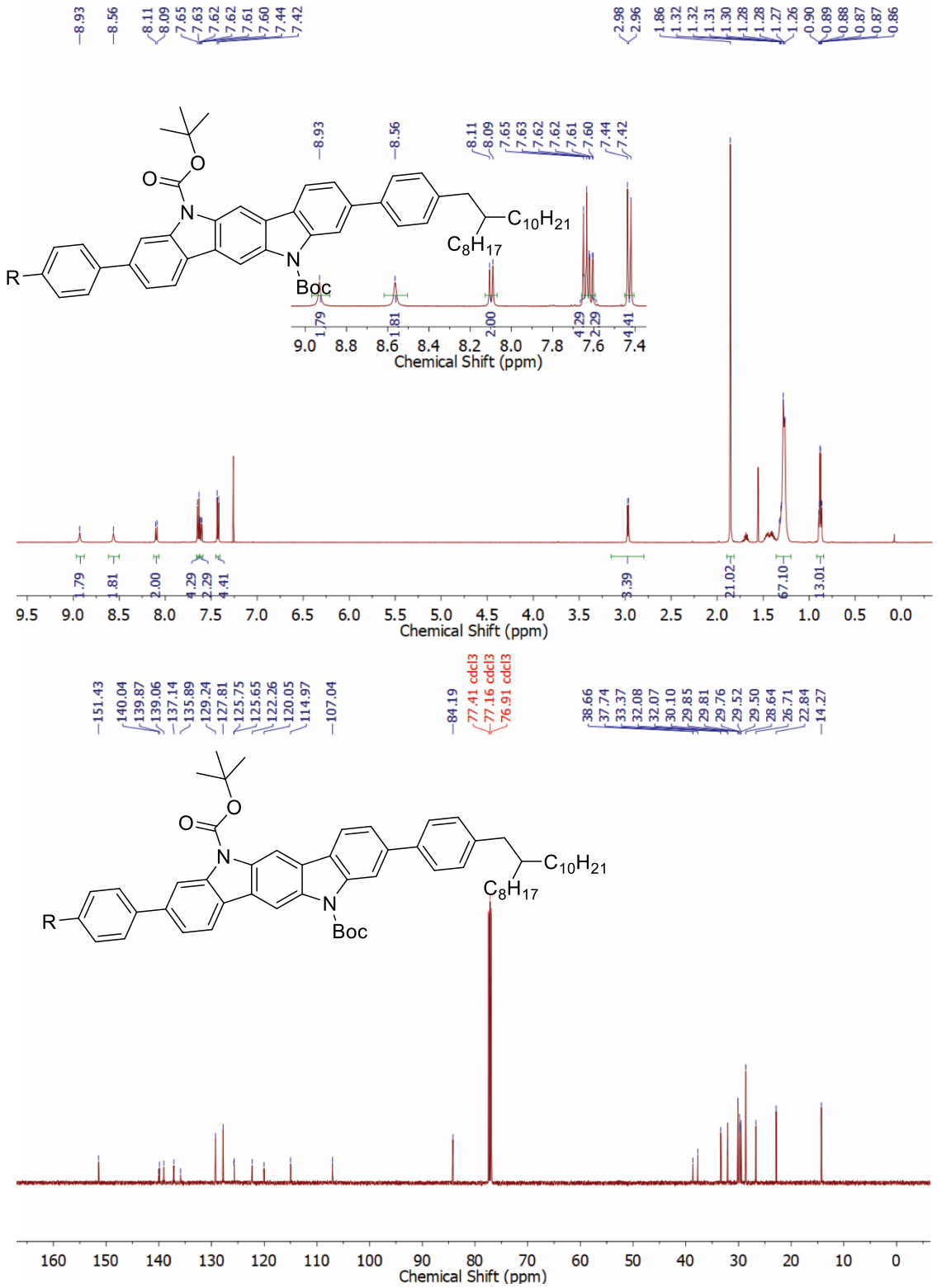

Figure 44. ^{1}H (500 MHz), $^{13}C\{^{1}H\}$ (100 MHz) NMR of Ph-IDCZ-Boc in CDCl3 at room temperature.

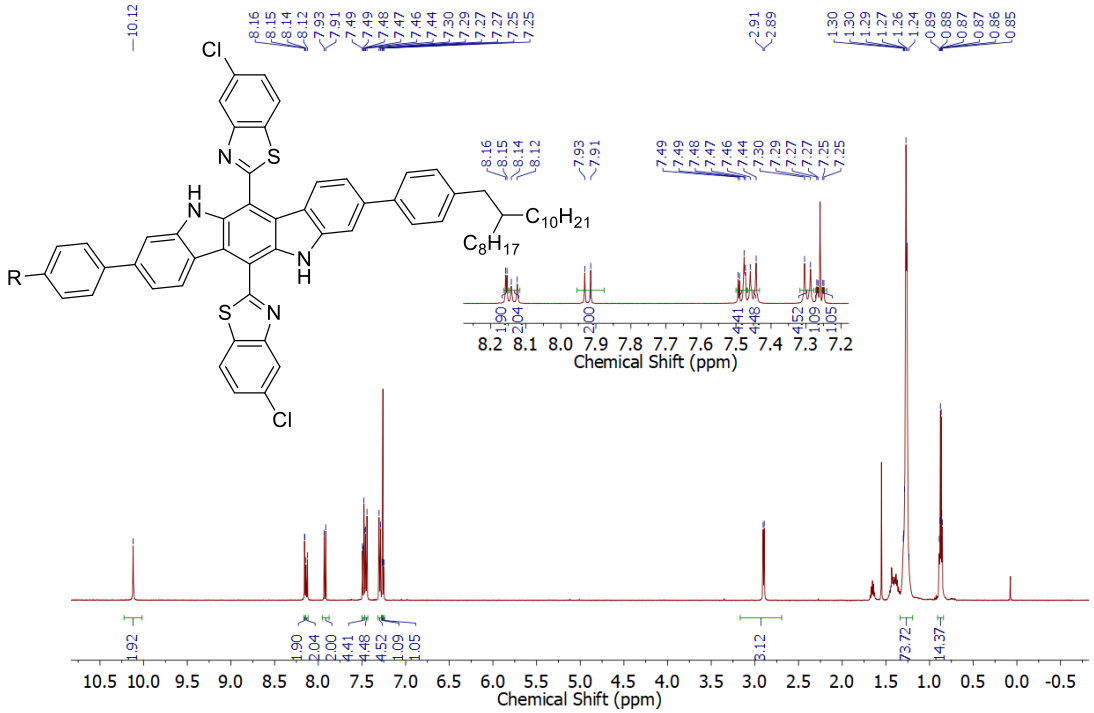

Figure 45. ^{1}H (500 MHz) NMR of pre-Ph-IDCZ-Cl-BTh in $CDCl_3$ at room temperature.

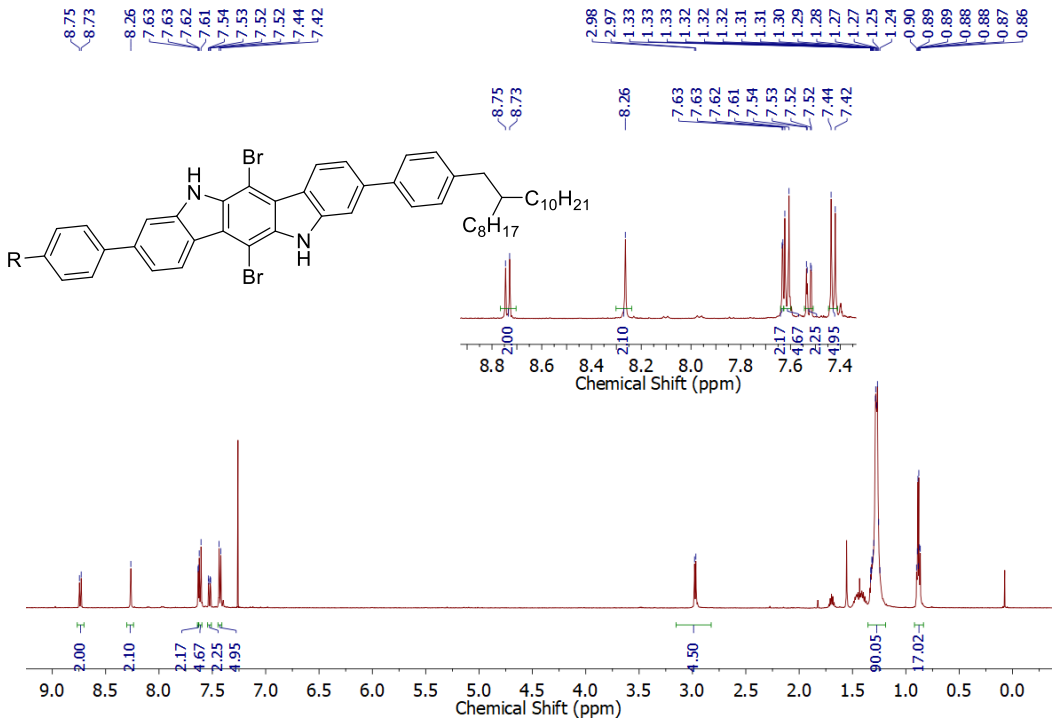

Figure 46. ^{1}H (500 MHz) NMR of Ph-IDCZ in $CDCl_3$ at room temperature.

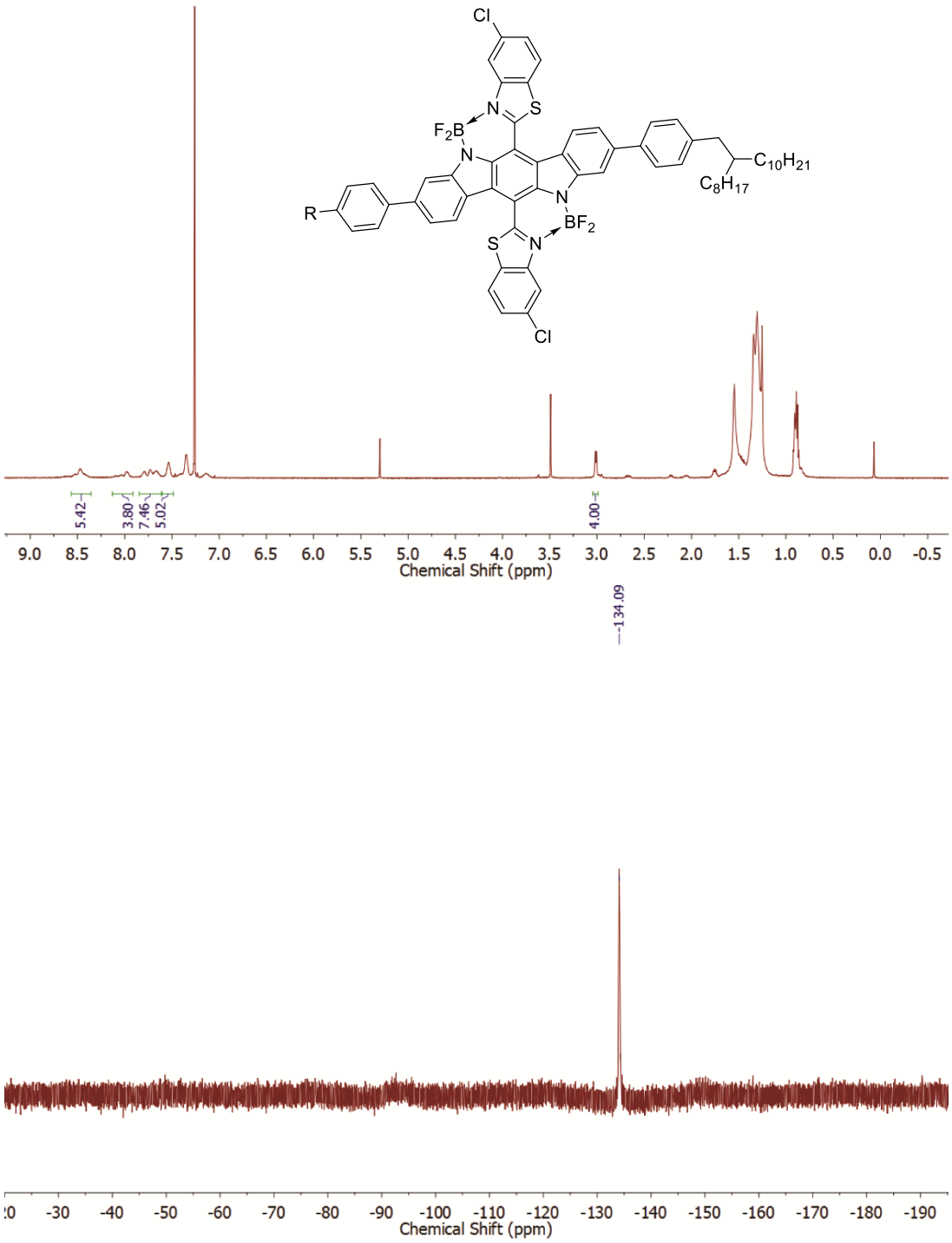

Figure 47. ^{1}H (500 MHz) and ^{19}F (470.4 MHz) NMR of Ph-IDCZ-Cl-BTh in $CDCl_3$ at room temperature.

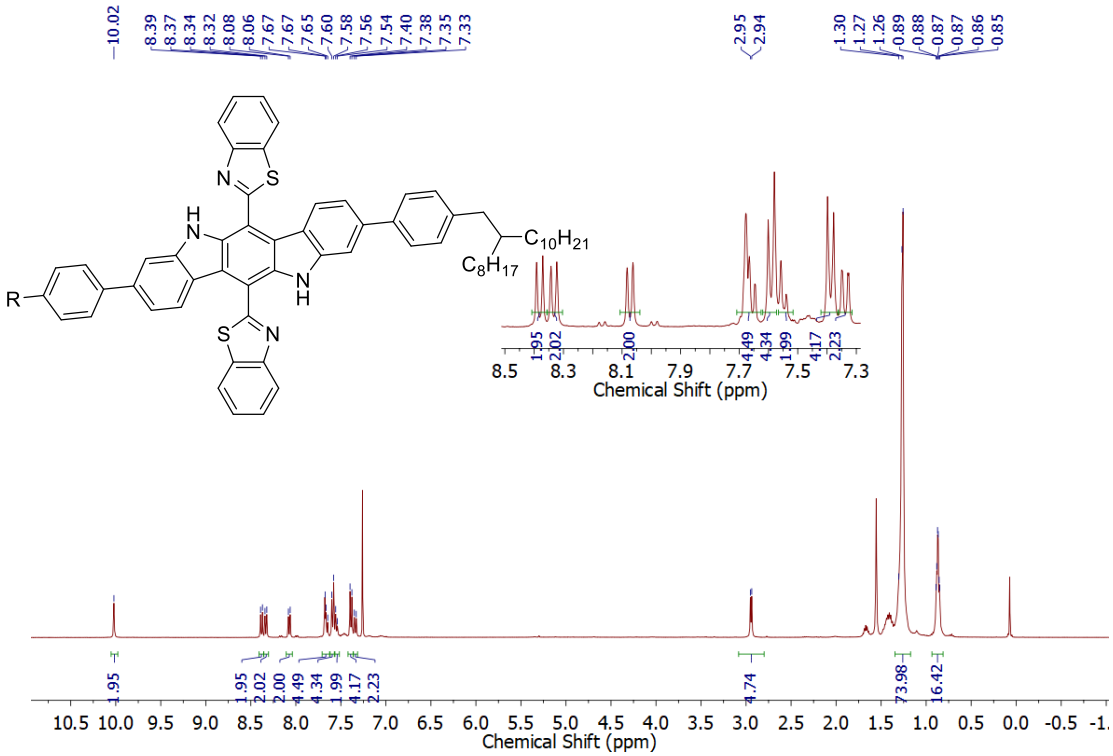

Figure 48. ^{1}H (500 MHz) NMR of pre-Ph-IDCZ-BTh in $CDCl_3$ at room temperature.

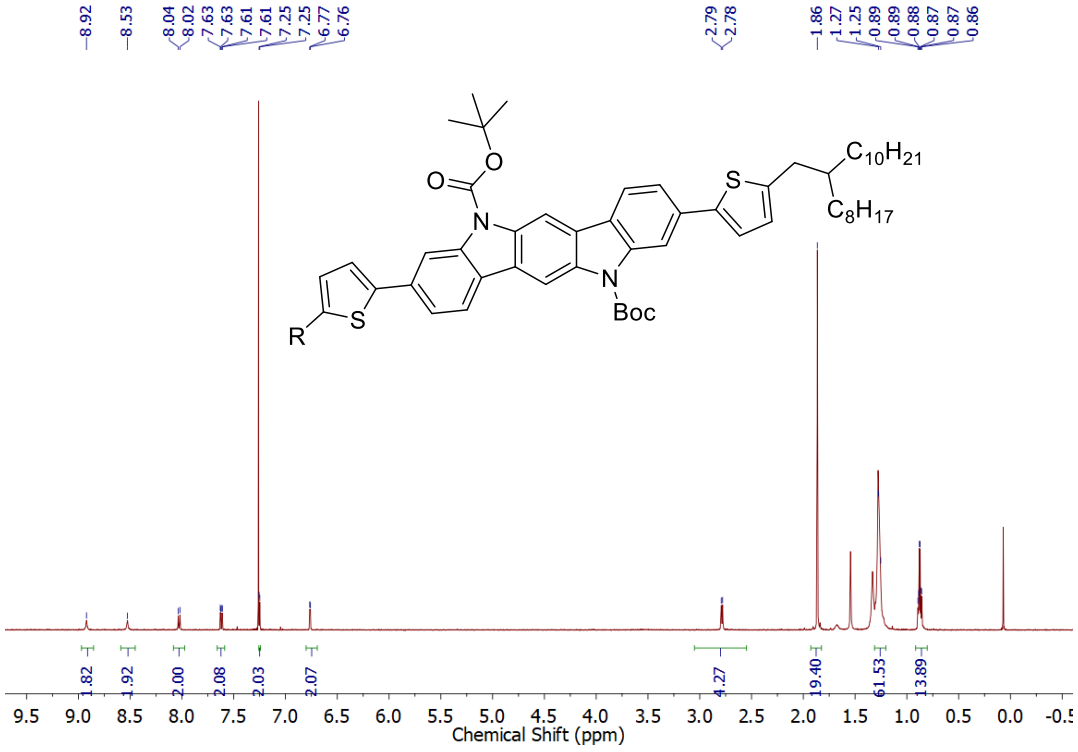

Figure 49. ^{1}H (500 MHz) NMR of IDCZ-Boc-Th in $CDCl_3$ at room temperature.

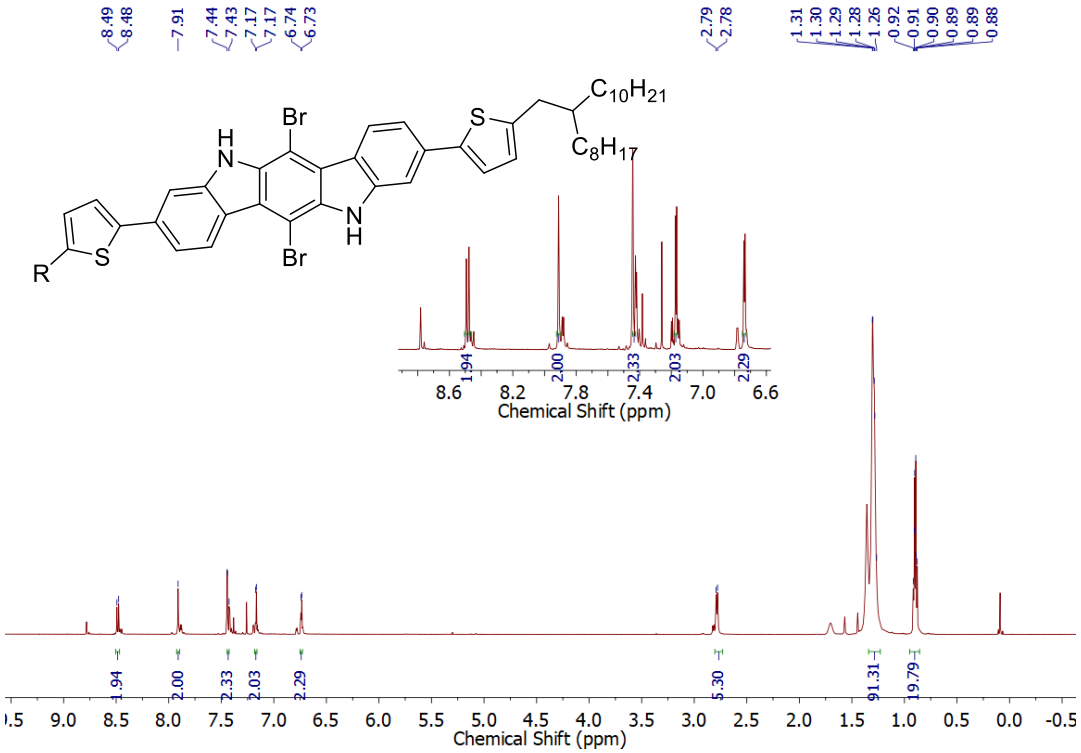

Figure 50. ^{1}H (500 MHz) NMR of Th-IDCZ in $CDCl_3$ at room temperature.

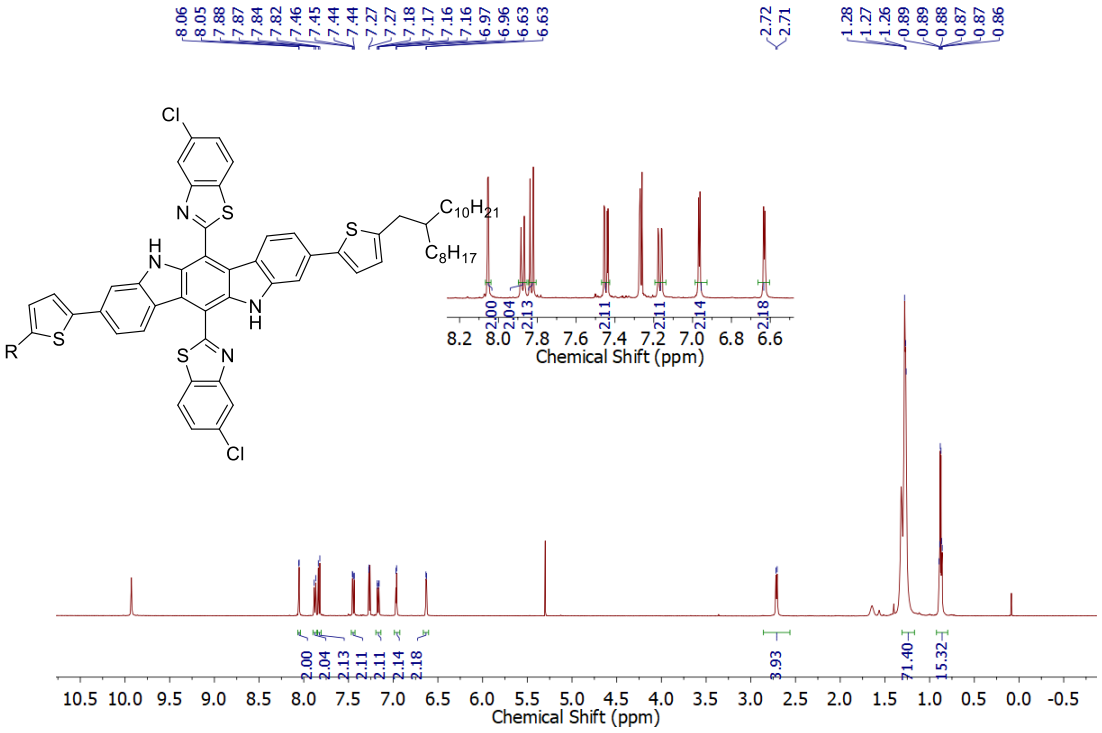

Figure 51. ^{1}H (500 MHz) NMR of pre-Th-IDCZ-Cl-BTh in $CDCl_3$ at room temperature.

3.4.3 UV-Vis Absorption and Fluorescence Emission

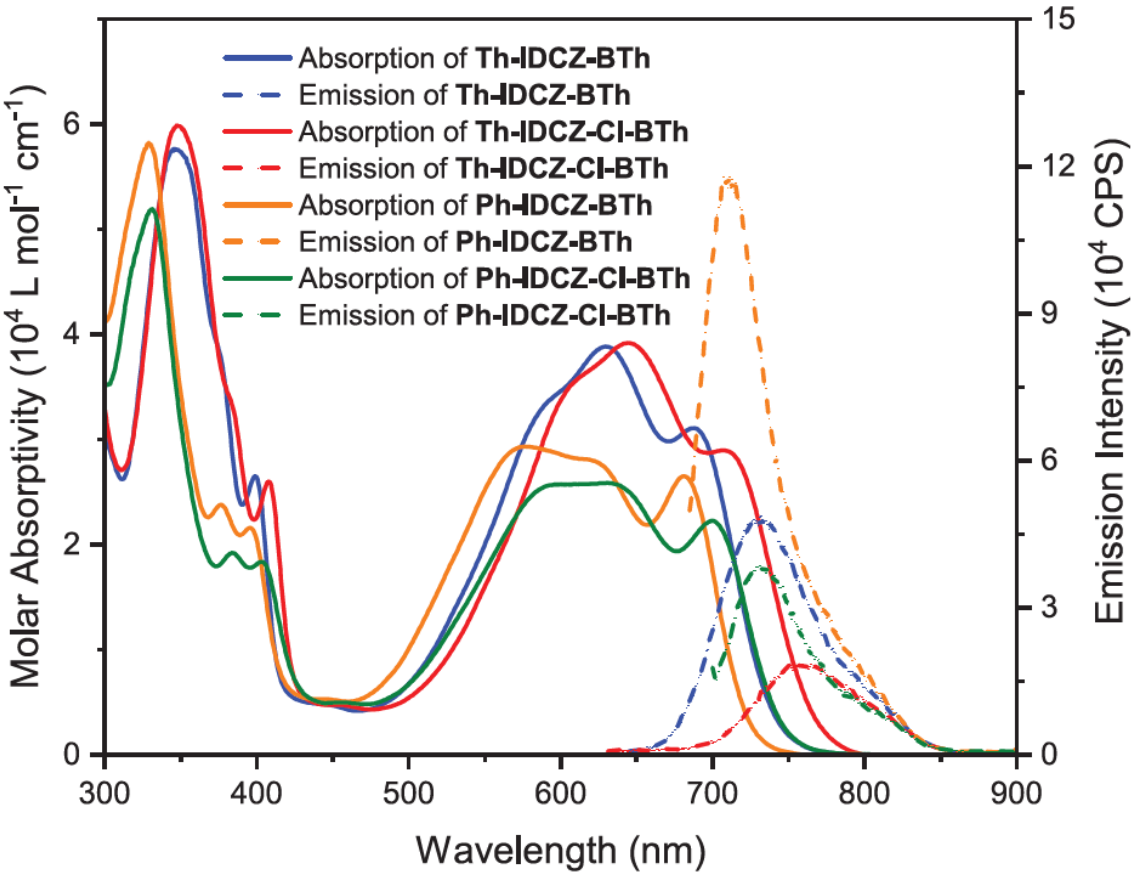

Figure 52. UV-Vis and fluorescence emission spectra of the four compounds Ph-IDCZ-Cl-BTh, Ph-IDCZ-BTh, Th-IDCZ-Cl-BTh and Th-IDCZ-BTh.

CHAPTER IV SYNTHESIS AND SUPRAMOLECULAR CHEMISTRY OF CENTRIPETAL AZA-POLYCYLIC COMPOUNDS

4.1 Introduction

Helicenes are defined as polycyclic aromatic compounds with nonplanar screw-shaped skeletons formed by ortho-fused benzene or other aromatic rings.[158-160] Dated back to the discovery of first helicenes in 1903,[161] the development of helicenes witnessed a quick surge after the late 1990s. More and more novel strategies for the synthesis of helicenes with good yields and enantioselectivities have been developed, thanks to the wide employment of organometallic catalysts.

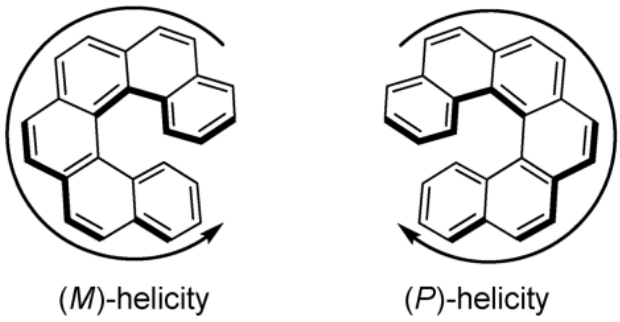

Figure 53. Schematic representation of helicity. From "Helicenes: Synthesis and Applications", by Yun Shen and Chuan-Feng Chen, *Chem. Rev.* 2012, *112* (3), 1463-1535.

A defining property of helicenes is its intrinsic chiral structure due to the lack of *Sn* symmetry. Helicenes wind in opposite directions to form helical structures and distort the backbone to mitigate the hindrance between terminal groups. Such a structural feature confers to this family of compounds chirality and therefore, chiroptical properties. According to the helicity rule proposed by Cahn, Ingold and Prelog in 1966, a left-handed helix is assigned "minus" and denoted by **M** whereas the opposite is assigned as "plus" and denoted by **P**.[162] In addition, on account of the nonplanar structural distortion, the solubility of helicenes is often higher than that of their planar counterparts due to the weaker π-π stacking.[163] To enhance the configurational stability of helicenes, bulky substituents on the terminal rings are often introduced to hinder the racemization process by increasing the corresponding barrier.[164]

Due to the special chiral feature and its functionalization versatility, helicenes have been perceived as potential ligands or chiral auxiliaries to promote stereoselective transformations. In one example, [5]helicenylphosphine served as chiral ligands to catalyze allylic substitution reactions to achieve high yield and stereoselectivity.[165] The mechanism underlying the high stereoselectivity was elucidated by DFT simulations demonstrating that enantiopure helicene ligand transferred the chirality to the metal center to favor one direction of nucleophilic attack on the allylic motif. Besides helicene phosphine ligands,[166,167] there have been reports on helicene alcohols[168] and azahelicenes,[169-171] along with their respective catalysis applications.

Despite these attractive catalytic applications, the promising chiral cavity has not been thoroughly exploited. Previously reported helicene ligands only have the

catalytically-active heteroatoms located on one specific site. However, the persistent central cavity of helicene molecules often remained unfunctionalized. From a broader perspective beyond helicenes, most reported polycyclic aromatic compounds had heteroatoms decorated on the outer rim,[56,172-175] and it is more challenging to achieve structures with heteroatoms decorating the inner pocket. I designed centripetal azahelicenes where the yellow spots are functionalized with nitrogen atoms, as shown in **Figure 54**. Every pair of adjacent nitrogen atoms mimicked the organization of the common ligand phenanthroline. It is envisioned here that these molecules will function as remarkable ligands binding with metal ions and other guest molecules. Another benefit of these ligands is that the configurational stability owing to the rigid helical backbone will be transferred to the metal center, forming enantiopure metal complexes.

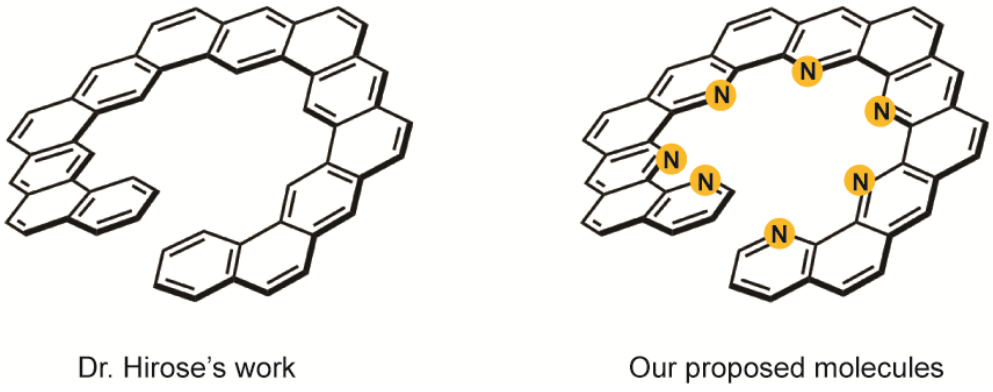

Figure 54. Schematic representation of Dr Matsuda's work and our proposed novel molecules.

A potential underlying challenge is the lack of effective synthetic methods to realize these electron-deficient structures. Despite the many annulation methods available to achieve polycyclic aromatic compounds, most of these methods work efficiently only on electron-rich substrates. Ring closing metathesis (RCM) was selected as the major strategy to fuse the backbone of the desired helicenes. The RCM reaction is advantageous for these purposes because its nature of thermodynamic control promotes high conversion to stable products, and allows for "error-checking" and "proof-reading" through reversibility.[176,177] Earlier, we achieved nearly quantitative conversions of RCM in a number of challenging scenarios, including the synthesis of defect-free ladder polymers[152,178,179], as well as annulation of polymer networks in the solid state[180] and in suspended nanoparticles[181]. In an earlier paper by Dr Hirose's group, RCM was successfully employed as the key strategy to construct the fully fused backbone of a non-nitrogen carbo-helicene composed of 13 rings.[182]

4.2 Molecular Design and Simulation

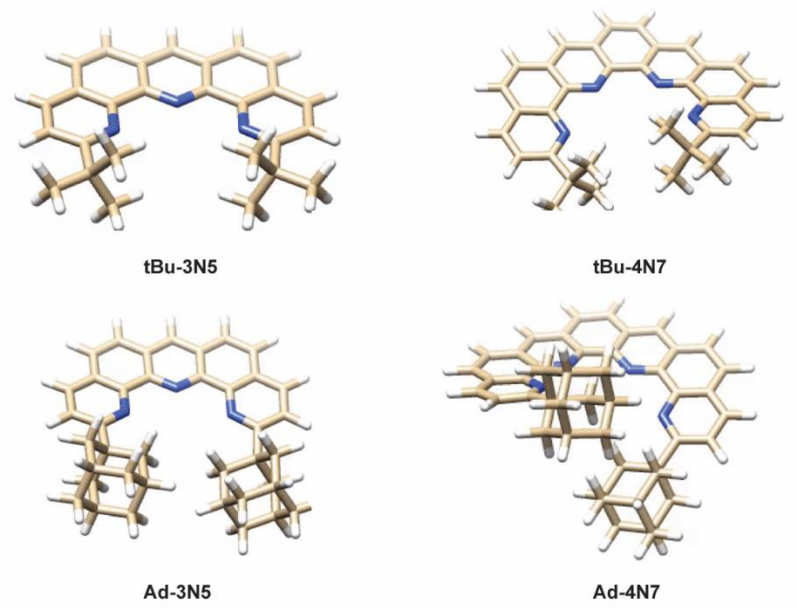

Figure 55. DFT simulation of centripetal azahelicenes with -tBu and -Ad as the terminal end group [B3LYP/6-31G].

Before moving on to the synthesis of these proposed molecules, DFT simulations (B3LYP/6-31G) were carried out to understand the correlation between the geometry, the size of the molecules and the bulkiness of the terminal end groups. The optimized geometry was demonstrated in **Figure 55**. It was elucidated that the geometry was closely related to the number of rings in the system and the bulkiness of terminal end groups. The helical conformation was formed with the increased number of rings and the bulkiness of terminal groups. For example, the molecule **tBu-3N5** was predicted to be fully coplanar whereas

the molecule **Ad-4N7** had a significantly contorted backbone due to the crowdedness by two proximate adamantyl groups. To reduce the number of rings required to form the helical conformation, it was decided to start from the molecules with -Ad as the terminal bulky group.

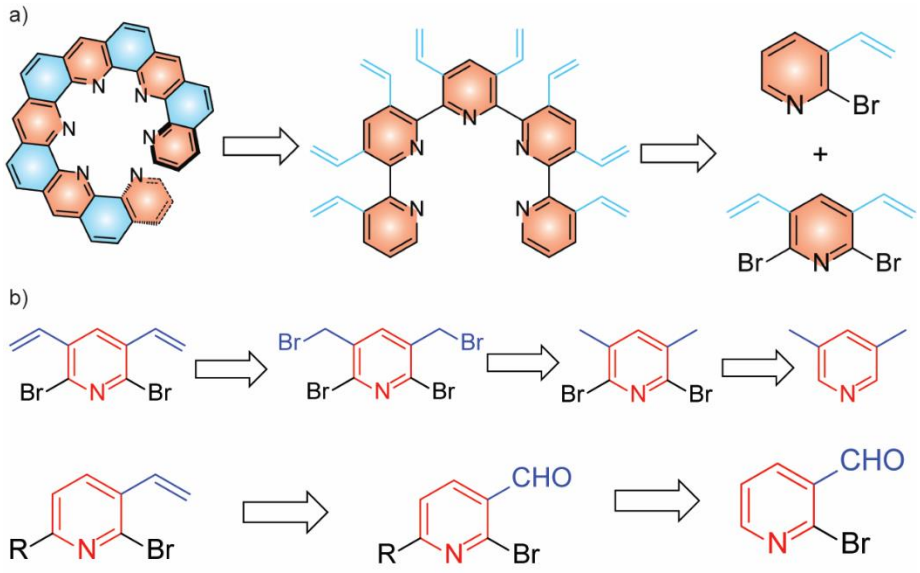

Figure 56. Retrosynthesis of a) the backbone and b) the building blocks of the proposed molecules.

In a retrosynthetic analysis for the target azahelicene molecules (**Figure 56**), the blue rings of the backbone are annulated via RCM reactions, and the precursors with pendant double bonds are achieved via cross coupling from two kinds of building blocks. For the central building blocks with two vinyl groups, those two double bonds come from

bromomethyl groups via Wittig olefination. Next, these two bromomethyl groups are generated via radical bromination on methyl groups. Finally, the two bromide atoms on the pyridine ring can be installed via electrophilic substitution. On the other hand, the double bond on the terminal building block comes from an aldehyde group via Wittig olefination. Next, the terminal alkyl group, either tert-butyl group or adamantyl group, is installed onto the pyridine ring, taking advantage of the Minisci radical alkylation reaction. Thus far, the designed molecules have been traced back to widely available materials, from which we would implement our synthesis.

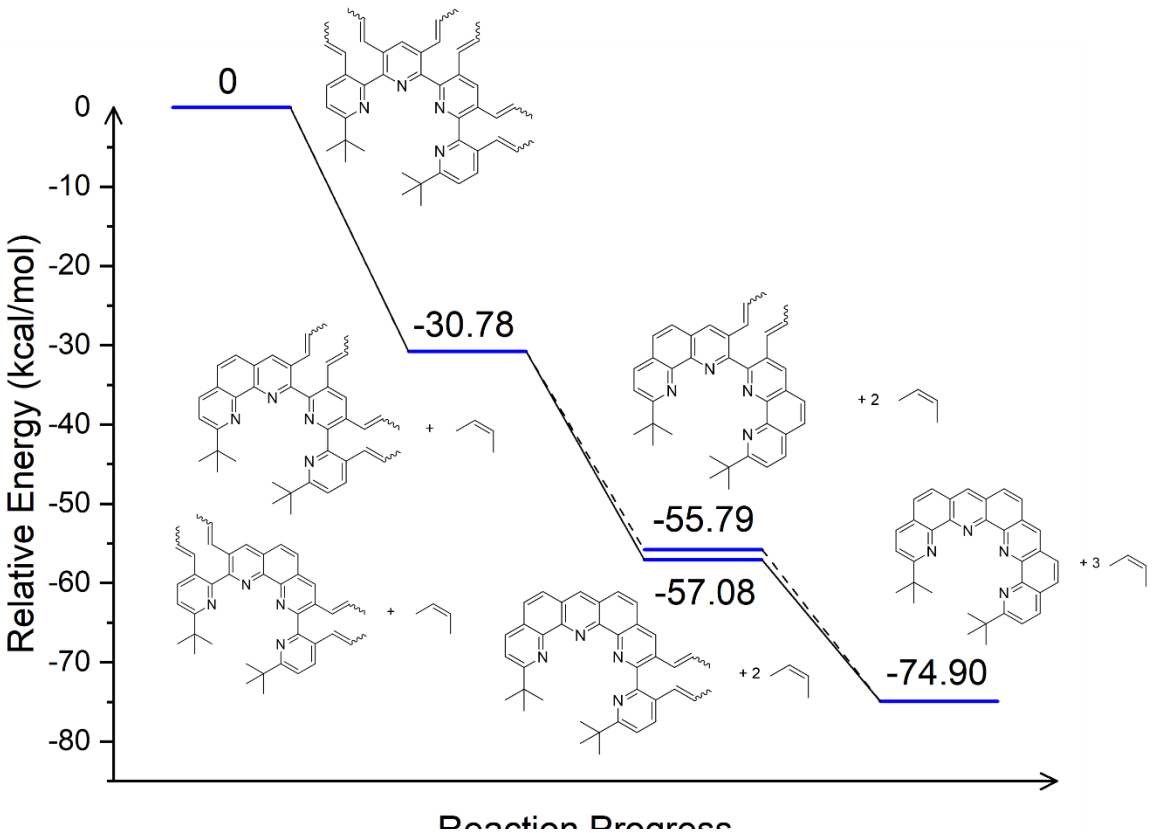

Figure 57. Reaction coordinate diagram of the RCM step on the tetramer precursor substrate.

To verify the feasibility of the employment of RCM in the final step, simulation on the reaction energy profile was performed to understand the thermodynamical favorability. Assigning the free energy of the starting material as zero, the relative energy levels of the intermediates with one, two and three rings annulated were computed and summarized in **Figure 57**. The benefit due to each ring closure was 30.78, 25.01 and 19.11 kcal/mol respectively, giving an overall energetic favorability of -74.90 kcal/mol. This implied that the final product was as hypothesized significantly lower in free energy compared to the starting material so that RCM should be directed to the desired final product. However, the marginal benefit to close more rings was predicted to decrease presumably due to the stronger strain accompanied by the longer backbone.

4.3 Results and Discussion

4.3.1 Preliminary Attempts

The conditions towards those building blocks were first optimized according to the retrosynthesis discussed above. First, the commercially available starting material **C1** was subjected to electrophilic substitution under harsh conditions, with oleum being the solvent and liquid bromine being the bromide source at an elevated temperature and extended reaction time to get brominated pyridine derivative **C2**. Afterwards, radical bromination was applied to the two methyl groups on **C2** using NBS as the bromide source and benzoyl peroxide as the radical initiator. This step afforded intermediate **C3** which featured two bromomethyl groups. In the last step, the two bromomethyl groups were converted to

corresponding phosphonium salt, which was later subjected to Wittig reaction under basic conditions to afford the desired building block **v-Br1Br** with two pendant vinyl groups.

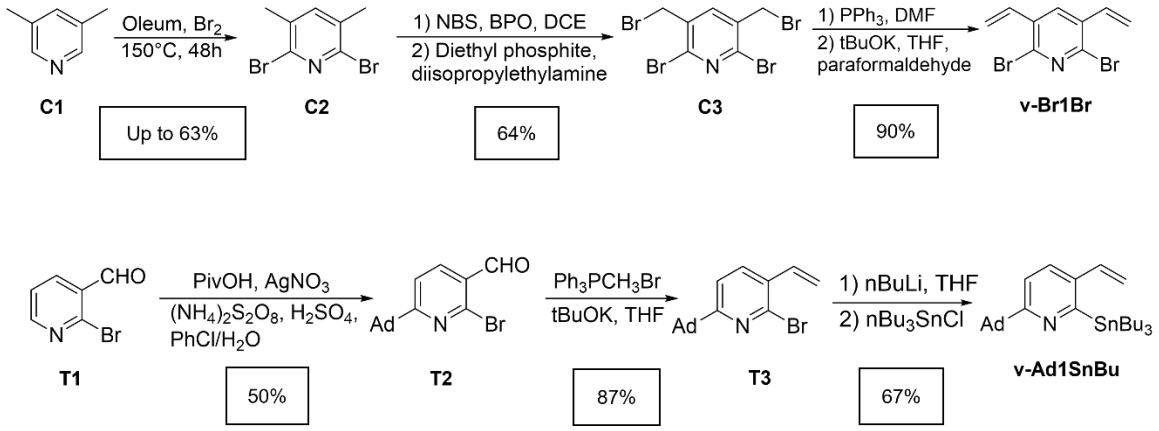

Figure 58. Synthetic scheme of preliminary synthetic attempts towards building blocks v-Br1Br and v-1SnBu.

On the other hand, the synthesis of terminal building block started off from **T1**. **T1** was subjected to Minisci radical alkylation to install the adamantyl group onto the pyridine ring to form **T2**. In this reaction, the aliphatic acid was used as the source of alkyl group and was required to form the corresponding radical steadily. **T2** reacted with methylphosphonium bromide under basic conditions to convert the aldehyde group to vinyl group and produce **T3**. **T3** further underwent lithium exchange reaction with n-butyllithium and stannylation to generate stannylated intermediate **v-Ad1SnBu**. All these

steps to synthesize building blocks have been optimized to show efficient yields (**Figure 58**).

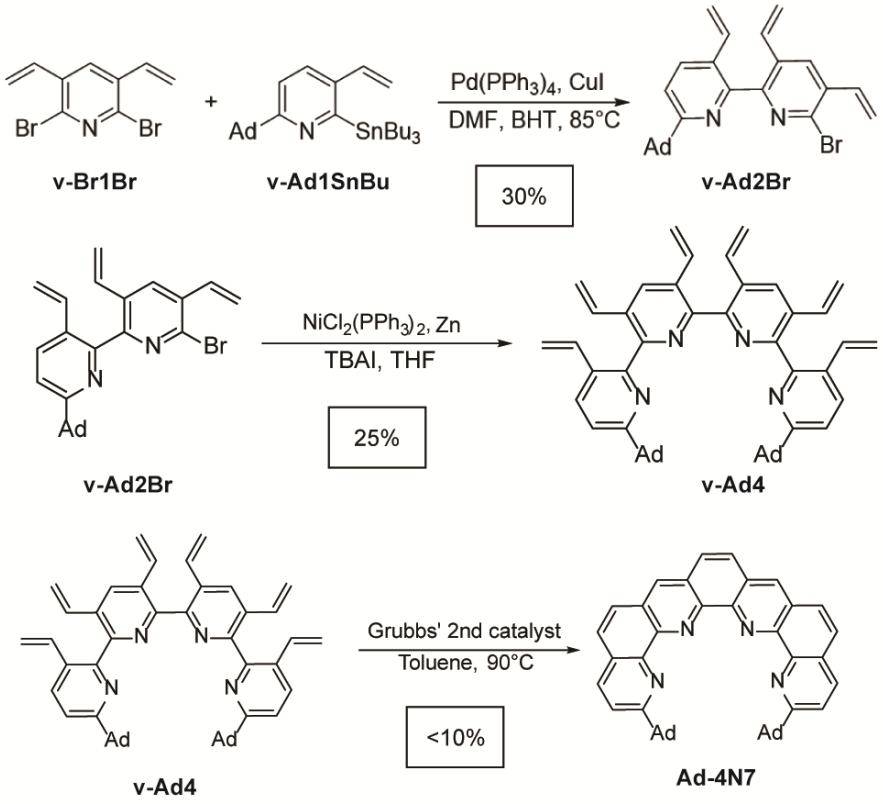

Figure 59. The synthetic scheme towards oligomer v-Ad2Br, v-Ad4 and final product Ad-4N7 with Stille coupling, oxidative homocoupling and ring closing metathesis.

Following the successful synthesis of **v-Br1Br** and **v-Ad1SnBu**, Stille reaction was carried out to couple them together. For the Stille coupling, extensive screening on reaction

conditions, including catalyst, ligand, solvent, temperature *etc.*, were conducted for optimization. Out of various combinations, it was found that the best combination of $Pd(PPh_3)_4$/CuI in DMF at 85°C offered the brominated dimer **v-Ad2Br** in a 30% yield. Next, **v-Ad2Br** was subjected to nickel-catalyzed oxidative homocoupling to get **v-Ad4**. $NiCl_2(PPh_3)_2$ was employed as the precatalyst, and was reduced to Ni(0) *in situ* to form the active catalytic species. Afterwards, the backbone of the precursor **v-Ad4** was annulated with ring closing metathesis to get the desired final product **Ad-4N7** (**Figure 59**, **60**).

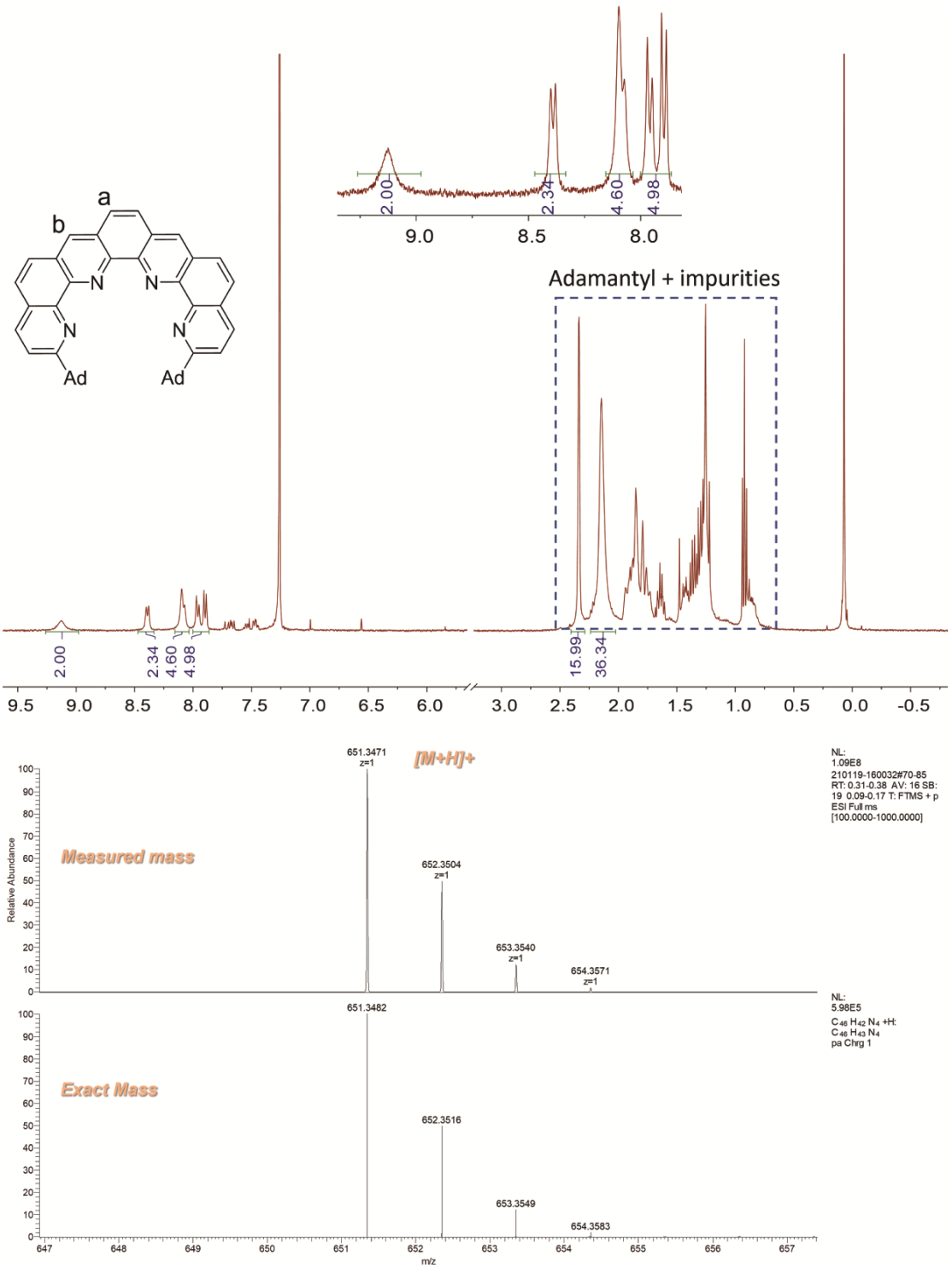

Figure 60. ^{1}H NMR spectrum in $CDCl_3$ and ESI mass spectrum of Ad-4N7.

Grubbs' 2nd generation catalyst was utilized as the catalyst, and an elevated temperature at

90°C was used to promote the complete conversion. It is noteworthy that due to the known thermal instability of Grubbs' 2nd generation catalyst,[183] the solution of the catalyst had to be injected into the reaction mixture dropwise to guarantee activity of the catalyst at the high reaction temperature.

Table 4. Strain analysis of the backbone of azahelicenes 3N5, 4N7, 5N9, 6N11.

Compound	Strain-free hypothetical energy (kcal/mol)	Calculated energy(kcal/mol)	Strain (kcal/mol)
Triaza[5]helicene (3N5)	6.10	6.10	0
Tetraaza[7]helicene (4N7)	6.10 / 2 * 3 = 9.15	10.32	1.17
Pentaaza[9]helicene (5N9)	6.10 / 2 * 4 = 12.20	15.53	3.33
Hexaaza[11]helicene (6N11)	6.10 / 2 * 5 = 15.25	20.95	5.70

Despite the success of these oligomerization and ring closing metathesis steps, there remains room for improvement in each of these steps. In the Stille coupling above, both the reactivity and conversion were low. The yield was only 30%, and a significant amount of the unreacted central building block was recovered. Besides, the building block **v-Ad1SnBu** had a similar polarity and size to the desired dimer **v-Ad2Br**, which made it

difficult to purify with either flash chromatography or prep GPC. More challenges were identified as the **Ad-4N7** product quickly decomposed even when stored in the freezer. This instability was presumably attributed to the high strain brought about by the bulky -Ad groups. Simulation on the strain of the backbone without any substituent was conducted to understand the intrinsic strain from the backbone (**Table 4**).

It could be seen from the table above that the strain values due to the extended backbone were 1.17, 3.33 and 5.70 kcal/mol respectively. These low strain values implied that the intrinsic strain alone due to the backbone should not hinder the synthesis. The instability of the synthesized **Ad-4N7** was inferred due to the extremely bulky adamantyl terminal group. Thus, in our next round of synthetic attempt, -Ad was changed to -tBu to alleviate the undesired high strain.

4.3.2 Synthesis Modification on Oligomerization

To address the difficulties mentioned above, the intermediate structures and synthetic strategies were modified accordingly (**Figure 61**). First, regarding the low reactivity of the Stille coupling, the tributylstannyl group on **v-tBu1SnBu** was changed to the trimethylstannyl group to form **v-tBu1SnMe**. The smaller size of the surrounding alkyl group was expected to favor the approaching of organotin compound to the palladium complex in the transmetalation step.[184] In addition, the vinyl groups were replaced by propenyl groups to suppress the potential Heck reaction and binding from the olefin to palladium center.

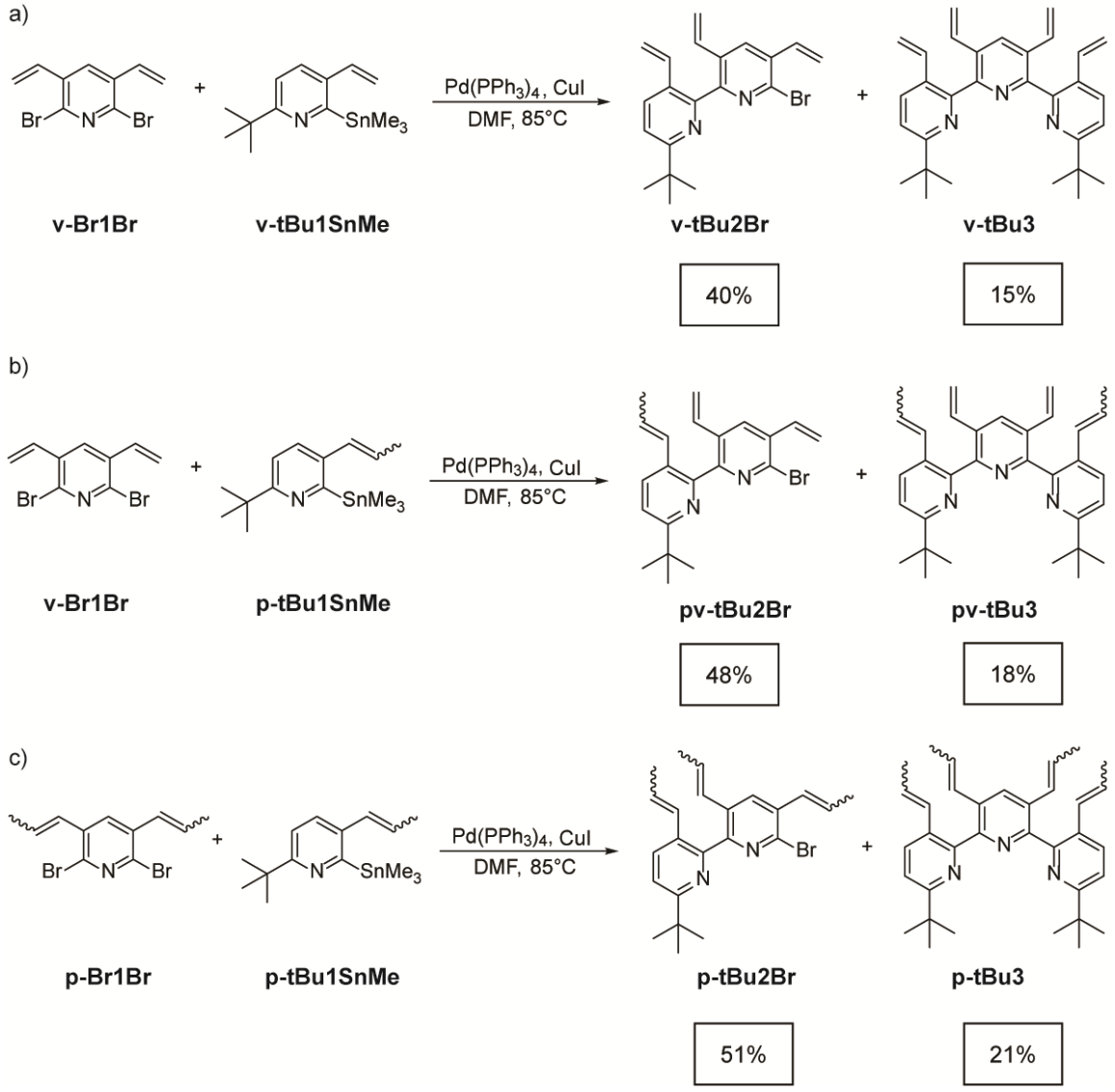

Figure 61. Synthetic scheme and their respective yields after a) changing -$SnBu_3$ to -$SnMe_3$ on stannyl compound in Stille coupling, b) changing the vinyl group on the terminal building block to propenyl group and c) changing the vinyl group on both the terminal and central building block to propenyl group.

As a result of such modifications, significant improvements have been witnessed in the synthesis of these oligomeric intermediates. First, as hypothesized, changing the

tributylstannyl group to the trimethylstannyl group increased the yield by about 10%, demonstrating stronger activity of -$SnMe_3$ group. Next, upon changing the vinyl group on the terminal building block, the efficacy of the reaction was moderately increased to about 48%. This was believed due to the extra methyl group that hampered binding between the olefin and the palladium center. Electronically, the slightly higher electron density of propenyl elevated the LUMO energy level, which prevented π-backdonation from d-orbital of palladium to olefin.[185] Sterically, The larger steric hinderance due to the extra methyl group rendered the association harder. In a combination of these two factors, the undesired association between palladium and olefin was suppressed, so that the reductive elimination was facilitated. In addition, the possibility of Heck reaction that competes against Stille coupling was reduced with the attachment of methyl groups on the double bonds.[186] Based on such improvement, the vinyl groups on the central building block were also changed into propenyl groups, but this time only slight improvement of up to 3% was recorded.

Gratifyingly, the oxidative homocoupling in the next step was improved as well, as shown in **Figure 62**. It is hypothesized that the weaker binding between olefin and palladium was the key reason for the higher efficiency by facilitating the generation of vacant sites for oxidative addition.[187,188] In the final RCM step, the product **tBu-4N7** was afforded with a yield lower than 30% with some impurities. The unidentified peak on the NMR spectrum was deduced to belong to impurities from decomposed Grubbs' catalyst, which failed to be conveniently separated from the desired product. As expected, this molecule was more stable than the counterpart with -Ad as the bulky group, which implied milder strain in the backbone.

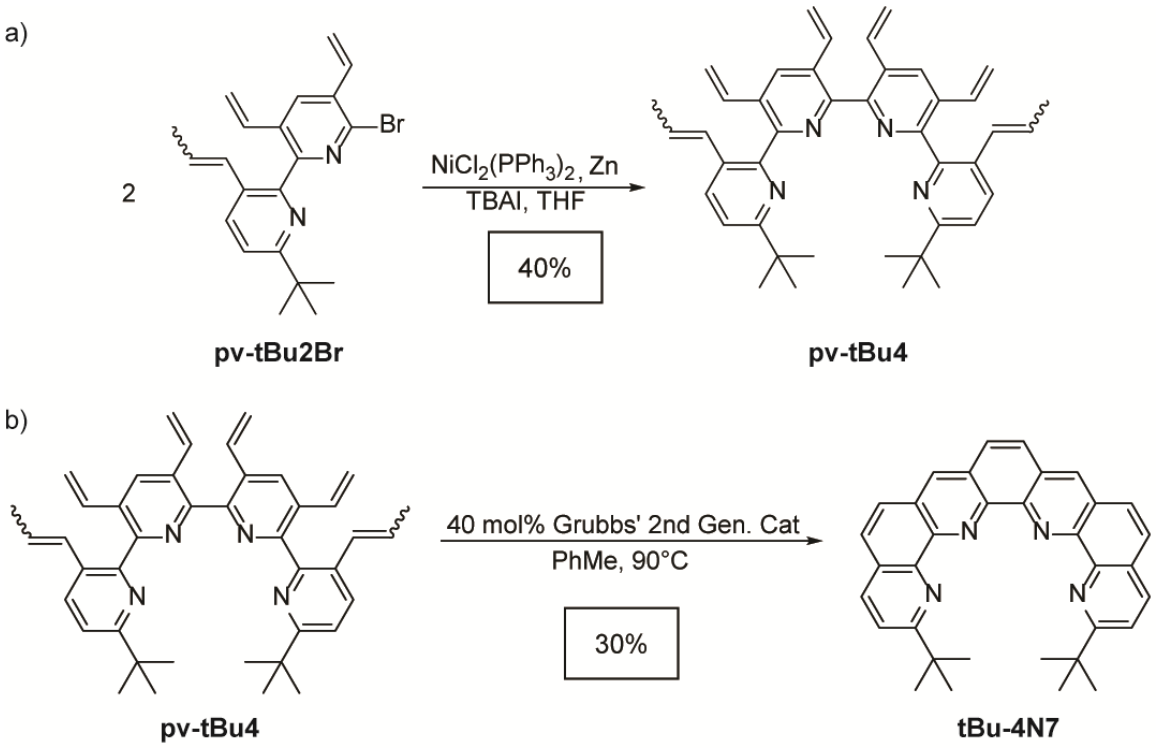

Figure 62. Synthetic scheme of a) oxidative homocoupling and b) RCM step after terminal group was changed to -tBu and the vinyl group on the terminal building block was changed to propenyl.

Another puzzle to solve is the low reproducibility of the oxidative homocoupling, likely due to the heterogeneous nature of this reaction. Despite the ultrasonication employed to guarantee the complete mixture between the solid zinc powder and $NiCl_2(PPh_3)_2$ crystals, the yield of this reaction fluctuated significantly from no conversion to around 40%. From the NMR spectrum, the major side product was the de-brominated product, which implied a reductive elimination process to form a new C—H bond, but it remained unknown where the hydrogen came from. More detailed mechanistic studies

needed to be conducted to gain a deeper insight into the reason for the fluctuations in this reaction. To overcome this issue, we decided to take a detour and utilize the iterative stannylation-Stille strategy. Although it took one more step than direct oxidative homocoupling, it allowed more versatility to achieve longer helicenes instead of that composed of four pyridine rings.

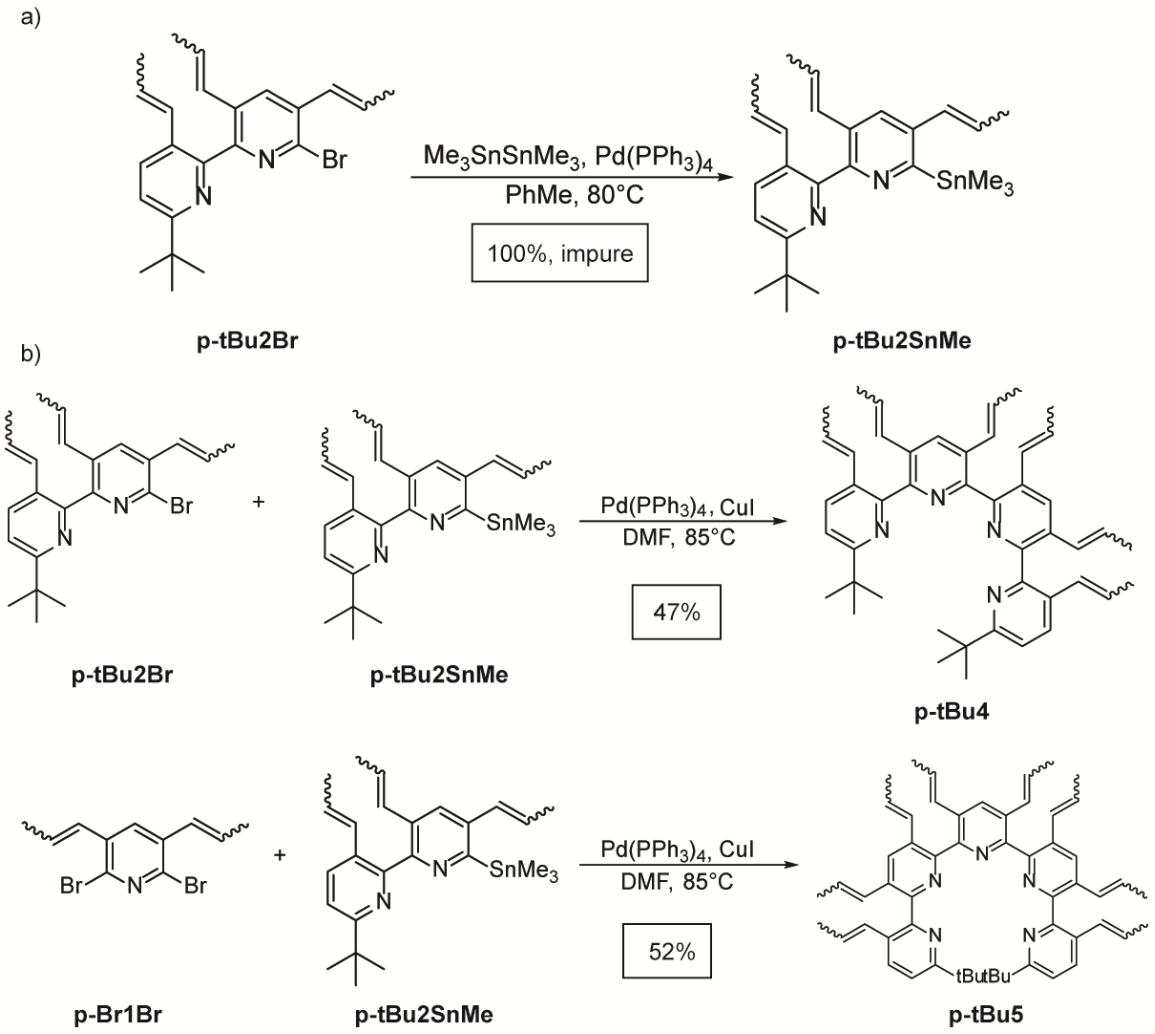

Figure 63. Synthetic scheme of a) palladium catalyzed stannylation, b) Stille coupling between brominated dimer p-tBu2Br and stannylated dimer p-tBu2SnMe and c) backbone extension to obtain the precursor p-tBu5 with five pyridine rings.

At the first attempt, the lithium exchange method was utilized to realize the stannylation, but only unidentified side products similar in size to one pyridine ring were obtained, which suggested the cleavage of the C—C bond between two pyridine rings. Consequently, focus was shifted to palladium-catalyzed stannylation method (**Figure 63**). It turned out that $Pd(PPh_3)_4$ alone was powerful enough to realize this transformation, and the semi-pure product **p-tBu2SnMe** was used directly in the next step Stille coupling with **p-tBu2Br** without further purification. The overall yield of two steps to get **p-tBu4** was close to around 47%, and it was more reliable and reproductive compared to the oxidative homocoupling method, giving stable results across different batches. Inspired by such success, this strategy was applied to achieve longer oligomeric precursors. Excessive amount of **p-tBu2SnMe** was subjected to Stille coupling with **p-Br1Br** to afford the precursor with five pyridine rings **p-tBu5**, the precursor of the helicene **tBu-5N9**. This success implied that this strategy could be applied to synthesize longer precursors without much sacrifice in the yield. Based on such success, we also tried RCM on the precursor **p-tBu5** to afford **tBu-5N9**, and although the purification turned difficult, the desired product was detected by the mass spectroscopy (**Figure 64**).

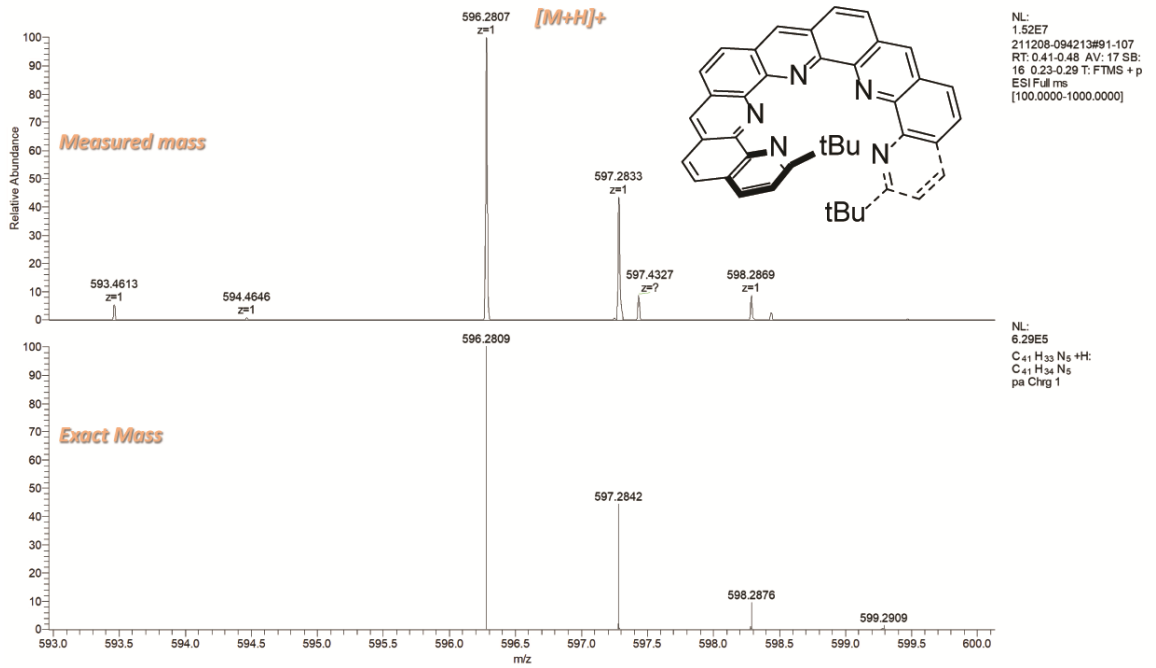

Figure 64. ESI mass spectrum of tBu-5N9, m/z $[M + H]^+$ Calcd for $C_{41}H_{34}N_5$ 596.2809; Found 596.2807.

4.3.3 Synthesis Modification on RCM

From the previous discussion, the knowledge of RCM on polypyridyl substrates was still limited, producing **tBu-4N7** only in a yield less than 30% with impurities. To obtain more insight into RCM on molecules featuring polypyridyl backbone, the precursor **pv-tBu3** was employed as the model compound as shown in **Figure 65**.

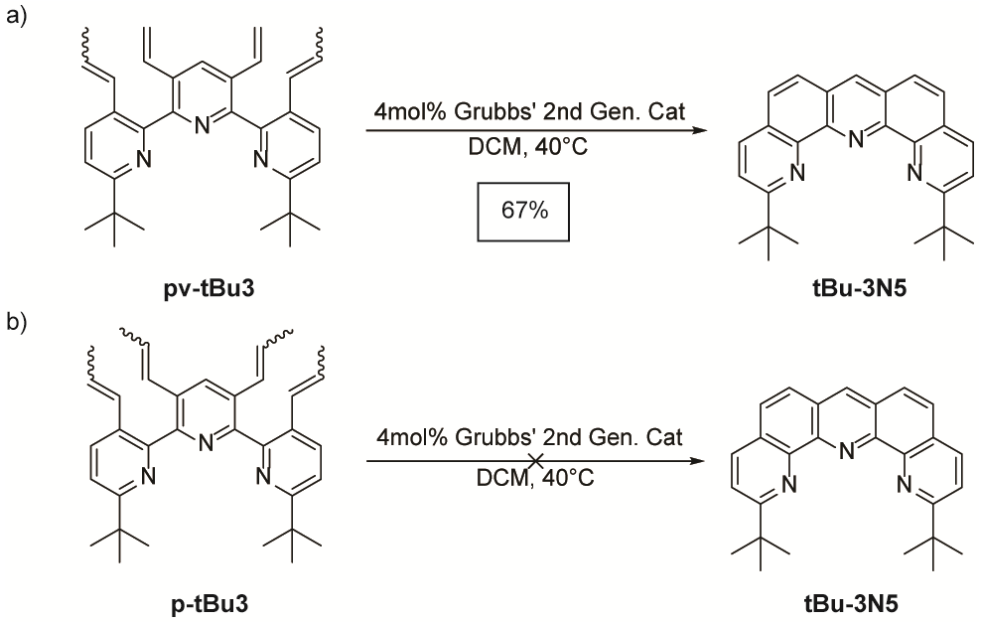

Figure 65. Synthetic scheme of RCM reaction on model compounds a) pv-tBu3 and b) p-tBu3.

Fortunately, the RCM reaction on the substrate **pv-tBu3** worked efficiently, affording the desired product **tBu-3N5** in a 67% yield with a low catalyst loading of 4 mol%. It is noteworthy that the product failed to be purified with normal phase silica gel due to its strong affinity to the stationary phase, so prep GPC was used for the purification purpose. The successful synthesis of **tBu-3N5** was undoubtedly verified by NMR spectrum, including ^{1}H NMR, ^{13}C NMR and COSY, and mass spec. **tBu-3N5** was a promising ligand, showing desirable binding strength towards metal ions like Zn^{2+} and Co^{2+}. Upon mixing with 0.5 equiv. $Zn(OTf)_2$ in acetonitrile at room temperature for 30 min, a near quantitative conversion was observed by ^{1}H NMR to form the metal complex $ZnL_2(OTf)_2$. Efforts to

grow the single crystals of these metal complexes are being committed in the lab. However, it caught our attention that the same conditions did not work on the fully-propenyl substrates **p-tBu3**. Only isomerization towards *trans* conformation around each double bond was observed, which was known to be a competitive process against the desired metathesis process. There is still debate over the mechanism of ruthenium-promoted olefin metathesis, and there have been extensive simulation studies to compare the feasibility of various mechanisms.[189,190] The most common mechanisms included hydride pathway,[191] Nolan-Prunet η^2-alkylidene/alkene mechanism,[192] van Rensburg η^3-allyl complex mechanism[193,194] *etc*. The hydride mechanism was deduced to be more compatible with our experimental observations, since it involved the hydride on the extra methyl group.

Despite the success of RCM reaction on **tBu-3N5**, it was not our final purpose to synthesize the compounds with only three pyridine rings. For this purpose, a wide range of conditions was tested to compare their efficiencies. First, the precursor **pv-tBu3** was acidified with trifluoroacetic acid and then subjected to the same RCM conditions, but the only observed product was the protonated starting material. After the RCM reaction, the protonated nitrogen atoms had to be organized in a centripetal manner. In the pristine RCM reaction, the cavity was large enough to accommodate lone pairs electrons of nitrogen atoms. However, when nitrogen atoms were protonated, the cavity was too crowded to fit the extra protons. Another reason might be that the protonation of nitrogen atoms made the precursor **pv-tBu3** more electron-deficient and lowered the HOMO energy level, rendering the olefins harder to bind to the ruthenium catalyst in the initial step in the catalytic cycle. Besides, various metal ions were mixed in the reaction mixture to be coordinated by the

formed **tBu-3N5** *in situ*, but this attempt did not work properly presumably due to the decomposition of the active Grubbs' catalyst via ligand exchange with external metal ions.

4.4 Conclusion

In summary, a series of novel centripetal azahelicenes and a feasible synthetic route to accomplish the synthesis of them have been designed. Guided by rationalized retrosynthesis design, the synthesis of building blocks was achieved in an efficient manner. Afterwards, the condition of oligomerization was extensively screened for the Stille coupling and nickel-catalyzed oxidative homocoupling.

To further improve the efficiency of oligomer synthesis, structural modifications and route change were adopted. These changes included changing tributylstannyl groups to trimethylstannyl groups to enhance reactivity, changing adamantyl groups to tert-butyl groups to alleviate strain and changing some of the vinyl groups to propenyl groups to reduce undesired binding between olefin and metal center. So far, the precursors with pendant olefins containing up to five pyridine rings can be efficiently synthesized.

However, more efforts are still required to realize the efficient and selective application of RCM reaction to annulate the backbone of proposed helicenes, despite the preliminary success of synthesis on **tBu-3N5** which was composed of three pyridine rings. The pristine RCM reactions did afford higher helicenes **tBu-4N7**, **Ad-4N7** and **tBu-5N9** in low yields and required a higher catalyst loading which hindered effective separation from impurities. External additives, including acid and metal ions, did not show benefit to

boost the transformation. Ongoing efforts are being made to find an optimal solution to strike a balance between the amount of catalyst required and the efficiency of purification.

4.5 Experimental Section

4.5.1 General Methods and Materials

Starting materials and reagents were purchased from commercial sources and were used as received without further purification. THF was dried and distilled under nitrogen from sodium using benzophenone as the indicator. Toluene was dried using an inert pure solvent system and used without further treatment. An oil bath was used for those reactions that required heating. ^{1}H and ^{13}C NMR spectra were recorded on a 500 MHz or 400 MHz spectrometer. The ^{1}H and $^{13}C\{^{1}H\}$ NMR chemical shifts were reported in ppm relative to the signals corresponding to the residual non-deuterated solvents ($CDCl_3$: ^{1}H 7.26 ppm, ^{13}C 77.23 ppm) or the internal standard (tetramethylsilane: ^{1}H 0.00 ppm). Abbreviations for reported signal multiplicities are as follows: s, singlet; d, doublet; t, triplet; q, quartet; m, multiplet; br, broad. The broad singlet at ~1.55 ppm on ^{1}H NMR spectra represents the resonance signal of H_2O in $CDCl_3$. Column chromatography was carried out on a normal phase SiO_2. Preparative size exclusive chromatography (SEC) purifications were performed at room temperature using chloroform as the eluent at a flow rate of 14 mL/min.

4.5.2 Synthesis

2,6-dibromo-3,5-dimethylpyridine (C2). 3,5-dimethylpyridine (**C1**, 20 mmol, 2.144 g) was added into 16 mL fresh oleum dropwise at 0°C in a pressure tube. Afterwards, liquid bromine (60 mmol, 9.589 g) was added into the mixture dropwise, and the mixture was stirred at this temperature for 1 h. After this 1 h period, the whole reaction mixture was heated at 150°C and stirred for 48 h. Next, the reaction mixture was allowed to cool down to room temperature naturally, after which it was poured onto 200 mL ice slowly. Afterwards, 6 M NaOH solution was added portion-wise to adjust the pH of the solution until it is basic. Precipitate was observed along with the increasing pH value. After desired pH value was achieved, 1 M $Na_2S_2O_4$ solution was added until the orange color faded away. The solution was extracted with DCM in three portions, and organic portions were combined and washed with brine solution. The volatile solvent was removed under reduced pressure, and the crude product was purified with column chromatography (SiO2, hexane/CH2Cl2 1:1 to 1:9) to afford **C2** as while solid in a 58% yield. ^{1}H NMR (500 MHz, $CDCl_3$) δ = 7.35 (s, 1H), 2.31 (s, 6H).

2,6-dibromo-3,5-bis(bromomethyl)pyridine (C3). In a pressure tube, **C2** (5 mmol, 1.325 g), NBS (20 mmol, 3.560 g) and AIBN (1 mmol, 0.164 g) were mixed in 10 mL of dichloroethane. The mixture was stirred and heated at 90°C for 3 h. Afterwards, the solution was cooled back to room temperature, and quenched with water. The mixture was extracted with DCM. The organic phase was dried over Na_2SO_4, and the transferred to a round bottom flask. The volatile solvent was removed under reduced pressure and dissolved in anhydrous THF again. To the solution, diisopropylethylamine (DIPEA, 13.33

mmol, 1.723 g) and diethylphosphite (DEP, 13.33 mmol, 1.841 g) were added to the THF solution sequentially. The mixture was stirred for 30 minutes and quenched with water. The mixture was extracted with DCM, and the organic phase was combined and washed with brine solution. The volatile solvent was removed under reduced pressure, and the crude product was purified with column chromatography (SiO2, hexane/CH2Cl2 1:1 to 1:9) to afford **C3** as while solid in a 64% yield. ^{1}H NMR (500 MHz, $CDCl_3$) δ = 7.81 (s, 1H), 4.50 (s, 4H).

2,6-dibromo-3,5-divinylpyridine (v-Br1Br). **C3** (0.3 mmol, 0.1268 g) and triphenylphosphine (0.75mmol, 0.1967 g) were dissolved in 2 mL anhydrous DMF in nitrogen atmosphere. The mixture was heated and stirred at 80°C overnight. Afterwards, the suspension was poured into diethyl ether. The precipitate was collected via vacuum filtration and dried in vacuum. The phosphonium salt was suspended in 2 mL anhydrous THF, and to this suspension was added 2 g paraformaldehyde. Potassium tert-butoxide (0.75 mmol, 85 mg) was slowly added to the suspension with stirring at 0°C, and the mixture was allowed to warm back to room temperature overnight. After the completion of the reaction, water was added to quench the reaction, and excessive paraformaldehyde was removed through a cotton ball. The mixture was extracted with DCM, and the organic phase was combined and washed with brine solution. The volatile solvent was removed under reduced pressure, and the crude product was purified with column chromatography (SiO2, hexane/CH2Cl2 1:1 to 1:9) to afford **v-Br1Br** as while crystal in 85% yield. ^{1}H NMR (400 MHz, $CDCl_3$) δ = 7.86 (s, 1H), 6.91 (dd, 2H), 5.81 (d, 2H), 5.54 (d, 2H). ESI-MS: m/z $[M + H]^+$ Calcd for $C_9H_7NBr_2$ 289.8998; Found 289.8993.

p-Br1Br. The synthesis is similar to **v-Br1Br**, except that acetaldehyde was used in the place of paraformaldehyde and the product was collected as colorless oil in 90% yield. ^{1}H NMR (400 MHz, $CDCl_3$) δ = 7.45-7.72 (sss, 1H), 5.95-6.65 (m, 4H), 1.78-1.96 (m, 6H). The strict assignment of peaks was rendered unfeasible due to the mixture of E/Z isomers.

T2. In a 250 mL round bottom flask, **T1** (10 mmol, 1.860 g), $AgNO_3$ (2.5 mmol, 0.425 g), adamantyl acid (70 mmol, 12.6 g) and ammonium persulfate (35 mmol, 7.987 g) were suspended in a mixture solvent of 20 mL dichloroethane and 100 mL water. To this suspension was added 2 mL concentrated sulfuric acid. The suspension was stirred and heated to reflux at 100°C, covered with aluminum foil. After 24 h, the mixture was filtered through a cotton ball to remove the insoluble parts. The clear solution was extracted with DCM, and the organic phase was combined and washed with brine solution. The volatile solvent was removed under reduced pressure, and the crude product was purified with column chromatography (SiO2, hexane/CH2Cl2 1:1 to 1:9) to afford **T2** as white solid in 45% yield. ^{1}H NMR (500 MHz, $CDCl_3$) δ = 10.29 (s, 1H), 8.09 (d, 1H), 7.35 (d, 1H), 1.74-2.14 (m, 15H).

tBu-T2. The synthesis was similar to T2, and pivalic acid (50 mmol, 6.10 g) was used in the place of adamantyl acid. The product is colorless oil and the yield was 70%.^{1}H NMR (500 MHz, $CDCl_3$) δ = 10.30 (s, 1H), 8.08 (d, 1H), 7.42 (d, 1H), 1.37 (m, 9H).

T3. In a Schlenk tube filled with nitrogen, methyltriphenylphosphonium bromide (3.03 mmol, 1.083 g) was suspended in 8 mL anhydrous THF, and tBuOK (3.03 mmol, 0.340 g) was added to the suspension to observe a bright yellow color. After one hour at

room temperature, **T2** (2.53 mmol, 0.809 g) was dissolved in 8 mL THF, and the solution was injected into the Schlenk tube slowly. The mixture was stirred at room temperature overnight and quenched with water after 24 h. The mixture was extracted with DCM, and the organic phase was combined and washed with brine solution. The volatile solvent was removed under reduced pressure, and the crude product was purified with column chromatography (SiO2, hexane/CH2Cl2 1:1 to 1:9) to afford **T3** as while crystal in 86% yield. ^{1}H NMR (400 MHz, $CDCl_3$) δ = 7.72 (d, 1H), 7.19 (d, 1H), 6.96 (dd, 1H), 5.68 (d, 1H), 5.39 (d, 1H), 1.74-2.10 (m, 15H).

v-tBuT3. The synthesis was similar to **T3**, except that **tBu-T2** used in the place of **T2**. The product was obtained as colorless oil in 84% yield. ^{1}H NMR (500 MHz, $CDCl_3$) δ = 7.72 (d, 1H), 7.28 (d, 1H), 6.96 (dd, 1H), 5.69 (d, 1H), 5.42 (d, 1H), 1.35 (s, 9H).

p-tBuT3. In a Schlenk tube filled with nitrogen, ethyltriphenylphosphonium bromide (4.5 mmol, 1.671 g) was suspended in 6 mL anhydrous THF at 0°C, and 1.6 M nBuLi in hexane solution (4.5 mmol, 2.8 mL) was injected into the suspension to observe a deep orange color change. The mixture was stirred at 0°C for 1 h, after which tBu-T2 (3 mmol, 0.726 g) was dissolved in 3 mL anhydrous THF and injected into the ylide solution, and gradual color diminishment was witnessed. The mixture was allowed back to room temperature overnight and quenched with water after 24 h. The mixture was extracted with DCM, and the organic phase was combined and washed with brine solution. The volatile solvent was removed under reduced pressure, and the crude product was purified with column chromatography (SiO2, hexane/CH2Cl2 1:1 to 1:9) to afford **p-tBuT3** as colorless oil in 86% yield. ^{1}H NMR (400 MHz, $CDCl_3$) δ = 7.48-7.63 (d + d, 1H), 7.20-7.25 (d + d,

1H), 5.8-6.7 (m, 2H), 1.76-1.94 (d + d, 3H), 1.33-1.35 (s + s, 9H). A mixture of E/Z isomers were obtained.

v-Ad1SnBu. **T3** (2 mmol, 0.636 g) was dissolved in 6 mL anhydrous THF in a flame dried Schlenk flask at -78°C using dry ice and acetone. To this solution was injected 1.6 M n-BuLi solution in hexane (2.2 mmol, 1.4 mL) very slowly to observe a formation of orange color. The mixture was stirred at -78°C for 1 h. After 1 h, tributyltin chloride (2.6 mmol, 0.846 g) was injected into the flask slowly. The mixture was allowed back to room temperature overnight. After 24 h, the reaction was quenched with water, and the solution was extracted with DCM, and the organic phase was combined and washed with brine solution. After being dried over Na_2SO_4, the volatile solvent was removed with reduced pressure, and the crude product was purified with prep GPC to afford **v-Ad1SnBu** as yellow oil in 78% yield. ^{1}H NMR (500 MHz, $CDCl_3$) δ = 7.65 (d, 1H), 7.04 (d, 1H), 6.73 (dd, 1H), 5.63 (d, 1H), 5.27 (d, 1H), 1.74-2.10 (m, 42H).

v-tBu1SnBu. **v-tBuT3** (0.5 mmol, 0.120 g) was dissolved in 3 mL anhydrous THF in a flame dried Schlenk flask at -78°C using dry ice and acetone. To this solution was injected 1.6 M n-BuLi solution in hexane (0.6 mmol, 0.38 mL) very slowly to observe a formation of orange color. The mixture was stirred at -78°C for 1 h. After 1 h, tributyltin chloride (0.7 mmol, 0.228 g) was injected into the flask slowly. The mixture was allowed back to room temperature overnight. After 24 h, the reaction was quenched with water, and the solution was extracted with DCM, and the organic phase was combined and washed with brine solution. After being dried over Na_2SO_4, the volatile solvent was removed with reduced pressure, and the crude product was purified with prep GPC to afford **v-tBu1SnBu**

as yellow oil in 78% yield. ^{1}H NMR (500 MHz, $CDCl_3$) δ = 7.64 (d, 1H), 7.12 (d, 1H), 6.74 (dd, 1H), 5.62 (d, 1H), 5.27 (d, 1H), 1.34 (s, 9H), 0.70-1.75 (m, 27H).

p-tBu1SnMe. **p-tBuT3** (2 mmol, 0.508 g) was dissolved in 10 mL anhydrous THF in a flame dried Schlenk flask at -78°C using dry ice and acetone. To this solution was injected 1.6 M n-BuLi solution in hexane (2.4 mmol, 1.5 mL) very slowly to observe a formation of orange color. The mixture was stirred at -78°C for 1 h. After 1 h, 0.5 M of trimethyltin chloride in hexane (1.3 mmol, 2.6 mL) was injected into the flask slowly. The mixture was allowed back to room temperature overnight. After 24 h, the reaction was quenched with water, and the solution was extracted with DCM, and the organic phase was combined and washed with brine solution. After being dried over Na_2SO_4, the volatile solvent was removed with reduced pressure, and the crude product was purified with prep GPC to afford **p-tBu1SnMe** as yellow oil in 78% yield. ^{1}H NMR (400 MHz, $CDCl_3$) δ = 7.48-7.64 (d + d, 1H), 7.20-7.25 (d + d, 1H), 5.89-6.68 (m, 2H), 1.76-1.94 (d + d, 3H), 1.33-1.35 (s + s, 9H). A mixture of E/Z isomers were obtained.

v-Ad2Br. **v-Br1Br** (0.6 mmol, 0.173 g) and **v-Ad1SnBu** (0.5 mmol, 0.263 g) were dissolved in 3 mL anhydrous DMF. The solution was degassed by freeze-pump-thaw three times in liquid nitrogen. Afterwards, tetrakis (0.075 mmol, 87 mg) and CuI (0.05 mmol, 8 mg) along with a few crystals of BHT were added to the solution. The entire mixture was stirred at 85°C overnight. After the completion of the reaction, the mixture was extracted with DCM, and washed with water once and brine twice. The organic phase was combined and dried over Na_2SO_4. The crude product was purified via column chromatography (SiO2, hexane/CH2Cl2 1:1 to 1:9) to provide a semi-pure product. Such semi-product was further

purified with prep GPC to afford **v-Ad2Br** in 30% yield. ^{1}H NMR (500 MHz, $CDCl_3$) δ = 8.06 (s, 1H), 7.90 (d, 1H), 7.29 (d, 1H), 7.04 (dd, 1H), 6.55-6.64 (m, 2H), 5.84 (d, 1H), 5.72 (d, 1H), 5.64 (d, 1H), 5.53 (d, 1H), 5.27 (d, 1H), 5.21 (d, 1H), 1.76-2.08 (m, 15H).

v-tBu2Br. The synthesis was similar to **v-Ad2Br**, except that **v-tBu1SnBu** was used in the place of **v-Ad1SnBu**, and the yield was 40%. ^{1}H NMR (500 MHz, $CDCl_3$) δ = 8.06 (s, 1H), 7.89 (d, 1H), 7.35 (d, 1H), 7.04 (dd, 1H), 6.55-6.65 (m, 2H), 5.85 (d, 1H), 5.72 (d, 1H), 5.65 (d, 1H), 5.54 (d, 1H), 5.24 (d, 1H), 5.22 (d, 1H), 1.35 (s, 9H). ESI-MS: m/z $[M + H]^+$ Calcd for $C_{20}H_{22}N2Br$ 369.0961; Found 369.0959.

pv-tBu2Br and **pv-tBu3**. The synthesis was similar to **v-tBu2Br**, except that **p-tBu1SnMe** was used in the place of **v-tBu1SnBu**, and the yield for **pv-tBu2Br** was 48%, the yield for **pv-tBu3** was 18%. ^{1}H NMR (400 MHz, $CDCl_3$) for **pv-tBu2Br** δ = 7.34-8.06 (m, 3H), 5.23-7.44 (m, 8H), 1.68-1.79 (d + d, 3H), 1.33-1.36 (s + s, 9H). ^{1}H NMR (400 MHz, $CDCl_3$) for **pv-tBu3** δ = 7.23-8.24 (m, 5H), 5.20-6.64 (m, 10H), 1.67-1.80 (m, 6H), 1.31-1.34 (m, 18H). Due to the larger number of isomers, the exact assignment of peaks was not feasible.

p-tBu2Br. The synthesis was similar to **pv-tBu2Br**, except that **p-Br1Br** was used in the place of **v-Br1Br**. ^{1}H NMR (400 MHz, $CDCl_3$) δ = 7.25-7.92 (m, 3H), 5.92-6.75 (m, 6H), 1.66-1.99 (m, 9H), 1.32-1.37 (m, 9H). Due to the larger number of isomers, the exact assignment of peaks was not feasible.

v-Ad4. $NiCl_2(PPh_3)_2$ (0.088 mmol, 56 mg) and tetrabutylammonium iodide (0.221 mmol, 82 mg) were suspended in 1.5 mL anhydrous THF, and then zinc powder (0.378 mmol, 25 mg) was added to the flask. The suspension was degassed by freeze-pump-thaw

three times with liquid nitrogen. The mixture was stirred at room temperature for 2 h. Afterwards, **v-Ad2Br** (0.221 mmol, 102 mg) was dissolved in 1.5 mL and injected to the flask. The reaction mixture was stirred at 55°C for 24 h. After the completion of the reaction, the reaction mixture was poured into the 30% ammonium hydroxide, and was extracted with DCM, and the organic phase was combined and washed with brine solution. After being dried over Na_2SO_4, the volatile solvent was removed with reduced pressure, and the crude product was purified with column chromatography (SiO2, hexane/CH2Cl2 1:1 to 1:9) to afford **v-Ad4** as yellow oil in a 25% yield. ^{1}H NMR (400 MHz, $CDCl_3$) δ = 8.23 (s, 2H), 7.87 (d, 2H), 7.23 (d, 2H), 6.86 (dd, 2H), 6.62-6.75 (m, 4H), 5.14-5.82 (m, 12H), 2.06 (s, 6H), 1.96 (s, 12H), 1.75 (s, 12H). ESI-MS: m/z $[M + H]^+$ Calcd for $C_{52}H_{55}N_4$ 735.4421; Found 735.4393.

pv-tBu4. The synthesis was similar to **v-Ad4**, except that **pv-tBu2Br** was used in the place of **v-Ad2Br** to afford **pv-tBu4** in a 40% yield. ^{1}H NMR (400 MHz, $CDCl_3$) δ = 8.24 (s, 2H), 7.76 (d, 2H), 7.25 (d, 2H), 5.22-6.93 (m, 16H), 1.74-1.76 (m, 6H), 1.29-1.30 (m, 18H).

p-tBu2SnMe. **p-tBu2Br** (0.188 mmol, 78 mg) and $(SnMe_3)_2$ (0.37 mmol, 0.121 g) were added to a Schlenk flask with 1.5 mL anhydrous toluene, and the solution was degassed three times with liquid nitrogen. Afterwards, tetrakis (0.0188 mmol, 22 mg) was added to the mixture, and stirred at 80°C for 24 h. After the completion of the reaction, the reaction was quenched with water, and extracted with DCM. The organic phase was washed with water and brine and dried over Na_2SO_4. The volatile solvent was removed under reduced pressure, and the crude product was purified with prep GPC to obtain the

semi-pure product in near 100% yield. The product was directly used in the next step without further purification. ^{1}H NMR (400 MHz, $CDCl_3$) δ = 7.09-7.80 (m, 3H), 5.40-6.45 (m, 6H), 1.48-1.85 (m, 9H), 1.22-1.25 (m, 9H), 0.10-0.30 (m, 9H). Due to the larger number of isomers, the exact assignment of peaks was not feasible.

p-tBu4. **p-tBu2Br** (0.145 mmol, 60 mg) and **p-tBu2SnMe** (0.145 mmol, 72 mg) were dissolved in 1 mL anhydrous DMF. The solution was degassed by freeze-pump-thaw three times in liquid nitrogen. Afterwards, tetrakis (0.022 mmol, 25 mg) and CuI (0.029 mmol, 5 mg) were added to the solution. The entire mixture was stirred at 85°C overnight. After the completion of the reaction, the mixture was extracted with DCM, and washed with water once and brine twice. The organic phase was combined and dried over Na_2SO_4. The crude product was purified via column chromatography (SiO2, hexane/CH2Cl2 1:1 to 1:9) to provide a semi-pure product. Such semi-product was further purified with prep GPC to afford **p-tBu4** in 42% yield. ^{1}H NMR (400 MHz, $CDCl_3$) δ = 7.20-8.10 (m, 6H), 5.60-6.65 (m, 12H), 1.70-1.90 (m, 18H), 1.25-1.42 (m, 18H). Due to the larger number of isomers, the exact assignment of peaks was not feasible.

tBu-3N5. In a Schlenk flask, **pv-tBu3** (0.12 mmol, 55 mg) and Grubbs' 2nd generation catalyst (0.0024 mmol, 2 mg) were dissolved in 6 mL DCM, and degassed with freeze-pump-thaw three times with liquid nitrogen. The mixture was stirred with mild heat at 40°C overnight, and after the completion of the reaction, the volatile solvent was removed under reduced pressure, and the crude product was purified with prep GPC to obtain the product in 68% yield as yellow powder. ^{1}H NMR (400 MHz, $CDCl_3$) δ = 8.74 (s, 1H), 8.19 (d, 2H), 7.90 (d, 2H), 7.79 (d + d, 4H), 1.71 (s, 18H). $^{13}C\{^{1}H\}$ NMR (100

MHz, $CDCl_3$) δ = 169.78, 136.02, 127.87, 126.98, 126.86, 125.61, 120.53, 38.97, 30.53. ESI-MS: m/z $[M + H]^+$ Calcd for $C_{27}H_{28}N3$ 394.2278; Found 394.2273.

tBu-4N7. **pv-tBu4** (0.092 mmol, 53 mg) and Grubbs' 2nd generation catalyst (0.0092 mmol, 8 mg) were dissolved in 2 mL anhydrous toluene. The solution was degassed by freeze-pump-thaw three times with liquid nitrogen. On the other hand, another batch of Grubbs' 2nd generation catalyst (0.0184 mmol, 16 mg) was dissolved in 4 mL anhydrous toluene. The extra batch of catalyst solution was injected into the reaction mixture slowly by syringe pump over 3 h, and meanwhile the reaction mixture was stirred at 90°C. After the completion of the injection, the mixture was further stirred overnight. After the completion of the reaction, the toluene was removed by vacuum, and the crude product was purified with prep GPC to obtain the semi-pure product in 30% yield as brown powder. ^{1}H NMR (500 MHz, $CDCl_3$) δ = 8.67 (s, 2H), 8.18 (d, 2H), 7.82 (d + d, 8H), 1.42 (s, 18H). ESI-MS: m/z $[M + H]^+$ Calcd for $C_{34}H_{31}N_4$ 495.2543; Found 495.2539.

Ad-4N7. The synthesis of **Ad-4N7** was similar to **tBu-4N7**, except that the starting material **v-Ad4** was used in the place of **pv-tBu4** to afford semi-pure product in less than 10% yield. ^{1}H NMR (400 MHz, $CDCl_3$) δ = 9.13 (s, 2H), 8.39 (d, 2H), 7.89-8.10 (m, 8H), 1.85-2.33 (s, 30H). ESI-MS: m/z $[M + H]^+$ Calcd for $C_{46}H_{42}N_4$ 651.3482; Found 651.3476.

p-tBu5. **p-Br1Br** (0.084 mmol, 27 mg) and **p-tBu2SnMe** (0.167 mmol, 83 mg) were dissolved in 1.5 mL anhydrous DMF. The solution was degassed by freeze-pump-thaw three times in liquid nitrogen. Afterwards, tetrakis (0.0126 mmol, 15 mg) and CuI (0.017 mmol, 3 mg) were added to the solution. The entire mixture was stirred at 85°C overnight. After the completion of the reaction, the mixture was extracted with DCM, and

washed with water once and brine twice. The organic phase was combined and dried over Na_2SO_4. The crude product was purified via prep GPC to afford semi-pure **p-tBu5** in 52% yield. ^{1}H NMR (400 MHz, $CDCl_3$) δ = 7.50-8.00 (m, 7H), 5.55-6.60 (m, 16H), 1.70-1.97 (m, 24H), 1.25-1.42 (m, 18H). Due to the larger number of isomers, the exact assignment of peaks was not feasible. ESI-MS: m/z $[M + H]^+$ Calcd for $C_{57}H_{66}N_5$ 820.5313; Found 820.5307.

4.5.3 NMR Spectra

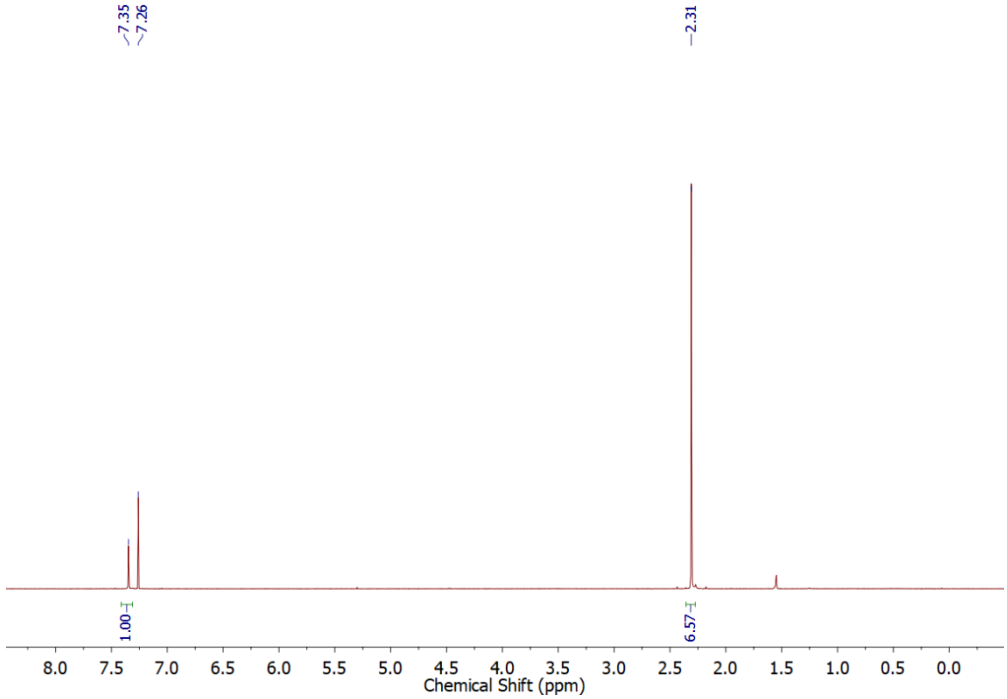

Figure 66. ^{1}H (500 MHz) NMR of C2 in $CDCl_3$ at room temperature.

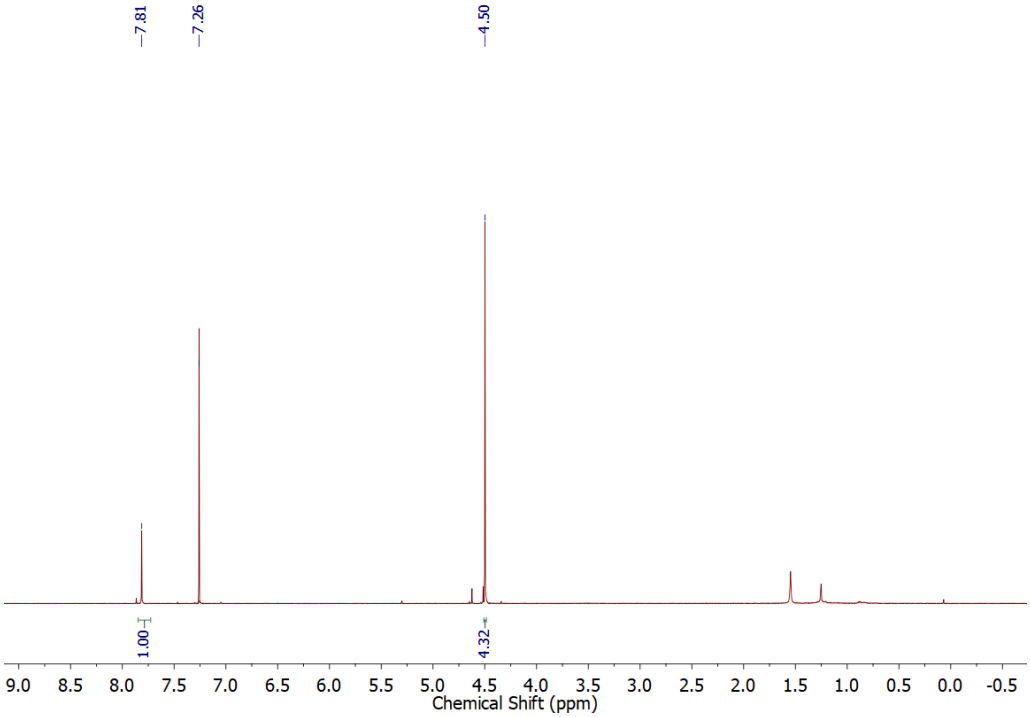

Figure 67. ^{1}H (500 MHz) NMR of C3 in $CDCl_3$ at room temperature.

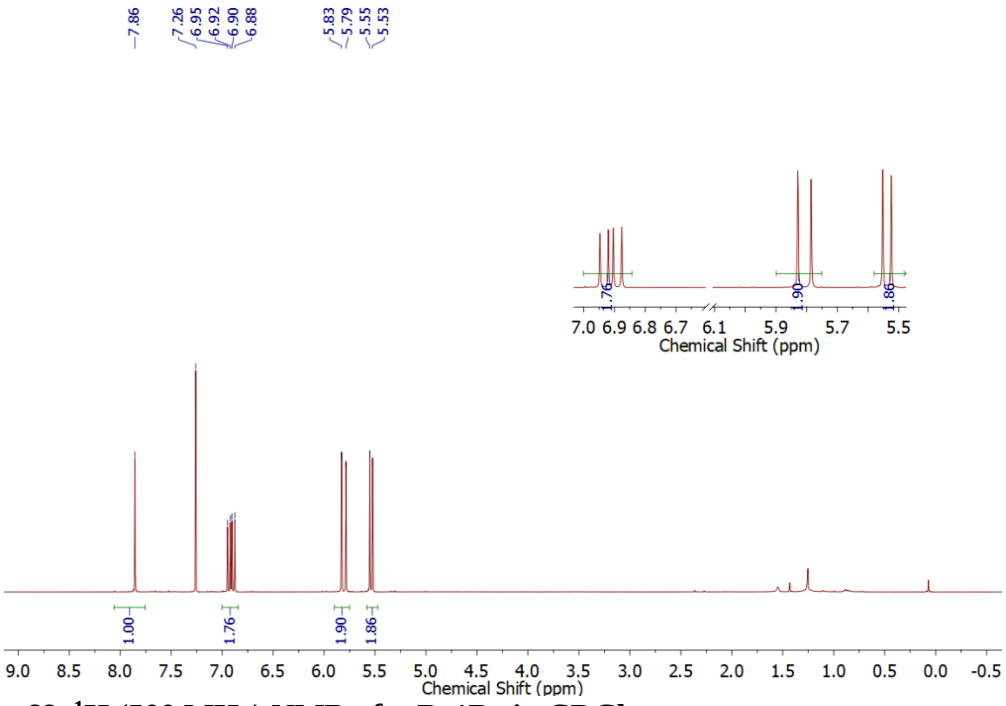

Figure 68. ^{1}H (500 MHz) NMR of v-Br1Br in $CDCl_3$ at room temperature.

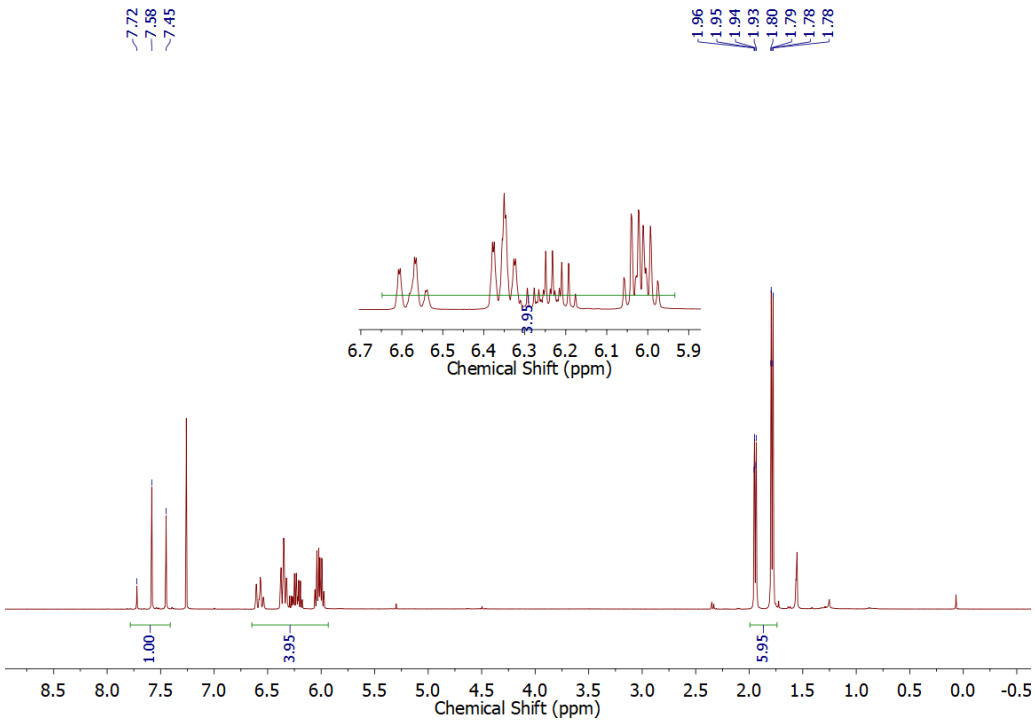

Figure 69. ^{1}H (500 MHz) NMR of p-Br1Br in $CDCl_3$ at room temperature.

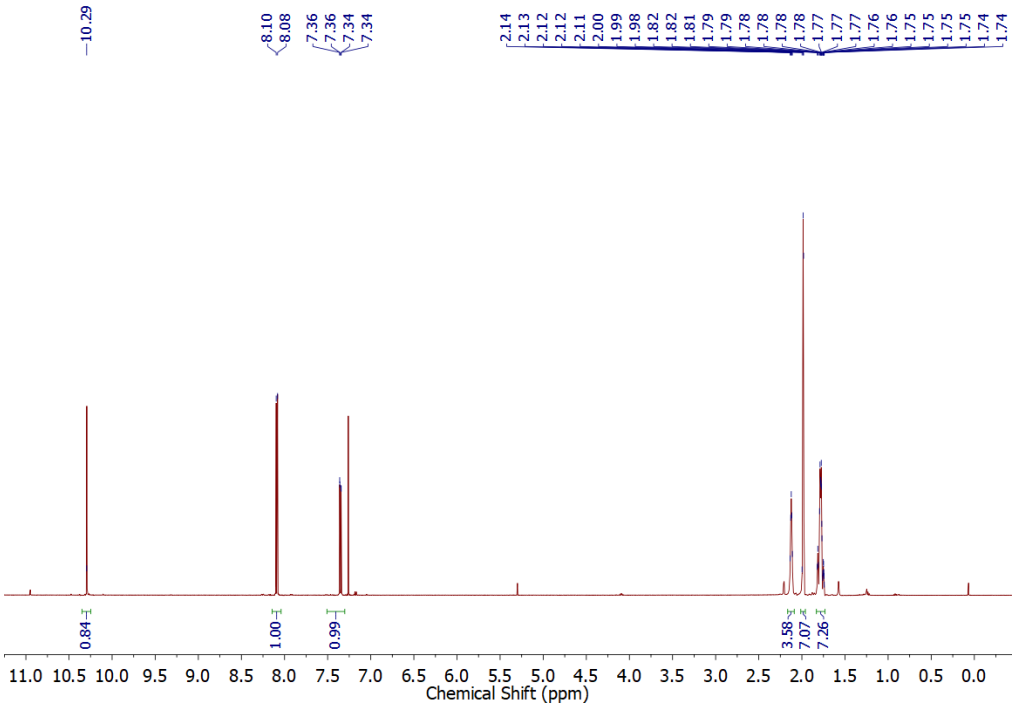

Figure 70. ^{1}H (500 MHz) NMR of T2 in $CDCl_3$ at room temperature.

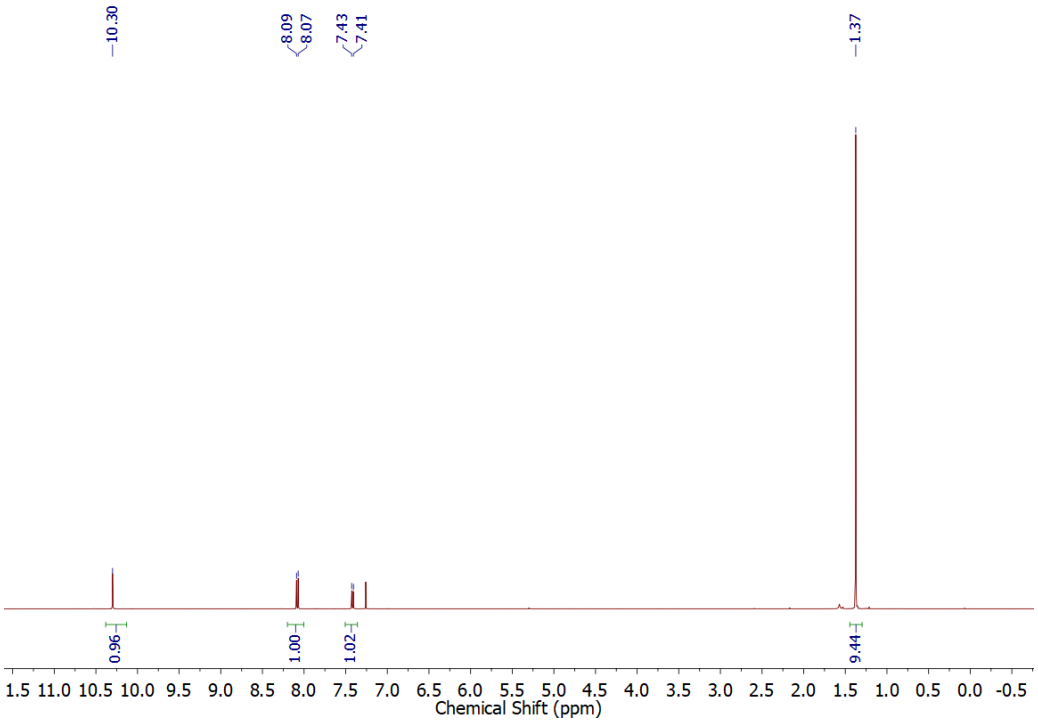

Figure 71. ^{1}H (500 MHz) NMR of tBu-T2 in $CDCl_3$ at room temperature.

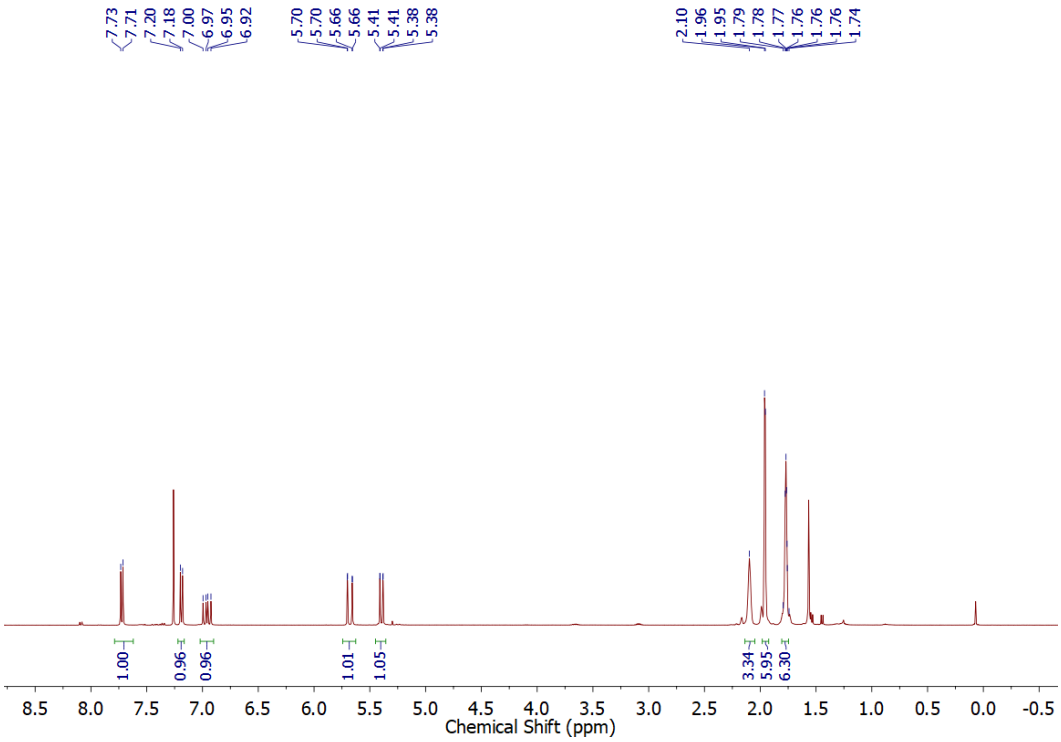

Figure 72. ^{1}H (500 MHz) NMR of T3 in $CDCl_3$ at room temperature.

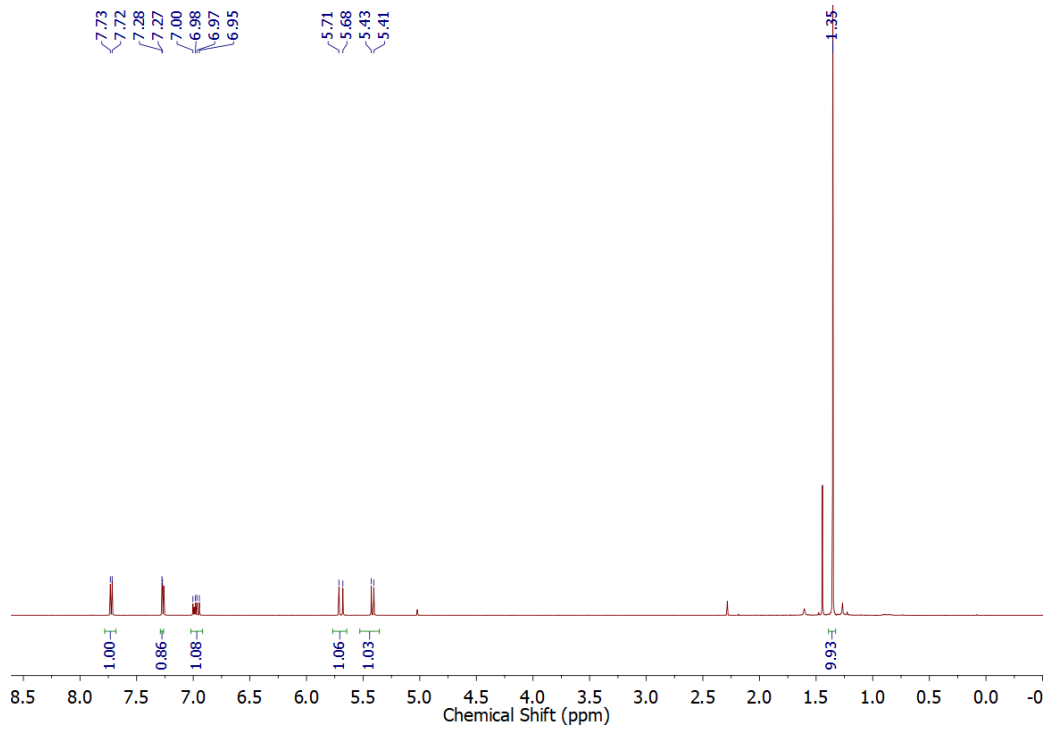

Figure 73. ^{1}H (500 MHz) NMR of v-tBuT3 in $CDCl_3$ at room temperature.

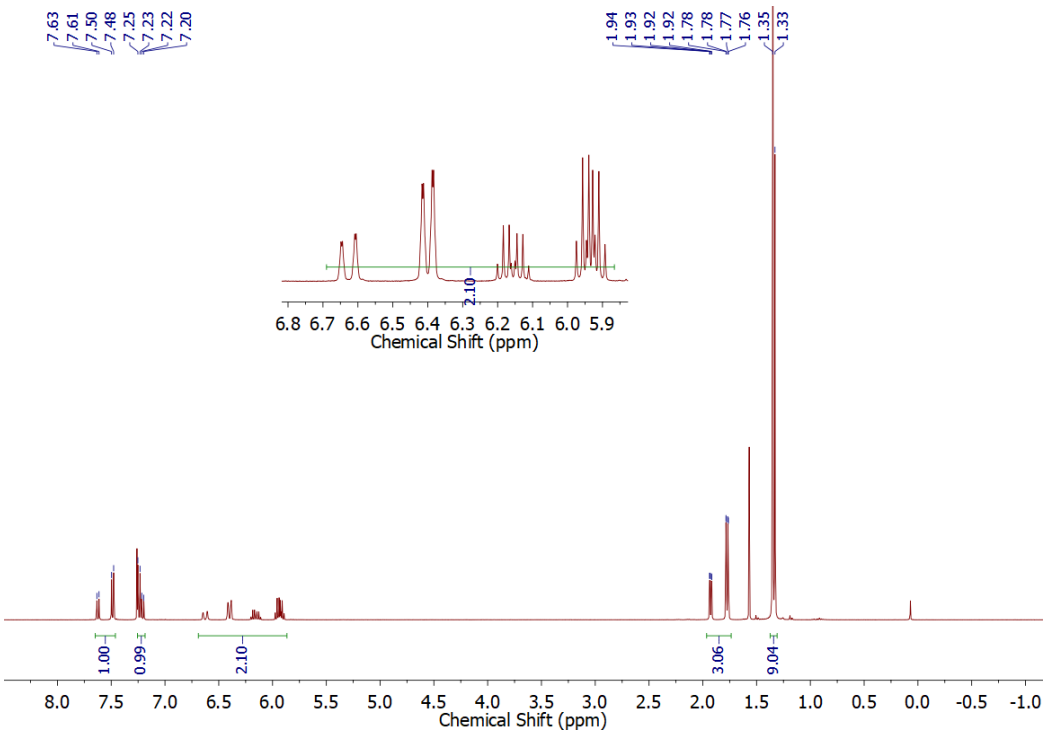

Figure 74. ^{1}H (400 MHz) NMR of p-tBuT3 in $CDCl_3$ at room temperature.

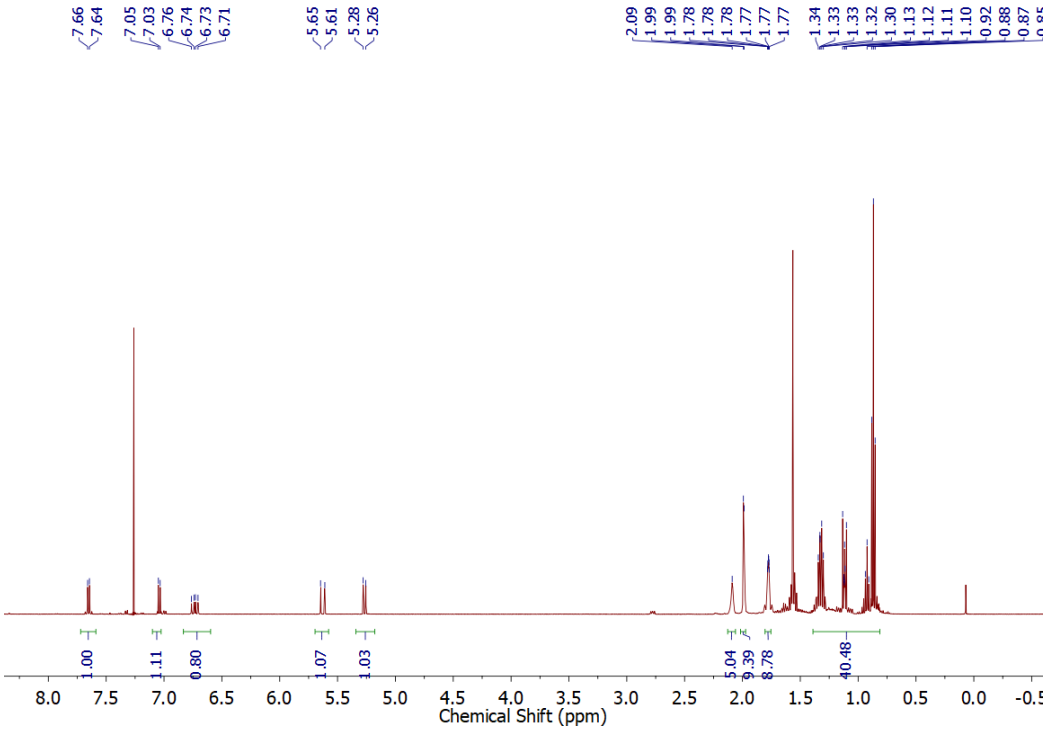

Figure 75. ^{1}H (500 MHz) NMR of v-Ad1SnBu in $CDCl_3$ at room temperature.

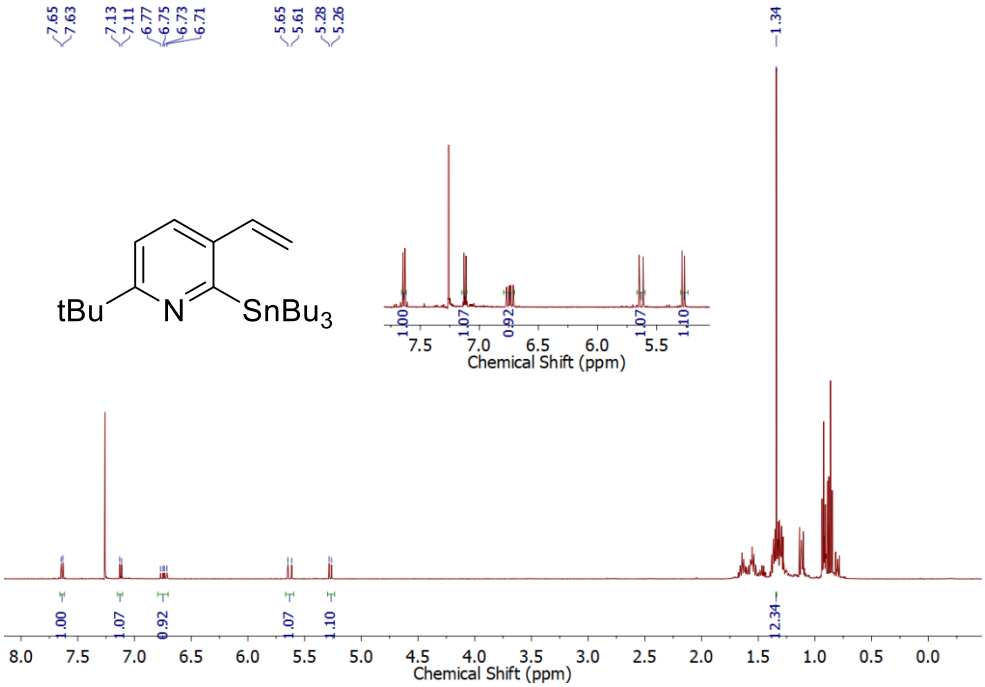

Figure 76. ^{1}H (500 MHz) NMR of v-tBu1SnBu in $CDCl_3$ at room temperature.

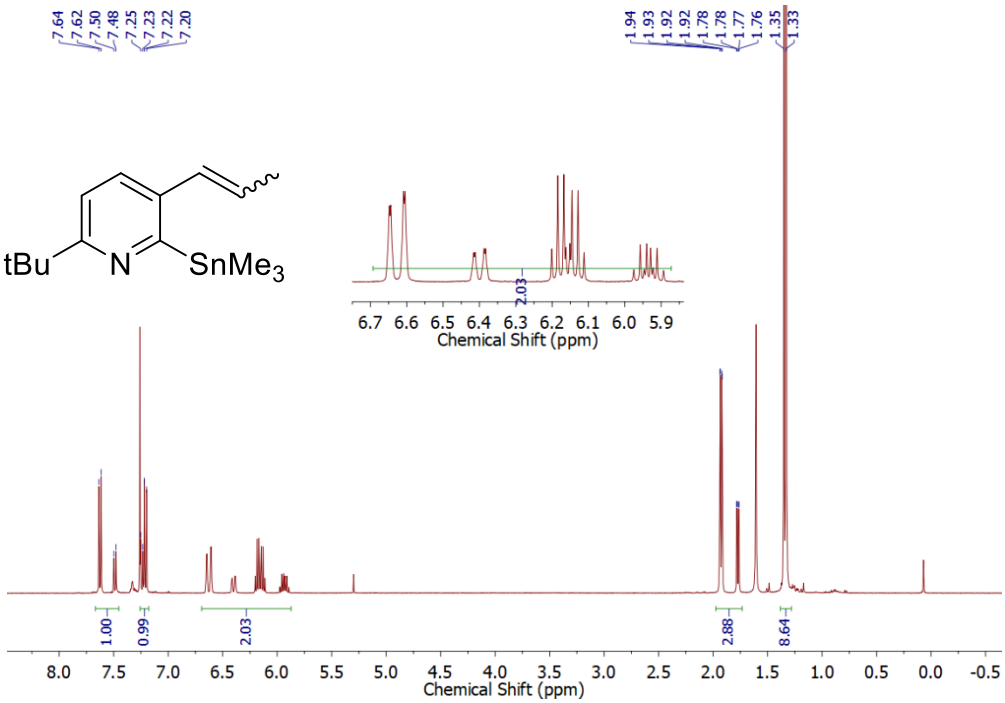

Figure 77. ^{1}H (400 MHz) NMR of p-tBu1SnMe in $CDCl_3$ at room temperature.

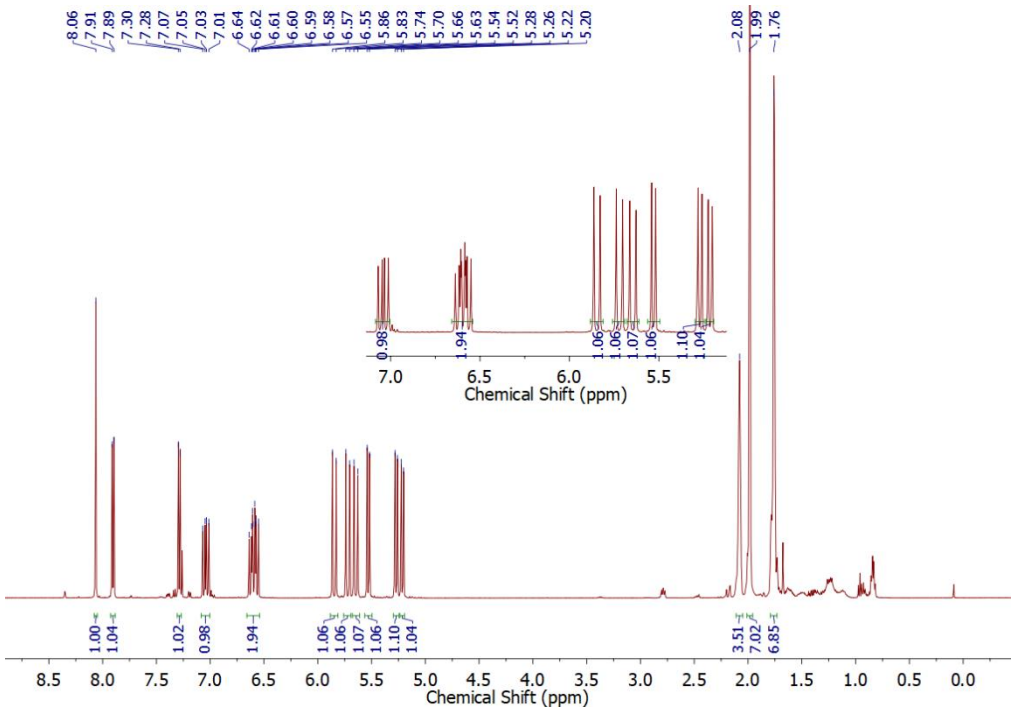

Figure 78. ^{1}H (500 MHz) NMR of v-Ad2Br in $CDCl_3$ at room temperature.

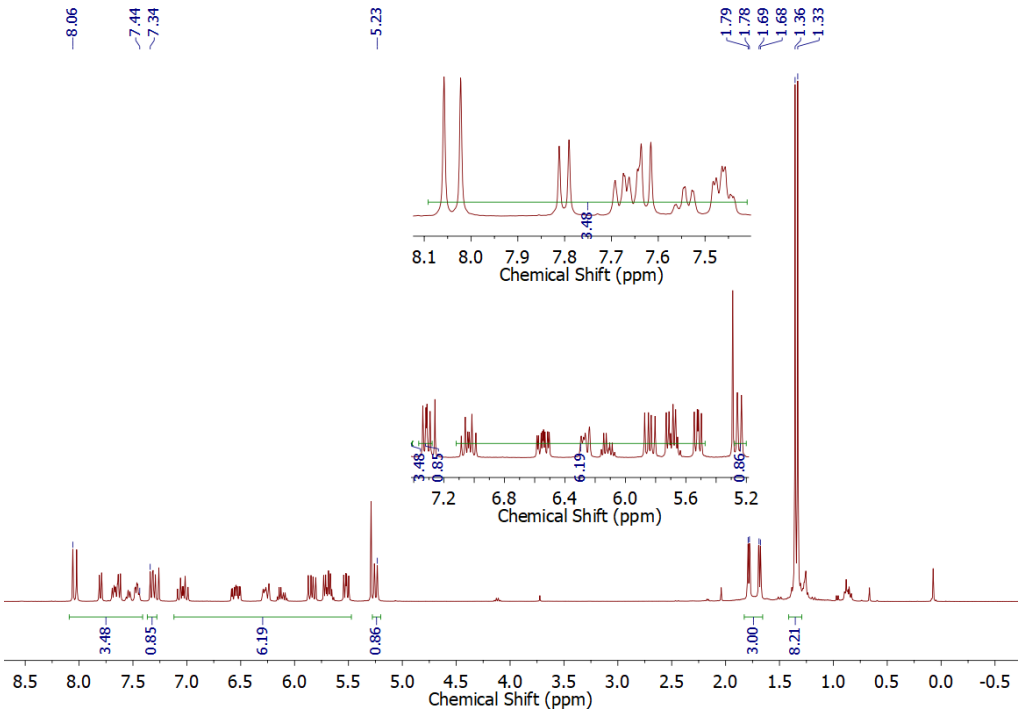

Figure 79. ^{1}H (400 MHz) NMR of pv-tBu2Br in $CDCl_3$ at room temperature.

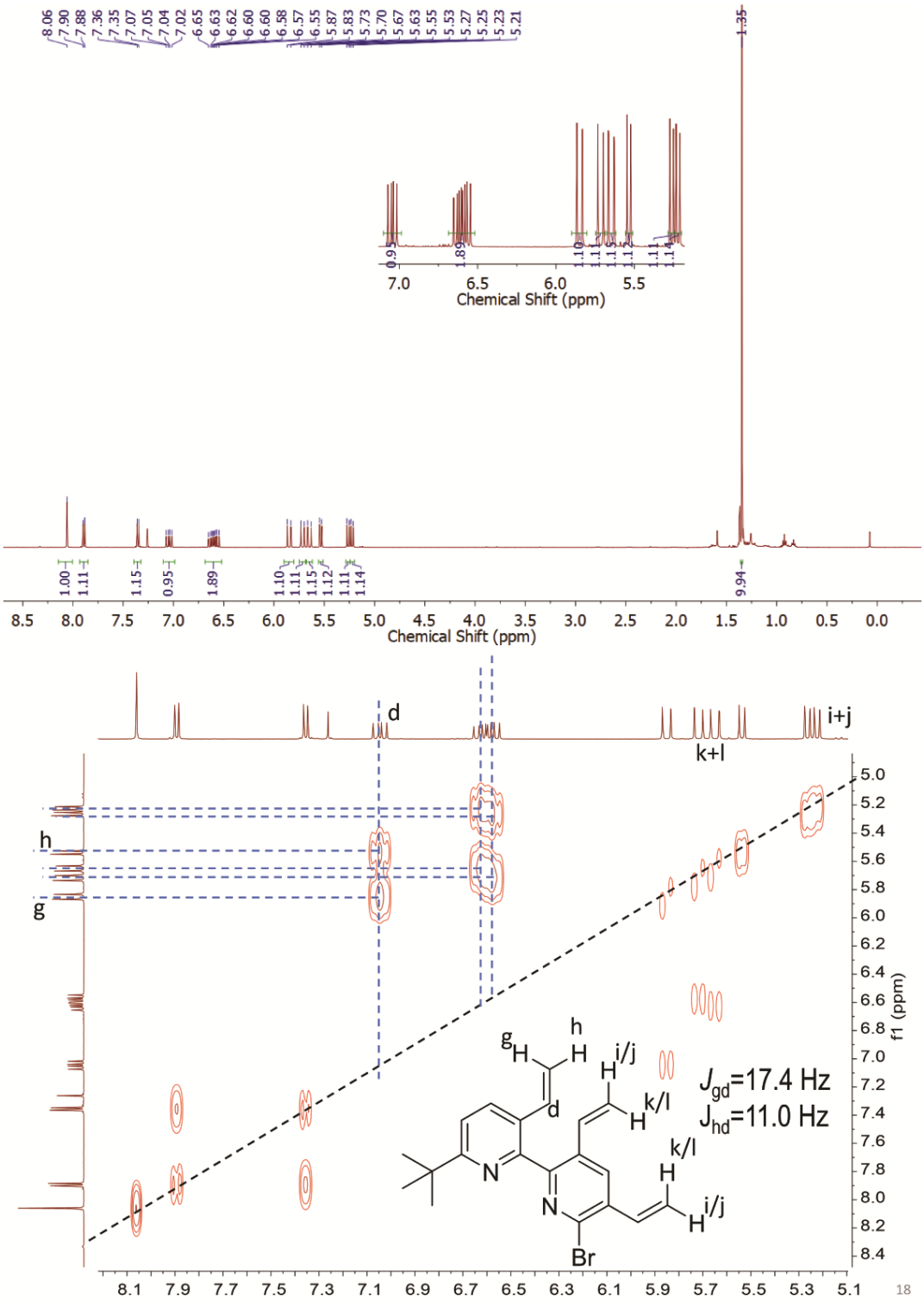

Figure 80. ^{1}H (500 MHz) NMR and ^{1}H-^{1}H COSY of v-tBu2Br in $CDCl_3$ at room temperature.

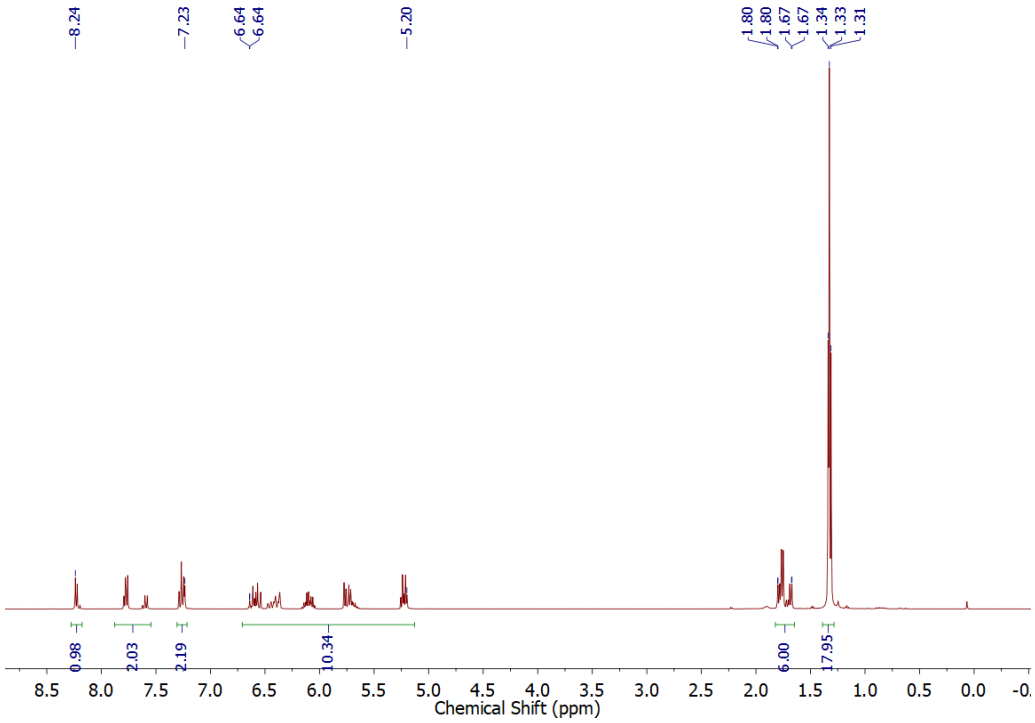

Figure 81. ^{1}H (400 MHz) NMR of pv-tBu3 in $CDCl_3$ at room temperature.

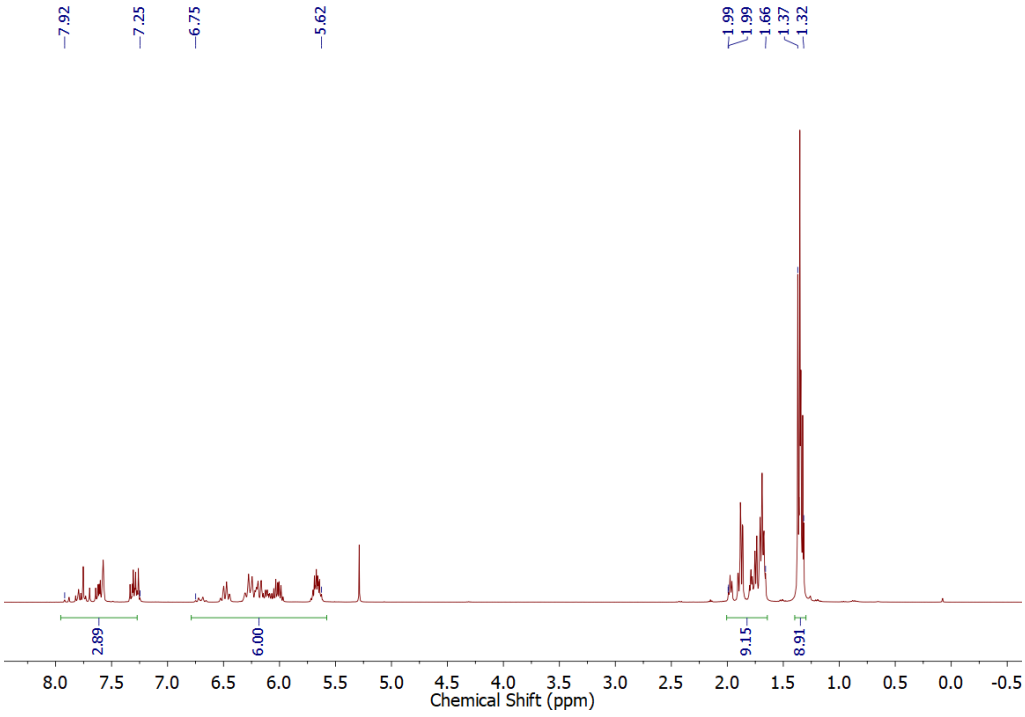

Figure 82. ^{1}H (400 MHz) NMR of p-tBu2Br in $CDCl_3$ at room temperature.

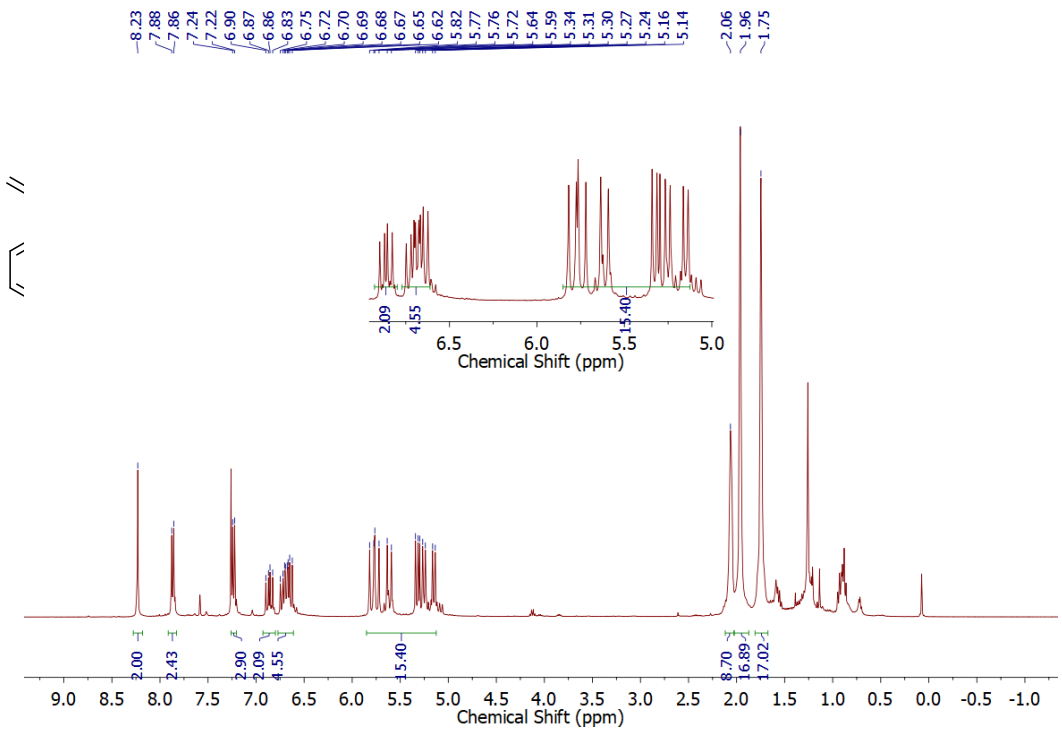

Figure 83. ^{1}H (400 MHz) NMR of v-Ad4 in $CDCl_3$ at room temperature.

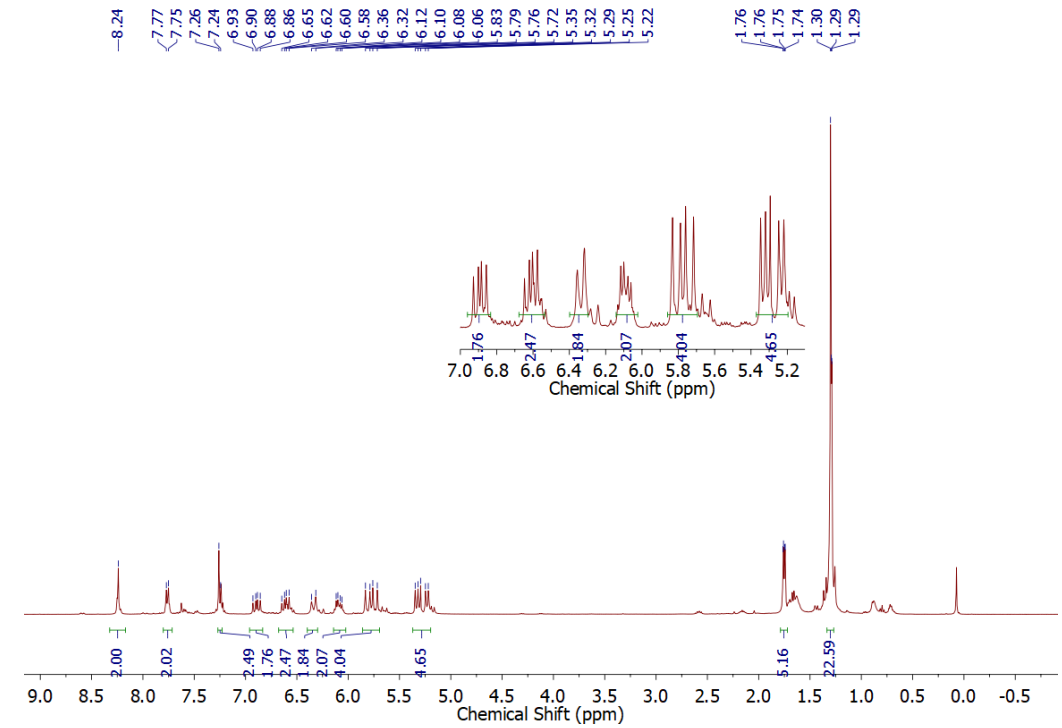

Figure 84. ^{1}H (400 MHz) NMR of pv-tBu4 in $CDCl_3$ at room temperature.

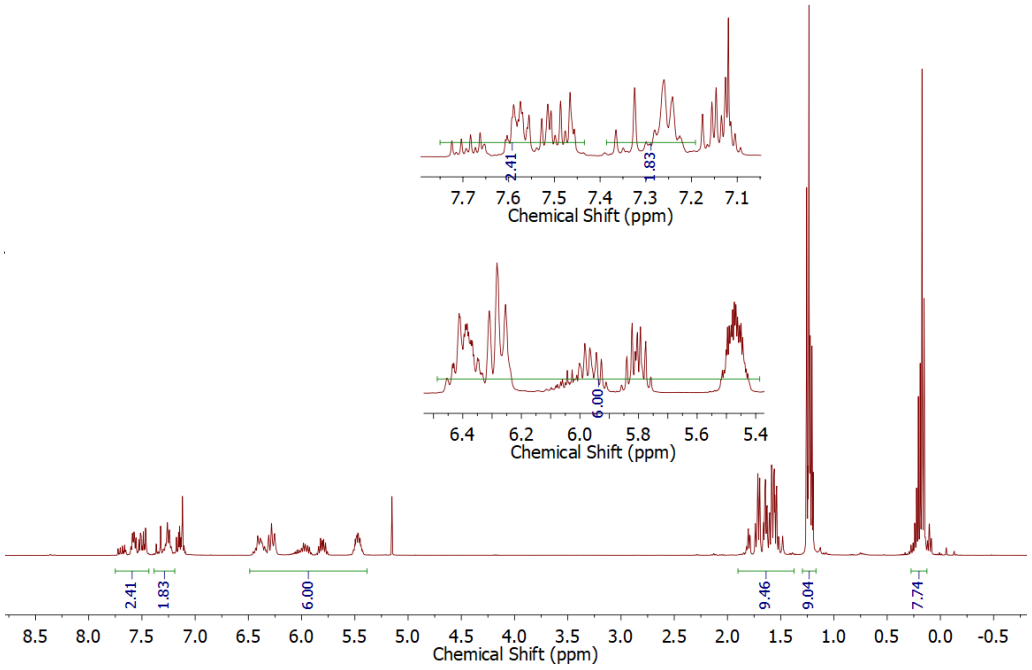

Figure 85. ^{1}H (400 MHz) NMR of p-tBu2SnMe in $CDCl_3$ at room temperature.

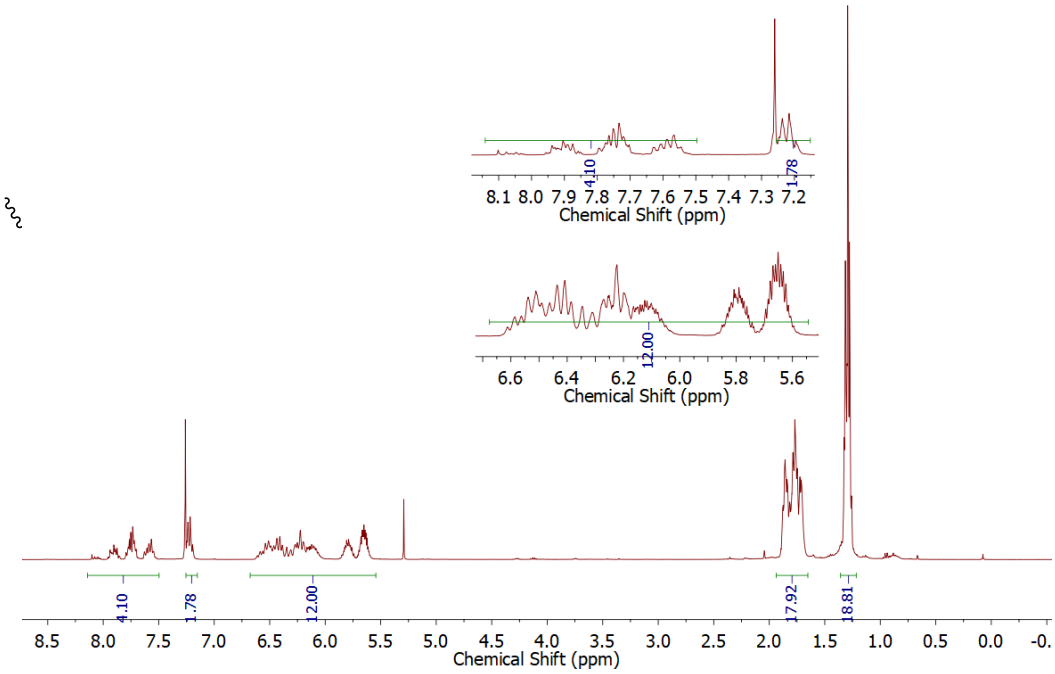

Figure 86. ^{1}H (400 MHz) NMR of p-tBu4 in $CDCl_3$ at room temperature.

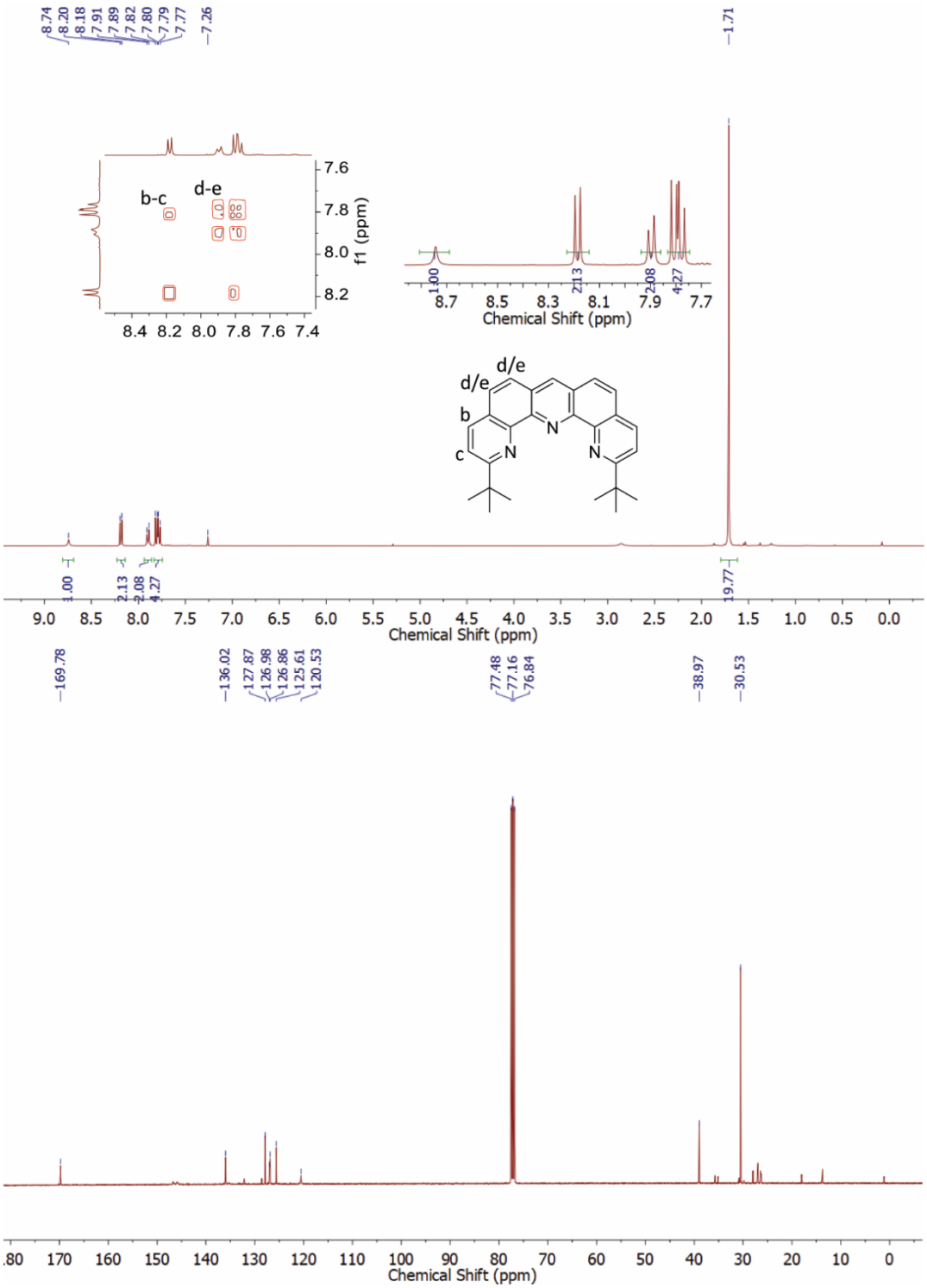

Figure 87. ^{1}H (500 MHz) NMR, 1H-1H COSY and ^{13}C{^{1}H} (100 MHz) NMR of p-tBu4 in $CDCl_3$ at room temperature.

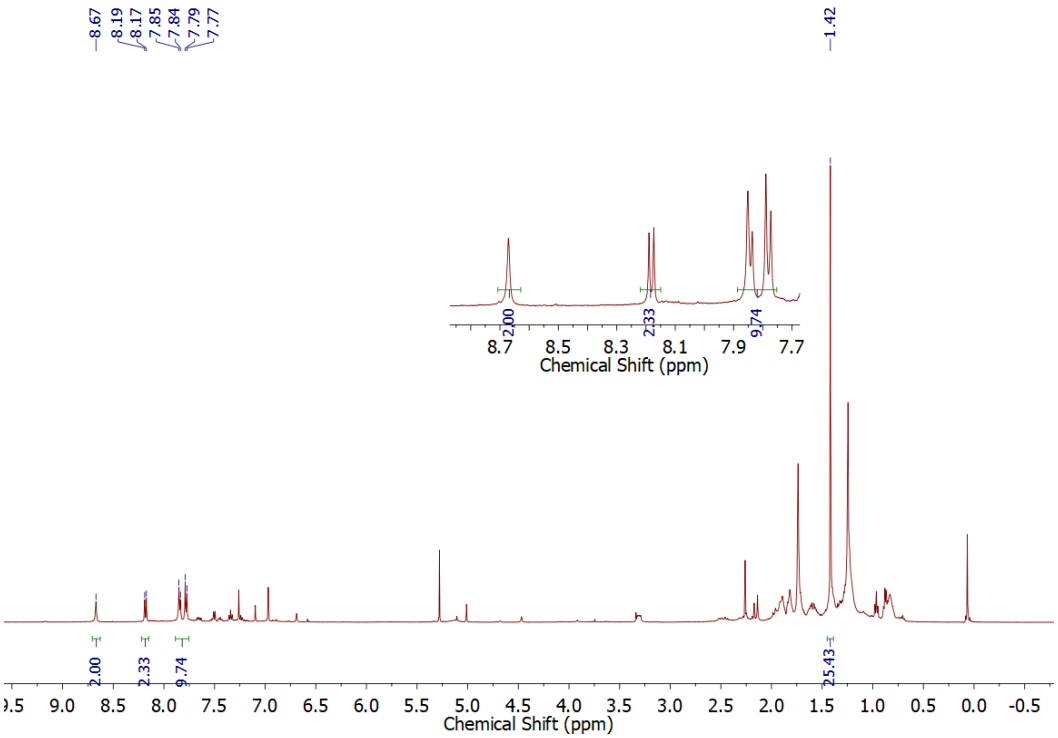

Figure 88. ^{1}H (500 MHz) NMR of tBu-4N7 in $CDCl_3$ at room temperature.

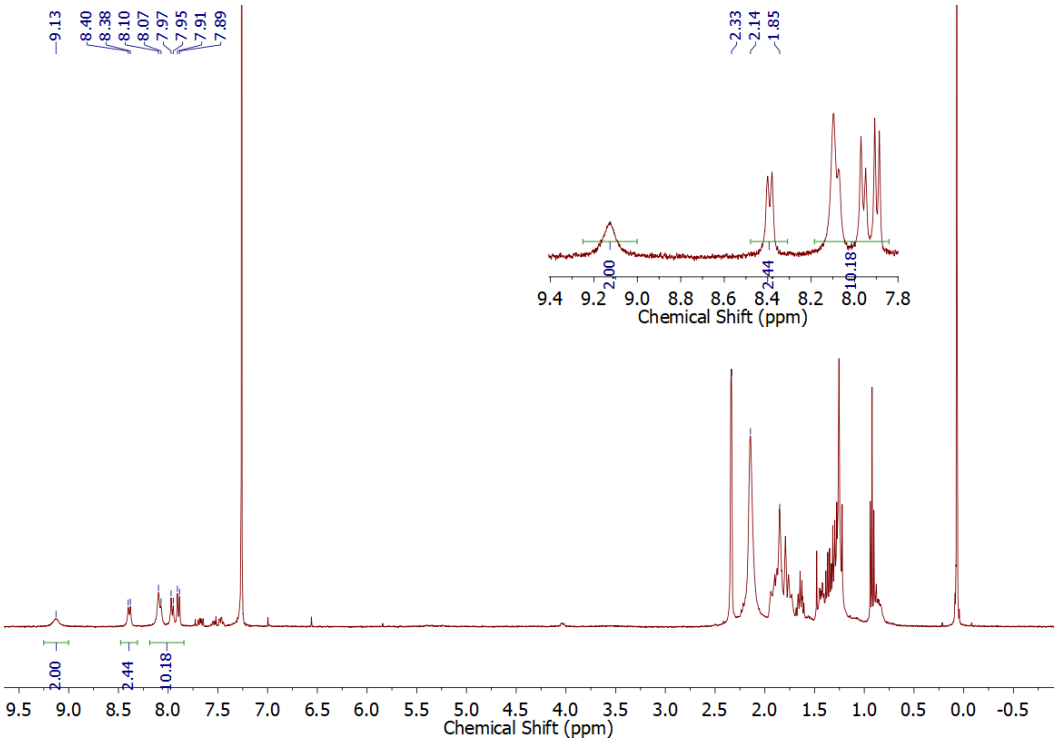

Figure 89. ^{1}H (400 MHz) NMR of Ad-4N7 in $CDCl_3$ at room temperature.

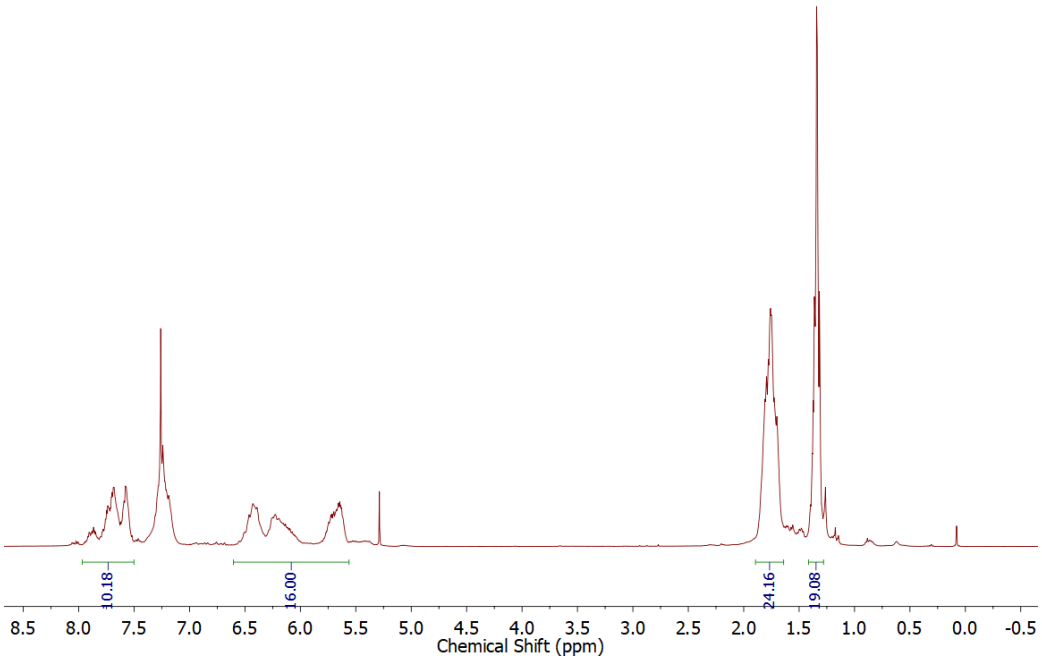

Figure 90. ^{1}H (400 MHz) NMR of p-tBu5 in $CDCl_3$ at room temperature.

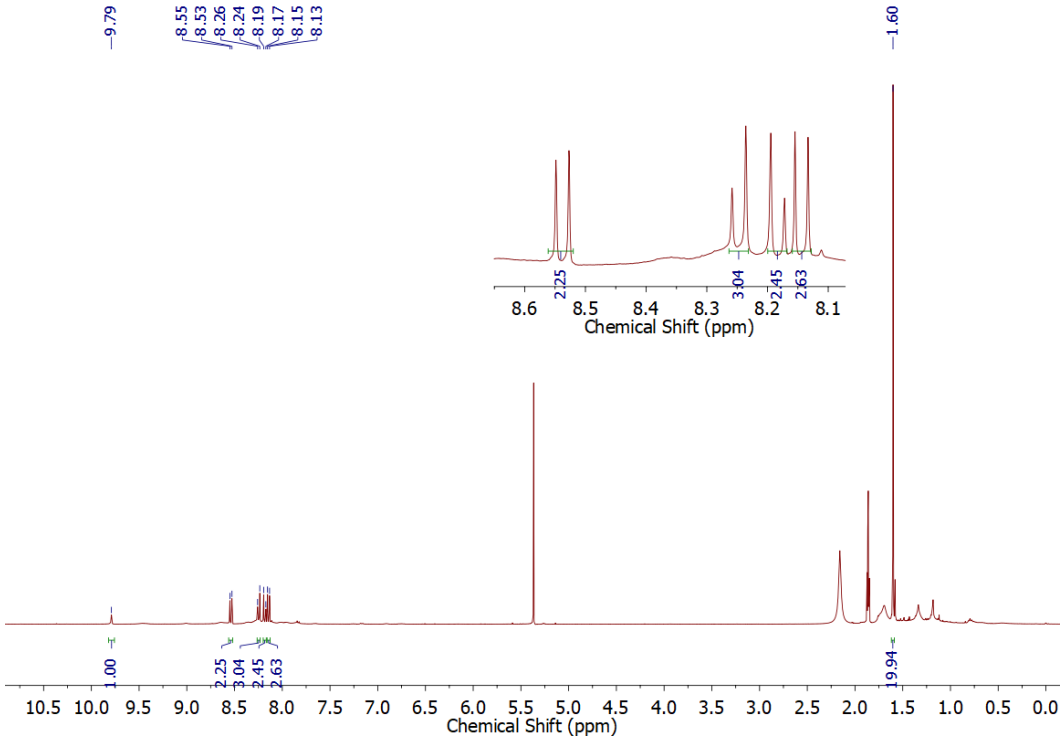

Figure 91. ^{1}H (400 MHz) NMR of $ZnL_2(OTf)_2$ in CD_3CN at room temperature, L = tBu-3N5.

CHAPTER V

DEVELOPMENT OF ORGANIC TEACHING LAB BASED ON "NOBEL PRIZE REACTIONS"

5.1 Introduction

Chemistry is a laboratory science which cannot be effectively taught without a robust laboratory experience for students at undergraduate level.[195] Laboratory experience is important not only for those majoring in chemistry to prepare them for more specific studies, but also for those majoring in other subjects to enhance their general science common sense and skills. Despite a survey result that students participating in the lab course pay most attention to their final grades, it was also mentioned that the experience during the course significantly impacted their focus.[196] In this context, the design of lab course topics, the clear instructions by the instructor, *etc*. all play an important role in the effective communication of scientific concepts.

In the contemporary curriculum design, the organic teaching labs are commonly supposed to be a complementary component of the theoretical organic chemistry course, and they usually progress synchronously with the theoretical course. Although this strengthens the understanding of chemical concepts, the experiments covered in teaching labs are usually quite conventional. Taking the organic teaching labs in Texas A&M University as an example, the topics include S_N1 reaction, oxidation of alcohol, reduction of camphor, diazonium and indigo dyes, *etc*. These reactions exemplify classical reaction categories, but the only organometallic reaction is Grignard reaction, which was proposed

over 100 years ago.[197] The absence of cutting-edge reactions in the teaching lab is critically impacting the efficiency of contemporary organic laboratory education.

Looking back at the methodologies developed in the last 50 years, there have been so many discoveries that revolutionized the field of organic chemistry. Among them cross coupling and olefin metathesis are the most notable examples as they are the topics of the Nobel Prize in Chemistry in 2010 and 2005, respectively. Tremendous attention has been attracted to these strategies, owing to their supreme power and versatility to construct more sophisticated molecules.[198,199] According to a survey in 2014, Suzuki was ranked as the second most frequently used reaction in the field of pharmaceuticals.[200] Bringing these impactful reactions into the chemical teaching lab will introduce the state-of-the-art chemical knowledge to undergraduates and transmit an idea of how these methods facilitate organic synthesis.

There have been a number of literature examples adopting Suzuki coupling and olefin metathesis in teaching lab. For Suzuki coupling, cases conducted in open air,[201] protected with nitrogen balloon,[202] using Schlenk line,[203] catalyzed with nickel catalyst,[204] *etc*. were reported. For the olefin metathesis, most of the reactions required nitrogen protection,[205] and the majority of these previous examples were cross metathesis instead of ring closing metathesis.[206] Herein we describe a novel design of sequential Suzuki coupling and ring closing metathesis to synthesize a common and simple polycyclic aromatic compound phenanthrene. Despite the simplicity of the final target compound, the underlying novelty and challenge are the requirement for simple experiment setup without

Schlenk line or liquid nitrogen degassing and the efficiency considering the time restriction and equipment restrictions for undergraduate laboratories.

5.2 Results and Discussion

The designed synthesis of phenanthrene is composed of two steps (**Figure 92**). In the first step, 2-bromostyrene and styrene boronic acid are coupled together via Suzuki coupling to afford the biphenyl derivative with pendant vinyl groups. Afterwards, this intermediate is subjected to RCM reaction to annulate the adjacent vinyl groups to obtain phenanthrene.

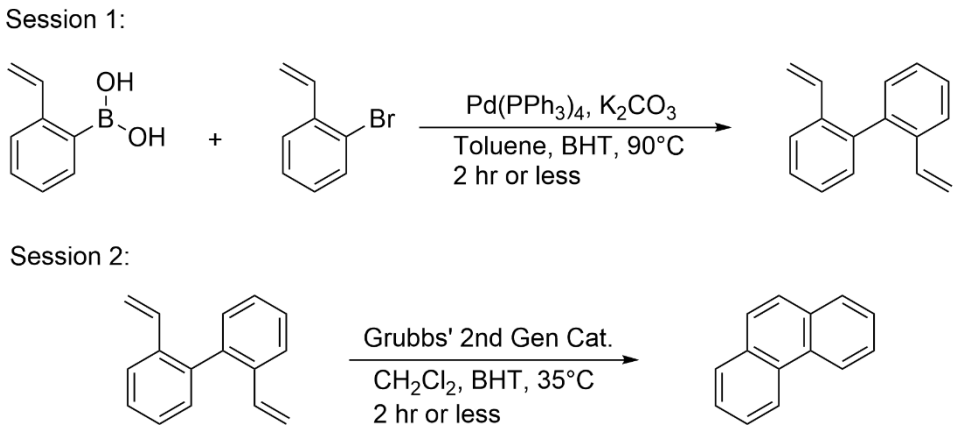

Figure 92. Synthetic scheme of the proposed teaching lab which contains Suzuki coupling and ring closing metathesis sequentially.

It would be a straightforward protocol if these experiments were to be conducted in a research lab scenario with liquid nitrogen, Schlenk line, glovebox, *etc*. However, these conditions had to be as simple as possible, and ambient conditions would be optimal for a teaching lab. Based on this situation, our strategy to find a feasible condition that would work in a teaching lab scenario was to start from the research lab conditions and gradually remove those specific requirements without significantly compromising the yields.

Table 5. Reaction condition optimization for the first step Suzuki coupling.

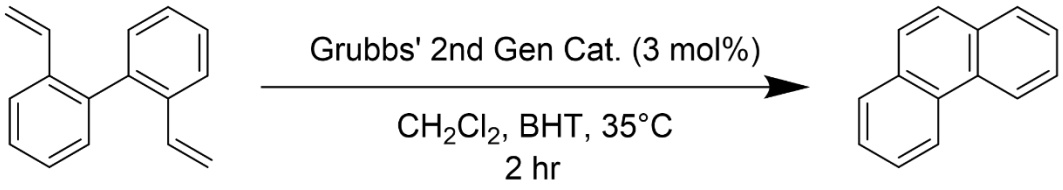

Entry	Reaction time	Method	Yield
1	2 h	Freeze, pump, thaw	60%
2	2 h	Open air	57%

For the first step of Suzuki coupling, a known working condition was to employ $Pd(PPh_3)_4$ as the catalyst, potassium carbonate as the base in toluene as the solvent, and BHT as the radical scavenger at 90°C. Considering the sensitivity of $Pd(PPh_3)_4$ to oxygen, the degassing method represented the key challenge. Another important factor was the

length of reaction time. Thus, we kept decreasing the complexity of the degassing method and reaction time to find a condition reasonable in the teaching lab and supplying decent yields. The summary of our trials is listed in **Table 5**. In the strictest condition, the yield was up to 80%. Next, the reaction time was shortened to only 2 hours, which enabled the reaction to be finished within a normal 3-hour lab course session. The yield was significantly decreased to 47% due to the incomplete conversion, but it was perceived as acceptable considering the short time. The step of freeze-pump-thaw step was further removed to simplify the reaction protocol, and nitrogen was bubbled into the reaction mixture for 15 min before the reaction. Gratifyingly, this change only decreased the yield slightly to 45%. This protocol was considered optimal considering the balance between simplicity and the yield.

Regarding the purification of the intermediate after the Suzuki step, column chromatography was selected as the key strategy, considering its special importance in organic synthesis. Based on the restriction of the teaching lab, a mini pipette filled with silica gel served as a flash column. Hexane was chosen as the eluent alone considering the low polarity of the product. The purification process usually afforded pure intermediates, with rare exceptions due to the difficulty to realize a complete separation between the intermediate and the starting material 2-bromostyrene under a high flow rate.

Table 6. Reaction condition optimization for the second step ring closing metathesis.

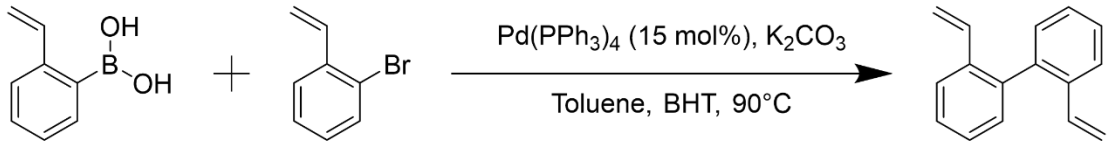

Entry	Reaction time	Degassing method	Yield
1	24 h	Freeze, pump, thaw	80%
2	2 h	Freeze, pump, thaw	47%
3	2 h	N_2 bubbling	45%

Afterwards, the optimization on the ring closing metathesis step was conducted. First, it was verified that 3 mol % of Grubbs' 2nd generation catalyst in DCM worked perfectly after being degassed with freeze-pump-thaw strategy. The removal of the freeze-pump-thaw strategy did not hamper the reaction, giving a similar yield and demonstrating desirable robustness of the catalyst towards this substrate. Regarding the purification method, a flash column worked well giving a yield of up to 80%. However, to expand the scope of purification methods taught in this course, recrystallization methods were examined. Ethanol and water served as a mixed solvent to realize the purification purpose to obtain flake-like crystals, and the yield by recrystallization was about 57%.

With the successful implementation of these two steps, the last factor before putting the lab to real practice is the cost and the safety issues. In terms of the cost, both 2-bromostyrene and styrene boronic acid were affordable. Although $Pd(PPh_3)_4$ and Grubbs'

2nd generation catalyst were more expensive, the overall cost was affordable as well considering the low catalyst loading required. Regarding safety concern, there were not significant hazards like high pressure or corrosive chemicals, but normal safety rules would be practiced assuring the lab would be carried out in a safe manner. In the fall semester of 2021, this lab was successfully implemented in the organic lab CHEM234 at Texas A&M University, which involved chemistry-majored second year undergraduates.

5.3 Conclusion

In conclusion, a teaching lab course that covered two Nobel prize winning reactions, Suzuki coupling and ring closing metathesis, was developed. The development of this lab addressed the concern that most of the topics covered in undergraduate lab courses are outdated and key metal-catalyzed reactions are missing in the current teaching curriculum. A simple polycyclic compound phenanthrene was chosen as the synthetic target which was designed to be achieved in two sequential steps, Suzuki coupling followed by ring closing metathesis. By carefully screening the reaction conditions viable in the context of a teaching lab, we successfully found a complete protocol that started from easily available starting materials to the final product that can be steadily characterized. The participation in this lab enabled students to not only learn state-of-the-art knowledge of chemistry and especially organometallic chemistry, but also review essential practical skills in chemical labs, like recrystallization, flash chromatography, *etc*.

The designed teaching lab has been successfully implemented. Next, a detailed plan to collect the statistics about the running status of this new lab, including the success rate

of students, students' feedback, amount of chemicals used, *etc*., is needed. In the upcoming semester, we will introduce quantitative survey to capture students' learning outcomes and instructors' feedback on these experiments.

5.4 Experimental Section

5.4.1 General Methods and Materials

Starting materials and reagents were purchased from commercial sources and were used as received without further purification. THF was dried and distilled under nitrogen from sodium using benzophenone as the indicator. Toluene was dried using an inert pure solvent system and used without further treatment. An oil bath was used for those reactions that required heating. ^{1}H and ^{13}C NMR spectra were recorded on a 500 MHz or 400 MHz spectrometer. The ^{1}H and $^{13}C\{^{1}H\}$ NMR chemical shifts were reported in ppm relative to the signals corresponding to the residual non-deuterated solvents ($CDCl_3$: ^{1}H 7.26 ppm, ^{13}C 77.23 ppm) or the internal standard (tetramethylsilane: ^{1}H 0.00 ppm). Abbreviations for reported signal multiplicities are as follows: s, singlet; d, doublet; t, triplet; q, quartet; m, multiplet; br, broad. The broad singlet at ~1.55 ppm on ^{1}H NMR spectra represents the resonance signal of H_2O in $CDCl_3$. Column chromatography was carried out on a normal phase SiO_2.

5.4.2 Synthesis

2,2'-divinyl-1,1'-biphenyl. In an open 25 mL round bottom flask equipped with a stir bar, 2-bromostyrene (1 mmol, 0.183 g), (2-vinylphenyl)boronic acid (1.2 mmol, 0.178

g), fresh tetrakis (0.15 mmol, 173 mg), potassium carbonate (3 mmol, 0.414 g) and a few crystal of BHT were mixed in 5 mL toluene. Nitrogen was purged into the mixture through a needle for 15 minutes. Afterwards, the mixture was heated up to 90°C with a refluxing apparatus. The reaction lasted for 2 hours, after which it was cooled down to room temperature, and washed with water. A simple extraction was conducted in a large test tube with DCM, and the bottom organic phase was combined and dried over Na2SO4. Next, the dried organic phase was subjected to reduced pressure to remove volatile solvent, and the crude product was dissolved in 1 mL hexane again. The 1 mL hexane solution was charged onto the top of pre-packed silica gel column, and a rubber bulb was used to apply pressure slowly to allow the eluent to flow through the mini column. The first fraction was collected as the colorless oil as the product in a 45% yield without further purification. ^{1}H NMR (500 MHz, $CDCl_3$) δ = 7.67 (d, 2H), 7.37 (t, 2H), 7.29 (t, 2H), 7.16 (d, 2H), 6.41 (dd, 2H), 5.66 (d, 2H), 5.10 (d, 2H).

Phenanthrene. All the product from the last step was transferred into a 25mL round bottom flask, and 10 mL of DCM was used to wash the initial flask and then combined into the new reaction flask. To this solution, Grubbs' 2nd generation catalyst (0.015 mmol, 12 mg) was added to the flask. The mixture solution was stirred for 2 hours. Afterwards, the solvent was directly removed under reduced pressure. The crude product was purified with recrystallization by ethanol as the good solvent and water as the poor solvent. The product was collected as white flakes in a 60% yield. ^{1}H NMR (4z00 MHz, $CDCl_3$) δ = 8.70 (d, 2H), 7.90 (d, 2H), 7.65-7.69 (m, 2H), 7.59-7.63 (m, 2H).

5.4.2 NMR Spectra

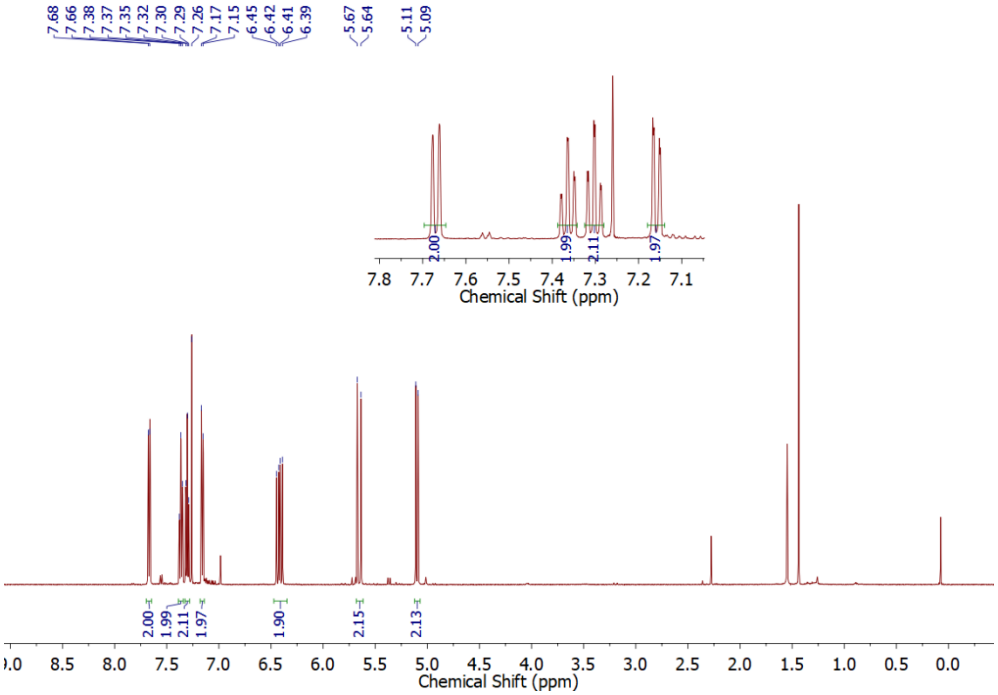

Figure 93. ^{1}H (500 MHz) NMR of 2,2'-divinyl-1,1'-biphenyl in $CDCl_3$ at room temperature.

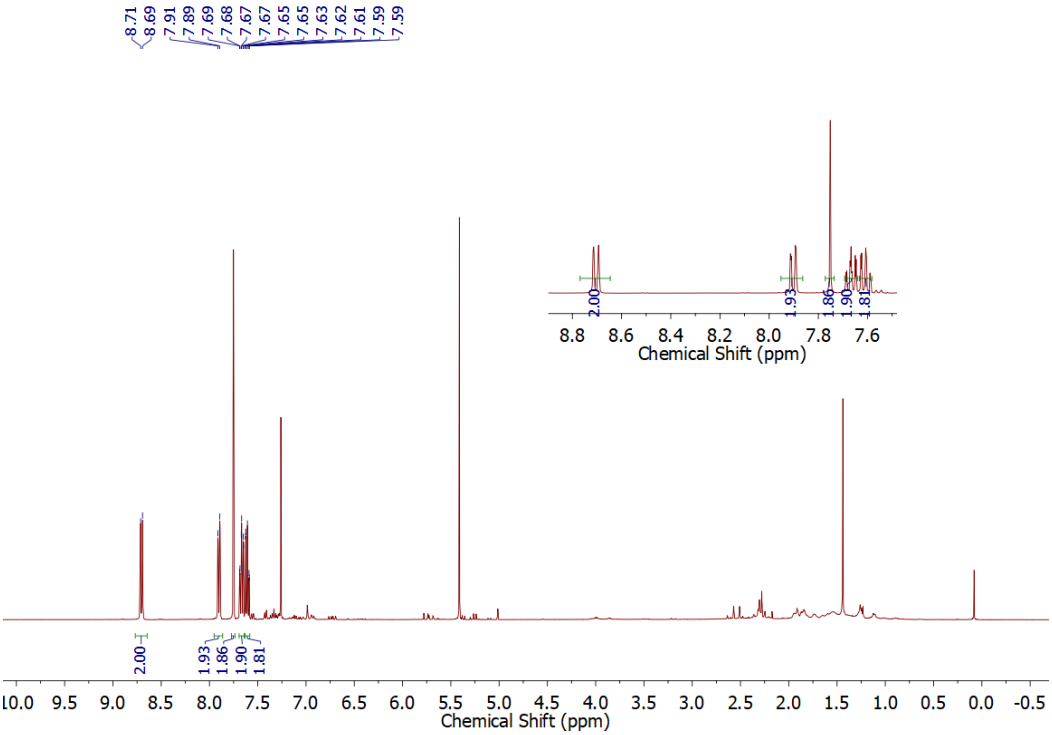

Figure 94. ^{1}H (400 MHz) NMR of phenanthrene in $CDCl_3$ at room temperature.

CHAPTER VI

CONCLUSIONS AND PERSPECTIVES

6.1 Ladder Type Small Molecule Embedding B←N Coordinative Bonds

B←N coordinative bonds have been demonstrated by our previous members that they can enforce a rigid and coplanar conformation in π-conjugated molecules. The introduction of B←N coordinative bonds on an indolocarbazole core enabled robust and reversible redox states.

In the first project, I integrated the indolocarbazole core with indaceno[2,1-d:6,5-d′]dithiazole and employed efficient borylation reaction to construct a ladder type molecule **BN-1** with 23 fused rings featuring four B—N covalent bonds and four B←N coordinative bonds. Various characterization methods implied that these B—N bonds not only rigidified the backbone but also decreased the frontier orbitals along with the bandgap compared to the counterpart with C—C bonds in the place of B—N bonds.

Second, I also successfully installed aryl groups with different electronic properties onto the indolocarbazole core and examined the structure-property relationship. Four molecules, **Th-IDCZ-BTh**, **Th-IDCZ-Cl-BTh**, **Ph-IDCZ-BTh** and **Ph-IDCZ-Cl-BTh**, were proposed and synthesized. The theoretical simulation results and experimental data on the bandgap matched well with our expectations based on the nature of the chosen aryl groups. GIWAXS data suggested a high crystallinity thanks to the rigidified backbone. Later, the electron transport mobilities of these molecules were tested but only moderate readings were recorded on the fabricated OTFTs.

Following the previous success, I achieved the synthesis of several novel molecules whose backbone was rigidified by the introduction of B←N bonds. However, these molecules did not show high performances as *n*-type semiconductors. There could be a couple of reasons for the unsatisfaction. First, the LUMO energy level was still not low enough. For example, **BN-1** still had a LUMO energy level -3.48 eV, and the other four molecules mentioned in Chapter III had the lowest LUMO energy level of -3.69 eV. These values did not meet the empirical criteria that a desirable LUMO value for *n*-type organic semiconductor is as low as -4.0 eV.

In fact, the sole introduction of B—N bonds seemed insufficient to achieve remarkable mobility data. To address this concern of molecular design, other common moieties in *n*-type organic semiconductors, like cyano groups, PDI/NDI, DPP, *etc*. can be tested Currently, there has been significant progress regarding the compounds based on isoindigo and benzobisimidazole structures (**Figure 95**), and more detailed characterization data will demonstrate their properties including device data.

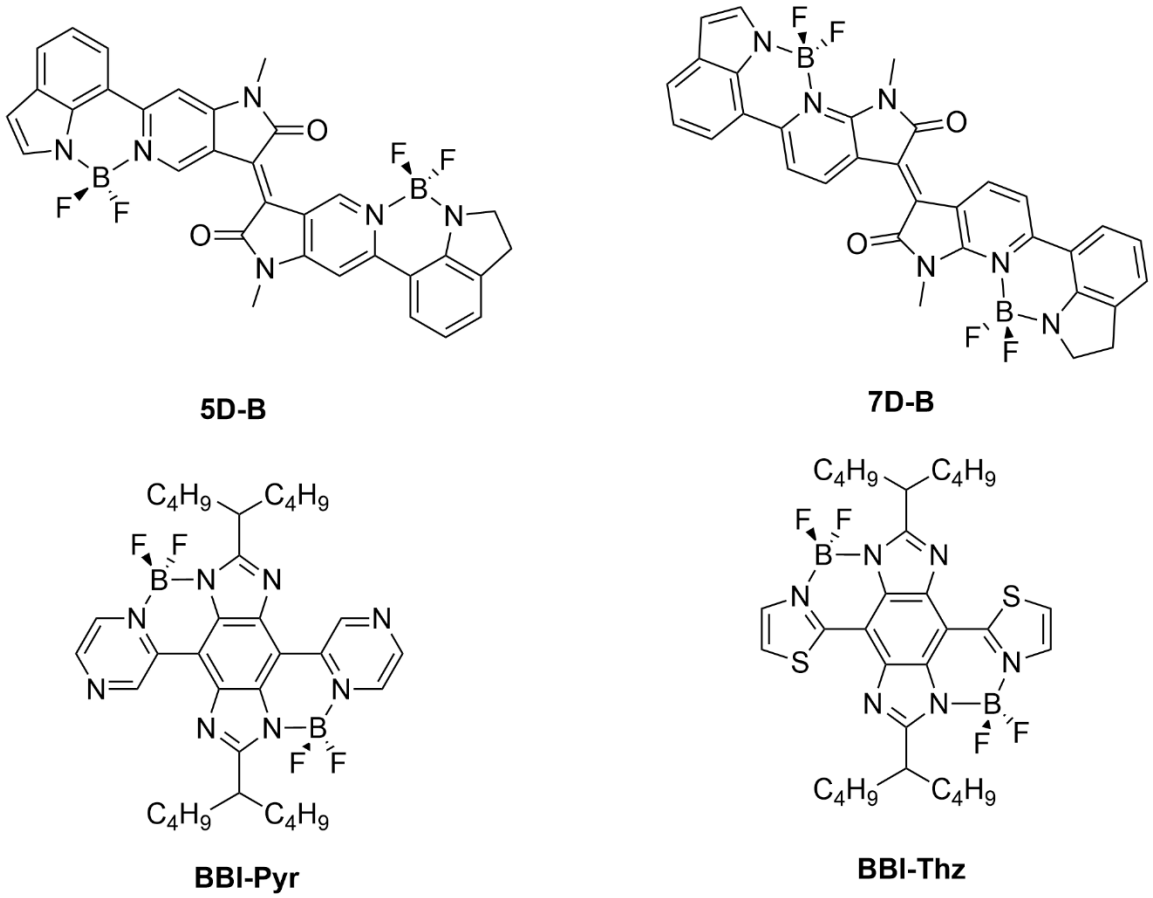

Figure 95. Perspective target molecules for research in our lab with different moieties.

6.2 Synthesis and Supramolecular Chemistry of Centripetal Azahelicenes

Despite the previous literature on azahelicenes, helicenes with nitrogen atoms decorating the inner rim remain unexplored. Importantly, this family of compounds were envisioned to function as strong ligands considering its preorganization of nitrogen atoms to avoid entropy penalty. Thus, I proposed a synthetic route towards these helicenes employing RCM as the key strategy to annulate the backbone.

Guided by the retrosynthesis on the proposed centripetal azahelicenes, I accomplished efficient synthesis of the building blocks with pendant olefins. Preliminary attempts on oligomerization and RCM witnessed a low to moderate yield, despite the mass spec and NMR spectrum on the helicene **Ad-4N7** with adamantyl as the steric group. Reflecting on the strain, the bulky group was changed to tert-butyl to accommodate strain. In addition, detailed modifications, such as changing the stannyl group, changing the propenyl group to vinyl group, *etc*. were continuously made to improve the synthetic efficiency. The initial oxidative homocoupling was discarded due to its low efficiency reproducibility. The iterative stannylation-Stille method was adopted to achieve precursors before RCM reaction. This change not only enhanced the reproducibility of this step, but also enabled the synthesis of longer precursors instead of those limited to tetramer. In the last step RCM reaction, semi-pure pseudo-helicene **tBu-4N7** was achieved.

Despite the preliminary success, there remains room for improvement regarding synthesis. The RCM reaction currently only worked well on the model compound **tBu-3N5**, which prompted us to find better conditions to optimize the yield of this reaction. With the experience on the synthesis on tetramer, exploration will take place to synthesize longer precursors containing five, six and even seven pyridine rings. With the satisfactory search for RCM conditions, these precursors will be annulated to afford the proposed centripetal azahelicenes (**Figure 96**).

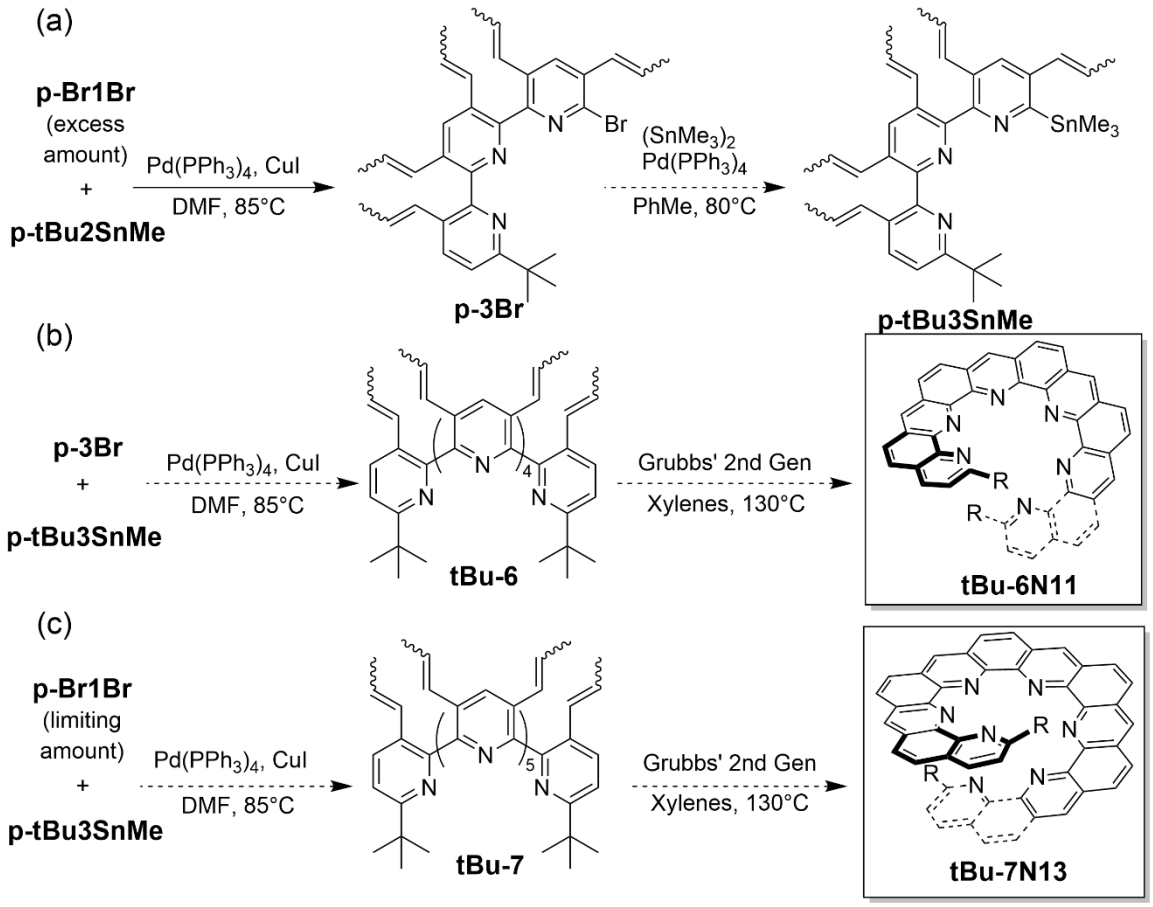

Figure 96. Perspective synthesis of precursors and final azahelicenes with six and seven nitrogen atoms.

Following the successful synthesis of these azahelicenes, their intriguing supramolecular properties will be explored. The proposed rigid ligands are anticipated to exhibit extraordinary affinity and sharp selectivity in coordinating large sized metal cations. They are particularly promising ligands for *f*-block lanthanide (Ln) cations, which are challenging to bind with high affinity and selectivity due to (i) the lack of

stereoelectronic preference that are seen on transition metals and (ii) the demand on a large coordination number from the ligand(s).[207] The important factors governing the coordination here are the supramolecular principles on size matching, multivalency, and preorganization, which are the inherent structural features designed into centripetal azahelicenes. For affinity, the rigid and multivalent nitrogen sites of these rigid polypyridyl ligands provide the large coordination number from a single ligand molecule. Moreover, the fused-ring backbone eliminates the undesired 3,3′-H-H repulsion and minimizes binding entropy penalty to further boost the affinity. The association constants of the proposed ligands vs appropriate Ln(III) are expected to be in the range of $10^9 \sim 10^{15}$ mol^{-1}.

The binding selectivity of polypyridine ligands vs various Ln(III) ions is mainly determined by the ligand strain energy (U) after forming the complex, which is balanced between the 3,3′-H-H repulsion raised by complex-driven planarization, and the forced change of ligand curvature upon chelating (**Figure 97**). The ionic radii of Ln(III) ions contract from La (1.032 Å) and Ce (1.01 Å) to late lanthanides such as Lu (0.861 Å). For conventional polypyridine ligands, the balance of ligand strain U often results in a favorable binding affinity with a middle lanthanide, such as Sm(III).[208] We anticipated that our ligands will have a much steeper change of the U value upon coordinating size-mismatched Ln(III) ions, due to significantly higher rigidity. We will test the binding affinities of them vs various Ln(III) ions by titration and competition experiments. The rigid ligands are expected to exert significantly sharper selectivity in favoring certain early

Ln(III) ions. These results will be critical for important applications involving separation, purification, and extraction of lanthanides.[209,210]

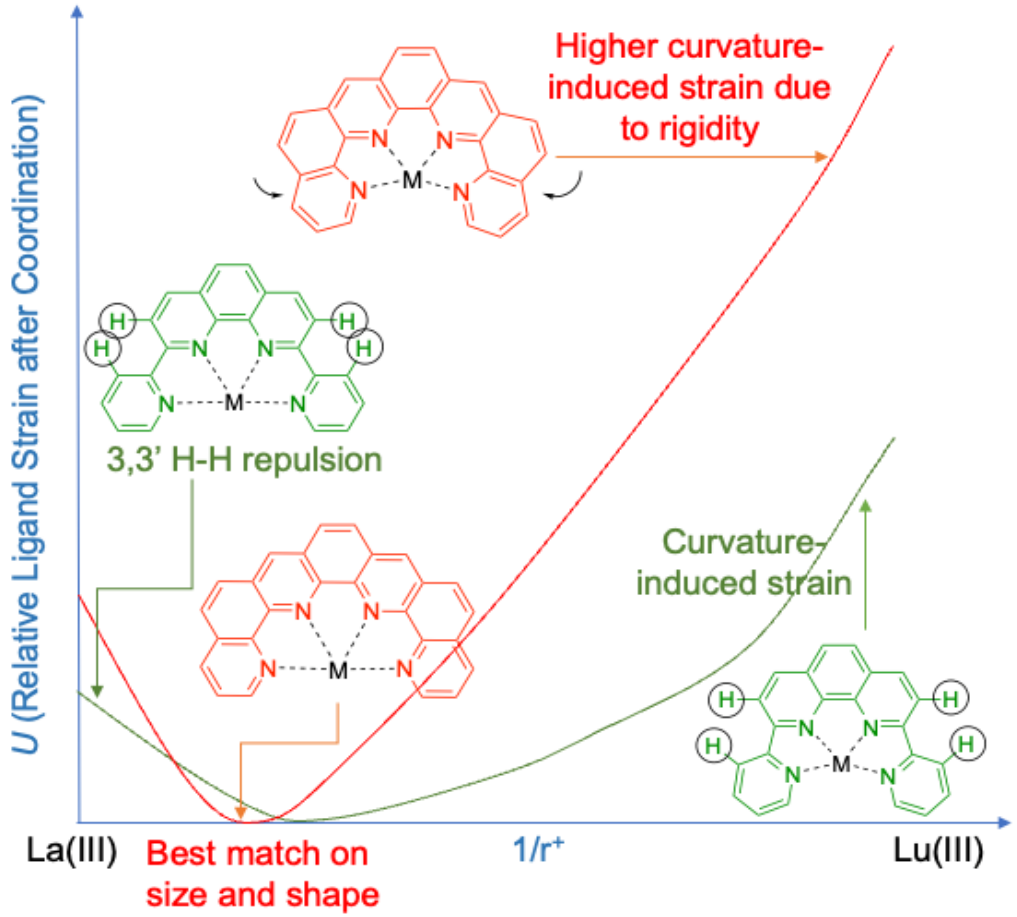

Figure 97. Schematic figure to demonstrate the selectivity on lanthanide by helicenes.

REFERENCES

1. Griffiths, J., Introduction: The Evolution of Present-Day Dye Technology. In *The Chemistry and Application of Dyes*, Waring, D. R.; Hallas, G., Eds. Springer US: Boston, MA, 1990; pp 1-16.

2. Meyer, J. C.; Geim, A. K.; Katsnelson, M. I.; Novoselov, K. S.; Booth, T. J.; Roth, S., The structure of suspended graphene sheets. *Nature* **2007,** *446* (7131), 60-63.

3. Rieger, R.; Müllen, K., Forever young: polycyclic aromatic hydrocarbons as model cases for structural and optical studies. *J. Phys. Org. Chem.* **2010,** *23* (4), 315-325.

4. Tour, J. M., Top-Down versus Bottom-Up Fabrication of Graphene-Based Electronics. *Chem. Mater.* **2014,** *26* (1), 163-171.

5. Narita, A.; Wang, X.-Y.; Feng, X.; Müllen, K., New advances in nanographene chemistry. *Chem. Soc. Rev.* **2015,** *44* (18), 6616-6643.

6. Wu, J.; Pisula, W.; Müllen, K., Graphenes as Potential Material for Electronics. *Chem. Rev.* **2007,** *107* (3), 718-747.

7. Wang, Y.; Shao, Y.; Matson, D. W.; Li, J.; Lin, Y., Nitrogen-Doped Graphene and Its Application in Electrochemical Biosensing. *ACS Nano* **2010,** *4* (4), 1790-1798.

8. Nguyen, D. K.; Tran, N. T. T.; Chiu, Y.-H.; Gumbs, G.; Lin, M.-F., Rich essential properties of Si-doped graphene. *Sci. Rep.* **2020,** *10* (1), 12051.

9. Zhu, Y.; Murali, S.; Stoller, M. D.; Ganesh, K. J.; Cai, W.; Ferreira, P. J.; Pirkle, A.; Wallace, R. M.; Cychosz, K. A.; Thommes, M.; Su, D.; Stach, E. A.; Ruoff, R. S., Carbon-based supercapacitors produced by activation of graphene. *Science* **2011,** *332* (6037), 1537-41.

10. Li, M.; Zhang, L.; Xu, Q.; Niu, J.; Xia, Z., N-doped graphene as catalysts for oxygen reduction and oxygen evolution reactions: Theoretical considerations. *J. Catal.* **2014,** *314*, 66-72.

11. Kuzmin, A. V.; Shainyan, B. A., Single Si-Doped Graphene as a Catalyst in Oxygen Reduction Reactions: An In Silico Study. *ACS Omega* **2020,** *5* (25), 15268-15279.

12. Gutzler, R.; Perepichka, D. F., π-Electron Conjugation in Two Dimensions. *J. Am. Chem. Soc.* **2013,** *135* (44), 16585-16594.

13. Qian, G.; Wang, Z. Y., Near-Infrared Organic Compounds and Emerging Applications. *Chem. Asian J.* **2010,** *5* (5), 1006-1029.

14. Sun, Z.; Wu, J., Higher Order Acenes and Fused Acenes with Near-infrared Absorption and Emission. *Aust. J. Chem.* **2011,** *64* (5), 519-528.

15. Pawlicki, M.; Collins, H. A.; Denning, R. G.; Anderson, H. L., Two-Photon Absorption and the Design of Two-Photon Dyes. *Angew. Chem. Int. Ed.* **2009,** *48* (18), 3244-3266.

16. Sreejith, S.; Divya, K. P.; Jayamurthy, P.; Mathew, J.; Anupama, V. N.; Philips, D. S.; Anees, P.; Ajayaghosh, A., Heteroaromatic donors in donor–acceptor–donor based fluorophores facilitate zinc ion sensing and cell imaging. *Photochem. Photobiol. Sci.* **2012,** *11* (11), 1715-1723.

17. Jin, E.; Yang, Q.; Ju, C.-W.; Chen, Q.; Landfester, K.; Bonn, M.; Müllen, K.; Liu, X.; Narita, A., A Highly Luminescent Nitrogen-Doped Nanographene as an Acid- and Metal-Sensitive Fluorophore for Optical Imaging. *J. Am. Chem. Soc.* **2021,** *143* (27), 10403-10412.

18. Arai, S.; Hida, M., Polycyclic Aromatic Nitrogen Cations. In *Adv. Heterocycl. Chem.*, Katritzky, A. R., Ed. Academic Press: 1992; Vol. 55, pp 261-358.

19. Zeng, Z.; Shi, X.; Chi, C.; López Navarrete, J. T.; Casado, J.; Wu, J., Pro-aromatic and anti-aromatic π-conjugated molecules: an irresistible wish to be diradicals. *Chem. Soc. Rev.* **2015,** *44* (18), 6578-6596.

20. Draper, S. M.; Gregg, D. J.; Schofield, E. R.; Browne, W. R.; Duati, M.; Vos, J. G.; Passaniti, P., Complexed Nitrogen Heterosuperbenzene: The Coordinating Properties of a Remarkable Ligand. *J. Am. Chem. Soc.* **2004,** *126* (28), 8694-8701.

21. Gregg, D. J.; Bothe, E.; Höfer, P.; Passaniti, P.; Draper, S. M., Extending the Nitrogen-Heterosuperbenzene Family: The Spectroscopic, Redox, and Photophysical Properties of "Half-Cyclized" N-1/2HSB and Its Ru(II) Complex. *Inorg. Chem.* **2005,** *44* (16), 5654-5660.

22. Wijesinghe, L. P.; Lankage, B. S.; Máille, G. M. Ó.; Perera, S. D.; Nolan, D.; Wang, L.; Draper, S. M., Methoxy functionalisation: exerting synthetic control of the supramolecular and electronic structure of nitrogen-doped nanographenes. *Chem. Commun.* **2014,** *50* (73), 10637-10640.

23. Graczyk, A.; Murphy, F. A.; Nolan, D.; Fernández-Moreira, V.; Lundin, N. J.; Fitchett, C. M.; Draper, S. M., Terpyridine-fused polyaromatic hydrocarbons generated via cyclodehydrogenation and used as ligands in Ru(ii) complexes. *Dalton Trans.* **2012,** *41* (25), 7746-7754.

24. Stock, A.; Pohland, E., Borwasserstoffe, IX.: B3N3H6. *Berichte der deutschen chemischen Gesellschaft (A and B Series)* **1926,** *59* (9), 2215-2223.

25. Hatakeyama, T.; Hashimoto, S.; Oba, T.; Nakamura, M., Azaboradibenzo[6]helicene: Carrier Inversion Induced by Helical Homochirality. *J. Am. Chem. Soc.* **2012,** *134* (48), 19600-19603.

26. Wang, X.; Zhang, F.; Liu, J.; Tang, R.; Fu, Y.; Wu, D.; Xu, Q.; Zhuang, X.; He, G.; Feng, X., Ladder-Type BN-Embedded Heteroacenes with Blue Emission. *Org. Lett.* **2013,** *15* (22), 5714-5717.

27. Dou, C.; Ding, Z.; Zhang, Z.; Xie, Z.; Liu, J.; Wang, L., Developing Conjugated Polymers with High Electron Affinity by Replacing a C□C Unit with a B←N Unit. *Angew. Chem. Int. Ed.* **2015,** *54* (12), 3648-3652.

28. Dou, C.; Long, X.; Ding, Z.; Xie, Z.; Liu, J.; Wang, L., An Electron-Deficient Building Block Based on the B←N Unit: An Electron Acceptor for All-Polymer Solar Cells. *Angew. Chem. Int. Ed.* **2016,** *55* (4), 1436-1440.

29. Lu, J.-S.; Ko, S.-B.; Walters, N. R.; Kang, Y.; Sauriol, F.; Wang, S., Formation of Azaborines by Photoelimination of B,N-Heterocyclic Compounds. *Angew. Chem. Int. Ed.* **2013,** *52* (17), 4544-4548.

30. Wang, S.; Yang, D.-T.; Lu, J.; Shimogawa, H.; Gong, S.; Wang, X.; Mellerup, S. K.; Wakamiya, A.; Chang, Y.-L.; Yang, C.; Lu, Z.-H., In Situ Solid-State Generation of (BN)2-Pyrenes and Electroluminescent Devices. *Angew. Chem. Int. Ed.* **2015,** *54* (50), 15074-15078.

31. Wang, X.-Y.; Zhuang, F.-D.; Wang, R.-B.; Wang, X.-C.; Cao, X.-Y.; Wang, J.-Y.; Pei, J., A Straightforward Strategy toward Large BN-Embedded π-Systems: Synthesis,

Structure, and Optoelectronic Properties of Extended BN Heterosuperbenzenes. *J. Am. Chem. Soc.* **2014,** *136* (10), 3764-3767.

32. Dosso, J.; Tasseroul, J.; Fasano, F.; Marinelli, D.; Biot, N.; Fermi, A.; Bonifazi, D., Synthesis and Optoelectronic Properties of Hexa-peri-hexabenzoborazinocoronene. *Angew. Chem. Int. Ed.* **2017,** *56* (16), 4483-4487.

33. Fresta, E.; Dosso, J.; Cabanillas-González, J.; Bonifazi, D.; Costa, R. D., Origin of the Exclusive Ternary Electroluminescent Behavior of BN-Doped Nanographenes in Efficient Single-Component White Light-Emitting Electrochemical Cells. *Adv. Funct. Mater.* **2020,** *30* (33), 1906830.

34. Allemann, O.; Duttwyler, S.; Romanato, P.; Baldridge, K. K.; Siegel, J. S., Proton-Catalyzed, Silane-Fueled Friedel-Crafts Coupling of Fluoroarenes. *Science* **2011,** *332* (6029), 574-577.

35. Ko, S.-B.; Lu, J.-S.; Wang, S., Chelation-Assisted Photoelimination of B,N-Heterocycles. *Org. Lett.* **2014,** *16* (2), 616-619.

36. Yang, D.-T.; Mellerup, S. K.; Peng, J.-B.; Wang, X.; Li, Q.-S.; Wang, S., Substituent Directed Phototransformations of BN-Heterocycles: Elimination vs Isomerization via Selective B–C Bond Cleavage. *J. Am. Chem. Soc.* **2016,** *138* (36), 11513-11516.

37. Yang, D.-T.; Shi, Y.; Peng, T.; Wang, S., BN-Heterocycles Bearing Two BN Units: Influence of the Linker and the Location of BN Units on Electronic Properties and Photoreactivity. *Organometallics* **2017,** *36* (14), 2654-2660.

38. Zhu, C.; Kalin, A. J.; Fang, L., Covalent and Noncovalent Approaches to Rigid Coplanar π-Conjugated Molecules and Macromolecules. *Acc. Chem. Res.* **2019,** *52* (4), 1089-1100.

39. Vagedes, D.; Kehr, G.; König, D.; Wedeking, K.; Fröhlich, R.; Erker, G.; Mück-Lichtenfeld, C.; Grimme, S., Formation of Isomeric BAr3 Adducts of 2-Lithio-N-methylimidazole. *Eur. J. Inorg. Chem.* **2002,** *2002* (8), 2015-2021.

40. Job, A.; Wakamiya, A.; Kehr, G.; Erker, G.; Yamaguchi, S., Electronic Tuning of Thiazolyl-Capped π-Conjugated Compounds via a Coordination/Cyclization Protocol with B(C6F5)3. *Org. Lett.* **2010,** *12* (23), 5470-5473.

41. Wakamiya, A.; Taniguchi, T.; Yamaguchi, S., Intramolecular B–N Coordination as a Scaffold for Electron-Transporting Materials: Synthesis and Properties of Boryl-Substituted Thienylthiazoles. *Angew. Chem. Int. Ed.* **2006,** *45* (19), 3170-3173.

42. Ishida, N.; Moriya, T.; Goya, T.; Murakami, M., Synthesis of Pyridine−Borane Complexes via Electrophilic Aromatic Borylation. *J. Org. Chem.* **2010,** *75* (24), 8709-8712.

43. Wong, B. Y.-W.; Wong, H.-L.; Wong, Y.-C.; Chan, M.-Y.; Yam, V. W.-W., Air-Stable Spirofluorene-Containing Ladder-Type Bis(alkynyl)borane Compounds with Readily Tunable Full Color Emission Properties. *Chem. Eur. J.* **2016,** *22* (42), 15095-15106.

44. Yusuf, M.; Liu, K.; Guo, F.; Lalancette, R. A.; Jäkle, F., Luminescent organoboron ladder compounds via directed electrophilic aromatic C–H borylation. *Dalton Trans.* **2016,** *45* (11), 4580-4587.

45. Li, Y.; Meng, H.; Yan, D.; Li, Y.; Pang, B.; Zhang, K.; Luo, G.; Huang, J.; Zhan, C., Synthesis of B←N embedded indacenodithiophene chromophores and effects of bromine atoms on photophysical properties and energy levels. *Tetrahedron* **2018,** *74* (32), 4308-4314.

46. Li, D.; Zhang, H.; Wang, Y., Four-coordinate organoboron compounds for organic light-emitting diodes (OLEDs). *Chem. Soc. Rev.* **2013,** *42* (21), 8416-8433.

47. Fu, Y.; Qiu, F.; Zhang, F.; Mai, Y.; Wang, Y.; Fu, S.; Tang, R.; Zhuang, X.; Feng, X., A dual-boron-cored luminogen capable of sensing and imaging. *Chem. Commun.* **2015,** *51* (25), 5298-5301.

48. Sun, L.; Zhang, F.; Wang, X.; Qiu, F.; Xue, M.; Tregnago, G.; Cacialli, F.; Osella, S.; Beljonne, D.; Feng, X., Geometric and Electronic Structures of Boron(III)-Cored Dyes Tailored by Incorporation of Heteroatoms into Ligands. *Chem. Asian J.* **2015,** *10* (3), 709-714.

49. Ammon, F.; Sauer, S. T.; Lippert, R.; Lungerich, D.; Reger, D.; Hampel, F.; Jux, N., Unexpected formation of [5]helicenes from hexaarylbenzenes containing pyrrole moieties. *Org. Chem. Front.* **2017,** *4* (5), 861-870.

50. Reger, D.; Schöll, K.; Hampel, F.; Maid, H.; Jux, N., Pyridinic Nanographenes by Novel Precursor Design. *Chem. Eur. J.* **2021,** *27* (6), 1984-1989.

51. Pigulski, B.; Ximenis, M.; Shoyama, K.; Würthner, F., Synthesis of polycyclic aromatic hydrocarbons by palladium-catalysed [3 + 3] annulation. *Org. Chem. Front.* **2020,** *7* (19), 2925-2930.

52. Feng, B.-B.; Liu, J.-Q.; Wang, X.-S., Cu(OAc)2-Catalyzed Aerobic Oxidative Dehydrogenation Coupling: Synthesis of Heptacyclic Quinolizino[3,4,5,6-kla]perimidines. *J. Org. Chem.* **2017,** *82* (3), 1817-1822.

53. Xie, J.; Shi, K.; Cai, K.; Zhang, D.; Wang, J.-Y.; Pei, J.; Zhao, D., A NIR dye with high-performance n-type semiconducting properties. *Chem. Sci.* **2016,** *7* (1), 499-504.

54. Zagranyarski, Y.; Skabeev, A.; Ma, Y.; Müllen, K.; Li, C., Facile synthesis of annulated heterocyclic benzo[kl]acridine derivatives via one-pot N–H/C–H coupling. *Org. Chem. Front.* **2016,** *3* (11), 1520-1523.

55. Wang, Y.; Allemann, O.; Balaban, T. S.; Vanthuyne, N.; Linden, A.; Baldridge, K. K.; Siegel, J. S., Chiral Atropisomeric Indenocorannulene Bowls: Critique of the Cahn‐Ingold–Prelog Conception of Molecular Chirality. *Angew. Chem. Int. Ed.* **2018,** *57* (22), 6470-6474.

56. Chen, F.; Hong, Y. S.; Kim, D.; Tanaka, T.; Osuka, A., Sequential N-Alkylations of Tetrabenzotetraaza[8]circulene as a Tool To Tune Its Optical Properties. *ChemPlusChem* **2017,** *82* (7), 1048-1051.

57. Shuler, W. G.; Parvathaneni, S. P.; Rodriguez, J. B.; Lewis, T. N.; Berges, A. J.; Bardeen, C. J.; Krische, M. J., Synthesis and Photophysical Properties of Soluble N-Doped Rubicenes via Ruthenium-Catalyzed Transfer Hydrogenative Benzannulation. *Chem. Eur. J.* **2021,** *27* (15), 4898-4902.

58. Bazzini, C.; Brovelli, S.; Caronna, T.; Gambarotti, C.; Giannone, M.; Macchi, P.; Meinardi, F.; Mele, A.; Panzeri, W.; Recupero, F.; Sironi, A.; Tubino, R., Synthesis

and Characterization of Some Aza[5]helicenes. *Eur. J. Org. Chem.* **2005,** *2005* (7), 1247-1257.

59. Caronna, T.; Mele, A.; Famulari, A.; Mendola, D.; Fontana, F.; Juza, M.; Kamuf, M.; Zawatzky, K.; Trapp, O., A Combined Experimental and Theoretical Study on the Stereodynamics of Monoaza[5]helicenes: Solvent-Induced Increase of the Enantiomerization Barrier in 1-Aza-[5]helicene. *Chem. Eur. J.* **2015,** *21* (40), 13919-13924.

60. Abbate, S.; Bazzini, C.; Caronna, T.; Fontana, F.; Gangemi, F.; Lebon, F.; Longhi, G.; Mele, A.; Natali Sora, I., Experimental and calculated circular dichroism spectra of monoaza[5]helicenes. *Inorg. Chim. Acta* **2007,** *360* (3), 908-912.

61. Waghray, D.; Zhang, J.; Jacobs, J.; Nulens, W.; Basarić, N.; Meervelt, L. V.; Dehaen, W., Synthesis and Structural Elucidation of Diversely Functionalized 5,10-Diaza[5]Helicenes. *J. Org. Chem.* **2012,** *77* (22), 10176-10183.

62. Aloui, F.; Abed, R. E.; Hassine, B. B., Synthesis of a new N-containing hexahelicene. *Tetrahedron Lett.* **2008,** *49* (9), 1455-1457.

63. Aloui, F.; Abed, R. E.; Marinetti, A.; Hassine, B. B., Synthesis and resolution of a new helically chiral azahelicene. *Tetrahedron Lett.* **2008,** *49* (26), 4092-4095.

64. Míšek, J.; Teplý, F.; Stará, I. G.; Tichý, M.; Šaman, D.; Císařová, I.; Vojtíšek, P.; Starý, I., A Straightforward Route to Helically Chiral N-Heteroaromatic Compounds: Practical Synthesis of Racemic 1,14-Diaza[5]helicene and Optically Pure 1- and 2-Aza[6]helicenes. *Angew. Chem. Int. Ed.* **2008,** *47* (17), 3188-3191.

65. Roithová, J.; Schröder, D.; Míšek, J.; Stará, I. G.; Starý, I., Chiral superbases: the proton affinities of 1- and 2-aza[6]helicene in the gas phase. *J. Mass Spectrom.* **2007,** *42* (9), 1233-1237.

66. Nakai, Y.; Mori, T.; Inoue, Y., Theoretical and Experimental Studies on Circular Dichroism of Carbo[n]helicenes. *J. Phys. Chem. A* **2012,** *116* (27), 7372-7385.

67. Schmidt, K.; Brovelli, S.; Coropceanu, V.; Beljonne, D.; Cornil, J.; Bazzini, C.; Caronna, T.; Tubino, R.; Meinardi, F.; Shuai, Z.; Brédas, J.-L., Intersystem Crossing Processes in Nonplanar Aromatic Heterocyclic Molecules. *J. Phys. Chem. A* **2007,** *111* (42), 10490-10499.

68. Isla, H.; Srebro-Hooper, M.; Jean, M.; Vanthuyne, N.; Roisnel, T.; Lunkley, J. L.; Muller, G.; Williams, J. A. G.; Autschbach, J.; Crassous, J., Conformational changes and chiroptical switching of enantiopure bis-helicenic terpyridine upon Zn2+ binding. *Chem. Commun.* **2016,** *52* (35), 5932-5935.

69. Takenaka, N.; Sarangthem, R. S.; Captain, B., Helical Chiral Pyridine N-Oxides: A New Family of Asymmetric Catalysts. *Angew. Chem. Int. Ed.* **2008,** *47* (50), 9708-9710.

70. Šámal, M.; Chercheja, S.; Rybáček, J.; Vacek Chocholoušová, J.; Vacek, J.; Bednárová, L.; Šaman, D.; Stará, I. G.; Starý, I., An Ultimate Stereocontrol in Asymmetric Synthesis of Optically Pure Fully Aromatic Helicenes. *J. Am. Chem. Soc.* **2015,** *137* (26), 8469-8474.

71. Žádný, J.; Jančařík, A.; Andronova, A.; Šámal, M.; Vacek Chocholoušová, J.; Vacek, J.; Pohl, R.; Šaman, D.; Císařová, I.; Stará, I. G.; Starý, I., A General Approach

to Optically Pure [5]-, [6]-, and [7]Heterohelicenes. *Angew. Chem. Int. Ed.* **2012,** *51* (24), 5857-5861.

72. Klívar, J.; Jančařík, A.; Šaman, D.; Pohl, R.; Fiedler, P.; Bednárová, L.; Starý, I.; Stará, I. G., [2+2+2] Cycloisomerisation of Aromatic Cyanodiynes in the Synthesis of Pyridohelicenes and Their Analogues. *Chem. Eur. J.* **2016,** *22* (40), 14401-14405.

73. Weimar, M.; Correa da Costa, R.; Lee, F.-H.; Fuchter, M. J., A Scalable and Expedient Route to 1-Aza[6]helicene Derivatives and Its Subsequent Application to a Chiral-Relay Asymmetric Strategy. *Org. Lett.* **2013,** *15* (7), 1706-1709.

74. Nakamura, K.; Furumi, S.; Takeuchi, M.; Shibuya, T.; Tanaka, K., Enantioselective Synthesis and Enhanced Circularly Polarized Luminescence of S-Shaped Double Azahelicenes. *J. Am. Chem. Soc.* **2014,** *136* (15), 5555-5558.

75. Tanaka, M.; Shibata, Y.; Nakamura, K.; Teraoka, K.; Uekusa, H.; Nakazono, K.; Takata, T.; Tanaka, K., Gold-Catalyzed Enantioselective Synthesis, Crystal Structure, and Photophysical/Chiroptical Properties of Aza[10]helicenes. *Chem. Eur. J.* **2016,** *22* (28), 9537-9541.

76. Quinn, J. T. E.; Zhu, J.; Li, X.; Wang, J.; Li, Y., Recent progress in the development of n-type organic semiconductors for organic field effect transistors. *J. Mater. Chem. C* **2017,** *5* (34), 8654-8681.

77. Zhu, C.; Ji, X.; You, D.; Chen, T. L.; Mu, A. U.; Barker, K. P.; Klivansky, L. M.; Liu, Y.; Fang, L., Extraordinary Redox Activities in Ladder-Type Conjugated Molecules Enabled by B ← N Coordination-Promoted Delocalization and Hyperconjugation. *J. Am. Chem. Soc.* **2018,** *140* (51), 18173-18182.

78. Ito, H.; Ozaki, K.; Itami, K., Annulative π-Extension (APEX): Rapid Access to Fused Arenes, Heteroarenes, and Nanographenes. *Angew. Chem. Int. Ed.* **2017,** *56* (37), 11144-11164.

79. Ito, H.; Segawa, Y.; Murakami, K.; Itami, K., Polycyclic Arene Synthesis by Annulative π-Extension. *J. Am. Chem. Soc.* **2019,** *141* (1), 3-10.

80. Miao, Q., *Polycyclic Arenes and Heteroarenes: Synthesis, Properties, and Applications*. John Wiley & Sons: 2015.

81. Zhang, L.; Cao, Y.; Colella, N. S.; Liang, Y.; Brédas, J.-L.; Houk, K. N.; Briseno, A. L., Unconventional, Chemically Stable, and Soluble Two-Dimensional Angular Polycyclic Aromatic Hydrocarbons: From Molecular Design to Device Applications. *Acc. Chem. Res.* **2015,** *48* (3), 500-509.

82. Cai, Z.; Awais, M. A.; Zhang, N.; Yu, L., Exploration of Syntheses and Functions of Higher Ladder-type π-Conjugated Heteroacenes. *Chem* **2018,** *4* (11), 2538-2570.

83. Bendikov, M.; Wudl, F.; Perepichka, D. F., Tetrathiafulvalenes, Oligoacenenes, and Their Buckminsterfullerene Derivatives: The Brick and Mortar of Organic Electronics. *Chem. Rev.* **2004,** *104* (11), 4891-4946.

84. Zheng, T.; Cai, Z.; Ho-Wu, R.; Yau, S. H.; Shaparov, V.; Goodson, T.; Yu, L., Synthesis of Ladder-Type Thienoacenes and Their Electronic and Optical Properties. *J. Am. Chem. Soc.* **2016,** *138* (3), 868-875.

85. Daniel Głowacki, E.; Leonat, L.; Irimia-Vladu, M.; Schwödiauer, R.; Ullah, M.; Sitter, H.; Bauer, S.; Serdar Sariciftci, N., Intermolecular hydrogen-bonded organic semiconductors—Quinacridone versus pentacene. *Appl. Phys. Lett.* **2012,** *101* (2), 023305.

86. Chen, L.; Hernandez, Y.; Feng, X.; Müllen, K., From Nanographene and Graphene Nanoribbons to Graphene Sheets: Chemical Synthesis. *Angew. Chem. Int. Ed.* **2012,** *51* (31), 7640-7654.

87. Gu, Y.; Muñoz-Mármol, R.; Wu, S.; Han, Y.; Ni, Y.; Díaz-García, M. A.; Casado, J.; Wu, J., Cove-Edged Nanographenes with Localized Double Bonds. *Angew. Chem. Int. Ed.* **2020,** *59* (21), 8113-8117.

88. Bonal, V.; Muñoz-Mármol, R.; Gordillo Gámez, F.; Morales-Vidal, M.; Villalvilla, J. M.; Boj, P. G.; Quintana, J. A.; Gu, Y.; Wu, J.; Casado, J.; Díaz-García, M. A., Solution-processed nanographene distributed feedback lasers. *Nat. Commun.* **2019,** *10* (1), 3327.

89. Han, Y.; Xue, Z.; Li, G.; Gu, Y.; Ni, Y.; Dong, S.; Chi, C., Formation of Azulene-Embedded Nanographene: Naphthalene to Azulene Rearrangement During the Scholl Reaction. *Angew. Chem. Int. Ed.* **2020,** *59* (23), 9026-9031.

90. Povie, G.; Segawa, Y.; Nishihara, T.; Miyauchi, Y.; Itami, K., Synthesis of a carbon nanobelt. *Science* **2017,** *356* (6334), 172-175.

91. Povie, G.; Segawa, Y.; Nishihara, T.; Miyauchi, Y.; Itami, K., Synthesis and Size-Dependent Properties of [12], [16], and [24]Carbon Nanobelts. *J. Am. Chem. Soc.* **2018,** *140* (31), 10054-10059.

92. Nielsen, C. B.; Holliday, S.; Chen, H.-Y.; Cryer, S. J.; McCulloch, I., Non-Fullerene Electron Acceptors for Use in Organic Solar Cells. *Acc. Chem. Res.* **2015,** *48* (11), 2803-2812.

93. Yan, C.; Barlow, S.; Wang, Z.; Yan, H.; Jen, A. K. Y.; Marder, S. R.; Zhan, X., Non-fullerene acceptors for organic solar cells. *Nat. Rev. Mater.* **2018,** *3* (3), 18003.

94. Shan, B.; Miao, Q., Molecular design of n-type organic semiconductors for high-performance thin film transistors. *Tetrahedron Lett.* **2017,** *58* (20), 1903-1911.

95. Naibi Lakshminarayana, A.; Ong, A.; Chi, C., Modification of acenes for n-channel OFET materials. *J. Mater. Chem. C* **2018,** *6* (14), 3551-3563.

96. Dou, J.-H.; Yu, Z.-A.; Zhang, J.; Zheng, Y.-Q.; Yao, Z.-F.; Tu, Z.; Wang, X.; Huang, S.; Liu, C.; Sun, J.; Yi, Y.; Cao, X.; Gao, Y.; Wang, J.-Y.; Pei, J., Organic Semiconducting Alloys with Tunable Energy Levels. *J. Am. Chem. Soc.* **2019,** *141* (16), 6561-6568.

97. Chen, J.; Yang, K.; Zhou, X.; Guo, X., Ladder-Type Heteroarene-Based Organic Semiconductors. *Chem. Asian J.* **2018,** *13* (18), 2587-2600.

98. Wang, Y.; Guo, H.; Ling, S.; Arrechea-Marcos, I.; Wang, Y.; López Navarrete, J. T.; Ortiz, R. P.; Guo, X., Ladder-type Heteroarenes: Up to 15 Rings with Five Imide Groups. *Angew. Chem. Int. Ed.* **2017,** *56* (33), 9924-9929.

99. Bunz, U. H. F.; Engelhart, J. U.; Lindner, B. D.; Schaffroth, M., Large N-Heteroacenes: New Tricks for Very Old Dogs? *Angew. Chem. Int. Ed.* **2013,** *52* (14), 3810-3821.

100. Lopez, S. A.; Sanchez-Lengeling, B.; de Goes Soares, J.; Aspuru-Guzik, A., Design Principles and Top Non-Fullerene Acceptor Candidates for Organic Photovoltaics. *Joule* **2017,** *1* (4), 857-870.

101. Liu, K.; Lalancette, R. A.; Jäkle, F., Tuning the Structure and Electronic Properties of B–N Fused Dipyridylanthracene and Implications on the Self-Sensitized Reactivity with Singlet Oxygen. *J. Am. Chem. Soc.* **2019,** *141* (18), 7453-7462.

102. Vanga, M.; Lalancette, R. A.; Jäkle, F., Controlling the Optoelectronic Properties of Pyrene by Regioselective Lewis Base-Directed Electrophilic Aromatic Borylation. *Chem. Eur. J.* **2019,** *25* (43), 10133-10140.

103. Crossley, D. L.; Cade, I. A.; Clark, E. R.; Escande, A.; Humphries, M. J.; King, S. M.; Vitorica-Yrezabal, I.; Ingleson, M. J.; Turner, M. L., Enhancing electron affinity and tuning band gap in donor–acceptor organic semiconductors by benzothiadiazole directed C–H borylation. *Chem. Sci.* **2015,** *6* (9), 5144-5151.

104. Mellerup, S. K.; Wang, S., Boron-based stimuli responsive materials. *Chem. Soc. Rev.* **2019,** *48* (13), 3537-3549.

105. Huang, Z.; Wang, S.; Dewhurst, R. D.; Ignat'ev, N. V.; Finze, M.; Braunschweig, H., Boron: Its Role in Energy-Related Processes and Applications. *Angew. Chem. Int. Ed.* **2020,** *59* (23), 8800-8816.

106. Zhuang, F.-D.; Sun, Z.-H.; Yao, Z.-F.; Chen, Q.-R.; Huang, Z.; Yang, J.-H.; Wang, J.-Y.; Pei, J., BN-Embedded Tetrabenzopentacene: A Pentacene Derivative with Improved Stability. *Angew. Chem. Int. Ed.* **2019,** *58* (31), 10708-10712.

107. Min, Y.; Dou, C.; Liu, D.; Dong, H.; Liu, J., Quadruply B←N-Fused Dibenzo-azaacene with High Electron Affinity and High Electron Mobility. *J. Am. Chem. Soc.* **2019,** *141* (42), 17015-17021.

108. Fischer, G. M.; Daltrozzo, E.; Zumbusch, A., Selective NIR chromophores: Bis(Pyrrolopyrrole) Cyanines. *Angew. Chem. Int. Ed.* **2011,** *50* (6), 1406-1409.

109. Shimogawa, H.; Murata, Y.; Wakamiya, A., NIR-Absorbing Dye Based on BF2-Bridged Azafulvene Dimer as a Strong Electron-Accepting Unit. *Org. Lett.* **2018,** *20* (17), 5135-5138.

110. Zhu, C.; Guo, Z.-H.; Mu, A. U.; Liu, Y.; Wheeler, S. E.; Fang, L., Low Band Gap Coplanar Conjugated Molecules Featuring Dynamic Intramolecular Lewis Acid–Base Coordination. *J. Org. Chem.* **2016,** *81* (10), 4347-4352.

111. Han, Y.; Barnes, G.; Lin, Y.-H.; Martin, J.; Al-Hashimi, M.; AlQaradawi, S. Y.; Anthopoulos, T. D.; Heeney, M., Doping of Large Ionization Potential Indenopyrazine Polymers via Lewis Acid Complexation with Tris(pentafluorophenyl)borane: A Simple Method for Improving the Performance of Organic Thin-Film Transistors. *Chem. Mater.* **2016,** *28* (21), 8016-8024.

112. Grandl, M.; Rudolf, B.; Sun, Y.; Bechtel, D. F.; Pierik, A. J.; Pammer, F., Intramolecular N→B Coordination as a Stabilizing Scaffold for π-Conjugated Radical Anions with Tunable Redox Potentials. *Organometallics* **2017,** *36* (14), 2527-2535.

113. Grandl, M.; Kaese, T.; Krautsieder, A.; Sun, Y.; Pammer, F., Hydroboration as an Efficient Tool for the Preparation of Electronically and Structurally Diverse N→B-Heterocycles. *Chem. Eur. J.* **2016,** *22* (40), 14373-14382.

114. Min, Y.; Dou, C.; Tian, H.; Geng, Y.; Liu, J.; Wang, L., n-Type Azaacenes Containing B←N Units. *Angew. Chem. Int. Ed.* **2018,** *57* (7), 2000-2004.

115. Sun, H.; Guo, X.; Facchetti, A., High-Performance n-Type Polymer Semiconductors: Applications, Recent Development, and Challenges. *Chem* **2020,** *6* (6), 1310-1326.

116. Long, X.; Ding, Z.; Dou, C.; Zhang, J.; Liu, J.; Wang, L., Polymer Acceptor Based on Double B←N Bridged Bipyridine (BNBP) Unit for High-Efficiency All-Polymer Solar Cells. *Adv. Mater.* **2016,** *28* (30), 6504-6508.

117. Mula, S.; Leclerc, N.; Lévêque, P.; Retailleau, P.; Ulrich, G., Synthesis of Indolo[3,2-b]carbazole-Based Boron Complexes with Tunable Photophysical and Electrochemical Properties. *J. Org. Chem.* **2018,** *83* (23), 14406-14418.

118. Koppel, I.; Koppel, J.; Maria, P.-C.; Gal, J.-F.; Notario, R.; Vlasov, V. M.; Taft, R. W., Comparison of brönsted acidities of neutral NH-acids in gas phase, dimethyl sulfoxide and water. *Int. J. Mass Spectrom. Ion Processes* **1998,** *175* (1), 61-69.

119. Barłóg, M.; Zhang, X.; Kulai, I.; Yang, D. S.; Sredojevic, D. N.; Sil, A.; Ji, X.; Salih, K. S. M.; Bazzi, H. S.; Bronstein, H.; Fang, L.; Kim, J.; Marks, T. J.; Guo, X.; Al-Hashimi, M., Indacenodithiazole-Ladder-Type Bridged Di(thiophene)-Difluoro-Benzothiadiazole-Conjugated Copolymers as Ambipolar Organic Field-Effect Transistors. *Chem. Mater.* **2019,** *31* (22), 9488-9496.

120. Qiu, F.; Zhang, F.; Tang, R.; Fu, Y.; Wang, X.; Han, S.; Zhuang, X.; Feng, X., Triple Boron-Cored Chromophores Bearing Discotic 5,11,17-Triazatrinaphthylene-Based Ligands. *Org. Lett.* **2016,** *18* (6), 1398-1401.

121. Menges, N., Computational study on aromaticity and resonance structures of substituted BODIPY derivatives. *Comput Theor Chem.* **2015,** *1068*, 117-122.

122. Meng, F.; Bu, Y.; Liu, C., Theoretical study of the pyridine–BF3 complex. *Journal of Molecular Structure: THEOCHEM* **2002,** *588* (1), 1-8.

123. Tao, J.; Sun, D.; Sun, L.; Li, Z.; Fu, B.; Liu, J.; Zhang, L.; Wang, S.; Fang, Y.; Xu, H., Tuning the photo-physical properties of BODIPY dyes: Effects of 1, 3, 5, 7-substitution on their optical and electrochemical behaviours. *Dyes and Pigments* **2019,** *168*, 166-174.

124. Yang, J.; Cai, F.; Desbois, N.; Huang, L.; Gros, C. P.; Bolze, F.; Fang, Y.; Wang, S.; Xu, H.-J., Synthesis, spectroscopic characterization, one and two-photon absorption properties and electrochemistry of π-expanded BODIPYs dyes. *Dyes and Pigments* **2020,** *175*, 108173.

125. Ie, Y.; Ueta, M.; Nitani, M.; Tohnai, N.; Miyata, M.; Tada, H.; Aso, Y., Air-Stable n-Type Organic Field-Effect Transistors Based on 4,9-Dihydro-s-indaceno[1,2-b:5,6-b′]dithiazole-4,9-dione Unit. *Chem. Mater.* **2012,** *24* (16), 3285-3293.

126. *APEX3 "Program for Data Collection on Area Detectors"*, BRUKER AXS Inc.

127. SADABS, S., G.M. *"Program for Absorption Correction of Area Detector Frames"*, BRUKER AXS Inc.

128. Sheldrick, G., SHELXT - Integrated space-group and crystal-structure determination. *Acta Crystallographica Section A* **2015,** *71* (1), 3-8.

129. Dolomanov, O. V.; Bourhis, L. J.; Gildea, R. J.; Howard, J. A. K.; Puschmann, H., OLEX2: a complete structure solution, refinement and analysis program. *J. Appl. Crystallogr.* **2009,** *42* (2), 339-341.

130. Forrest, S. R., *Organic Electronics: Foundations to Applications*. Oxford University Press: 2020.

131. Fukuda, K.; Takeda, Y.; Yoshimura, Y.; Shiwaku, R.; Tran, L. T.; Sekine, T.; Mizukami, M.; Kumaki, D.; Tokito, S., Fully-printed high-performance organic thin-film transistors and circuitry on one-micron-thick polymer films. *Nat. Commun.* **2014,** *5* (1), 4147.

132. Kaltenbrunner, M.; Sekitani, T.; Reeder, J.; Yokota, T.; Kuribara, K.; Tokuhara, T.; Drack, M.; Schwödiauer, R.; Graz, I.; Bauer-Gogonea, S.; Bauer, S.; Someya, T., An ultra-lightweight design for imperceptible plastic electronics. *Nature* **2013,** *499* (7459), 458-463.

133. Mei, J.; Diao, Y.; Appleton, A. L.; Fang, L.; Bao, Z., Integrated Materials Design of Organic Semiconductors for Field-Effect Transistors. *J. Am. Chem. Soc.* **2013,** *135* (18), 6724-6746.

134. He, Y.; Hong, W.; Li, Y., New building blocks for π-conjugated polymer semiconductors for organic thin film transistors and photovoltaics. *J. Mater. Chem. C* **2014,** *2* (41), 8651-8661.

135. Yuan, Y.; Giri, G.; Ayzner, A. L.; Zoombelt, A. P.; Mannsfeld, S. C. B.; Chen, J.; Nordlund, D.; Toney, M. F.; Huang, J.; Bao, Z., Ultra-high mobility transparent organic thin film transistors grown by an off-centre spin-coating method. *Nat. Commun.* **2014,** *5* (1), 3005.

136. Luo, C.; Kyaw, A. K. K.; Perez, L. A.; Patel, S.; Wang, M.; Grimm, B.; Bazan, G. C.; Kramer, E. J.; Heeger, A. J., General Strategy for Self-Assembly of Highly Oriented

Nanocrystalline Semiconducting Polymers with High Mobility. *Nano Lett.* **2014,** *14* (5), 2764-2771.

137. Zaumseil, J.; Sirringhaus, H., Electron and Ambipolar Transport in Organic Field-Effect Transistors. *Chem. Rev.* **2007,** *107* (4), 1296-1323.

138. Brixi, S.; Melville, O. A.; Mirka, B.; He, Y.; Hendsbee, A. D.; Meng, H.; Li, Y.; Lessard, B. H., Air and temperature sensitivity of n-type polymer materials to meet and exceed the standard of N2200. *Sci. Rep.* **2020,** *10* (1), 4014.

139. Guo, X.; Watson, M. D., Conjugated Polymers from Naphthalene Bisimide. *Org. Lett.* **2008,** *10* (23), 5333-5336.

140. Kang, B.; Kim, R.; Lee, S. B.; Kwon, S.-K.; Kim, Y.-H.; Cho, K., Side-Chain-Induced Rigid Backbone Organization of Polymer Semiconductors through Semifluoroalkyl Side Chains. *J. Am. Chem. Soc.* **2016,** *138* (11), 3679-3686.

141. Hwang, Y.-J.; Ren, G.; Murari, N. M.; Jenekhe, S. A., n-Type Naphthalene Diimide–Biselenophene Copolymer for All-Polymer Bulk Heterojunction Solar Cells. *Macromolecules* **2012,** *45* (22), 9056-9062.

142. Yang, J.; Xiao, B.; Tajima, K.; Nakano, M.; Takimiya, K.; Tang, A.; Zhou, E., Comparison among Perylene Diimide (PDI), Naphthalene Diimide (NDI), and Naphthodithiophene Diimide (NDTI) Based n-Type Polymers for All-Polymer Solar Cells Application. *Macromolecules* **2017,** *50* (8), 3179-3185.

143. Zhou, E.; Tajima, K.; Yang, C.; Hashimoto, K., Band gap and molecular energy level control of perylene diimide-based donor–acceptor copolymers for all-polymer solar cells. *J. Mater. Chem.* **2010,** *20* (12), 2362-2368.

144. Zhou, E.; Cong, J.; Wei, Q.; Tajima, K.; Yang, C.; Hashimoto, K., All-Polymer Solar Cells from Perylene Diimide Based Copolymers: Material Design and Phase Separation Control. *Angew. Chem. Int. Ed.* **2011,** *50* (12), 2799-2803.

145. Guo, Y.; Li, Y.; Awartani, O.; Zhao, J.; Han, H.; Ade, H.; Zhao, D.; Yan, H., A Vinylene-Bridged Perylenediimide-Based Polymeric Acceptor Enabling Efficient All-Polymer Solar Cells Processed under Ambient Conditions. *Adv. Mater.* **2016,** *28* (38), 8483-8489.

146. Gruntz, G.; Lee, H.; Hirsch, L.; Castet, F.; Toupance, T.; Briseno, A. L.; Nicolas, Y., Nitrile Substitution Effect on Triphenodioxazine-Based Materials for Liquid-Processed Air-Stable n-Type Organic Field Effect Transistors. *Adv. Electron. Mater.* **2015,** *1* (6), 1500072.

147. Wang, C.; Zhang, J.; Long, G.; Aratani, N.; Yamada, H.; Zhao, Y.; Zhang, Q., Synthesis, Structure, and Air-stable N-type Field-Effect Transistor Behaviors of Functionalized Octaazanonacene-8,19-dione. *Angew. Chem. Int. Ed.* **2015,** *54* (21), 6292-6296.

148. Zhang, C.; Zang, Y.; Gann, E.; McNeill, C. R.; Zhu, X.; Di, C.-a.; Zhu, D., Two-Dimensional π-Expanded Quinoidal Terthiophenes Terminated with Dicyanomethylenes as n-Type Semiconductors for High-Performance Organic Thin-Film Transistors. *J. Am. Chem. Soc.* **2014,** *136* (46), 16176-16184.

149. Zhang, C.; Zang, Y.; Zhang, F.; Diao, Y.; McNeill, C. R.; Di, C.-a.; Zhu, X.; Zhu, D., Pursuing High-Mobility n-Type Organic Semiconductors by Combination of

"Molecule-Framework" and "Side-Chain" Engineering. *Adv. Mater.* **2016,** *28* (38), 8456-8462.

150. Xu, S.; Ai, N.; Zheng, J.; Zhao, N.; Lan, Z.; Wen, L.; Wang, X.; Pei, J.; Wan, X., Extended isoindigo core: synthesis and applications as solution-processable n-OFET materials in ambient conditions. *RSC Advances* **2015,** *5* (11), 8340-8344.

151. Dou, J.-H.; Zheng, Y.-Q.; Yao, Z.-F.; Yu, Z.-A.; Lei, T.; Shen, X.; Luo, X.-Y.; Sun, J.; Zhang, S.-D.; Ding, Y.-F.; Han, G.; Yi, Y.; Wang, J.-Y.; Pei, J., Fine-Tuning of Crystal Packing and Charge Transport Properties of BDOPV Derivatives through Fluorine Substitution. *J. Am. Chem. Soc.* **2015,** *137* (50), 15947-15956.

152. Lee, J.; Kalin, A. J.; Wang, C.; Early, J. T.; Al-Hashimi, M.; Fang, L., Donor–acceptor conjugated ladder polymer via aromatization-driven thermodynamic annulation. *Polymer Chemistry* **2018,** *9* (13), 1603-1609.

153. Krakowiak, K. E.; Bradshaw, J. S., Thermal Removal of Boc-Protecting Groups During Preparation of Open-Chain Polyamines. *Synth. Commun.* **1996,** *26* (21), 3999-4004.

154. Yumusak, C.; Sariciftci, N. S.; Irimia-Vladu, M., Purity of organic semiconductors as a key factor for the performance of organic electronic devices. *Mater. Chem. Front.* **2020,** *4* (12), 3678-3689.

155. Okamoto, T.; Kumagai, S.; Fukuzaki, E.; Ishii, H.; Watanabe, G.; Niitsu, N.; Annaka, T.; Yamagishi, M.; Tani, Y.; Sugiura, H.; Watanabe, T.; Watanabe, S.; Takeya, J., Robust, high-performance n-type organic semiconductors. *Sci. Adv. 6* (18), eaaz0632.

156. Jiang, Z.; Li, X.; Strzalka, J.; Sprung, M.; Sun, T.; Sandy, A. R.; Narayanan, S.; Lee, D. R.; Wang, J., The dedicated high-resolution grazing-incidence X-ray scattering beamline 8-ID-E at the Advanced Photon Source. *J. Synchrotron Rad.* **2012,** *19* (4), 627-636.

157. Jiang, Z., GIXSGUI: a MATLAB toolbox for grazing-incidence X-ray scattering data visualization and reduction, and indexing of buried three-dimensional periodic nanostructured films. *J. Appl. Crystallogr.* **2015,** *48* (3), 917-926.

158. Shen, Y.; Chen, C.-F., Helicenes: Synthesis and Applications. *Chem. Rev.* **2012,** *112* (3), 1463-1535.

159. Dhbaibi, K.; Favereau, L.; Crassous, J., Enantioenriched Helicenes and Helicenoids Containing Main-Group Elements (B, Si, N, P). *Chem. Rev.* **2019,** *119* (14), 8846-8953.

160. Gingras, M., One hundred years of helicene chemistry. Part 1: non-stereoselective syntheses of carbohelicenes. *Chem. Soc. Rev.* **2013,** *42* (3), 968-1006.

161. Meisenheimer, J.; Witte, K., Reduction von 2-Nitronaphtalin. *Berichte der deutschen chemischen Gesellschaft* **1903,** *36* (4), 4153-4164.

162. Cahn, R. S.; Ingold, C.; Prelog, V., Specification of Molecular Chirality. *Angewandte Chemie International Edition in English* **1966,** *5* (4), 385-415.

163. Paruch, K.; Vyklický, L.; Wang, D. Z.; Katz, T. J.; Incarvito, C.; Zakharov, L.; Rheingold, A. L., Functionalizations of [6]- and [7]Helicenes at Their Most Sterically Hindered Positions. *J. Org. Chem.* **2003,** *68* (22), 8539-8544.

164. Milton, M.; Schuster, N. J.; Paley, D. W.; Hernández Sánchez, R.; Ng, F.; Steigerwald, M. L.; Nuckolls, C., Defying strain in the synthesis of an electroactive bilayer helicene. *Chem. Sci.* **2019,** *10* (4), 1029-1034.

165. Yamamoto, K.; Shimizu, T.; Igawa, K.; Tomooka, K.; Hirai, G.; Suemune, H.; Usui, K., Rational Design and Synthesis of [5]Helicene-Derived Phosphine Ligands and Their Application in Pd-Catalyzed Asymmetric Reactions. *Sci. Rep.* **2016,** *6* (1), 36211.

166. Graule, S.; Rudolph, M.; Vanthuyne, N.; Autschbach, J.; Roussel, C.; Crassous, J.; Réau, R., Metal−Bis(helicene) Assemblies Incorporating π-Conjugated Phosphole-Azahelicene Ligands: Impacting Chiroptical Properties by Metal Variation. *J. Am. Chem. Soc.* **2009,** *131* (9), 3183-3185.

167. Graule, S.; Rudolph, M.; Shen, W.; Williams, J. A. G.; Lescop, C.; Autschbach, J.; Crassous, J.; Réau, R., Assembly of π-Conjugated Phosphole Azahelicene Derivatives into Chiral Coordination Complexes: An Experimental and Theoretical Study. *Chem. Eur. J.* **2010,** *16* (20), 5976-6005.

168. Dreher, S. D.; Katz, T. J.; Lam, K.-C.; Rheingold, A. L., Application of the Russig−Laatsch Reaction to Synthesize a Bis[5]helicene Chiral Pocket for Asymmetric Catalysis. *J. Org. Chem.* **2000,** *65* (3), 815-822.

169. Šámal, M.; Míšek, J.; Stara, I.; Stary, I., Organocatalysis with azahelicenes: The first use of helically chiral pyridine-based catalysts in the asymmetric acyl transfer reaction. *Collect. Czech. Chem. Commun.* **2009,** *74*.

170. Crittall, M. R.; Rzepa, H. S.; Carbery, D. R., Design, Synthesis, and Evaluation of a Helicenoidal DMAP Lewis Base Catalyst. *Org. Lett.* **2011,** *13* (5), 1250-1253.

171. Crittall, M. R.; Fairhurst, N. W. G.; Carbery, D. R., Point-to-helical chirality transfer for a scalable and resolution-free synthesis of a helicenoidal DMAP organocatalyst. *Chem. Commun.* **2012,** *48* (91), 11181-11183.

172. Chen, F.; Hong, Y. S.; Shimizu, S.; Kim, D.; Tanaka, T.; Osuka, A., Synthesis of a Tetrabenzotetraaza[8]circulene by a "Fold-In" Oxidative Fusion Reaction. *Angew. Chem. Int. Ed.* **2015,** *54* (36), 10639-10642.

173. Chen, F.; Tanaka, T.; Mori, T.; Osuka, A., Synthesis, Structures, and Optical Properties of Azahelicene Derivatives and Unexpected Formation of Azahepta[8]circulenes. *Chem. Eur. J.* **2018,** *24* (29), 7489-7497.

174. Pedersen, S. K.; Eriksen, K.; Ågren, H.; Minaev, B. F.; Karaush-Karmazin, N. N.; Hammerich, O.; Baryshnikov, G. V.; Pittelkow, M., A Fully Conjugated Planar Heterocyclic [9]Circulene. *J. Am. Chem. Soc.* **2020,** *142* (33), 14058-14063.

175. Matsuo, Y.; Kise, K.; Morimoto, Y.; Osuka, A.; Tanaka, T., Fold-in Synthesis of a Pentabenzopentaaza[10]circulene. *Angew. Chem. Int. Ed.* **2022,** *n/a* (n/a), e202116789.

176. Liu, C.; Park, E.; Jin, Y.; Liu, J.; Yu, Y.; Zhang, W.; Lei, S.; Hu, W., Surface-Confined Dynamic Covalent System Driven by Olefin Metathesis. *Angew. Chem. Int. Ed.* **2018,** *57* (7), 1869-1873.

177. Kravchenko, A.; Timmer, B. J. J.; Inge, A. K.; Biedermann, M.; Ramström, O., Stable CAAC‐based Ruthenium Complexes for Dynamic Olefin Metathesis Under Mild Conditions. *ChemCatChem* **2021,** *13* (22), 4841-4847.

178. Lee, J.; Rajeeva, B. B.; Yuan, T. Y.; Guo, Z. H.; Lin, Y. H.; Al-Hashimi, M.; Zheng, Y. B.; Fang, L., Thermodynamic synthesis of solution processable ladder polymers. *Chem. Sci.* **2016,** *7* (2), 881-889.

179. Lee, J.; Li, H. B.; Kalin, A. J.; Yuan, T. Y.; Wang, C. X.; Olson, T.; Li, H. Y.; Fang, L., Extended Ladder-Type Benzo[k]tetraphene-Derived Oligomers. *Angew. Chem. Int. Ed.* **2017,** *56* (44), 13727-13731.

180. Che, S.; Pang, J.; Kalin, A. J.; Wang, C.; Ji, X.; Lee, J.; Cole, D.; Li, J.-L.; Tu, X.; Zhang, Q.; Zhou, H.-C.; Fang, L., Rigid Ladder-Type Porous Polymer Networks for Entropically Favorable Gas Adsorption. *ACS Materials Letters* **2020,** *2* (1), 49-54.

181. Kalin, A. J.; Che, S.; Wang, C. X.; Mu, A. U.; Duka, E. M.; Fang, L., Solution-Processable Porous Nanoparticles of a Conjugated Ladder Polymer Network. *Macromolecules* **2020,** *53* (3), 922-928.

182. Nakakuki, Y.; Hirose, T.; Matsuda, K., Synthesis of a Helical Analogue of Kekulene: A Flexible π-Expanded Helicene with Large Helical Diameter Acting as a Soft Molecular Spring. *J. Am. Chem. Soc.* **2018,** *140* (45), 15461-15469.

183. Hong, S. H.; Wenzel, A. G.; Salguero, T. T.; Day, M. W.; Grubbs, R. H., Decomposition of Ruthenium Olefin Metathesis Catalysts. *J. Am. Chem. Soc.* **2007,** *129* (25), 7961-7968.

184. Espinet, P.; Echavarren, A. M., The Mechanisms of the Stille Reaction. *Angew. Chem. Int. Ed.* **2004,** *43* (36), 4704-4734.

185. Johnson, J. B.; Rovis, T., More than Bystanders: The Effect of Olefins on Transition-Metal-Catalyzed Cross-Coupling Reactions. *Angew. Chem. Int. Ed.* **2008,** *47* (5), 840-871.

186. Beletskaya, I. P.; Cheprakov, A. V., The Heck Reaction as a Sharpening Stone of Palladium Catalysis. *Chem. Rev.* **2000,** *100* (8), 3009-3066.

187. Amatore, C.; Broeker, G.; Jutand, A.; Khalil, F., Identification of the Effective Palladium(0) Catalytic Species Generated in Situ from Mixtures of Pd(dba)2 and Bidentate Phosphine Ligands. Determination of Their Rates and Mechanism in Oxidative Addition. *J. Am. Chem. Soc.* **1997,** *119* (22), 5176-5185.

188. Amatore, C.; Jutand, A.; Khalil, F.; M'Barki, M. A.; Mottier, L., Rates and mechanisms of oxidative addition to zerovalent palladium complexes generated in situ from mixtures of Pd0(dba)2 and triphenylphosphine. *Organometallics* **1993,** *12* (8), 3168-3178.

189. Ashworth, I. W.; Hillier, I. H.; Nelson, D. J.; Percy, J. M.; Vincent, M. A., Searching for the Hidden Hydrides: The Competition between Alkene Isomerization and Metathesis with Grubbs Catalysts. *Eur. J. Org. Chem.* **2012,** *2012* (29), 5673-5677.

190. Nelson, D. J.; Manzini, S.; Urbina-Blanco, C. A.; Nolan, S. P., Key processes in ruthenium-catalysed olefin metathesis. *Chem. Commun.* **2014,** *50* (72), 10355-10375.

191. McGrath, D. V.; Grubbs, R. H., The mechanism of aqueous ruthenium(II)-catalyzed olefin isomerization. *Organometallics* **1994,** *13* (1), 224-235.

192. Bourgeois, D.; Pancrazi, A.; Nolan, S. P.; Prunet, J., The Cl2(PCy3)(IMes)Ru(· CHPh) catalyst: olefin metathesis versus olefin isomerization. *J. Organomet. Chem.* **2002,** *643-644*, 247-252.

193. Janse van Rensburg, W.; Steynberg, P. J.; Meyer, W. H.; Kirk, M. M.; Forman, G. S., DFT Prediction and Experimental Observation of Substrate-Induced Catalyst Decomposition in Ruthenium-Catalyzed Olefin Metathesis. *J. Am. Chem. Soc.* **2004,** *126* (44), 14332-14333.

194. van Rensburg, W. J.; Steynberg, P. J.; Kirk, M. M.; Meyer, W. H.; Forman, G. S., Mechanistic comparison of ruthenium olefin metathesis catalysts: DFT insight into relative reactivity and decomposition behavior. *J. Organomet. Chem.* **2006,** *691* (24), 5312-5325.

195. Chapter 1 The Role of the Laboratory in Chemistry Teaching and Learning. In *Teaching and Learning in the School Chemistry Laboratory*, The Royal Society of Chemistry: 2022; pp 1-15.

196. Santos-Díaz, S.; Hensiek, S.; Owings, T.; Towns, M. H., Survey of Undergraduate Students' Goals and Achievement Strategies for Laboratory Coursework. *J. Chem. Educ.* **2019,** *96* (5), 850-856.

197. Peltzer, R. M.; Gauss, J.; Eisenstein, O.; Cascella, M., The Grignard Reaction – Unraveling a Chemical Puzzle. *J. Am. Chem. Soc.* **2020,** *142* (6), 2984-2994.

198. Campeau, L.-C.; Hazari, N., Cross-Coupling and Related Reactions: Connecting Past Success to the Development of New Reactions for the Future. *Organometallics* **2019,** *38* (1), 3-35.

199. Ogba, O. M.; Warner, N. C.; O'Leary, D. J.; Grubbs, R. H., Recent advances in ruthenium-based olefin metathesis. *Chem. Soc. Rev.* **2018,** *47* (12), 4510-4544.

200. Brown, D. G.; Boström, J., Analysis of Past and Present Synthetic Methodologies on Medicinal Chemistry: Where Have All the New Reactions Gone? *J. Med. Chem.* **2016,** *59* (10), 4443-4458.

201. Hamilton, A. E.; Buxton, A. M.; Peeples, C. J.; Chalker, J. M., An Operationally Simple Aqueous Suzuki–Miyaura Cross-Coupling Reaction for an Undergraduate Organic Chemistry Laboratory. *J. Chem. Educ.* **2013,** *90* (11), 1509-1513.

202. Callam, C. S.; Lowary, T. L., Suzuki Cross-Coupling Reactions: Synthesis of Unsymmetrical Biaryls in the Organic Laboratory. *J. Chem. Educ.* **2001,** *78* (7), 947.

203. Dai, J.; Lu, D.; Ye, T.; Yu, S.; Cheng, X., Experimenting with a Suzuki–Miyaura Cross-Coupling Reaction That Demonstrates Tolerance toward Aldehyde Groups To Teach Undergraduate Students the Fundamentals of Transition-Metal-Catalyzed Reactions. *J. Chem. Educ.* **2019,** *96* (11), 2672-2675.

204. Cooke, J., Syntheses of Four-Coordinate Nickel(II)-Phosphine Compounds and a Rapid Suzuki–Miyaura Cross-Coupling Reaction for Short Laboratory Sessions. *J. Chem. Educ.* **2019,** *96* (9), 2009-2014.

205. Pappenfus, T. M.; Hermanson, D. L.; Ekerholm, D. P.; Lilliquist, S. L.; Mekoli, M. L., Synthesis and Catalytic Activity of Ruthenium–Indenylidene Complexes for Olefin Metathesis. *J. Chem. Educ.* **2007,** *84* (12), 1998.

206. Taber, D. F.; Frankowski, K. J., Grubbs's Cross Metathesis of Eugenol with cis-2-Butene-1,4-diol To Make a Natural Product. An Organometallic Experiment for the Undergraduate Lab. *J. Chem. Educ.* **2006,** *83* (2), 283.

207. Mikami, K.; Terada, M.; Matsuzawa, H., "Asymmetric" Catalysis by Lanthanide Complexes. *Angew. Chem. Int. Ed.* **2002,** *41* (19), 3554-3572.

208. Hancock, R. D., The pyridyl group in ligand design for selective metal ion complexation and sensing. *Chem. Soc. Rev.* **2013,** *42* (4), 1500-24.

209. Li, X. Z.; Zhou, L. P.; Yan, L. L.; Dong, Y. M.; Bai, Z. L.; Sun, X. Q.; Diwu, J.; Wang, S.; Bunzli, J. C.; Sun, Q. F., A supramolecular lanthanide separation approach based on multivalent cooperative enhancement of metal ion selectivity. *Nat. Commun.* **2018,** *9* (1), 547.

210. Lumetta, G. J.; Gelis, A. V.; Carter, J. C.; Niver, C. M.; Smoot, M. R., The Actinide-Lanthanide Separation Concept. *Solvent Extr. Ion Exch.* **2014,** *32* (4), 333-347.